UNIVERSITY OF NOTTINGHAM

DEPARTMENT OF MECHANICAL ENGINEERING

Characterisation of Fabric Deformation Mechanisms during Preform Manufacture

by

Mark Blagdon

BEng

Thesis submitted to the University of Nottingham

for the degree of Doctor of Philosophy

October 1998

Contents

Abstract

Characterisation of Fabric Deformation Mechanisms during Preform Manufacture

by

Mark Blagdon

BEng

The use of composites for structural applications in the automotive industry has become more attractive due to the possible weight savings and part integration. Liquid moulding processes, where the reinforcement is prepared separately from the moulding operation, have been suggested as a suitable production method. However there are several obstacles to overcome before they can meet the high production volumes required. Whilst forming the preform, defects such as wrinkling and tearing can occur which can prevent successful moulding.

This thesis addresses problems in the design and production of preforms. Current preform manufacturing processes and modelling techniques are reviewed. A model based on kinematic principles to predict fibre architectures for biaxial fabrics draped over arbitrary surfaces is described. A technique based on grid strain analysis was used to measure the deformation of various stitch bonded fabrics, and compared to the kinematic drape model results. The pure shear assumptions of the kinematic drape model assume the fabric has zero resistance to shear. Experimental measurements of fabric in-plane shear resistance were undertaken and compared for a range of fabrics. This highlighted some important criteria in fabric selection and possible problems in the kinematic modelling approach. The results from the in-plane shear tests were compared with those from the grid strain analysis to determine which fabric variables were important to fabric formability. Problems in the application of constraints within the kinematic model were discovered, and methods for overcoming them were suggested. Criteria which must be considered when selecting suitable fabrics for high drape preforms are discussed.

Acknowledgements

The author would like to thank his supervisors Dr. C.D. Rudd and Dr. A.C. Long for their guidance and assistance during this research.

The funding for this project was supplied by Ford Motor Company, and their support has been gratefully received. Particular thanks to Dr. Ken Kendall, Mr. Carl Johnson and Dr. Mahmood Demeri for the use of their experimental facilities in Dearborn, and Dr. John Hill for moral support and accommodation.

The Head of Department, Professor Clayton, receives thanks for allowing the use of Department facilities. The technical assistance of Andrew Kingham, Roger Smith and Geoff Tomlinson was much appreciated.

Fellow researchers Dr Paul Smith, Dr Patrick Blanchard, Dan Morris, Dr Simon Gardener, Dr Chris Duffy, Mat Turner, Dr Mike Johnson, Dr Steve Knowles, Dr Alan McMillan and Dr Tom Corden provided encouragement and humour to relieve the stress, as well as proving to me that deadlines could be met.

Finally my long suffering partner Becky must be thanked for all her help and support, both emotional and domestic.

Glossary of Terms

Anisotropic - Having properties dependent upon the orientation of the material.

Areal density - Unit of measurement of surface density (weight per unit area) of a fabric.

Biaxial - Having fibres in two different directions.

Binder - A cohesive agent used to join fibres within a preform.

Braiding - A preforming technique which wraps the fibres around a mandrel.

C - A high level computer language with low level hardware access capabilities.

Catalyst - A chemical which initiates cure of the resin.

Chain stitch - A type of stitch used in fabric manufacture.

CNC - Computer Numerical Control.

Cure - A chemical reaction which permanently changes the state of a thermoset resin.

Drape - The ability of a fabric to conform to a complex surface.

Fibre - An individual strand of material.

Filament - The smallest unit of a fibrous material.

Filament winding - A composite manufacturing technique, which wraps fibres around a mandrel.

Geodesic - The shortest path between two points across a surface.

GUI - Graphical User Interface

Impregnation - The penetration of resin into a preform.

Injection gate - An inlet into the mould cavity through which resin flows.

Isotropic - Having properties which are independent of material orientation.

KDM - Kinematic Drape Model.

Laminate - An assembly of plies within a moulding.

Linear Density - The mass of a yarn per unit length.

LMP - Liquid Moulding Process.

Mandrel - A core used in braiding or filament winding.

Matrix -	Homogeneous material that encases the reinforcement.
Mould -	A cavity with the required component shape, which is used to contain the resin during cure.
NCF -	Non Crimp Fabric.
Newtonian Fluid -	A fluid whose viscosity is independent of shear rate.
Orthotropic -	Having mutually perpendicular planes of elastic symmetry.
PC -	Personal Computer.
Permeability -	The ease of fluid impregnation into a porous material.
Pitch -	The spacing between yarns or stitches.
Plies -	Multiple layers within a fabric or laminate.
Preform -	A collection of glass fibres assembled and formed into the desired geometry prior to injection of resin
Prepreg -	Pre-impregnated reinforcement.
Punch -	The male half of a mould.
Reinforcement -	A strong material bonded into the matrix to improve the mechanical properties.
Resin -	A liquid matrix.
Roving -	A number of strands collected into a parallel bundle with no twist (also called tow)
RTM -	Resin Transfer Moulding.
SBF -	Stitch Bonded Fabric.
SGI -	Silicon Graphics Interface, a computer workstation hardware manufacturer
Slip -	A fabric deformation mechanism increasing the pitch between yarns.
Simple shear -	Fabric deformation via rotation of the yarn intersections.
SRIM -	Structural Reaction Injection Moulding.
Stitch bonding -	Using warp knitting methods to produce reinforcement assembled by a light stitch.
Tex -	Unit of measurement of linear density of a fibre (g/km).
Thermoplastic -	A matrix material which can be reformed via heating.
Thermoset -	A matrix material which undergoes an irreversible chemical reaction upon cure.

Tow -	An untwisted bundle of continuous filaments, usually a bundle of glass fibres (also called roving)
Tricot stitch -	A type of stitch used in fabric manufacture.
Vent -	A port in a mould cavity that allows air and resin to be expelled.
Volume Fraction -	Fraction of volume taken by a particular item.
Warp -	Direction along the major axis of a fabric.
Weave -	A method of interlacing fibres to form a fabric
Weft -	Direction transverse to the warp.
Yarn -	A collection of continuous twisted fibres
Yield -	Imperial unit of measurement of linear density of a fibre (yards/lb)

Nomenclature

			Units
A	-	Area	mm^2
B	-	Boundary condition matrix	
C	-	Circumference of a circle	mm
D	-	Distance	mm
E	-	Elastic modulus	Pa
F	-	Force	N
L	-	Spacing between yarns or grid	mm
M	-	Transformation matrix	
P	-	Point on a surface	
R	-	Radius of a sphere	mm
S	-	Slippage parameter	
S	-	Shear stiffness	N/m.rad
S_m,S_n	-	Grid spacing within KDM	mm
S_o	-	Areal density	kg/m^2
U	-	Parameter matrix	
V	-	Volume fraction	
$V_{1,2}$	-	Vector between two points	
W	-	Width	mm
W	-	Parameter matrix	
X,Y,Z	-	Cartesian axes	
a,b,c,d	-	Planar coefficients	
a_n	-	Proportion of fibres orientated at α_n to applied load	
h	-	Height	mm
l	-	Length	mm
m	-	Linear mass of yarn	g/km
n	-	Number of items	
t	-	Thickness of a ply	mm
x,y,z	-	Cartesian distance or co-ordinates of a point	mm

α	-	Length of major axis of ellipse	mm
α_n	-	Fibre angle with respect to applied load	radians
β	-	Length of minor axis of ellipse	mm
δ	-	Change of	
ϕ	-	Inter yarn angle	degrees
γ	-	Out of plane angle of fibre	degrees
η	-	Reinforcement efficiency	
θ	-	Angle of inclination	degrees
θ_s	-	Inter-yarn shear angle	degrees
ρ	-	Density	kg/m^3
Φ	-	Included angle	degrees
Θ	-	Angle of fibre with respect to plane	degrees

Subscripts

Actual	-	Measured across surface.
c	-	Composite property.
f	-	Fibre property.
Frame	-	Parallelogram shear frame.
Glass	-	Glass property.
Int	-	Yarn Intersection.
lay	-	Layer.
m	-	Matrix property.
m,n	-	Position of grid intersection with respect to origin.
o	-	Original.
s	-	Shear property.
xhd	-	Crosshead.
Vec	-	Vector.
yarn	-	Yarn property.
θ	-	At angle theta.

Superscripts

‘	-	Measured value

Chapter 1 - Introduction

1.1 Background

Composite materials can be defined as a microscopic combination of two or more distinct materials having a recognisable interface between them [1], consisting of a reinforcement supported by a matrix. The reinforcement is usually in fibrous form which performs well in tension, but which tends to buckle under compressive loads. The matrix encases the reinforcement, protecting it and transferring any loads into the reinforcement. The properties of a composite material (laminate) can be optimised to suit the application by altering the material properties with respect to the loading, offering strength and weight advantages over traditional homogeneous materials.

Most composite manufacturing processes form the material and component geometry at the same time which has the advantage that the geometry is not restricted by the laminate forming properties. However the mechanical properties of the laminate are dependent upon the moulding process, part geometry and properties of the constituent parts.

The advantages of structural composites have seen them used in aerospace, offshore and military applications. These are generally low volume applications using materials such as glass, carbon or aramid fibres in a polyester, epoxy or vinyl-ester matrix. Many use composites for their weight saving and high strength (and therefore safety margin) properties which overcome the higher cost of the materials.

1.2 Composites in the Automotive Industry

The continuing growth in the number of automotive vehicles in use world-wide has led to most developed countries imposing greater demands on automobile manufacturers to reduce emissions and decrease fuel consumption on all new fossil fuel powered vehicles. Tighter US vehicle emission regulations defined in the 1997 Corporate Average Fuel Efficiency (CAFE) legislation [2] require increased fuel economy which can partly be met by producing lighter automobiles [3].

Initial uses of composites by mainstream automobile manufacturers were for non-structural components such as headlamp housings, spoilers and bumpers. The materials used were generally low cost, typically glass fibres combined with a polyester resin matrix. These demonstrated the weight saving potential of composites and indicated that their use in structural parts may be possible at the high volumes typically produced by the industry. The current fashion for low volume niche market vehicles requires flexible design methods, component integration and cheaper tooling to minimise the higher unit costs involved when producing smaller numbers of parts. Composites can satisfy these requirements with lighter panels and lower cost tooling, along with the added advantages of resistance to corrosion, low thermal expansion, formability, part integration and vibration damping. They also provide possibilities of improved automobile aerodynamics by allowing the production of larger, more complex curved body panels which may not be viable using more traditional materials such as steel and aluminium.

Since the mid 1980's moulding compounds have been used to produce car bonnets and semi-structural parts such as body panels for the Renault Espace, and tailgates for the Citroen AX and BX range [4], but the properties provided by the short fibres used in these technologies are not sufficient for use in structural parts that maintain the weight and cost savings. Several prototype structural parts have been produced using an automated liquid moulding process (LMP) [5] [6], which offers the strength advantage of long fibre reinforcement, along with fast cycle times, pre-colouring of the part and the ability to utilise cores and inserts to reduce weight and increase strength and stiffness.

1.3 Liquid Moulding Processes

There are two common types of liquid moulding process, Resin Transfer Moulding (RTM) and Structural Reaction Injection Moulding (SRIM). To increase the effective use of the mould, the process is usually split into two main stages [7]. These are preparing and forming of the reinforcement into a preform and the subsequent moulding operation (impregnation of fibre reinforcement and cure of the resin). In the preforming stage fibrous reinforcements in either mat, roving or fabric form are assembled, formed to the final part geometry and trimmed prior to insertion in the

mould. The use of polished nickel plated matched dies can provide two good surfaces on the finished part aiding release from the mould, reducing cycle time and the need for post moulding processes. The mould typically consists of a male and female pattern, which are normally heated to decrease the resin injection and cure time. The preform is placed in the mould cavity and the two halves are closed and clamped together. A thermoset resin is then injected through ports in the tool surface, forcing any air out of the mould cavity through vents. As the resin flows through the tool cavity it is heated by contact with the tool until it reaches its reaction temperature. The resin cures through a chemical reaction where an initiator starts a cross-linking process in the polymer chains producing an infusible material. After curing the part is removed from the mould. Post cure processing such as oven curing (to ensure all cross-linking of the polymer has occurred) and trimming may be required.

One of the problems preventing the increased use of composites over conventional materials such as metals in mainstream applications is cost, both of raw materials and processing. Costs can be reduced by integrating many components into one moulding (requiring more complex mouldings and hence preforms), shortening the cycle time of the moulding operation and reducing the amount of material used. Cycle time reduction is being addressed through advanced resin chemistry and optimisation of the injection and curing stage through improved tool design and heating methods. Major advances are now required in preform technology to bring the preforming cycle time in-line with current moulding cycle times, whilst allowing large and complex components to be produced reliably.

1.4 Preform Manufacture

A preform typically consists of bundles of fibres formed into the component shape prior to the moulding process. These fibres form the load bearing structure within the composite material. Various methods for preform manufacture exist such as braiding [8], direct fibre placement [9-11], slurry forming [12, 13] and the 'cut and sew' method [14]. The automated braiding method produces little waste material, but is slow and limited in the size, shape and production volumes that it can achieve. Direct fibre placement can produce larger preforms, but can be slow for large shapes and is still a developing technology. The slurry method uses chopped fibres (which produce a

weaker laminate than continuous fibres) to produce a random fibre distribution across the preform, and the cycle time is longer.

The cut and sew method is the most flexible of the methods, and has been used to produce large, highly complex preform shapes in a relatively short time [15]. To improve the speed and repeatability of the process, automated methods for manufacture, trimming and handling are under development [16, 17]. Typically fibres which have been pre-processed into a manageable form such as fabric sheet or matting are used [18], which can lead to inefficient use of the rollstock material. The sheet materials are trimmed to near net shape using devices such as CNC lasers or conventional scissors. The sheets are stacked in a predetermined sequence and orientation to form a lay-up, which is placed into a preforming tool. This typically has the same geometry as the moulding tool, and forms the lay-up into the component shape. A separate tool is used for preforming to increase effective use of the moulding tool and minimise the wear caused by the high abrasive properties of the glass. As the pressures are generally much lower during preforming the preform tool can be less stiff and therefore cheaper. The whole assembly can be rigidised using an internal or externally applied binding agent such as thermoplastic polyester powder.

When formed to complex or deep drawn shapes the fibres must realign within the fabric structure in order to conform to the tool surface. The alignment of the fibres after preforming determines the mechanical and processing properties of the laminate. Problems such as fabric tearing, bridging, wrinkling (leaving the tool surface) and folding can occur in the preform when the reinforcement reaches the limit of its formability. These can cause problems during moulding such as:-

i) Fast tracking of the resin: When the preform does not fill to the edge of the mould cavity, resin will flow more easily around the edge, which can trap a pocket of air in the tool cavity preventing complete impregnation of the preform [16].

ii) Non-closure of the mould: Excessive preform thickness or oversized preforms can prevent tool closure.

iii) Dry patches in the laminate: Incomplete resin impregnation caused by uneven resin flow during injection can cause dry spots in the laminate. This is due to

areas of low permeability in the preform caused by high glass volume fractions and highly orientated fibres.

1.5 Research At The University of Nottingham

Several research programmes have been undertaken at the University of Nottingham under Ford Motor Company sponsorship to assess the potential of liquid moulding for producing high volume structural automotive components and to transfer new technology to the production line. Optimisation of the processing cycle by reducing cycle times through the use of resin preheating [19, 20] and optimisation of the resin chemistry [21] were investigated along with improvements in component quality by optimising tool and preform design [22, 23] and aiding mould release [21]. This required work on materials characterisation [24], process measurement and control technology [25], preforming [9, 26] and process modelling [23, 27].

Long [26] investigated the change in laminate properties caused by fibre re-alignment during the preforming of glass fibre fabrics, and demonstrated that fibre movement had a predictable effect on preform processing and laminate mechanical properties. This led to the development of a kinematic based computer model to predict fibre orientations in biaxial fabric preforms, which provided the starting point for the work developed in this thesis.

1.6 Defining the Problem

To increase the use of LMPs for composite production in high volume applications, improvements in the cut and sew preform method are required through:-

i) Reduced cost: The preform cycle time can be reduced through simplification of the laminate ply assembly. This can be achieved partly through the use of high drape, stitch bonded fabrics to create a preform consisting of few large, complex plies rather than many smaller overlapping plies. This could also reduce raw material waste when cutting the net shape preform from roll stock.

ii) Improved part development: To reduce the time and effort required for preform and mould development, tools are required to predict preform fibre architecture, and to highlight problems in fabric forming such as wrinkling and tearing.

iii) Fabric formability characterisation: The deformation of a high drape fabric composed of aligned bundles of stitched fibres depends upon reinforcement parameters such as fibre diameter, tow thickness and local volume fraction and construction factors such as stitch type and pitch These factors will affect the amount and type of deformation that the fabric will undergo before damage occurs. Therefore fabric formability must be considered when selecting the reinforcement within a preform.

Prediction of the fibre architecture within a preform can be used to determine the optimal fabric orientation in the preform tool, ensuring that the part can be formed, and for determining the preform processing properties. Most of the existing fabric drape models use a kinematic approach based on simple shear. This approach assumes complete mapping of the fibres onto the surface, using simple shear assumptions, and thus is independent of the forces occurring during preforming and the type of fabric being formed.

1.7 Theme of Work

The aim of the work presented in this thesis is to characterise the deformation mechanisms occurring during preform manufacture with regard to fabric construction. This requires an understanding of the possible fabric deformation mechanisms and factors that affect fabric formability.

Chapter 2 reviews previous research concerning the possible fabric deformation mechanisms along with methods of predicting and measuring them. Four modes of deformation have been shown to occur during preform manufacture with three being within the plane of the fabric. The dominant mode has been suggested by Potter [28] to be inter-fibre shear whereby the fibre intersections act as pin-joints about which the fibres rotate.

Methods for predicting fibre orientations within a biaxial fabric draped over a surface have been reported by several authors [29-31]. Most methods are based on a geometric mapping approach, where the fabric is modelled as a pin-jointed net and mapped onto a mathematically described surface. The implementation of a kinematic

draping model based on work by Long and Rudd [29] is described in Chapter 3. The surface geometry is described by flat quadrilateral or triangular patches, so that any complex curved 3D geometry can be analysed. To provide a unique solution, constraints are provided by two initially perpendicular constrained fibres whose paths across the surface are predicted from an initial contact point.

The kinematic drape model takes no account of the forming forces involved and assumes that the fabric being modelled has no resistance to shear. Work reported on woven fabrics suggests a resistance to shear and a shear limit beyond which the fabric will not conform. To determine the useful limits of the kinematic method, a simple trellising rig was used to measure the in-plane shear resistance of various high drape fabrics. The test method involved clamping a fabric sample along its edges and measuring the shear resistance as the fabric underwent a large shear deformation. Comparison of the in-plane shear properties and shear deformation limits of common stitch bonded glass fibre fabrics (engineered fabrics) are described in Chapter 4.

Previous validation of the kinematic models has been qualitative, typically involving a visual comparison of the experimental fabric architecture with the predicted data. An experimental technique to measure fabric deformation within a preform using grid strain analysis to provide quantitative results is described in Chapter 5. The system measures the deformation of a known grid printed onto the fabric surface prior to preforming. The co-ordinates of each grid intersection were measured in three dimensions using two digital images of the preform. The data were processed to provide information on the grid angle (hence the inter-fibre shear angle) and strains. This allowed comparison of preform fibre architecture over different surface geometries at varying forming velocities, the results of which are presented in Chapter 6. A review of the effect of fabric parameters which define shear properties (as investigated in Chapter 4) on preform architecture is given in Chapter 7. The results were used to validate the kinematic drape model, and to investigate the occurrence of other fabric deformation methods such as fibre slip and wrinkling.

Chapter 2 - Literature Review

2.1 Introduction

This section reviews the development and current state of preform drape analysis. The mechanics of deformation and methods of modelling the forming of other sheet materials such as fibre reinforced thermoplastics have been examined, along with techniques for measuring the material properties used in the models.

The application of the predicted yarn orientations derived from drape modelling in the optimisation of preform design is reliant on accurate data for the formability and properties of deformed fabrics. A study of methods for measuring fabric properties and fabric deformation during forming, used for model validation, is also presented. Other methods for measuring sheet material and fabric properties have been investigated and evaluated for their use in obtaining fabric formability data.

2.2 Effect Of Preform Architecture on Laminate Properties

The injection phase of LMPs has been researched extensively to aid the design of the tooling and injection system. It has been proven that the preform fibre architecture affects the resin flow during the injection phase [23]. The ease of flow of the resin through the fibres, as characterised by the reinforcement permeability, has been researched extensively at low [24] and high pressures [32], and for sheared reinforcement [8]. Models to predict the flow of the resin through the mould cavity [27, 33-36], allowing optimisation of the number and placement of the injection and vent ports, have been implemented. The models are usually based on Darcy's law for flow through porous media [37] and require information on the principal fabric permeabilities and their orientation for each element in the model. The realignment of fibres during preforming produces permeability variations [35, 38], along with variations in physical properties such as modulus and strength.

The mechanical properties of a laminate depend upon the orientation of the reinforcement with respect to the load. A simple estimation of laminate stiffness can be calculated using a modified rule of mixtures:-

$$E_c = E_f . V_f . \eta + E_m (1 - V_f) \qquad (2.1)$$

where the efficiency factor of the reinforcement in the direction of the load is defined by Krenchel [39] as:-

$$\eta = \sum a_n . \cos^4 \alpha_n \qquad (2.2)$$

The theory ignores off axis deformation (and therefore the Poisson effect) and assumes perfect bonding, and hence load transfer, between reinforcement and matrix. This method was used by Long [26] to predict the tensile modulus variation in a wheel hub made from SBF where high fibre shear was predicted, although this was not validated experimentally.

2.3 Analysis of Fabric Deformation Mechanisms

Research into fabric formability has shown that fabrics may deform by one of a number of mechanisms as shown in Figure 2.1 [28]:-

i) inter-yarn shear.
ii) fibre extension.
iii) inter-yarn slip.
iv) inter-ply slip.
v) buckling of the fibres - within the plane of the fabric.
vi) wrinkling - fibres bending out of the plane of the fabric

The relative importance of each of these depends upon the materials, the process variables and part geometry. The most common deformation method in biaxial engineered fabrics is thought to be inter-yarn shear [28]. The angle between two yarns is called the inter-yarn angle (ϕ), with the change in inter-yarn angle defined as the inter-yarn shear angle (θ_s). For an initially orthotropic (90^o) fabric the shear angle can be defined as:-

$$\theta_s = 90^0 - \phi \qquad (2.3)$$

There is a limit to how much a fabric will deform through inter-yarn shear, normally due to the compaction limit of the fibres. As the fabric shears the angle between the yarn

decreases, the minimum angle between yarns that a fabric can deform to before wrinkling is defined as the fabric locking angle [41].

Due to the high modulus of individual glass fibres and the low forces involved in fabric forming, fibre extension is negligible. Inter-yarn slip (where individual yarns slide relative to each other within the fabric) which could cause fabric thinning at extreme deformation, has not been considered by many workers. Inter-ply slip occurs in multiple layer preforms where the separate fabric layers move relative to one another.

2.3.1. Modelling of Garment Draping

The earliest investigations into fabric properties and development of modelling methods were within the garment industry. The difference in conformability of knitted fabrics and woven cloths led to research into methods of predicting the fitting of textile fabrics to the human body. Mack and Taylor [42] established an early fabric draping algorithm. The cloth was assumed to be composed of inextensible fibres, with the cross over points of the warp and weft yarns acting as pin joints. The simulation assumed the cloth maintained complete contact with the surface. The fitting of the cloth to complex surfaces was examined theoretically, and differential equations were derived to predict the orientation of the yarns. A hemisphere was draped with 'leno' net to demonstrate the principles, but no comparison was made with the theoretical results.

More recent studies are more concerned with the 'hang' and movement of garment textiles under free drape conditions, as would be found in garments worn on the human body. Chen and Govindaraj [43] describe a FE method using shear flexible shell theory applied to a fabric draped over a square block. An alternative method based on interacting particles was used by Breen *et al* [44] to investigate the difference in corner folding of a variety of woven fabrics when draped over a table. The validation of such models is difficult, and they have only been used to show the effect of fabric stiffness on the hang of a garment.

2.4 Simulation of Sheet Composite Forming Processes

Sheet composites materials consisting of thermoset or thermoplastic resin impregnated fibres, are a middle ground between purely isotropic metal forming and

orthotropic fabrics. They usually consist of an isotropic fluid (resin) around fibres (in either unidirectional aligned yarn or fabric form) described as a pre-preg. The deformation mechanisms and methods of modelling sheet forming vary depending upon the reinforcement architecture.

2.4.1. Unreinforced or Randomly Orientated Fibre Reinforced Materials.

These materials can be modelled using similar methods to metals or other isotropic materials. For example, a finite element model using membrane elements was described by Taylor [45] and used to predict the wall thickness of various thermoplastics when vacuum formed into a box shape.

2.4.2. Unidirectional Reinforced Materials.

The deformation of unidirectional reinforced materials is dominated by the high stiffness of the reinforcing fibres, which limits axial deformation. A single ply of such a material will behave like a fibre-filled Newtonian fluid if stretched in the transverse direction, but an elastic solid if stretched in the fibre direction [46]. The major deformation mechanism will depend upon the applied load with regard to the reinforcement direction, with matrix shear being the most common during the forming of complex curvatures [46].

The theory of Ideal Fibre Reinforced Materials (IFRM) was developed by Pipkin and Rogers [47] and Spencer [48] for modelling highly anisotropic elastic and plastic materials. This assumes the material can be modelled as a transversely isotropic Newtonian fluid, which obeys the constraints of inextensibility in the fibre direction and incompressibility of the material. O Bradaigh and Pipes [49] integrated the IFRM equations into a finite element package called FEFORM to determine plane stresses in the plane of the fibres for various loading cases. The solution allowed the orientation of the fibres to be calculated at the end of each time step during the stamping process, thus updating the orientation of the inextensible fibre constraints in the model. The model was used to investigate the effect of process parameters on wrinkling in a centrally indented APC-2 carbon pre-preg, and showed good agreement between model and experiment [50].

A simplified method for predicting the fibre distribution of continuous uni-directional fibre reinforced thermoplastics formed over complex surfaces was described by Smiley *et al* [51]. The transverse fibre spacing was assumed to remain constant during the forming process, and could thus be modelled using the same kinematic principles suggested by Potter [28] as used in the modelling of bi-directional fabric forming described below.

2.4.3. Bi-directional Reinforced Materials

Bi-directional fabrics consist of yarns in either woven of stitched form, produced using a process adapted from the garment industry. Therefore the analysis of fabric based sheet materials is based on deformation mechanisms observed during earlier work performed by the garment industry, described in section 2.3.

Analysis of the Forming of Pre-Preg Sheet Thermoplastic Materials

Sheet forming of thermoplastic matrix composites has become more attractive recently, brought about by a desire to reduce the long cure cycle times associated with liquid moulding. Sheet thermoplastic pre-preg using random, unidirectional fibre or biaxial fabric reinforcement can be heated, formed and cooled relatively quickly, without degradation of the mechanical properties [52]. Murtagh and Mallon [53] have confirmed that bi-directional reinforced thermoplastic materials can deform by a number of mechanisms; initial yarn straightening, followed by inter-ply slip or intra-ply slip depending upon the material and lay up characteristics.

The finite element modelling of sheet forming has taken two routes, the explicit method as applied by de Luca *et al* [54], and the implicit method as used by O Bradaigh *et al* [49,50]. The implicit method is suitable for slower forming, and single curvature situations, and the explicit method for faster heat sensitive applications [55].

The finite element approach described by O Bradaigh *et al* [50] was modified by McEntee [55] to incorporate inter-ply slip and tool contact and hence model multiple ply laminates. The simulation of a multi ply pre-preg under simple three point bending was described. However the IFRM approach used by McEntee does not take account of the influence of processing conditions such as temperature and rate of loading, so is limited in its application.

An adaptation of the IFRM model to incorporate matrix viscosity was proposed by Johnson [56]. This was developed into a velocity and temperature dependent visco-elastic material law, where the viscous matrix properties were separated from the elastic fibre properties by de Luca *et al* [54, 57] and incorporated into a modified commercial finite element program (PAM-STAMP) based on shell elements [54]. The shell elements were able to represent ply buckling caused by in-plane compressive loads. Multiple plies were modelled by describing each layer individually, and applying a viscous-friction relationship between layers. The draping of a spherical ended, half-cylinder shaped 'sikken' was modelled for unidirectional and woven fabrics and compared visually with yarn angles and wrinkles obtained in experimental parts. An investigation was performed into the effect of varying forming conditions (velocity, laminate stack sequence and blank holder clamping) on the formation of wrinkles. Canavan *et al* [58] used the PAM-STAMP code to simulate the forming of a hemisphere and compared the results to the experimental forming of a woven fabric. The results were validated by manual measurement of the thickness and inter-yarn angle at locations around the hemisphere. They reported difficulty in measuring the inter-yarn angles manually which may have accounted for scatter in the results.

A numerical model integrated in to the ABAQUS finite element code was described by Blanlot [59], based on anisotropic hypoelastic constitutive equations. This assumes that the direction of yarn shear corresponds to that of the principal directions of strain and uses rigid body rotation to update the yarn directions during draping. The predicted values of inter-yarn angle over a hemisphere were compared with those obtained experimentally for a woven fabric, and showed close agreement up to 35° inter yarn shear. However there was no description of how the angles were measured.

Analysis of the Forming of Co-Mingled Thermoplastic Sheet Materials

A more recent development has been the use of commingled glass and thermoplastic fibres such as TWINTEX [60], which allows a higher degree of conformability than traditional sheet pre-preg materials [61]. The fabric is heated and deformed under pressure, melting the thermoplastic matrix, which impregnates the glass reinforcing fibres [62]. Modelling of these materials must include the impregnation [63] and consolidation phase [64, 65] as well as fabric shear.

Van West *et al* [66] used a kinematic drape model (similar to that described below) to predict the yarn re-orientation when formed to a surface, followed by a model of compaction pressures and a finite difference model of the impregnation process. This allowed the prediction of the consolidation time, forming pressure, laminate thickness and volume fraction for the press forming of commingled fabrics.

2.5 Simulation of Fabric Deformation

Increases in low cost computing power during the late 1980's and early 1990's have allowed the large number of calculations involved in analysing fibre movement during deformation to be achieved economically. Consequently, research into the modelling of fabric preforms has increased rapidly.

2.5.1 Development of Fabric Deformation Modelling

Potter [28, 67] researched the formability of three classes of material: two-dimensional random mats, pre-pregs of aligned, discontinuous fibres and sheet fabric reinforcements. He suggested that when a complex surface is draped with a bi-directional cloth, two extremes of deformation are possible. These are the pin-jointed deformation mechanism as suggested by Mack and Taylor [42], and a projection of the yarns onto the surface. Projecting the yarns onto the surface involves a finite amount of slip (increase in distance) between the yarn crossover points. Various woven reinforcements were examined to determine the mode of deformation that occurred when stretching +/-45° specimens, by measuring the lateral contraction. The results suggested that most bi-directional cloths can be modelled as a pin-jointed mesh, provided that the spacing between the yarns is small and that the applied biaxial stresses are of similar magnitude. Fabric drape was defined as the ability to form over three-dimensional shapes without being cut or applying undue force.

Robertson *et al* [30] developed a simple kinematic draping algorithm for a hemispherical surface, again assuming pin-jointed behaviour. This method (subsequently called the kinematic drape model (KDM)) predicts the orientation of the yarns over a complex surface using a mapping approach, and does not take into account forming forces. Hence inter-yarn slip or fibre buckling is not predicted. The equations for the surface were combined with two equations representing the possible co-ordinates

of the next yarn intersection to determine each yarn crossover point. To derive a unique solution the initial position and orientation of the crossover point of two yarns on the surface was required. This method was applied to the analysis of fibre distributions in a fabric draped over a hemispherical surface. Results were compared with components draped with woven cheesecloth by manually measuring the inter-yarn angle along the line of highest shear, and showed an excellent correlation between theory and experiment.

Van West *et al* [31] adapted the pure shear approach to simulate the draping of a bi-directional woven fabric over an arbitrary surface. The surface was represented by patches, each described by a bi-cubic polynomial. An iterative solution was therefore required to solve the equations of intersection. The model was applied to several shapes including hemispheres and conic-spherical surfaces, each geometry consisting of many curved surface patches. An adaptation of this approach was described by Bergsma [41], who redefined the constraints through a minimisation of energy method after each stage of the draping algorithm, for fabric draped over simple three-dimensional shapes. Unfortunately this method was not reliable when draping complex surfaces. A finite element analysis model was then developed, representing the yarns by a collection of beam elements that connect at the yarn intersections. This allowed buckling to be represented, which is not possible with kinematic drape modelling. A theoretical investigation was performed, to minimise the occurrence of wrinkling in a fabric draped over a rectangular box, by applying tension to the edge of the fabric.

A further kinematic drape model to predict yarn orientations over an arbitrary surface was developed by Long [26]. The difference between Long's model and those of previous authors was in describing the surface using flat patches (the mosaic method). The solutions could thus be calculated directly, as opposed to the iterative solutions required with curved patches, producing a faster solution. The model was applied to a number of automotive component geometries, with the surface geometries imported from PAFEC finite element data files. An investigation was undertaken, to minimise wrinkling in the recessed swage areas of a Ford Escort Cosworth Undershield by reorientation of the fabric. The yarn architecture of a woven fabric draped over a prototype wheel hub was also modelled, and validated by manual measurement of the inter-yarn angles and measurement of the glass volume fraction. The data produced for

of the next yarn intersection to determine each yarn crossover point. To derive a unique solution the initial position and orientation of the crossover point of two yarns on the surface was required. This method was applied to the analysis of fibre distributions in a fabric draped over a hemispherical surface. Results were compared with components draped with woven cheesecloth by manually measuring the inter-yarn angle along the line of highest shear, and showed an excellent correlation between theory and experiment.

Van West *et al* [31] adapted the pure shear approach to simulate the draping of a bi-directional woven fabric over an arbitrary surface. The surface was represented by patches, each described by a bi-cubic polynomial. An iterative solution was therefore required to solve the equations of intersection. The model was applied to several shapes including hemispheres and conic-spherical surfaces, each geometry consisting of many curved surface patches. An adaptation of this approach was described by Bergsma [41], who redefined the constraints through a minimisation of energy method after each stage of the draping algorithm, for fabric draped over simple three-dimensional shapes. Unfortunately this method was not reliable when draping complex surfaces. A finite element analysis model was then developed, representing the yarns by a collection of beam elements that connect at the yarn intersections. This allowed buckling to be represented, which is not possible with kinematic drape modelling. A theoretical investigation was performed, to minimise the occurrence of wrinkling in a fabric draped over a rectangular box, by applying tension to the edge of the fabric.

A further kinematic drape model to predict yarn orientations over an arbitrary surface was developed by Long [26]. The difference between Long's model and those of previous authors was in describing the surface using flat patches (the mosaic method). The solutions could thus be calculated directly, as opposed to the iterative solutions required with curved patches, producing a faster solution. The model was applied to a number of automotive component geometries, with the surface geometries imported from PAFEC finite element data files. An investigation was undertaken, to minimise wrinkling in the recessed swage areas of a Ford Escort Cosworth Undershield by reorientation of the fabric. The yarn architecture of a woven fabric draped over a prototype wheel hub was also modelled, and validated by manual measurement of the inter-yarn angles and measurement of the glass volume fraction. The data produced for

of the next yarn intersection to determine each yarn crossover point. To derive a unique solution the initial position and orientation of the crossover point of two yarns on the surface was required. This method was applied to the analysis of fibre distributions in a fabric draped over a hemispherical surface. Results were compared with components draped with woven cheesecloth by manually measuring the inter-yarn angle along the line of highest shear, and showed an excellent correlation between theory and experiment.

Van West *et al* [31] adapted the pure shear approach to simulate the draping of a bi-directional woven fabric over an arbitrary surface. The surface was represented by patches, each described by a bi-cubic polynomial. An iterative solution was therefore required to solve the equations of intersection. The model was applied to several shapes including hemispheres and conic-spherical surfaces, each geometry consisting of many curved surface patches. An adaptation of this approach was described by Bergsma [41], who redefined the constraints through a minimisation of energy method after each stage of the draping algorithm, for fabric draped over simple three-dimensional shapes. Unfortunately this method was not reliable when draping complex surfaces. A finite element analysis model was then developed, representing the yarns by a collection of beam elements that connect at the yarn intersections. This allowed buckling to be represented, which is not possible with kinematic drape modelling. A theoretical investigation was performed, to minimise the occurrence of wrinkling in a fabric draped over a rectangular box, by applying tension to the edge of the fabric.

A further kinematic drape model to predict yarn orientations over an arbitrary surface was developed by Long [26]. The difference between Long's model and those of previous authors was in describing the surface using flat patches (the mosaic method). The solutions could thus be calculated directly, as opposed to the iterative solutions required with curved patches, producing a faster solution. The model was applied to a number of automotive component geometries, with the surface geometries imported from PAFEC finite element data files. An investigation was undertaken, to minimise wrinkling in the recessed swage areas of a Ford Escort Cosworth Undershield by reorientation of the fabric. The yarn architecture of a woven fabric draped over a prototype wheel hub was also modelled, and validated by manual measurement of the inter-yarn angles and measurement of the glass volume fraction. The data produced for

fibre orientation and volume fraction in each patch was imported into a resin flow model developed by Rice [27], and used to predict the flow front pattern during moulding which were compared to experimental short shot mouldings.

Van Der Ween [68] compared the numerical accuracy and computational expense of three algorithms for draping biaxial cloths over arbitrarily curved surfaces. Three methods comprising of a minimisation of elastic energy method and two based on the kinematic drape approach were applied to a hemispherical surface. The mosaic approach was dominated by a constant error due to surface discretisation, but was the only method that allowed arbitrary surfaces such as those to generated from FE data to be described.

Trochu *et al* [69] took the kinematic drape method and applied it to parametric surface geometries which had been approximated from the true geometry by a dual 'kriging' interpolation process. This produces a continuous and differentiable surface model which overcomes the problems described by Van Der Ween [68] when there are discontinuities between the tangent plane or curvature across patches. However, it can only be applied to surfaces that are described by a single mathematical function.

A commercial finite element package called PATRAN 3 [70] provided a Laminate Modeller option, which used a kinematic drape model to produce ply data for a fabric layer over a FE mesh. The software assumes either pure shear deformation or projection of the grid onto the surface, and stops the draping simulation if a user input fabric locking angle is exceeded. This approach is also used in the FiberSIM program which is integrated within the Catia CAD system produced by Composites Design Technologies [71].

A mechanics based approach to drape modelling was reported by Boisse *et al* [73]. A finite element model was developed assuming minimisation of tensile strain energy within the fabric. This was used to predict the outline of a square piece of fabric deformed with a hemispherical punch and showed a good correlation with the measured profile. Data on the tensile and shear properties of a fabric were required and measured for a woven fabric using an off-axis tensile test and a trellising shear test (as described in section 2.7.2).

A method for predicting locking angle of woven fabrics, required by the programs mentioned above, is presented by Prodromou and Chen [72], based on the packing limit of a fabric unit cell. They suggest the locking angle depends upon the yarn spacing (L_{yarn}) and the yarn width (W_{yarn}) and can be defined by :-

$$\theta = \sin^{-1}\left(\frac{W_{yarn}}{L_{yarn}}\right) \qquad (2.4)$$

Hence a quick comparison of the locking angle of two woven fabrics can be made from their relative yarn width to yarn spacing. However this approach ignores factors such as yarn compaction and friction at yarn intersections, and the results they present showed these to be a major factor.

2.5.2 Drape Algorithms

Kinematic Approach

The kinematic approach has proved the most popular method of modelling fabric deformation as it assumes the fibres are stiff and inextensible, thus reducing the analysis to a geometry fitting problem. This allows the fabric to be modelled as a pin jointed mesh, where the co-ordinates of any yarn intersection (node) can be derived from the co-ordinates of three adjacent nodes. Each yarn intersection can be defined uniquely by relating its position within the grid matrix to the grid origin (0,0), along two axes (using two integers, m and n). Since it is assumed that the yarns rotate about the node points, any node in the net can be found from the intersection of the arcs defining possible yarn paths from two previous nodes (n-1,m and m-1,n) [Figure 2.2] and the equation of the surface [26]. The equations defining the possible intersection of two yarns restrained at previous node points are:-

$$S_m^2 = (x_{m,n} - x_{m-1,n})^2 + (y_{m,n} - y_{m-1,n})^2 + (z_{m,n} - z_{m-1,n})^2 \qquad (2.5)$$

$$S_n^2 = (x_{m,n} - x_{m,n-1})^2 + (y_{m,n} - y_{m,n-1})^2 + (z_{m,n} - z_{m,n-1})^2 \qquad (2.6)$$

Many ways of describing the surface mathematically have been suggested. Early work was performed on surfaces that could be described by simple mathematical equations, such as a hemisphere [30]. More complex symmetrical shapes, such as pyramid and top hat sections, were described by various authors [50, 74]. However,

describing the surface mathematically is limited in its applicability to modelling complex preform geometries.

A more general approach requires any surface geometry to be the input for the model. The simplest method describes the surface as flat quadrilateral or triangular patches. This is the so called mosaic approach [68], and allows direct solution of the equations, and thus a unique solution. The equation of the flat plane that the node lies on is defined by:-

$$ax_{m,n} + by_{m,n} + cz_{m,n} = d \qquad (2.7)$$

By solving the equations 2.5, 2.6 and 2.7 simultaneously two solutions to the co-ordinates of the next node can be found, with one set of co-ordinates being identical to a previous node (n-1,m-1) [Figure 2.2]. This was the approach used by Long [26] and allows any arbitrary surface to be modelled.

Another method of describing the geometry involves approximating the surface using parametric bicubic equations [31]. Each node is described by Cartesian co-ordinates and parameters that describe the plane of the surface at that point. This method can describe changes in slope, inflection points and twist in a surface. The equation defining each patch (p) is:-

$$p = UMBM^T W^T \qquad (2.8)$$

where U and W are parameter arrays of the co-ordinate system that lie on the surface patch, M is a transformation matrix that depends upon the surface model and continuity constraints and B is the patch boundary condition matrix defined by the four corner points. This method can describe curved surface geometries more accurately due to the existence of a second derivative term, but requires an iterative solution.

Modelling Fibre Slip

Another approach to draping (as suggested by Potter [28]) is to project the yarns from a plan view onto the surface. Projecting the yarns onto the surface involves a finite

amount of slip between the yarn crossover points. Since experimental work has shown inter-yarn shear to be the major mode of deformation, little work has been done to develop this modelling method.

A method for defining slip (change in yarn length between intersections) as a function of the shear angle for woven fabrics is described by Laroche and Vu-Khanh [74].

$$Slip = 1 + S.\left(1 - \frac{\phi}{90}\right) \tag{2.9}$$

The slippage parameter S must be determined experimentally, although Laroche does not explain how. This was investigated experimentally by Wang *et al* [75] who used a bias extension test to study the deformation of woven fabrics. They found no evidence of slip in areas where the shear was uniform, but recorded up to 4% slip in areas where there was a large change in shear angle. The slip only occurred in fabrics with carbon yarns, and the yarns in these areas were also constrained by the clamping method at one end.

2.5.3 Defining Constraints Within the Kinematic Model

In order to determine a unique drape solution for a given geometry, initial conditions or constraints are required. The majority of authors [26, 29, 30, 31, 69] assumed the constraints to be described by the paths of a known warp and weft yarn across the surface, known as constrained paths. The constrained paths are calculated prior to drape analysis as two geodesic [29] or projected lines [69] derived from an initial orientation and point of intersection of the fabric and the geometry. This has generally proved valid for geometries with planes or axes of symmetry such as a hemisphere or box. However, for geometries with high Gaussian curvature, such as a box, or non axi-symmetric surfaces this method can be unstable [70].

Van West *et al* [66] demonstrated the importance of constrained path selection, first by draping a beaded stiffener geometry symmetrically and then draping two beads sequentially using a pure shear drape simulation. The symmetric part showed no problems were likely in draping the part, whereas the more complex sequential bead geometry showed the possibility of fabric wrinkling and bridging around the second bead. However, they do not describe experimental validation of this finding. A similar

experiment was performed by Long [26] who demonstrated the effect of altering the initial fabric orientation when draping a box corner. When draped with the yarns initially parallel to the box edge, the minimum predicted inter-yarn angle was 16° along the leading edge. This could cause a wrinkle to form in the fabric depending upon the fabric properties and may affect the ability to preform the geometry. Long suggested that by rotating the fabric orientation by 45° this problem could be eliminated and the minimum angle increases to 22° along the edge face, although no experimental results were presented.

Bergsma [41] attempted a different approach to generating the constrained paths, by redefining the constraint as the position of each row of yarns was calculated. This method minimised the energy needed to deform the fabric and is analogous to a forming process, where as the fabric comes into contact with the geometry, its position is constrained. However, this method requires an iterative solution and is computationally expensive. The technique was applied successfully to complex shapes with little or no planes of symmetry such as a modified T box section, but the automated method was not robust and a manual option for path selection was added. The manual method required the user to chose which constraints looked valid from those the program calculated.

The Laminate Modeller option in PATRAN 3 provides several methods of applying constraints [70]. As well as the geodesic and projection approaches, a minimisation of energy method is described. From an initial start orientation the fabric grows a grid step at a time using a minimisation of shear criterion, which appears to be the same as that used by Bergsma [41]. This is suggested as an alternative to the geodesic method on surfaces with high Gaussian curvature. However, there has not been any experimental validation of this approach reported.

2.6 Characterising Sheet Deformation

The formability of sheet materials can be defined as a measure of the ability to undergo deformation to the desired shape without failure [76]. Early research into sheet steel was aimed at improving the quality of stamped sheet parts. The test methods used to characterise sheet metal forming may not be applicable to non-isotropic materials such as fibre reinforced materials.

2.6.1. Measuring Sheet Metal Formability

Sheet metal forming has become the main process in car body panel manufacture and has therefore been studied extensively. The process failure criteria are different to those for fabric forming, the main problems being thinning, wrinkling and ruptures in the blank which limit the depth of draw.

Formability of sheet metals can be evaluated by simple tests such as a tensile test to measure parameters related to formability such as yield point, but to evaluate accurately material formability requires more complex methods such as the Fukui conical cup test [77]. Formability may be represented by a forming limit (FLD) or Keeler-Goodwin diagram [78]. From test data, the major and minor principal surface strains are plotted at the onset of visible necking in a deformed sheet for a wide range of stress regimes. The maximum strain combinations that the material can withstand before failure are plotted. The forming limit diagram can be combined with strain results from a numerical forming simulation to predict safety margins or failure criteria in the part.

An automated method of measuring strains from deformed specimens, such as those occurring during metal forming, was developed by Vogel *et al* [79-81]. This technique, known as grid strain analysis (GSA), measured the co-ordinates of the intersections of a grid printed onto a sheet material prior to forming, and from a knowledge of the initial grid size, calculated the strain distribution across the surface. This approach is normally used for evaluating the forming feasibility of panels, as well as producing forming limit diagrams for sheet metals [79-82]. Figure 2.3 shows a sample of aluminium sheet with a grid etched on the surface and press formed to provide strain data for a FLD.

2.6.2. Measuring Sheet Polymer Formability

The deformation of most sheet polymer materials is a function of the shear characteristics of the matrix [55], and successful modelling of these materials requires information of the material viscosity at various temperatures. Therefore most of the work presented on this topic is concerned with measuring such properties.

A trellising shear rig was used by Breuer *et al* [83] to measure the shear characteristics of woven fabric impregnated with a polyamide matrix at 215°C. They

found that fabric wrinkling is dependent upon membrane stresses and showed for a carbon pre-preg that a 35° decrease in the locking angle was possible by applying a 20 MPa membrane stress. They used the findings to minimise fabric wrinkling in thermoformed fabrics by increasing membrane stress by tensioning the yarns using flexible roller blank holders. A similar method was described by Canavan *et al* [58] to determine the longitudinal and transverse viscosities of carbon fibre - epoxy woven material.

Murtagh and Mallon [53] performed a range of tests on thermoplastic laminates to characterise the processing properties of these materials with regard to temperature and pressures. A 90° V bend test was used to study inter-ply slip between multiple layers in experimental forming situations. A comparison of the shear stresses occurring during ply slip was made from ply pull out tests, where the force required to pull a single ply from a laminate stack was recorded. A bias extension test was used to validate a geometric inter-yarn shear versus bias extension relationship and determine the three material viscosities (i.e. longitudinal, transverse and inter-yarn shearing).

Most measurement of yarn angles used in the validation of sheet modelling techniques have been manual. Martin *et al* [84] demonstrated the use of a grid strain analysis technique similar to that described in section 2.6.1 to measure the principal strains in three types of thermoplastic sheet formed into a hemisphere by diaphragm forming. They concluded that laminates with two directions of fibre reinforcement act like bi-directional woven fabrics when formed over complex curved surfaces.

2.7 Characterising Fabric Deformation

The assumptions and equations used in any model require validation. The modelling of yarn orientations and volume fractions within a preform is only useful if the fabric properties pertaining to similar states can be measured. Existing validation work has focused mainly on comparing predicted fibre patterns with those derived from experimental preforms. Methods of measuring properties of isotropic materials, such as metals, are not always applicable to orthotropic materials, such as fabrics, and some of the properties obtained do not have relevance to modelling fabric deformation.

2.7.1. Determining Yarn Orientations Within a Preform

Two main methods of determining yarn orientations are direct measurement of the yarn orientation within the preform and measurement of the laminate properties affected by yarn orientation.

Direct Measurement Methods

Early measurement of inter-yarn angle were performed manually on a coarse woven cloth by Robertson *et al* [30] and Laroche and Vu-Khanh [85], which proved suitable for a simple shape such as a hemisphere, but could be time consuming for the validation of more complex shapes. An improved method using visual comparison of the deformation of a known size of grid printed onto the fabric prior to deformation, was performed by Long [26]. This allows a quick comparison of the inter-yarn angles over a much wider area, but still gives a subjective assessment of accuracy. A development of this method was to superimpose a simulation of the draping over a photograph of the experimental part, as performed by Van West *et al* [66].

A more objective method involving direct measurement of fibre orientations within a moulded part was described by Hull [86] who suggested that the orientation of a fibre can be determined by examining the elliptical projection of a fibre cut by a known plane. The orientation of the fibre relative to the plane can be determined from the orientation and dimensions of the major and minor axes of the ellipse. Figure 2.4 shows a fibre sectioned by a known plane. From an image of the cut sample, the co-ordinates of the each end of the major and minor ellipse axes, and the out of plane angle of the fibre (γ) with respect to the plane of the fabric, can be measured. The length of the major (α) and minor (β) ellipse axes can then be calculated, and the angle of the fibre (Θ) with respect to the section plane determined using:-

$$\Theta = \sin^{-1}\left[\frac{\beta}{\alpha}\right] \tag{2.10}$$

The automation of the image capture and analysis has been reported by many authors [87-89], mainly for measuring the orientation of short fibres for injection moulded components. Using computer based software, the speed with which fibre

angles can be measured has been greatly enhanced, and several errors in the process have been minimised by comparing the predicted area against the actual fibre area. However, the equations for calculating the fibre ellipticity (2.10) are sensitive to error when the fibre is nearly perpendicular to the section plane [89]. This can be minimised by taking two samples, or sectioning at an oblique angle to the fibre. This method was used by Smith [8] to measure fibre angles in continuous fibre braided components who used the manual measurement method to validate his braid model.

Measuring Laminate Properties

Determining the fibre volume fractions within a moulded part via ashing gives the average fibre volume fraction over the sample area and is thus not accurate in areas where there is high fibre reorientation within the sample. This method has been used to compare predicted and measured volume fractions by Long [26] as a method of verifying the kinematic drape model. Experimental results for yarn orientation and volume fraction were compared with those produced by modelling for a prototype wheel hub.

Laroche and Vu-Khanh [74] assumed that, for pre-preg sheets under diaphragm forming, the volume fraction of the deformed ply remains constant, and therefore the thickness (t) of the ply would be related to the inter-yarn angle (ϕ) and initial thickness (t_o) by:-

$$t = \frac{t_o}{\sin\phi} \tag{2.11}$$

However, this approach is sensitive to the accuracy in thickness measurement, which can be affected by surface defects such as uneven crimp in the weave. When used to measure the thickness variation of a woven carbon pre-preg draped around a radius topped cone significant scatter was seen in the data.

2.7.2 Measuring Material Properties of Engineered Fabrics

Traditional garment fabric characterisation methods, such as the Kawabata KES-F [90] range of tests, are aimed at measuring wear and feel characteristics of fabrics. Therefore, few of these tests may be applicable to the large deformations seen by

engineered fabrics, and may not produce the mechanical properties required by current and future drape models. Substantial work has been published on the measurement of processing properties such as the permeabilities of roll stock fabrics [24], but there have been relatively little data on processing properties of sheared fabric [8], which may be more relevant for complex shapes.

Kutz [91] researched fabric characterisation and drapability. Test methods used in evaluating the formability of sheet metals, garment fabrics and engineered fabrics were investigated. The results suggested that conventional methods such as the Kawabata KES-F system for measuring fabric conformability do not necessarily work for fabrics being formed under high loads and deformations. Along with Ko [92], they performed a comparison of the formability of five fabrics (two woven and three stitched), by comparing bending stiffness, force required to shear fabric by 1°, bias extension and hemisphere forming tests. They rated the performance of the fabrics after each test and found that the rankings for low deformation tests (bending and 1° shear) did not correspond to those for high deformation tests (bias extension and forming). This implies that the use of fabric test results for fabric selection relies upon the test method simulating similar amounts of deformation as that seen during the preforming process.

Yu *et a*l [93] applied existing fabric characterisation experiments devised for the textile industry to four woven carbon fabrics. Units from the Kawabata evaluation system which have been applied successfully to fabrics, rubber, leather, yarn and films, were used to measure tensile, compressive, shear and bending properties. Further experiments [94] which measured the energy required to form the same carbon woven fabrics into a hemisphere, were used to provide a formability rating. A comparison of the characterisation [93] and forming [94] results showed a correlation between the bending rigidity of the fabric and its relative formability (defined as energy required to form), and it was concluded that characterisation results could be used to assess the formability of textile preforms. However, these results are for carbon fibres which have a higher bending stiffness than glass fibres, and the results may not be applicable to glass fibre fabrics.

Most of the early work on inter-yarn shear properties was undertaken on woven garment textiles which exhibit a high shear stiffness and limited formability. The equipment used by Treloar and others [95-98] to measure in-plane shear properties deformed the fabric by applying a horizontal load to a vertically orientated sample under in-plane tension (similar to the Kawabata KES-F method). A schematic of a typical test set-up can be seen in Figure 2.5a. A mass was hung from the lower edge of the sample to tension the fabric, and a horizontal force was applied along the lower edge. The force was increased by adding weights in stages to a cable running over a pulley, and the angle of shear of the fabric was measured and plotted against the shearing force. Detection of wrinkling in the fabric denoted the end of the test. The fabrics used were mainly garment textiles with a fine weave and a correspondingly high in-plane shear stiffness. Consequently locking occurred at shear angles as low as 10^{o}.

A parallelogram based method [Figure 2.5b] was described by Culpin [99] for textiles, but the shear forces in the fabric were not calculated from the crosshead force (described fully in section 4.2.2). Skelton [100] proposed models for estimating shear stiffness and shear limits from existing data on fabric construction and shearing force (calculated from a parallelogram based shear test). The models were for woven garment textiles and were based on the change of fibre intersection area, and hence increase in rotational friction between the fibres, during shearing.

Prodromou and Chen [72] used a parallelogram rig, video equipment and image analysis equipment to plot shear angle versus load for various woven fabrics. They noted the occurrence of a locking angle in the fabric, which limited further shear and caused out-of plane wrinkling. Similar tests were performed by Breuer *et al* [83] on glass and carbon woven fabrics. Breuer *et al* also noted that the results were sensitive to the alignment of the fabric in the test fixture, with a 1^{o} misalignment of the yarns with respect to the parallelogram edge causing 1.5% strain in the fibres.

Measurement of the load-displacement characteristics of fabrics under 45^{o} bias tensile loading conditions [Figure 2.6], the so called bias extension method, have been reported [26, 73, 75, 97]. This test method places the fabric under tension as well as shear, and does not indicate the relative importance of the two effects, hence the physical

application of such data within current kinematic drape models is limited. A summary of the locking angle of various fabrics presented by previous authors, is shown in Table 2.1.

2.8 Conclusions

The re-orientation of yarns which occur when draping an engineered fabric over a 3-D geometry has been shown to have a large effect on the processing (permeability) and mechanical properties of the laminate. This has led to the development of models to predict the yarn reorientation during preforming.

The possible mechanisms of fabric deformation have been established and evaluated for their relevance in general fabric forming. The major deformation mode of engineered fabrics has been assumed to be inter-yarn shear, but in certain cases, for example where the yarns are close to their packing limit, other forms of deformation such as inter-yarn slip may be significant. The pure shear kinematic drape method has been shown to be the most common, which approximates the yarn intersections to pin-joints between stiff inextensible fibre links, and is analogous to mapping the yarns onto the part surface. No prediction of the forces involved in the forming process is made. Several authors have applied the technique to simulate the draping of simple shapes and validated the model through simple subjective test procedures. Because the kinematic drape models are based on a pure shear mapping approach they predict the same unique yarn orientation for each geometry regardless of which fabric is being considered.

The limitations of this method have proved to be the valid selection of boundary conditions and accurate representation of the surface geometry. There are an infinite number of possible yarn orientation configurations for modelling the drape of a fabric over a surface. To determine a unique solution, constraints must be applied. One method of achieving this is by defining the paths of a pair of warp and weft yarns across the surface using geodesic principles. This has proved the most common method, but can become erroneous on surfaces with high Gaussian curvature.

It has been shown that a pin-jointed 'shear only' model is suitable for application to simple shapes such as a cone or pyramid, but the validity of this model for all

orthotropic fabrics or when applied to more complex shapes has not been established. The validation of such models has been limited although various experimental techniques have been used to measure orientation of the fabric. Evaluation of the existing methods for validating the kinematic drape model predictions has shown them to be mainly simplistic and subjective, therefore a more objective method is required. However, it may be possible to adapt techniques for measuring metal formability, such as grid strain analysis, to measure preform deformation.

The kinematic drape method assumes that the fabrics being modelled exhibit zero resistance to inter-yarn shear and that all fabrics can undergo up to 90^{o} of inter-yarn shear. The results of shear tests have shown that there is a limit to the amount of shear that a fabric can undergo. This is called the fabric locking angle and is important in the application of current drape models as it indicates whether the KDM results are invalid.

Author	Fabric	Material	Locking angle	Method
Culpin [99]	Cotton	Hessian	84.5°	Parallelogram
Wang [74]	Carbon	Plain weave 189 g/m^2	37°	Bias extension.
Wang [74]	Carbon	5HS weave 289 g/m^2	28°	Bias extension.
Wang [74]	Glass	4HS weave 107 g/m^2	35°	Bias extension.
Wang [74]	Glass	8HS weave 289 g/m^2	36°	Bias extension.
Breuer [83]	Glass	Plain weave 345 g/m^2	50°	Parallelogram
Breuer [83]	Glass	Twill weave 295 g/m^2	35°	Parallelogram
Breuer [83]	Glass	Twill weave 167 g/m^2	38°	Parallelogram
Breuer [83]	Glass	Satin weave 294 g/m^2	52°	Parallelogram
Breuer [83]	Carbon	Plain weave 350 g/m^2	50°	Parallelogram
Breuer [83]	Carbon	Twill weave 204 g/m^2	30°	Parallelogram
Breuer [83]	Carbon	Satin weave 285 g/m^2	37°	Parallelogram
Prodromou [71]	Glass	Plain weave 250 g/m^2	32°	Parallelogram
Prodromou [71]	Glass	Plain weave 333 g/m^2	33°	Parallelogram
Prodromou [71]	Glass	Plain weave 200 g/m^2	24°	Parallelogram
Prodromou [71]	Glass	Plain weave 800 g/m^2	40°	Parallelogram
Prodromou [71]	Glass\Resin	Plain weave 800 g/m^2	47°	Parallelogram

Table 2.1 Summary of published fabric locking angle data.

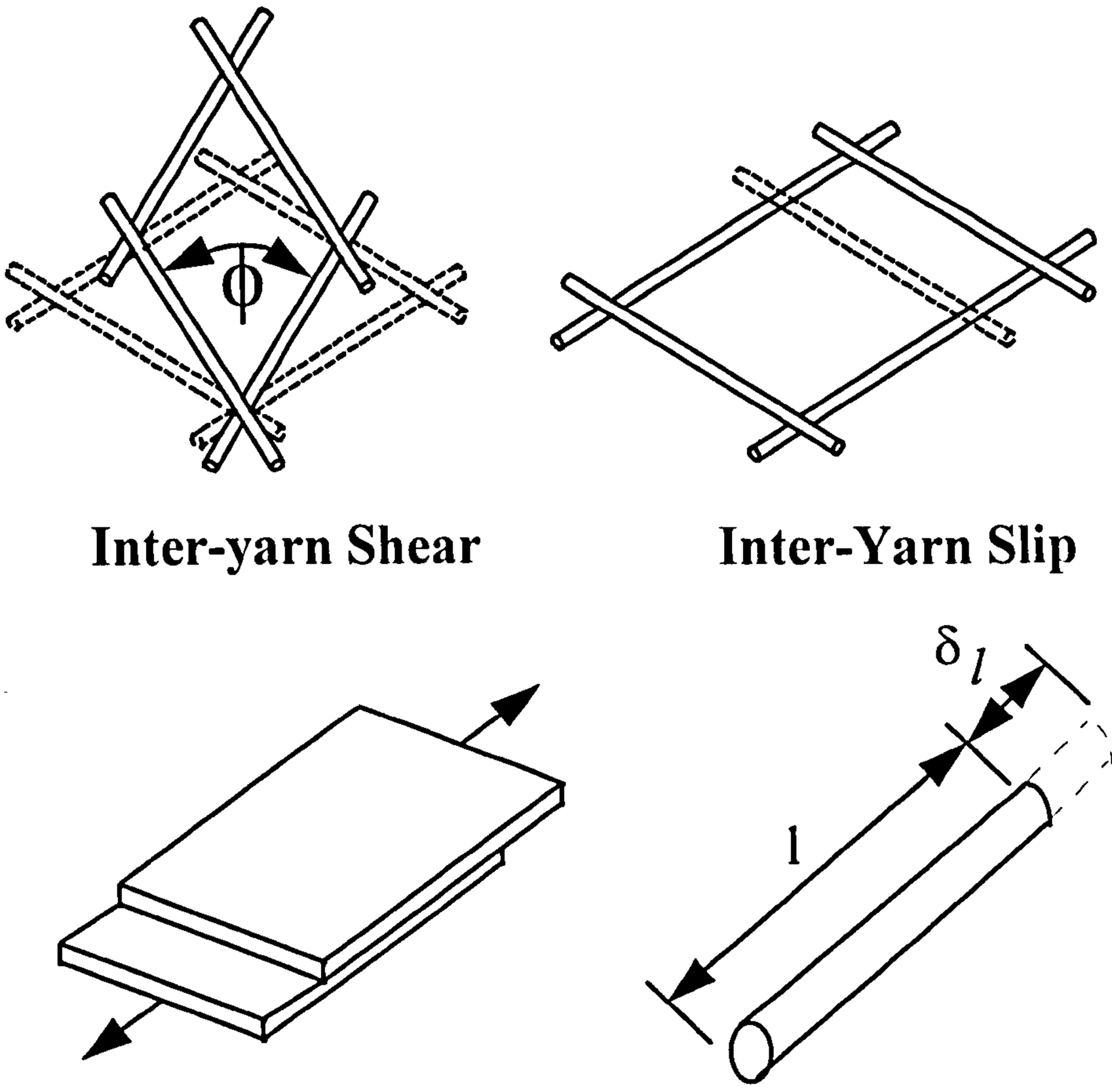

Figure 2.1 Mechanisms of fabric deformation

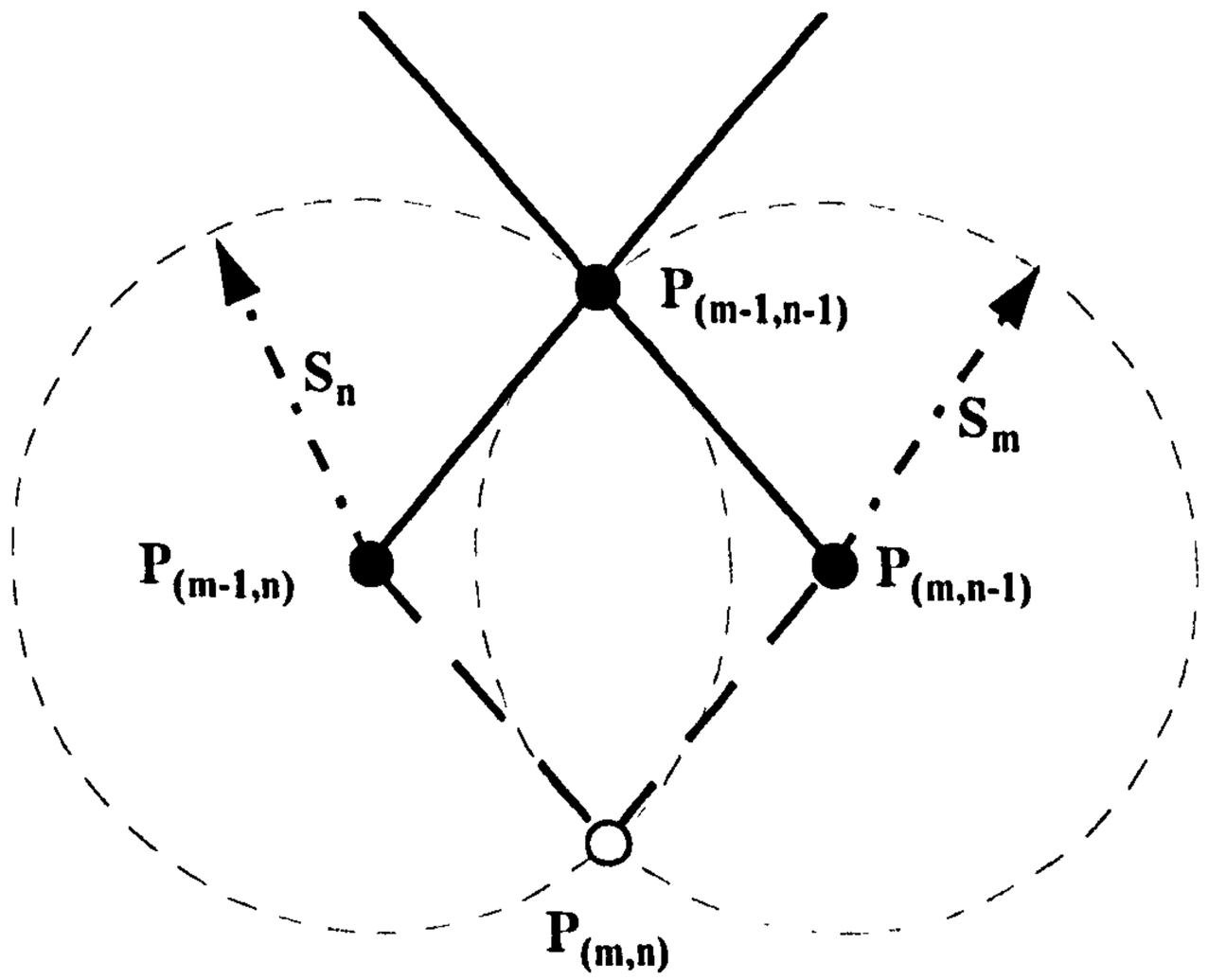

Figure 2.2 Node placement within a pin-jointed net

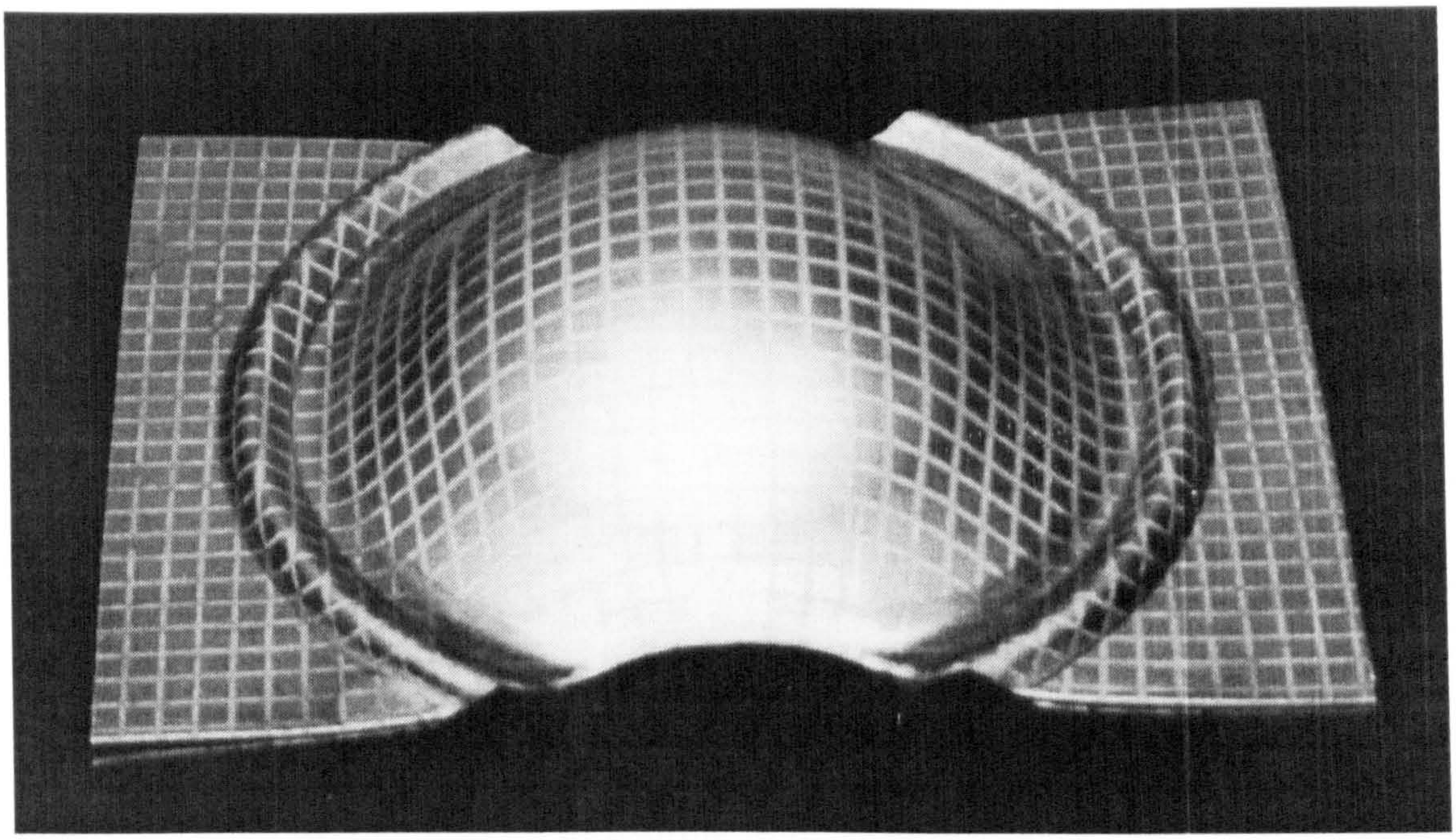

Figure 2.3 Gridded aluminium sheet as used in grid strain analysis technique.

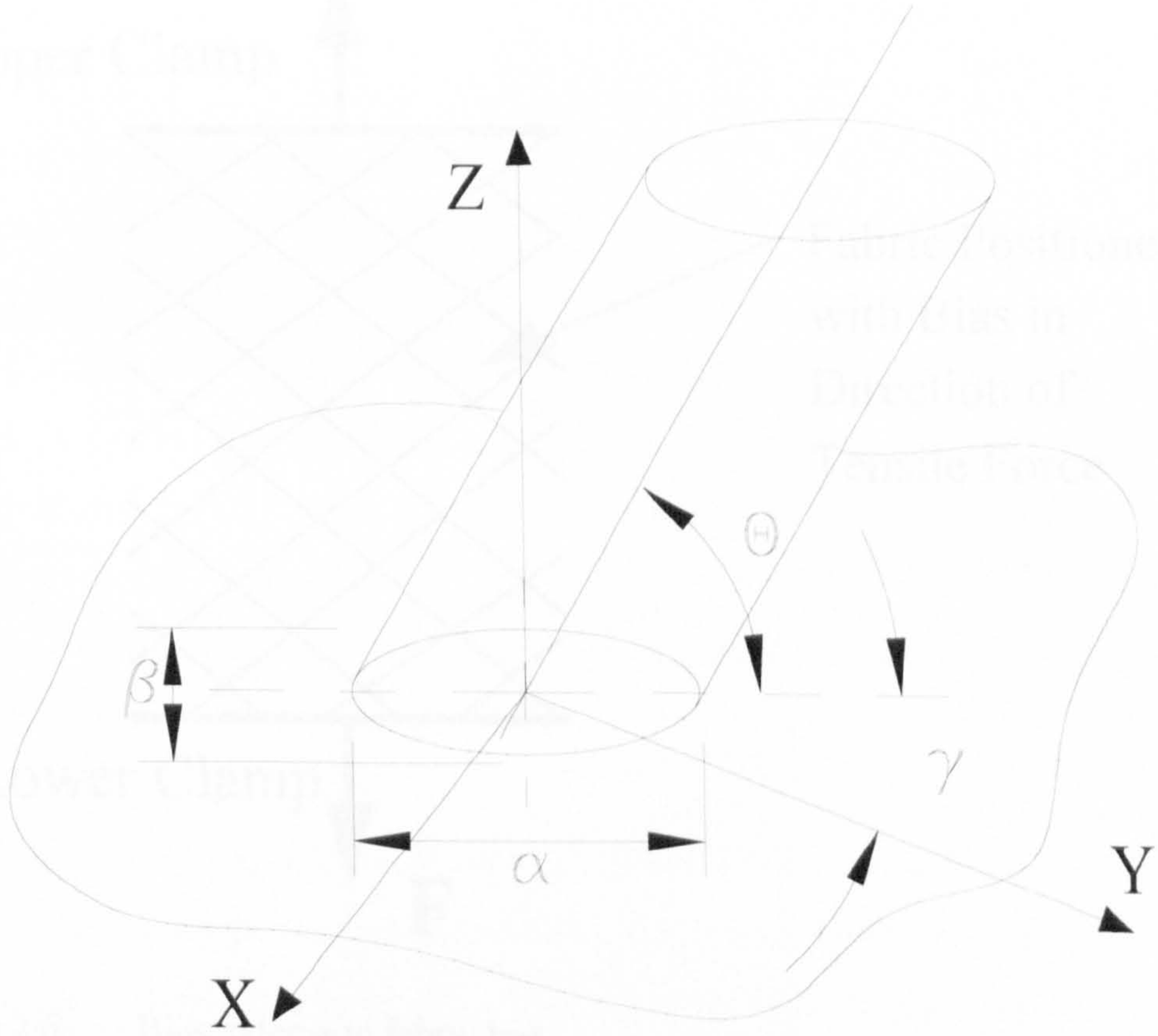

Figure 2.4 Method of calculating fibre orientation from elliptical projection of fibre through a cut plane.

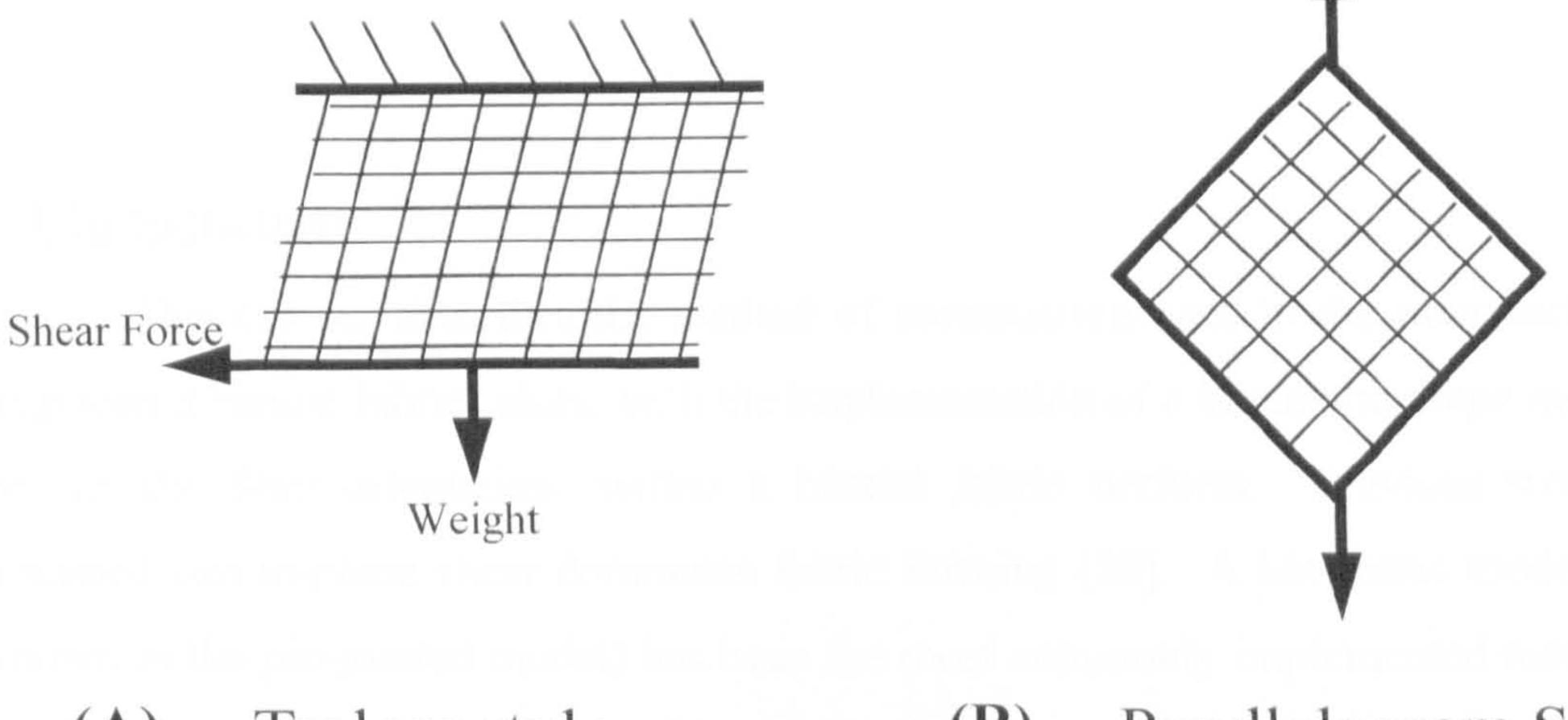

(A) Treloar style Shear Equipment

(B) Parallelogram Shear Equipment

Figure 2.5 Two methods for measuring fibre shear resistance.

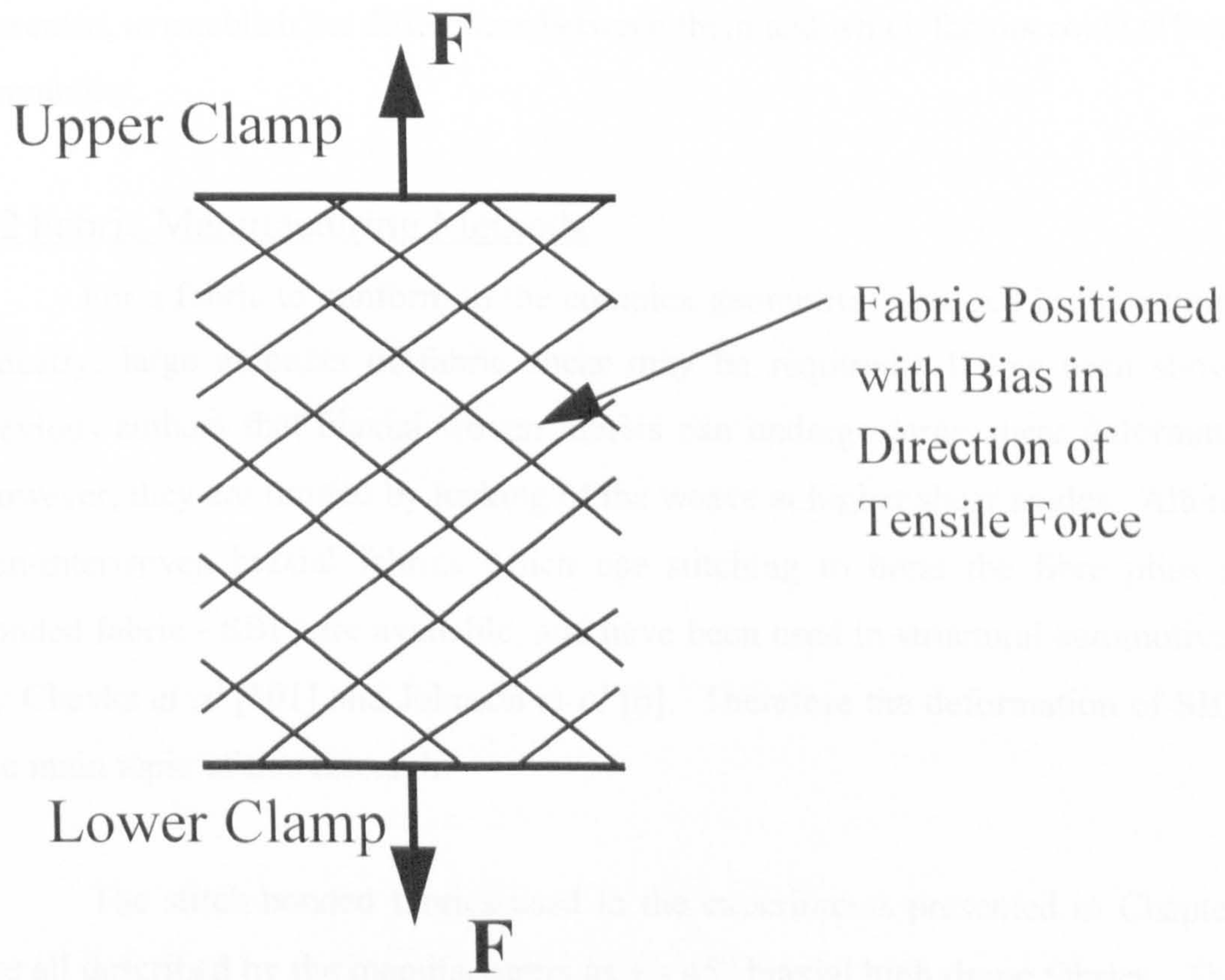

Figure 2.6 Bias extension fabric test.

Chapter 3 - Fabric Construction and Modelling

3.1 Introduction

This chapter describes the method of construction used in the manufacture of engineered biaxial fabrics along with the implementation of a kinematic drape model to predict the fibre orientations within a biaxial fabric preform. Previous work has assumed that in-plane shear dominates fabric forming [28]. A kinematic model (also known as the pin-jointed model) has been the most commonly implemented method of modelling such fabrics as reviewed in section 2.5. A model based on that described by Long [26] was developed in order to predict fibre orientations for comparisons with the experiments described in Chapter 5 and to evaluate the limitations of the kinematic approach. An examination of the manufacturing methods of a range of high drape fabrics used in subsequent experiments for validation of the kinematic drape model is presented, to establish the differences between them and which factors could affect their formability.

3.2 Fabric Manufacturing Methods

For a fabric to conform to the complex geometries required in the automotive industry, large amounts of fabric shear may be required. It has been shown by previous authors that biaxial woven fabrics can undergo large shear deformations. However, they are limited by locking of the weave at higher shear angles. Alternative non-interwoven biaxial fabrics which use stitching to bond the fibre plies (stitch bonded fabric - SBF) are available, and have been used in structural automotive parts by Chavka *et al* [101] and Johnson *et al* [6]. Therefore the deformation of SBFs are the main topic of this research.

The stitch-bonded fabrics used in the experiments presented in Chapters 4-7 are all described by the manufacturers as +/- 45° biaxial high drape fabrics. The high formability is claimed because of the use of a stitch to bond the fabric rather than the use of interwoven fibres. A range of fabrics from two manufacturers was used for the experiments described in this thesis. Additionally a 0°/90° plain weave fabric (from

Fibre Glass Industries) of similar areal density to the SBFs was used in the in-plane shear tests to provide a comparison. A summary of their properties is presented in Appendix 3.1. Three high drape COTECH +/- 45° fabrics from Tech Textiles were compared with four +/- 45° Biaxial Ulti Cloths (BUC) fabrics from the standard range of Flemmings Industrial Fabrics (BUC 440, BUC 600, BUC 800 and BUC 1200) and five prototype BUC fabrics made to the author's requirements (BUC 403, BUC 545, BUC 682, BUC, 784 and BUC 1600). The main variables examined were:-

i) Yarn linear density.

ii) Yarn spacing.

iii) Number of plies.

iv) Stitch type and spacing.

v) Fabrication method.

3.2.1 Fabric Constituents

The yarn linear density (m) and yarn spacing (L) define the areal density of the fabric. The areal density (S_o) is defined by:-

(3.1)

The linear density of the yarns used ranged from 300 Tex to 1200 Tex, with pitches ranging from 1.3 mm to 2.3 mm. The fabrics used were mainly 2 layer fabrics with one four layer fabric (Tech Textiles E-bBXhd 892) for comparison. This gave a range of areal densities from 403 g/m^2 to 1600 g/m^2, as summarised in Appendix 3.1.

3.2.2 Types of Stitch Used

Two types of stitch are used to assemble stitched fabrics. The most common is tricot stitch [102] (Figure 3.1) which was used in both the Tech Textiles and Flemmings range of reinforcements. A second type of stitch was used in the construction of the Flemmings Industrial Fabrics materials to hold the layers in position prior to joining with the tricot stitch. A chain stitch (Figure 3.2) was used to prevent movement in the yarns as they were fed into the stitching machine.

3.2.3 Manufacturing Method

The two Tech Textiles fabrics (E-BXhd 936 and E-bBXhd 892) that are produced in the UK are made on LIBA machines [103] using an improved fibre laydown method which LIBA call the perfect parallel or 'Parramax' method. This method [Figure 3.3] guides the yarns in a parallel path upon laydown. The Tech Textiles fabric (TT E-BX 948) that is produced in the USA is made on conventional Meyer machines [103] ('cross weft' method) that create a slight misalignment in the yarn pattern as they are passed across the bed (Figure 3.4). This results in an 88° to 92° angle between the yarns.

The Flemmings Industrial Fabrics are made using a modified weft insertion knitting process. Two separate layers of transverse weft yarn are formed and held with a chain stitch, and are then sheared to create the desired ply angle, before being fed into the sewing head to be joined with a tricot stitch. The exact process is commercially sensitive, so cannot be described in further detail [107].

3.2.4 Comparison of Fabric Construction Characteristics

The pure shear drape model described later in this chapter assumes that the yarn intersections act as pin-joints between inextensible fibres. This presumes that fabrics have no shear resistance and can undergo up to 90° shear. This is obviously not true, and an investigation into fabric shear limits is described in Chapter 4. In order to characterise those fabrics which the kinematic drape model can be applied to, and understand what is causing the differences in fabric formability, a comparison of the fundamental differences in fabric construction is made in Table 3.1.

Manufacturer	**Name**	**Manufacturing method**	**No of plies**	**Stitch type**	**Figure No.**
Tech Textiles	E-BXhd 936	Parramax	2	Tricot	Figure 3.5
Tech Textiles	E-BX 948	Cross weft	2	Tricot	Figure 3.6
Tech Textiles	E-bBXhd 892	Parramax	4	Tricot	Figure 3.7
Flemmings	BUC Range	Weft Insertion	2	Chain and Tricot	Figure 3.8

Table 3.1 Summary of fabric construction characteristics.

3.3 Modelling Fabric Deformation Using Pure Shear Assumptions

A kinematic drape model based on that described by Long [26] was implemented to allow investigation into the limits of this particular modelling technique. The kinematic method ignores the forces present during forming, and produces a mapping of a uniform grid, representing the yarn intersections within the fabric, onto the surface. It assumes that the position of every yarn intersection within a fabric can be calculated using the following assumptions [42]:-

i) The yarn intersections act as if they were pinned together at the intersections.

ii) The yarns can neither lengthen nor shorten.

iii) The yarns and nodes have negligible thickness or volume.

iv) The yarns take a straight line path between two nodes.

v) The network is always in contact with the surface.

3.3.1 Limitations of the Kinematic Drape Model

The assumptions made above may not be true in certain forming situations, which therefore define the limitations of the kinematic drape model, and must be considered when establishing its applicability to forming:-

i) It is likely for stitched high drape fabrics that as the amount of inter-yarn shear increases other deformation modes such as inter-yarn slip will occur in the fabric, altering the distance between yarn intersections.

ii) The effect of fibre thickness may be insignificant at low volume fractions, but as the fabric shear increases the local volume fraction will increase. Eventually the fibres will reach their packing limit, the so-called locking angle, beyond which it is not possible to deform the fabric through inter-yarn shear.

iii) At high shear values it is likely that compressive forces may occur in the fabric that will cause yarns to buckle in the plane of the fabric.

iv) Further compressive forces would cause wrinkling, which would cause the fabric to lift off the surface.

Therefore the fibre architecture prediction may depend upon the properties of the fabric. Interpretation of the results must take into account the fabric locking angle, and a check should be made as to whether the minimum inter-yarn angle predicted exceeds this value.

The kinematic model predicts the maximum fibre re-alignment required to form the fabric to the surface, and can be interpreted as the predicting the worst case [26]. This is because, in practice, the additional deformation mechanisms will reduce the amount of shearing which is necessary.

3.4 Implementation of the Kinematic Drape Model

A kinematic drape model was implemented on a Silicon Graphics Personal Iris workstation using ANSI C. The method of predicting the fibre arrangement within a preform requires a surface model and a set of constraints. The latter take the form of the paths of two initially perpendicular yarns across the surface. Thus a unique yarn pattern can be calculated for a given yarn spacing. From the results, a plot of the angle between the yarns can be produced to indicate the shear deformation required within the fabric.

3.4.1 Description of the Surface Geometry

The mosaic approach was used to describe the surface geometry, as this allows modelling of arbitrary surfaces. Figure 3.9 shows a wheel hub surface geometry defined using flat triangular and quadrilateral patches. The surface geometries were created using the PATRAN 3 pre-processor and exported to a file in PATRAN neutral file format. These were then converted to an AVS native format, using a program written by the author. This allowed the input files and model results to be viewed using AVS software in the early stages of the research, before the user interface was developed. The AVS format was simplified by stripping out all of the text fields and is illustrated in Appendix 3.2.

The input data were read from file, and processed to calculate geometric data such as constants describing the plane of each patch and patch connectivity. This reduced the run time by eliminating the need to recalculate the constants over successive stages.

3.4.2 Defining the Constraints within the Model

The constrained paths were calculated from a point on the surface and an initial surface vector using geodesic principles as described by Long [26]. Typically this would represent the first point of contact between the fabric and mould surface. This fixes the

initial orientation of the fabric. The paths of the two yarns were then extended to the boundary of the part. The constrained paths were assumed to take the shortest path to the boundary because this allegedly requires the minimum potential energy [26], although subsequent experimental work proved that this is not always valid [see Chapter 6]. The geodesic path was maintained by retaining a constant angle of incidence between the yarn and the patch boundary at the intersections between patches as described by Long [26]. The geodesic paths divide the surface into up to four quadrants that can be draped individually. For simple symmetric surfaces only one quadrant needs to be represented in the model as shown in Figure 3.9.

3.4.3 Solution of the Pure Shear Equations

The algorithm requires that each yarn intersection (node) is predicted from two previous node positions. This arises from the assumption of an inextensible pin jointed net. The co-ordinates of the node must lie on the mould surface and on the plane of intersection of two spheres centred on the two previous nodes.

The intersections of the yarns are described relative to the original yarn node point (m=0, n=0) using unique indices along each constrained path direction (m, n). The pin-jointed assumptions allow the position of a fibre intersection to be described as the intersection of the two spheres described by the radius of the fibre section about the two previously known intersection points in the m and n directions with the equation of the surface (see Figure 2.2). If the next node is on the same patch as the two nodes from which it is derived then its co-ordinates may be calculated from using vector addition, otherwise three simultaneous equations must be solved (Equations 2.5 to 2.7). A full explanation of the methods involved is described in Appendix 3.3.

As each node intersection is found, the angle between the yarns is calculated and stored. This is important for determining the shear angle, and hence volume fraction in each patch, as well as indicating whether wrinkling is likely. Once all the patches are filled, the data is written to a file for subsequent post processing. The basic algorithm for the kinematic drape model is described in Appendix 3.4.

3.5 Graphical User Interface

An interface to allow the user to interact with the model and display the results was jointly developed by the author and a software engineer. The interface allowed the user to load and display the part geometry. The initial point and vector of the constrained paths were placed on the geometry using cross hairs, and the constrained paths generated. Once the yarn spacing was input, the draping model was run, the output of which was displayed on the screen in real-time. The results were also output to a user specified text file for comparison with experimental data.

3.6 Examples

The drape model and graphical interface were used to predict and display the fibre orientations for each of the subsequent drape predictions shown in this thesis. The results for the simulated drape of a wheel hub as used for a basic visual comparison with the model produced by Long can be seen in Figure 3.10. Figure 3.11 shows a plot of the predicted fibre angles across the surface of a prototype wheel well which was taken from a larger component geometry described by Chavka *et al* [101]. The surface geometry is defined by triangular patches due to co-ordinate rounding errors when converting the geometry from the original PAFEC file. The red lines defining the position of the constrained path can be seen running diagonally across the surface from the centre. From this path the positions of the other node intersections were predicted. These were plotted on the geometry surface with their colour related to the inter-yarn angle.

3.7 Summary

An investigation into the differences between the fabrics used for the experiments in this thesis has been presented. The differences in constituent properties are due to the fibre linear density, fibre pitch and number of layers which define the fabric areal density. Other factors which can affect the fabric formability are stitch type and construction method.

A kinematic drape model for predicting yarn orientations of bi-directional fabrics draped over arbitrary surfaces, based on pure shear assumptions, has been implemented. The most suitable method for describing an arbitrary surface was deemed to be a mosaic approach, where the surface was described by flat triangular or quadrilateral patches.

This method allows direct solution of the equations describing the intersections between yarns and the surface geometry. The surface geometry was described by flat patches read from either an AVS input file or a PATRAN neutral file. The output from the model was displayed graphically using a colour scale to represent the angle between the fibres. The surfaces used in experiments described in subsequent chapters were approximated using flat triangular elements.

The results obtained using the kinematic drape model presented in this chapter are compared with experimental data in subsequent chapters to examine the applicability of the pin-jointed method.

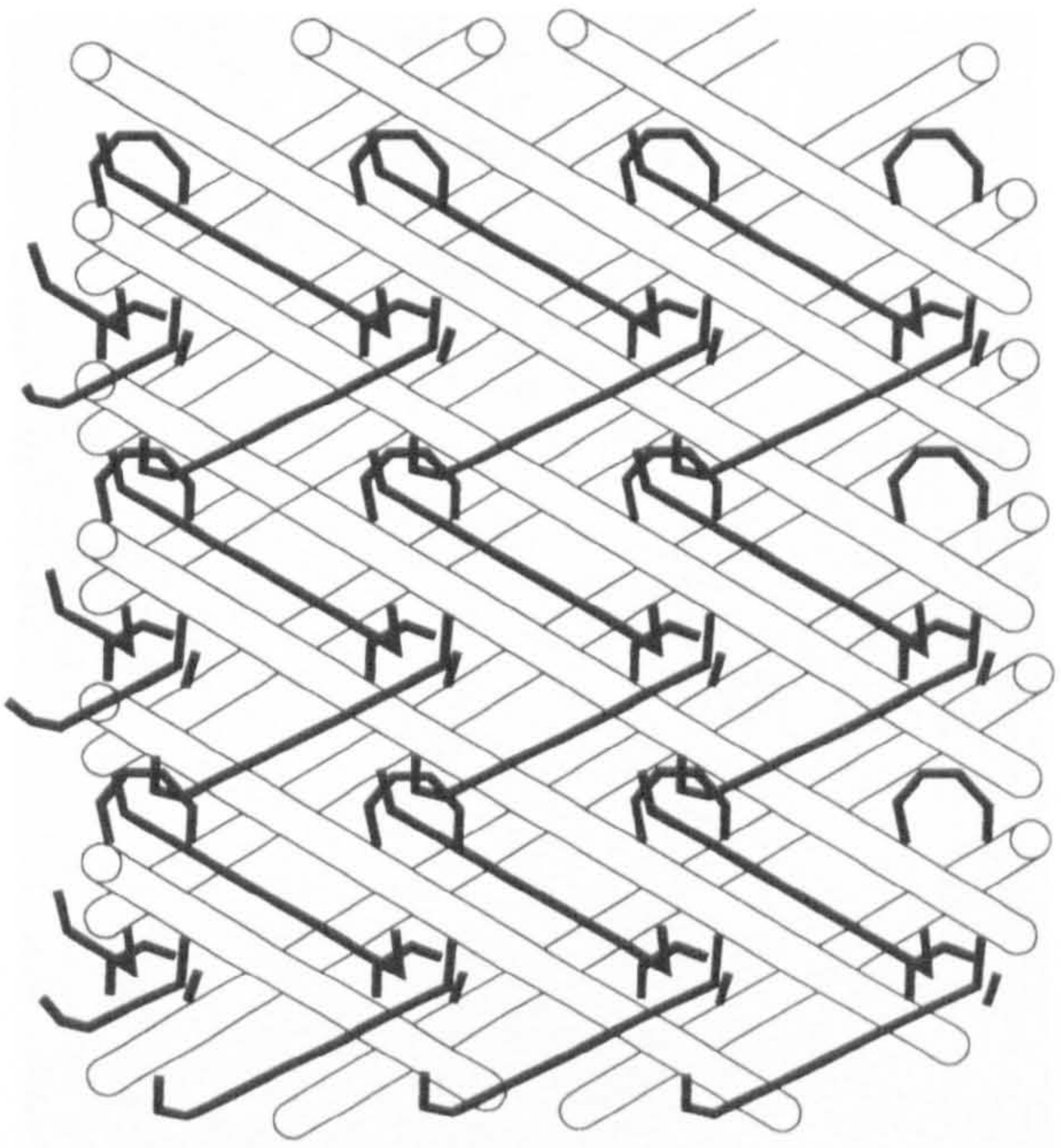

Figure 3.1 Diagram of tricot stitching.

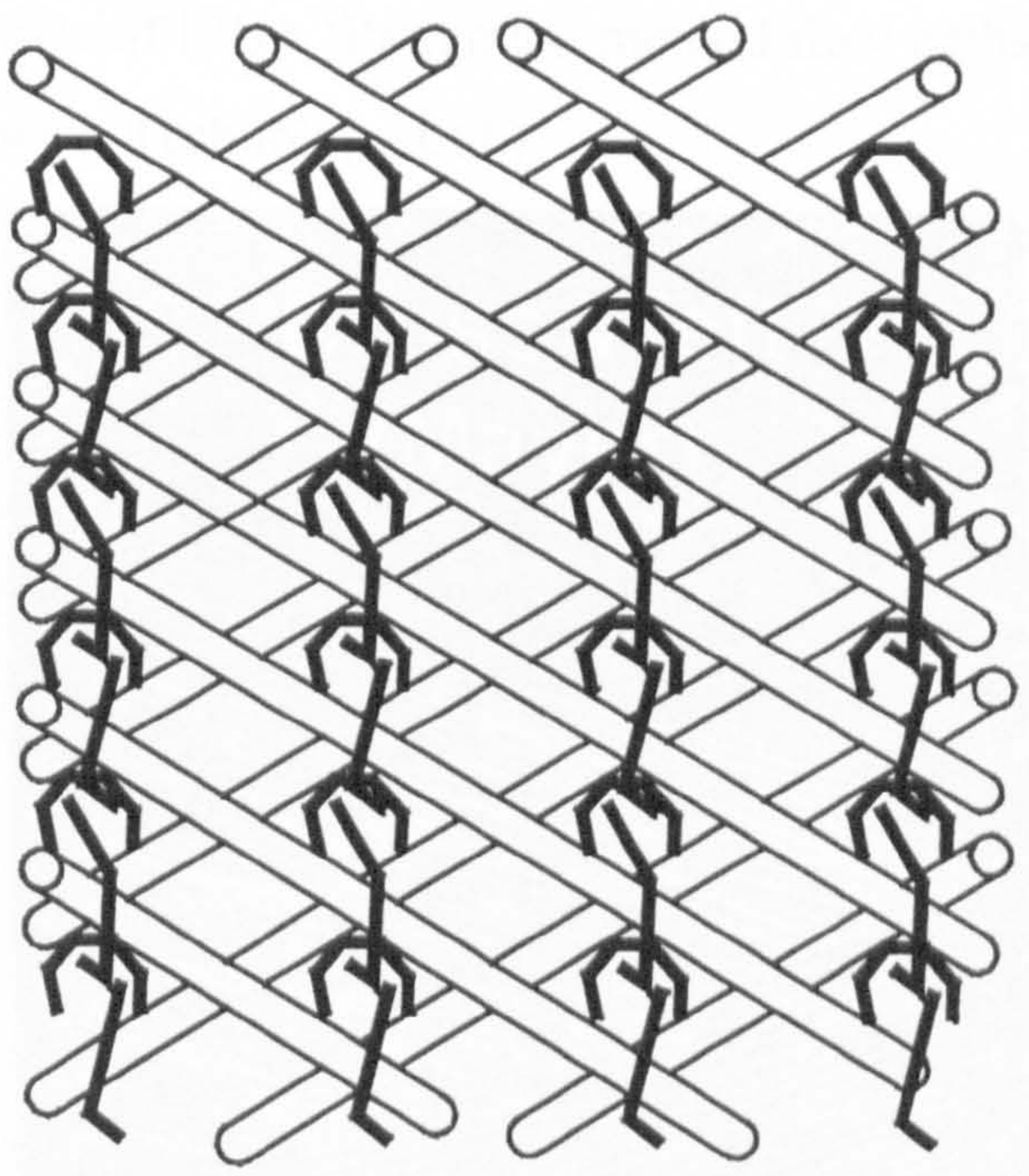

Figure 3.2 Diagram of chain stitching.

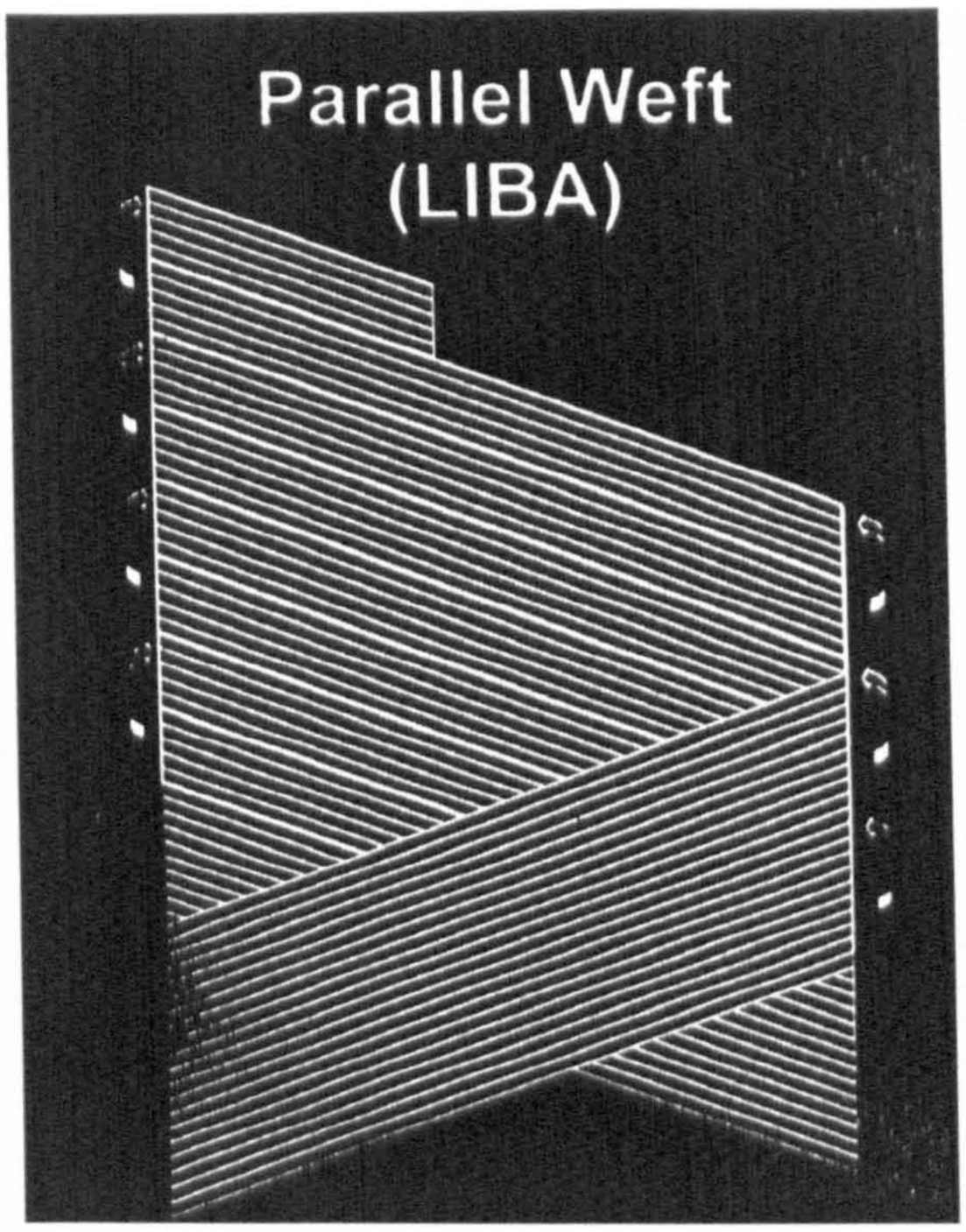

Figure 3.3 Schematic of LIBA 'Parramax' method fibre paths (Courtesy of Brunswick Technology Ltd.)

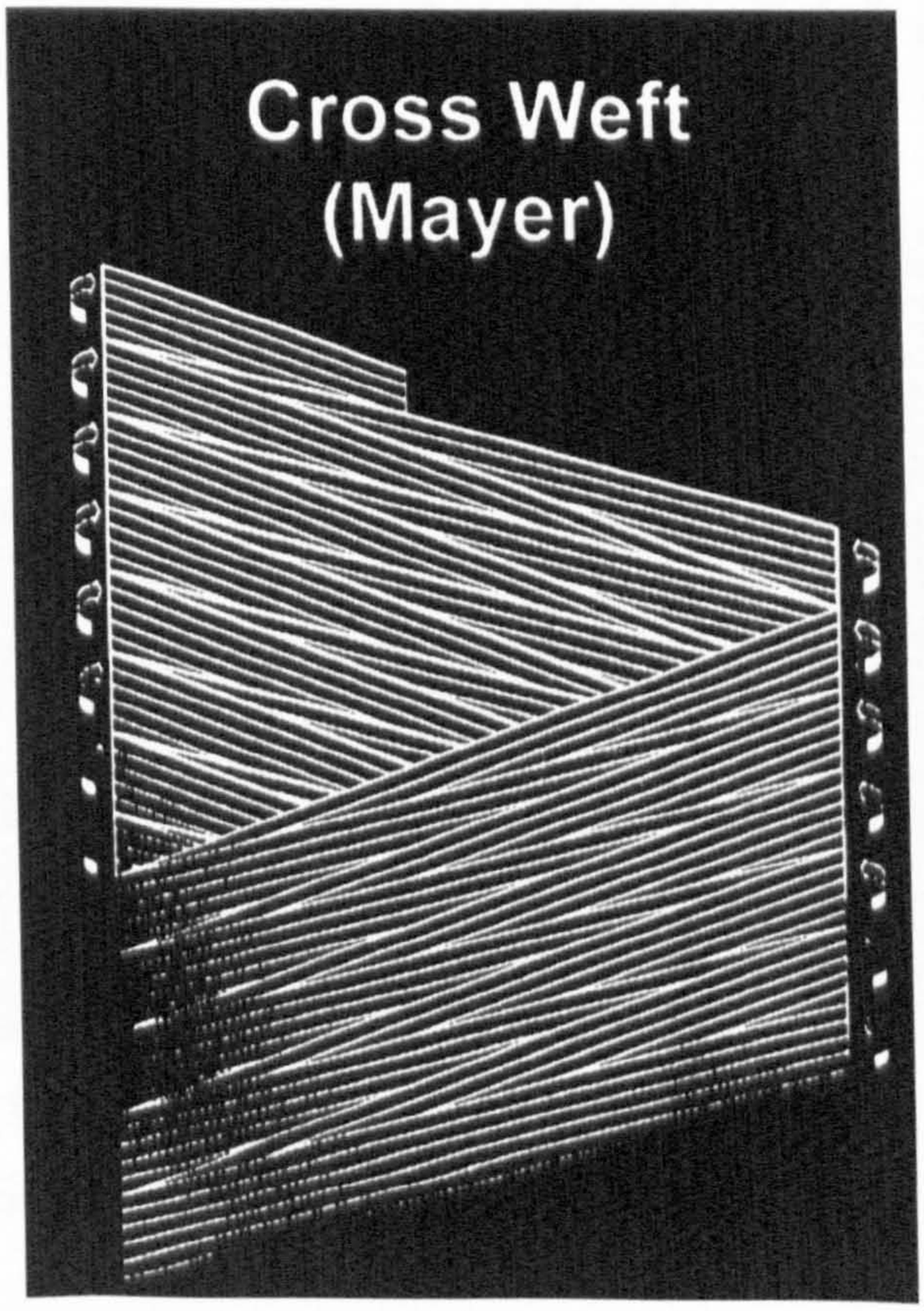

Figure 3.4 Schematic of conventional 'cross weft' fabric production fibre paths (Courtesy of Brunswick Technology Ltd.)

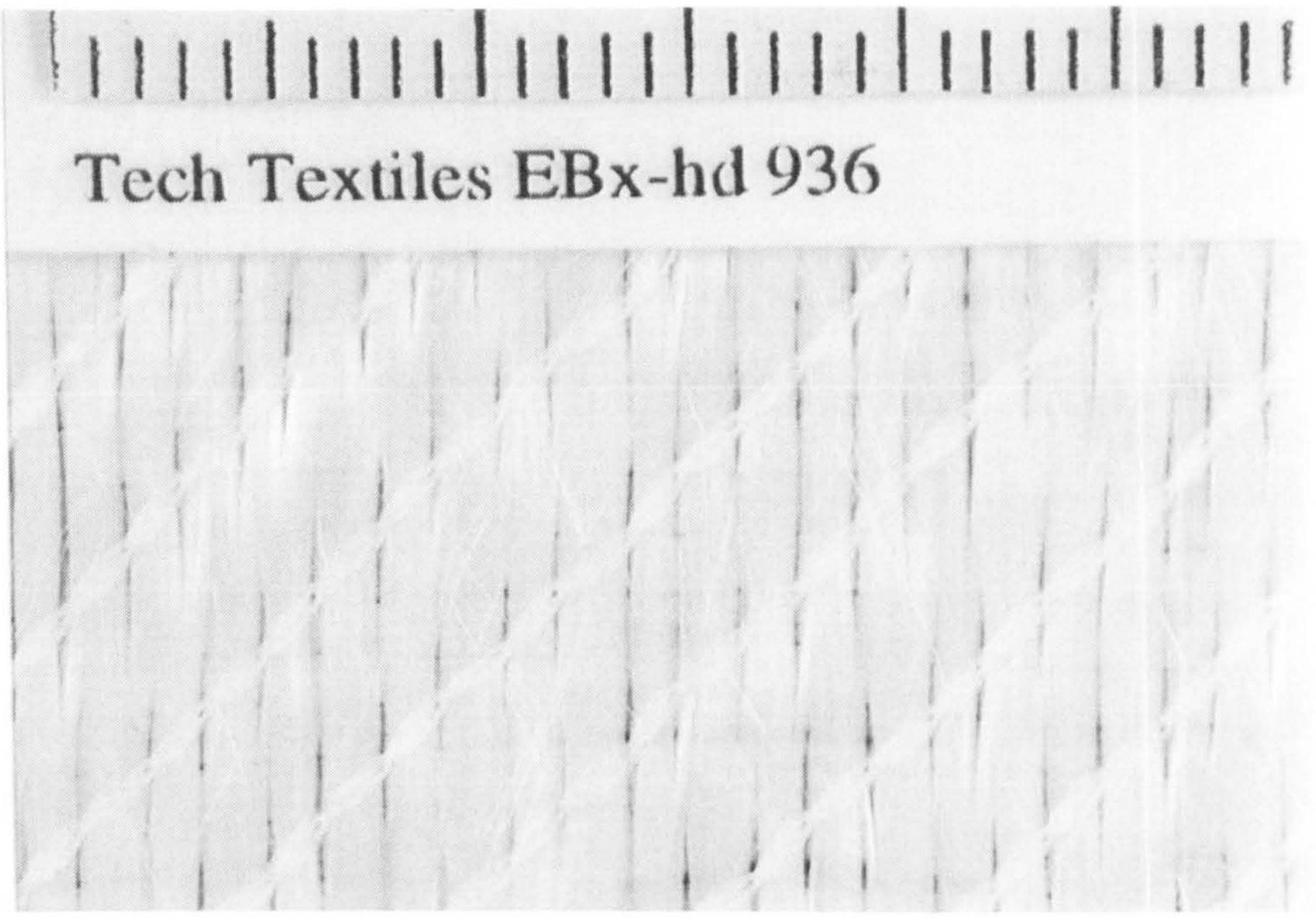

Figure 3.5 (a) Front face of Tech Textiles E-BXhd 936 fabric. 2 layer, tricot stitched, Parramax construction. Note parallel yarn paths.

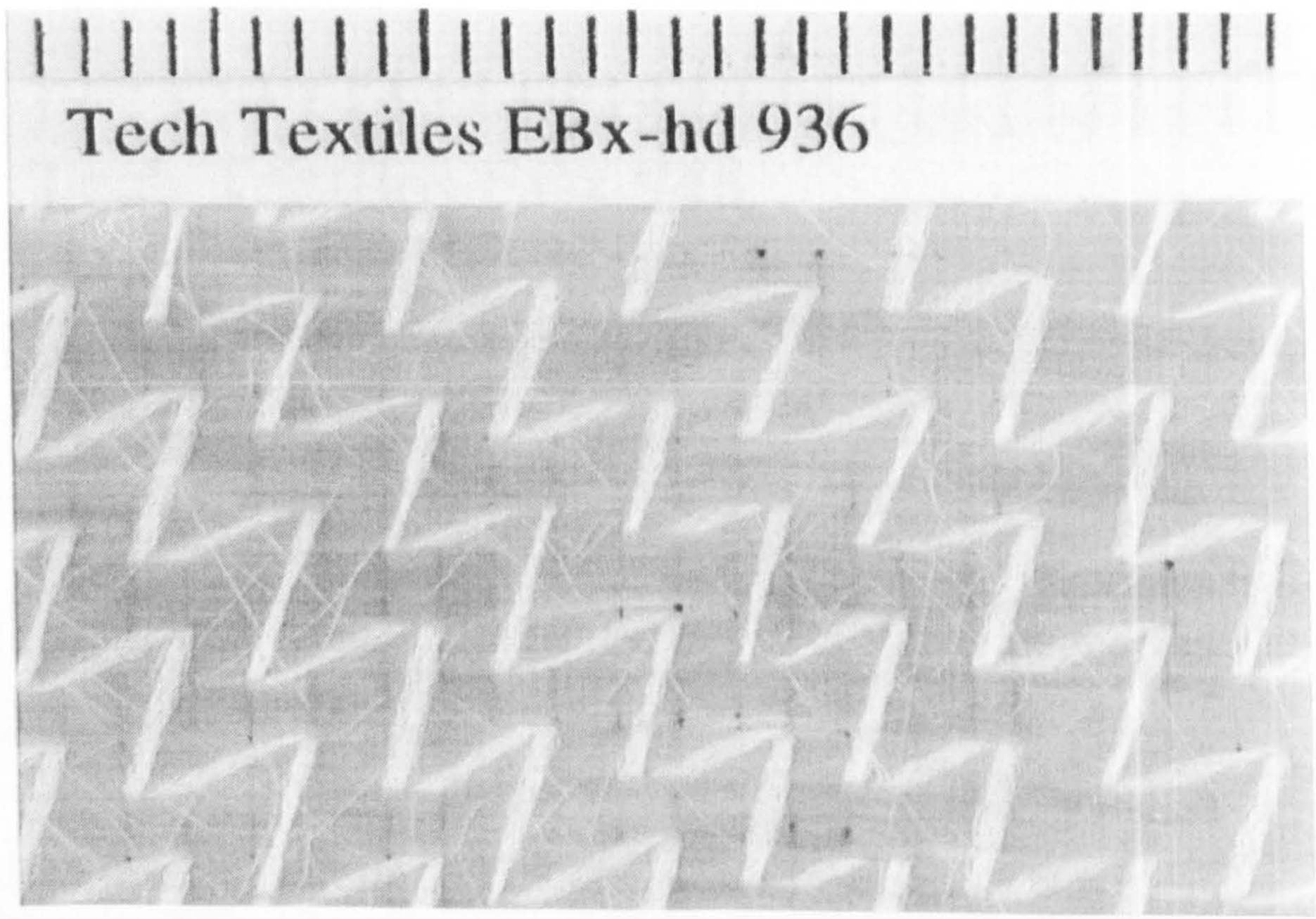

Figure 3.5 (b) Rear face of Tech Textiles E-BXhd 936 fabric. The zig-zag pattern of the tricot stitch is clearly seen.

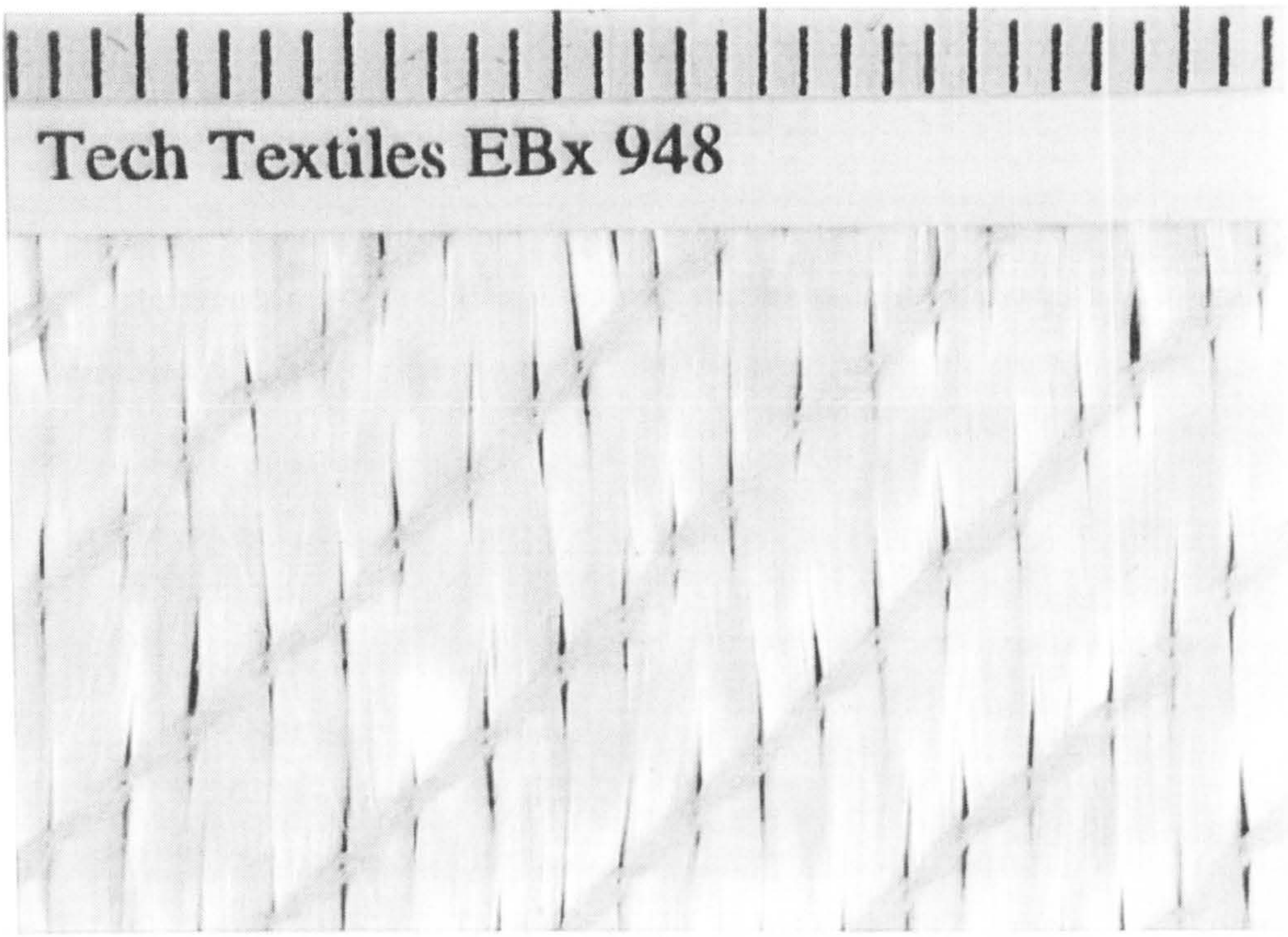

Figure 3.6 (a) Front face of Tech Textiles E-BX 948 fabric. 2 layer, tricot stitched, Crossweft construction. Note the yarns are not perfectly parallel.

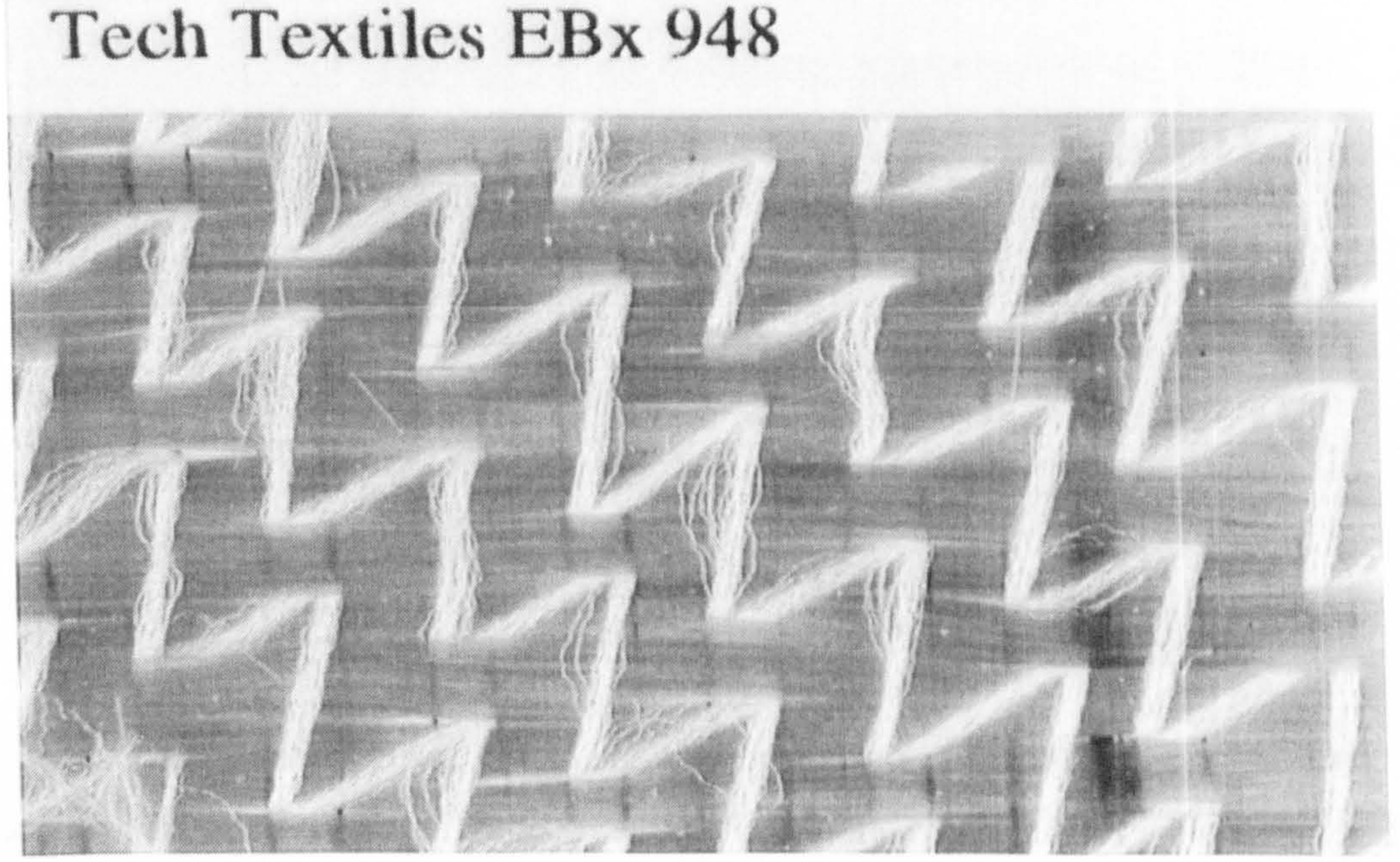

Figure 3.6 (b) Rear face of Tech Textiles E-BX 948 fabric.

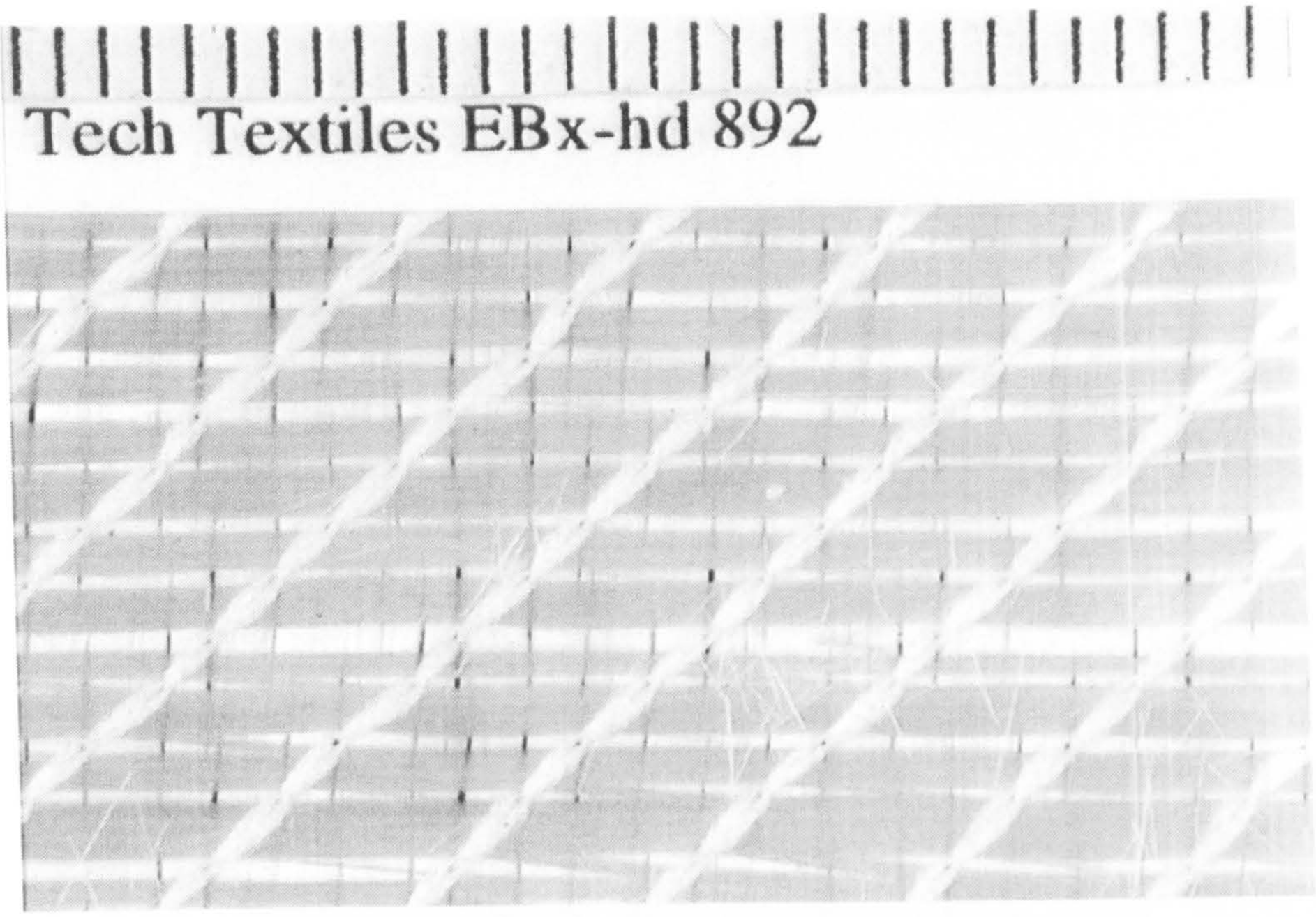

Figure 3.7 (a) Front face of Tech Textiles E-bBXhd 892 fabric. 4 layer, tricot stitched, Parramax construction.

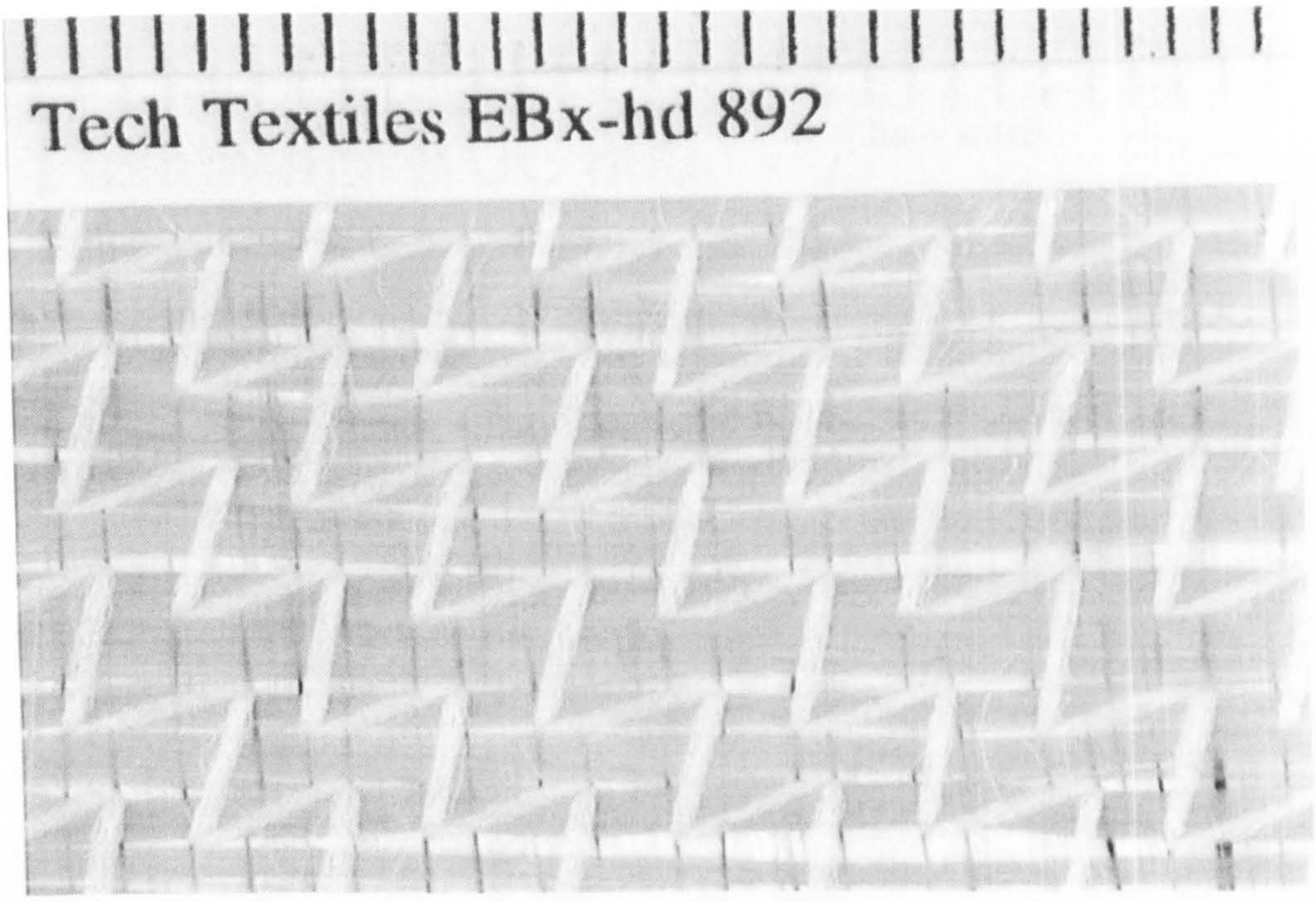

Figure 3.7 (b) Rear face of Tech Textiles E-bBXhd 892 fabric. Note outer fibre layers are both running in same direction, with double thickness inner layer.

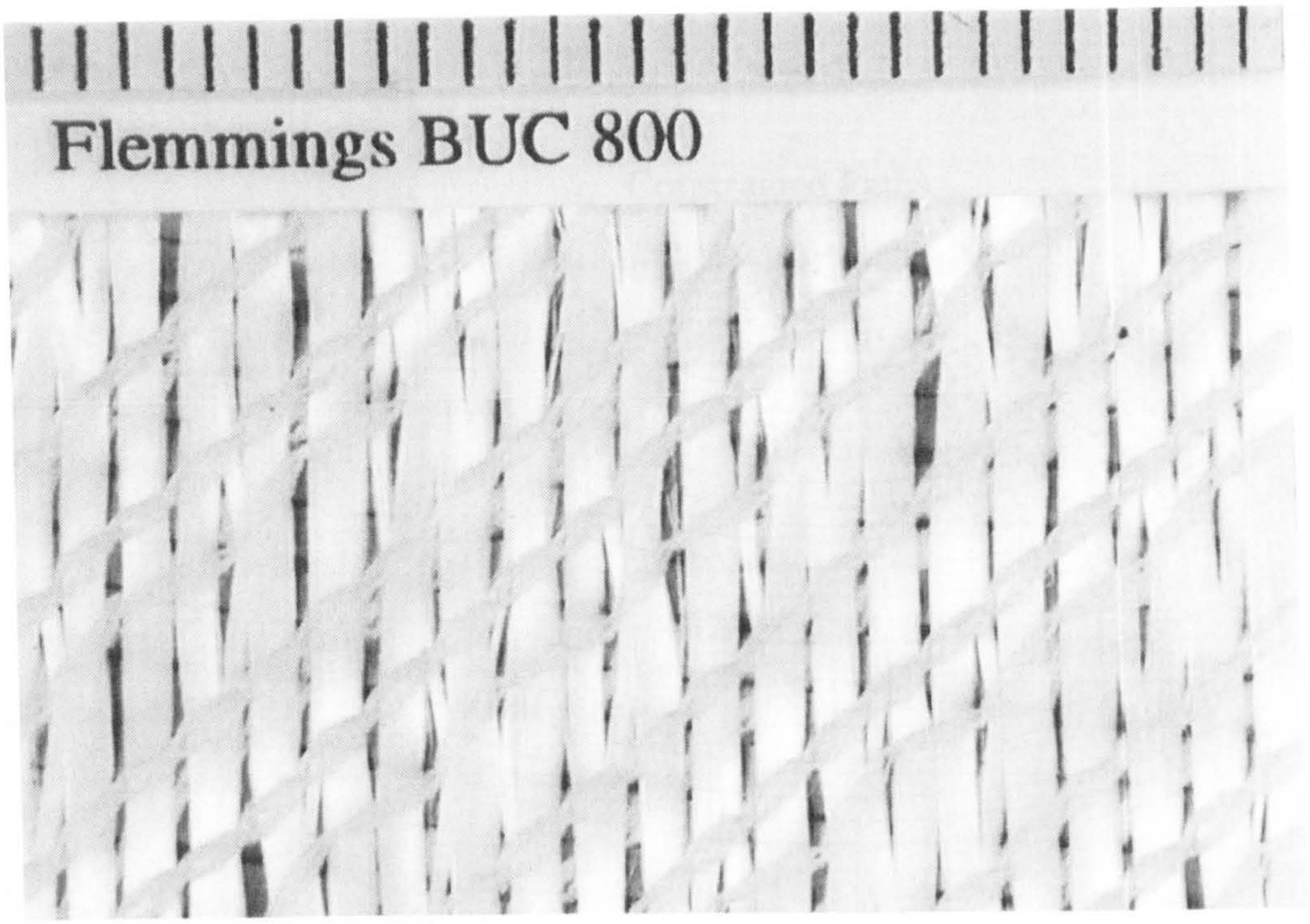

Figure 3.8 (a) Front face of Flemmings Industrial Fabrics BUC 800 fabric. 2 layer, chain and tricot stitched.

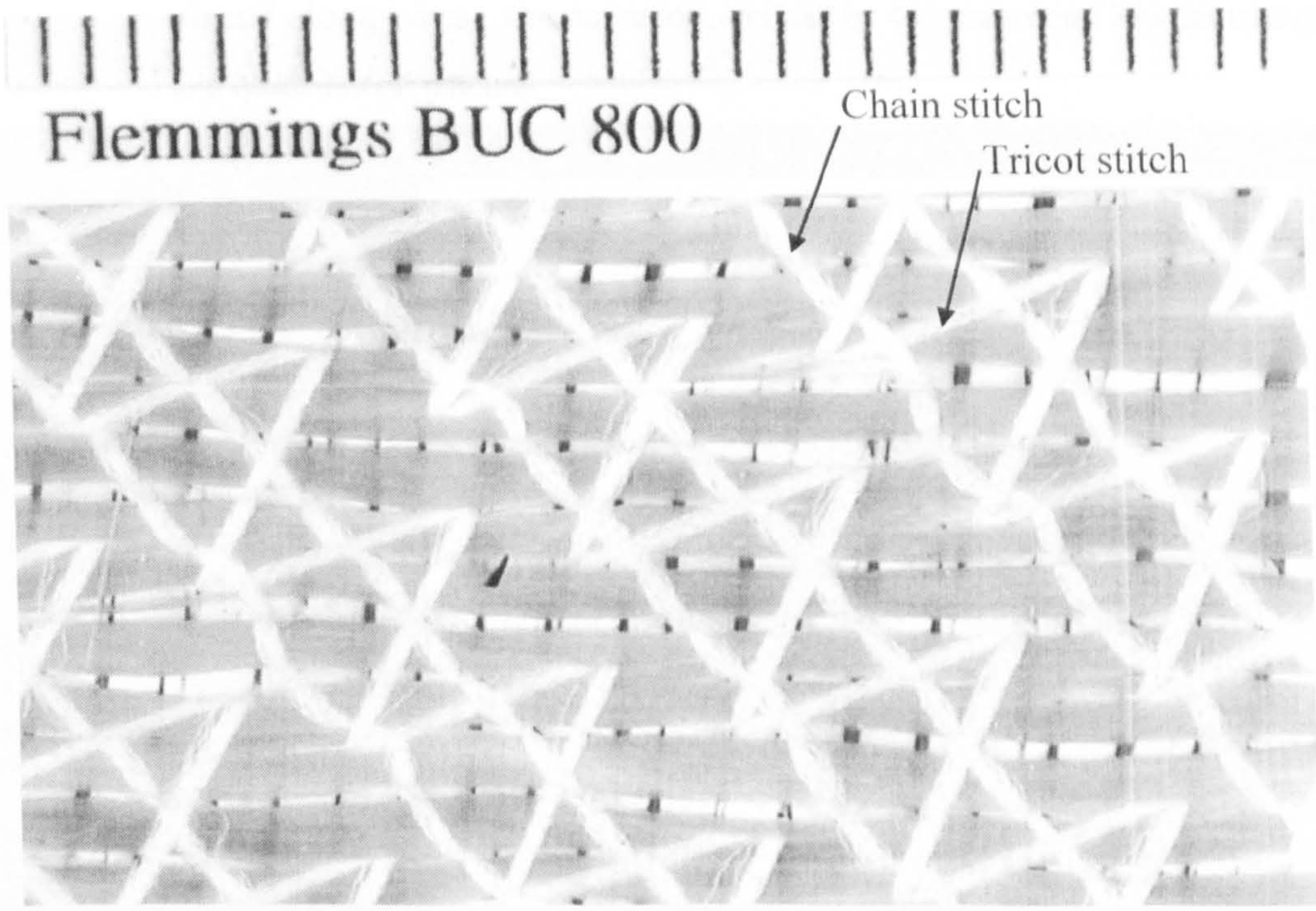

Figure 3.8 (b) Rear face of Flemmings Industrial Fabric BUC 800 fabric. Note the loose zig-zag tricot stitch and tight chain stitch. The inter-yarn angle is not 90° as would be expected but approximately 82°.

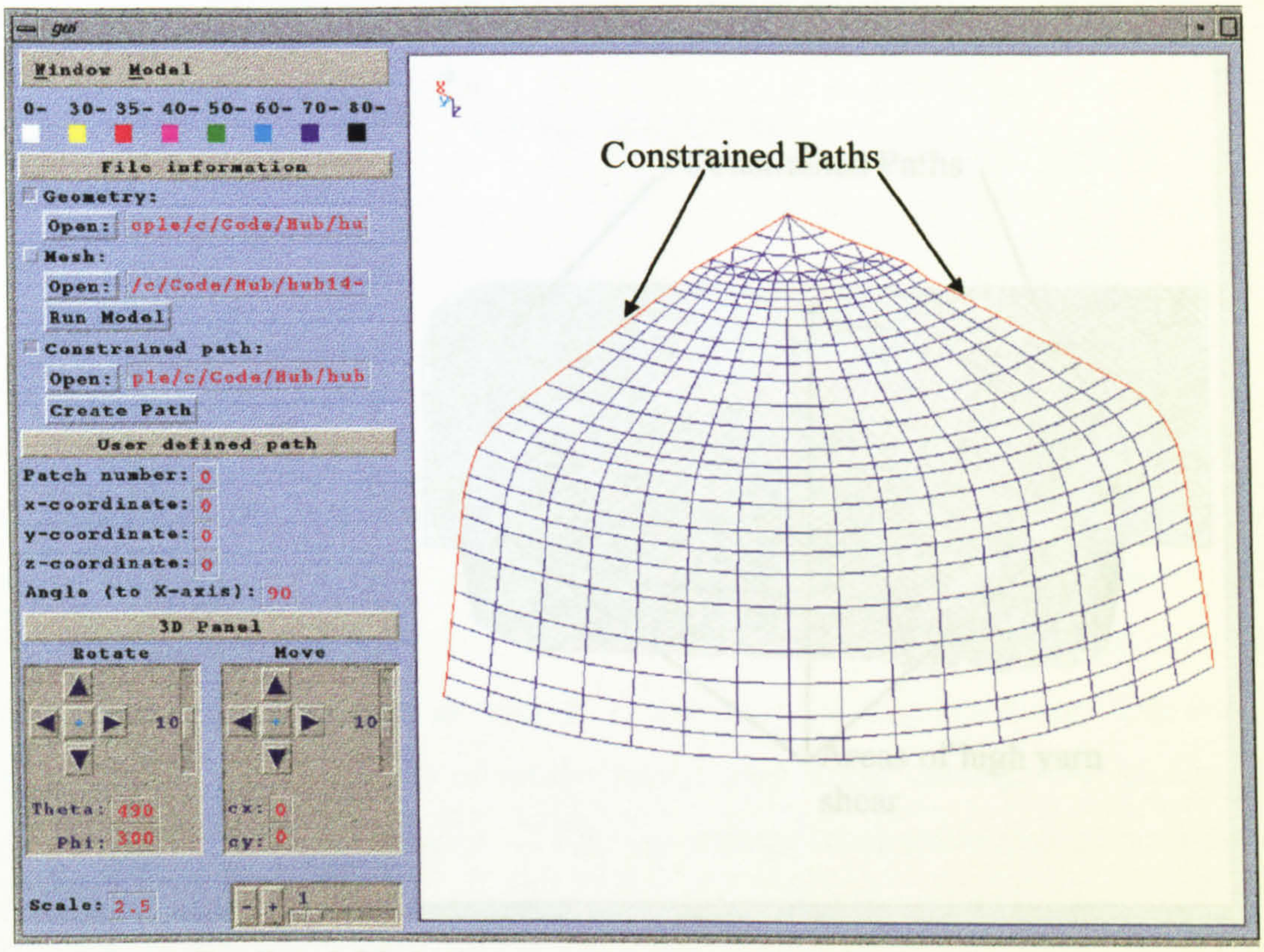

Figure 3.9 Wheel hub geometry with two constrained paths (defined by red lines) placed along edge. Quarter model, defined by 466 points and 396 flat triangular and quadrilateral patches.

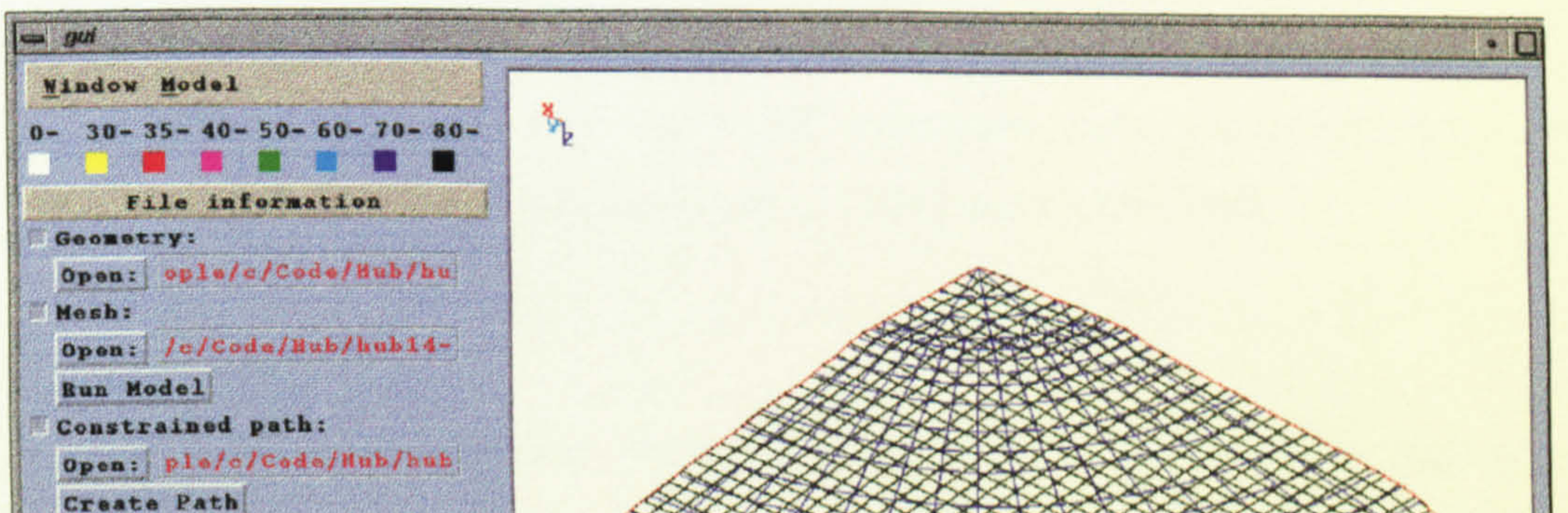

Figure 3.10 Predicted fabric drape over wheel hub - 6.4 mm grid spacing, minimum predicted inter-yarn angle 30°.

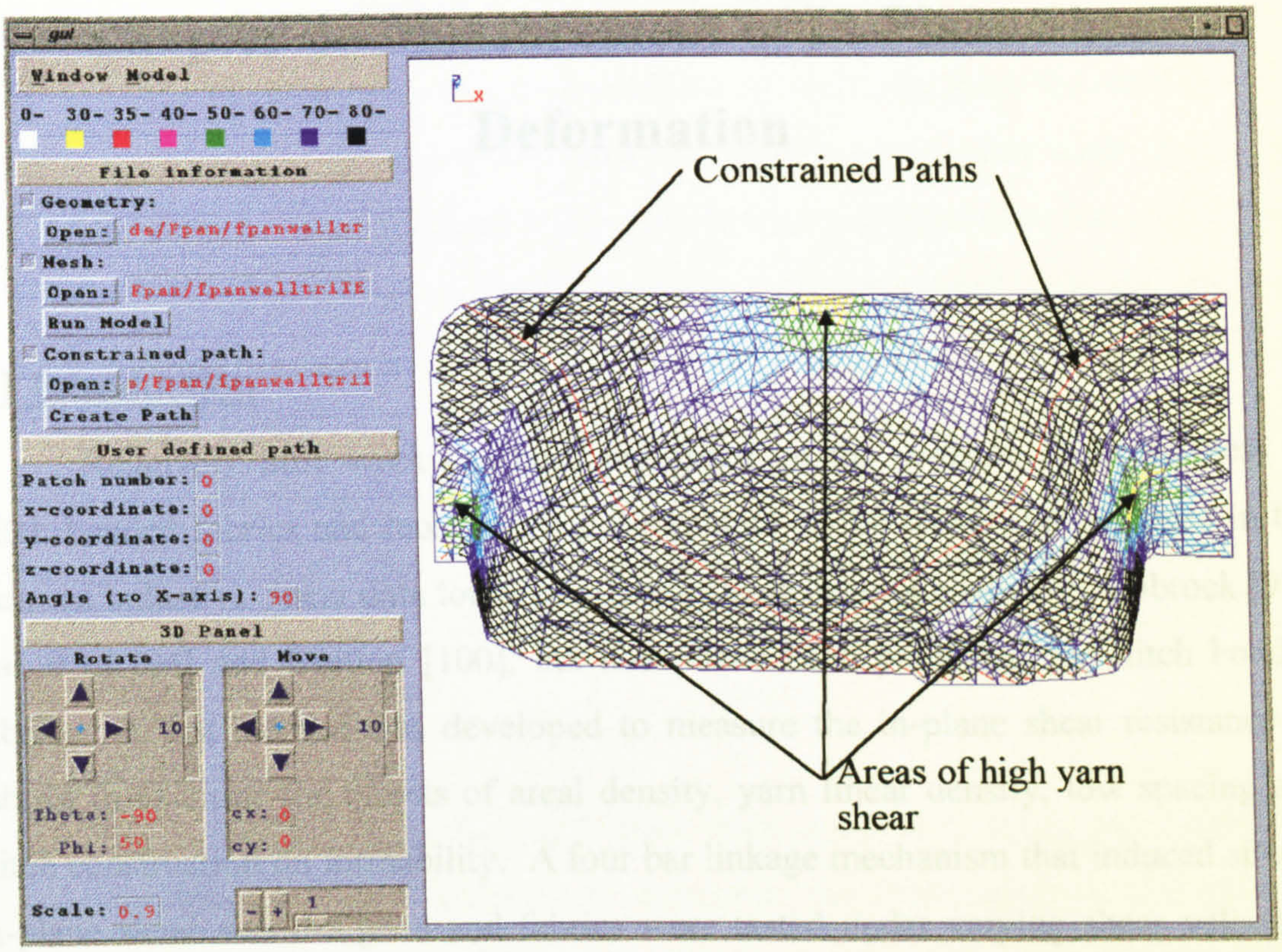

Figure 3.11 Predicted fabric drape over a prototype wheel well - half model defined by 294 points and 525 triangular patches, 6.4 mm grid spacing.

Chapter 4 - Measurement of In-Plane Shear Deformation

4.1 Introduction

Relatively little work has been published on the in-plane shear stiffness of stitch bonded fabrics and most existing data relate to the woven fabrics used in the garment industry. Shear data for woven fabrics have been published by Robroek [97], Cai *et al* [94] and Skelton [100], but none have been published for stitch bonded fabrics. A test method was developed to measure the in-plane shear resistance of fabrics to examine the effects of areal density, yarn linear density, tow spacing and stitch construction on formability. A four bar linkage mechanism that induced simple in-plane shear was designed and fabrics were tested under varying shear velocities and orientations. The data were processed for comparison with the in-plane shear resistance and locking angle of the fabrics described in section 3.2.

4.2 Test Method for Measuring In-Plane Shear

A method that would allow up to 58° inter-yarn shear was developed, similar to that reported by Skelton [100], Boisse *et al* [104] and Culpin [99].

4.2.1 Test Equipment

To induce pure in-plane shear deformation in a fabric, a test facility was required that would rotate the fibres without applying a tensile force. A parallelogram four bar linkage mechanism was designed similar to that described in section 2.7.2 (Figure 4.1) The frame was held in a computer controlled hydraulic load frame (MTS Systems) with the frame geometry initially square and at 45° to the horizontal (Figure 4.2) A sample of fabric 295 mm square was held in the fixture by rubber faced clamping bars and toggle clamps. The +/- 45° tricot stitched biaxial fabrics were clamped along four edges but the +/- 49° chain and tricot stitched fabrics were only clamped along the edges running normal to the warp fibres (Figure 4.3) to prevent tensile forces occurring in the weft fibres. A force was applied to opposite diagonals of the frame by moving the lower crosshead of the load frame, which

altered the parallelogram geometry and sheared the fabric. The crosshead travelled 127 mm (a limit of the data acquisition equipment) vertically from the starting (non-sheared) position and the resistance force and crosshead position were monitored. The resistance force was measured using a 500N load cell connected between the top of the parallelogram frame and the crosshead. The crosshead velocity remained constant throughout the travel but could be varied from 0 to 1020 mm/min (0.017 m/sec) under computer control. Due to the geometry of the four bar linkage the relationship between the crosshead displacement and the in-plane shear angle is non-linear throughout the crosshead displacement. The actual in-plane shear velocity for a nominal crosshead velocity of 68 mm/min can be seen in Figure 4.4.

4.2.2 Test Procedure

Fabric samples were cut using a sheet metal template to ensure repeatability of the sample dimensions and weighed to determine the fabric areal density prior to testing. The bi-directional +/- 45° tricot stitched samples were cut to ensure that the warp and weft fibres were perpendicular to the template edge. This sometimes required pre-shear of the fabric to ensure the fibres were not put under tension during the test. For the tricot and chain stitched fabrics where the fibres were not initially perpendicular (typically +/- 49°) the samples were cut so that one set of fibres would be perpendicular to the template edge. This was to ensure that when the fabric was clamped along only one edge, the fibres were perpendicular to the frame, as described in section 4.2.1. When clamping the samples into the frame, any perceived slack was removed by lightly tensioning the fabric to remove any waviness before locking the clamps.

A computer controlled data acquisition system (MTS Systems Corp. Testworks software v2.11b) was used for monitoring and control. The load cell reading was zeroed with the fixture and fabric sample in place to eliminate their weight from the test results. A test procedure was programmed into the control software to allow variable crosshead velocities and a maximum movement of 127 mm. The crosshead position, time and resistance force were sampled automatically by the software and output to a data file.

The raw data were processed using a spreadsheet (Excel 5.0) to provide a plot of in-plane shear force versus the inter-yarn shear angle (see Appendix 4.1 for further details). Previous workers [74, 104] have used the in-plane shear force versus axial strain relationship. The latter method does not provide comparative data such as the locking angle directly.

The in-plane shear angle and in-plane shear force are simple to calculate knowing the force measured by the load cell and the fixture geometry. Figure 4.5 shows the geometric arrangement and forces diagram, and Appendix 4.1 provides a more detailed explanation. The included angle between the parallelogram sides (hence the yarns in the sample), Φ_{Frame}, was determined by trigonometry based on the displacement of the crosshead. The in-plane shear force (F_S), (parallel to the fabric edge) can be calculated from the load cell force (F_{xhd}) by simple trigonometry. The equation used was:-

$$F_S = \frac{F_{xhd}}{2.\cos(\Phi_{Frame}/2)} \tag{4.1}$$

To establish the system noise, test repeatability and resistance to movement of the frame, tests were performed with the frame empty at different crosshead speeds. Figure 4.6 shows the shear force versus shear angle for the empty shear fixture. Results were taken for six tests at the two extremes of the velocity range used in subsequent experiments (68 mm/min and 1020 mm/min). It can be seen that the effect of friction in the empty fixture and the maximum error due to noise in the system is approximately +/-1.2 N.

Three replicates were made for each test condition and the average results presented, to minimise the errors due to variability in the fabric and misalignment in the test fixture. Figure 4.7 shows the results of three replicates using a biaxial tricot stitch bonded fabric at 68 mm/min with the stitching running perpendicular and parallel to the load direction. Comparing the load from the empty rig (Figure 4.6) with the results of the shear test (Figure 4.7) shows that the maximum noise level of 1.17 N is approximately 3.3% of the shear resistance of the fabric at the same angle and within the variation of the three tests. Therefore the force data were not trimmed

to remove the empty rig results. The variation in shear force when loaded perpendicular to the stitch was an average of approximately 4 N between the three tests with the largest error of approximately 9 N occurring at the largest inter-yarn shear angle of 58°. Results with the stitching running parallel to the load showed a similar variation but due to the higher shear force the effect of the error was less noticeable.

4.3 Interpretation of the Results

A typical plot of the average shear force vs. shear angle for the data shown in Figure 4.7, when loaded parallel to the stitch direction, is shown in Figure 4.8. At low shear angles the shear force rises steadily until a value of approximately 20 N where it starts to level off. This can be explained as follows: As the two layers of fibres rotate about their intersections they become more aligned and the area of contact between them increases. The friction couple between the layers of fibres increases proportional to the area of contact and therefore the force required to shear the fabric increases further.

If the fabric is sheared parallel to the stitching, then another factor is apparent. As the shear angle increases, the stitching which holds the fibre bundles together becomes tighter and restrains the fibre bundles. The stitch tension resists the shear force and the friction between intersecting yarns also increases due to the stitch tension. Eventually either the fibres reach their packing limit or the stitch locks and the shear stiffness increases sharply. Thus a 'locking angle' is demonstrated, in Figure 4.8 the locking angle is beyond 58° shear (therefore below 32° inter yarn angle).

An alternative method of comparing fabric shear characteristics is using shear stiffness (S) as defined by Skelton [100]. The shear stiffness is derived from the shear coupling in the fabric sample, and allows the area of the sheared element to be eliminated from the stiffness value. The shear stiffness of a fabric can be defined by:-

$$S = \frac{F_s.h}{h.l.\theta_s}(N/m.rad) \qquad (4.2)$$

where F_S is the shear force, h is the sample height and can be eliminated from the equation (i.e. distance between parallel clamping bars), l is the length of clamped edge and θ_s is the shear angle in radians.

Previous authors [93, 99, 100] have quoted a single figure for the shear stiffness of fabrics as the test range was small (maximum of 8°). Figure 4.9 shows the in-plane shear stiffness (as defined by Skelton) versus shear angle for the data shown in Figure 4.8, and indicates that a unique value of shear stiffness is more difficult to determine as the shear stiffness is a function of the shear angle.

In fabrics with high shear stiffness, the locking angle can be determined by the onset of wrinkling (as used by Dreby [95] for garment textiles). The present results suggest that a similar result might be deduced from the increasing shear stiffness. However, at the machine limitation of 127 mm crosshead movement (58° shear angle), the fabric did not appear to have locked fully (either visually or by examining the shear force), although the rate of change of shear force at 58° (Figure 4.8) suggests that locking is approached. Theoretically the shear force would tend to infinity when the fabric locked and therefore the rate of change of shear force would also tend to infinity. This will appear on the shear force versus shear angle plots as an increase in the curve's gradient and will indicate that the fabric is close to locking. However, in reality the fabric would start to wrinkle and the stitching would rupture before the force tended to infinity.

4.4 Comparison of Shear Stiffness of Stitch Bonded Fabrics under Varying Shear Conditions

4.4.1 Effect of Test Method on Shear Properties

To determine whether there was a fundamental difference between the two sided clamping used in determining textile shear stiffness based on the Kawabata KES-FB-1 method used by Yu *et al* [93], and the four sided constraint imposed by the parallelogram method, a comparison was performed. Figure 4.10 shows plots of shear force versus shear angle for two sided and four sided clamping for Tech Textiles E-BX 948 fabric. The area of fabric being sheared was approximately 54800 mm^2

when clamping along two edges and 63000 mm^2 when clamping along four edges. The results were normalised to compare the results over the same fabric area. Figure 4.10 indicates there is little difference between two and four sided clamping, with both sets of results following the same trend. The two sided clamping results show up to 10 N lower shear force occurred at the maximum shear angle (58°), which is probably due to reduced packing of the fibres along the unrestrained edges of the fabric. Thus it appears that the clamping method used in the test has little effect on the results, provided that an allowance is made for the difference in the area of the fabric being sheared.

4.4.2 Effect of Stitch Orientation on Shear Properties

Figure 4.11 shows shear force versus shear angle graphs for the same tricot stitched fabric with the stitch orientation running parallel and perpendicular to the applied load. As the construction of the fabric was identical in each direction apart from the stitching, the effect of the stitch can be seen as the difference in shear forces for each direction. When the force was applied parallel to the stitching, increasing tension occurred in the stitch as the shear angle increased. From an examination of the stitch, it appeared that initially the slack in the stitching was taken up with little effect upon the stiffness of the fabric. Since it would be expected that the force required to elongate the stitch thread is higher than that required to compact the fibre yarns at the intersections, the stitches tighten around the fibre tows increasing the resistance to rotation due to friction. Eventually the stitching restrains the deformation and prevents further shear deformation. Although it is difficult to determine conclusively from the data it appears that the rate of change of shear force at 58° shear is higher when the fabric is loaded parallel to the stitch direction. This suggests that the fabric loaded parallel to the stitch is closer to locking and that the maximum shear angle is lower than when the load is applied perpendicular to the stitch (i.e. the stitch is not in tension during deformation). Therefore it appears that the locking angle of stitch bonded fabrics is dependent upon the stitch (so called *stitch limited locking*) if the stitch is in tension and upon the fibre packing limit (so called *packing limited locking*) when the stitch is not in tension.

4.4.3 Effect of Shear Rate on Shear Properties

To study the effect of test velocity on the shear stiffness of the fabric, shear tests were performed at varying crosshead velocities. A biaxial tricot stitched fabric (Tech Textiles E-BX 948) was tested with the stitching running parallel and perpendicular to the loading direction at four crosshead velocities (between 68 mm/min and 1020 mm/min).

Figure 4.12 shows the average shear force against shear angle for four test velocities with the stitch running parallel to the load direction. The shear forces at the lowest forming velocity (68 mm/min) are approximately 18 N lower than those for the other three velocities. Although the results could suggest that the shear resistance of fabrics loaded parallel to the stitch may be velocity dependent, there is not a direct correlation between forming velocity and shear force.

Figure 4.13 shows the results under the same test conditions but with the stitch running perpendicular to the load direction. There is much less variation in the results and the effect of shear velocity appears to be smaller which may suggest that the stitch is the main cause of the variability shown in Figure 4.12. The lowest crosshead velocity (68 mm/min) again produces the lowest shear forces (allowing for noise in the 540 mm/min data) with the two higher velocities producing slightly higher forces suggesting that there may be a small effect on inter-fibre friction due to shear velocity.

The rippling effect seen in the data (particularly during the 540 mm/min tests) was due to noise in the hydraulics or data acquisition equipment, which could not be traced. Another possible cause of variation in the test results could be due to the variation in fibre alignment accuracy when loading the samples into the frame. This would cause tension in the fibres during shearing, pulling them from under the clamps. This caused fibre buckling due to excess length as the frame returned to the original unsheared position after the test. If this was noticed, then the data were ignored and the test repeated.

4.4.4 Effect of Stitch Pattern on Shear Properties

The most common stitch used in stitch bonded fabrics is the tricot stitch, as used in the high drape Tech Textiles fabrics (explained in section 3.2.2). Chain stitch was used during manufacture of the Flemmings BUC range of fabrics to hold each layer of fibres in place before being assembled using a tricot stitch in the same direction. This section looks at the effect of the stitch type on shear properties.

Figure 4.14 shows the in-plane shear stiffness versus shear angle for a tricot stitched fabric (Tech Textiles E-BXhd 936) and a chain and tricot stitched fabric (Flemmings BUC 800), loaded perpendicular and parallel to the stitch direction. The two fabrics have similar areal densities and were made from the same linear density fibres (800 Tex). It is clear that the chain stitched fabric was considerably stiffer than the tricot stitched fabric when loaded parallel to the stitches. At approximately 12° shear angle the chain stitched fabric locked and the fabric wrinkled. There was no gradual stiffening (as in the tricot stitched fabric) and the chain stitch appeared to lock abruptly. As the fabric was deformed further the stitching ruptured as seen by the knee at approximately 40° shear. When the chain stitched fabric was loaded perpendicular to the stitching, a more typical resistance curve was observed. The shear resistance was higher than that seen in the tricot stitched fabric as the chain and tricot stitched fabric had an initial ply angle of approximately +/- 49° rather than the +/- 45° of the tricot stitched fabric. This meant that the area of intersection between the fibres was initially higher, hence the friction force between the fibres would also be higher. Also some of the weft fibres near the edge of the +/- 49° fabric were clamped at one end during the test (See Figure 4.3) and must slide across the warp fibres during the test. These effects would increase the shear resistance of the fabric.

4.4.5 Effect of Fabric Construction on Shear Properties

The effect of fabric construction on the shear resistance of stitched fabrics was investigated by comparing three fabrics with similar areal densities, but differing in their construction method. A two layer +/-45° Parramax constructed fabric (E-BXhd 936) and a two layer +/- 45° cross weft fabric (E-BX 948) were compared with a four layer -45/+45/+45/-45 Parramax fabric (E-bBXhd 892) from the same manufacturer (Tech Textiles). The fabric construction methods and constituent properties are described in Chapter 3.

Figure 4.15 compares the shear resistance of Parramax and cross weft fabrics at a crosshead speed of 1020 mm/min. The Parramax fabric has a shear force approximately half that of the cross weft fabric, which could be due to yarn waviness which was evident in the cross weft fabric. The yarn linear density in the Parramax fabric is approximately 16% lower than that in the cross weft fabric, which may also contribute to this effect. The stitch tension was also considered as a contributing factor, but as the difference in shear resistance is noticeable when loaded in the perpendicular direction this would not appear to be the cause. The rate of change of shear force (shear rigidity) at 58° shear are summarised in Table 4.1. This indicates that the cross weft fabric (6.76 N/deg) is marginally closer to locking than the Parramax fabric (5.3 N/deg), although the difference cannot be determined exactly.

Figure 4.16 compares the shear resistance of a two layer and four layer, tricot stitched fabric. There appears to be little difference between the fabrics, although the 2 layer fabric was 18% stiffer at 58° shear angle when loaded perpendicular to the stitch, but approximately the same when loaded parallel to the stitch. The 4 layer fabric had an 11% lower areal density which may account for the lower shear resistance as the stitch tightens and the yarns compress at high shear angles.

To examine the effect of the fabric construction parameters such as yarn linear density and pitch on in-plane shear resistance, custom fabrics with an identical stitch type were commissioned (using a combination of chain and tricot stitch) from Flemmings Industrial Fabrics.

The yarn linear density was varied from 408 Tex to 1200 Tex, giving areal densities of 545 g/m^2, 800 g/m^2, 1200 g/m^2 and 1600 g/m^2. Figure 4.17 shows the shear characteristics when loaded parallel to the stitch direction. Due to the chain stitch, all the fabrics locked at approximately 12° shear and started to wrinkle as can be seen by the drop in shear force. Up to this point it can be seen that the heavier yarns produced the highest resistance, as might be expected due to the larger area of intersection between the yarns. The resistance of the two fabrics using lighter yarns was approximately equal up to the point of locking. Testing perpendicular to the stitch direction (Figure 4.18) shows that as the yarn linear density increases so does the shear force. As the fabrics approach the shear limit of the test equipment the in-

plane shear resistance of the fabrics are in proportion to their fibre linear densities. The heaviest fabric started to lock at 50^{o} shear (40^{o} inter-yarn angle) due to compaction of the yarns. Beyond this point the fabric started wrinkling, which can be seen as a knee in the shear force (Point B). For the other fabrics, there is a variation in the rate of change of shear resistance suggesting that the lighter yarns (and lower areal density) resulted in lower locking angles.

Figures 4.19 and 4.20 indicate that the effect of decreasing the fibre pitch for the same yarn (408 Tex) within a fabric is similar to that of increasing the fibre linear density. Figure 4.19 shows the in-plane shear force when loaded parallel to the stitching. The fabrics locked at approximately 12^{o} with the heavier fabrics having a higher shear resistance up to the point of locking. Figure 4.20 shows the in-plane shear force of the same fabrics when loaded perpendicular to the stitch. As seen previously (Figure 4.19) the in-plane shear resistance of the fabrics increases with the areal density and the locking angle of the heavier fabrics would appear higher than the lighter ones.

Finally two fabrics with similar areal densities but made from different linear density yarns (hence different yarn pitch) were tested. The fabrics were constructed from a 600 Tex yarn (areal density 800 g/m^2, 1.5 mm yarn pitch) and a 900 Tex yarn (areal density 786 g/m^2, 2.3 mm yarn pitch). Figure 4.21 shows little difference in the fabric shear resistance when loaded parallel to the stitch up to the stitch locking angle of approximately 12^{o}. Figure 4.21 also shows the shear resistance of the fabrics when loaded perpendicular to the stitch. The shear resistance of the fabric constructed from lighter yarn was approximately half that of the fabric constructed from the heavier yarn. This suggests that the shear resistance of a fabric loaded perpendicular to the stitch is not related directly to the fabric areal density.

Examination of the number of yarn intersections for the two fabrics shows that the fabric with the larger yarn spacing has a lower number of yarn intersections in the fabric (2.3 mm pitch gives 189,035 crossovers per square metre, whereas 1.5 mm pitch gives 444,444). The ratio of number of crossovers are approximately the same as the ratio of the shear resistances (yarn crossover ratio = 2.35:1 and shear resistance = 2:1). However this does not take into account the difference in yarn linear density.

Figure 4.22 shows a comparison of the crossover area within the fabric versus shear rigidity at the linear portion of the shear plots for all chain and tricot stitched fabrics.

By measuring the yarns using a vernier calliper, a width to height ratio was estimated at 3:1. By assuming the yarns were rectangular in cross section, the width of each yarn was calculated from its linear density. The area of an unsheared yarn intersection was calculated by squaring the width. A calculation of the number of yarns per square metre was made from the yarn pitch, and hence a ratio of yarn intersection area to fabric area was produced. The slope of the shear force plots in the linear region (from 8 to 32°) was calculated and plotted against the intersection area ratio. The data (Figure 4.22) shows that there is an almost linear relationship between inter-layer yarn contact and fabric shear resistance. The complete method of calculating this data is shown in Appendix 4.2.

4.4.6 Effect of Reinforcement Type on Shear Properties

A comparison of the shear resistance of a stitch bonded fabric and a plain weave with similar superficial densities is shown in Figure 4.23. At low shear angles (0° to 30°) the fabrics show similar in-plane shear resistance, but at higher shear angles the interlocking of the yarns within the plain weave and the larger yarn linear density (2200 Tex versus 305 Tex) provide a much larger resistance to shear than for the non-interlocked (stitched) fabric. At the end of the test small wrinkles started to appear in the fabric, suggesting that the woven fabric was starting to lock, which is also indicated by the high shear rigidity at 58° shear (15.9 N/deg). This suggests that the high drape stitch bonded fabrics may only provide an advantage in preform geometries where more than 35° shear is expected.

4.5 Conclusions

A test procedure to measure the shear characteristics of biaxial fabrics has been established. Twelve stitch bonded fabrics were tested and the results processed to indicate in-plane shear force and fabric locking angle as summarised in Table 4.1.

The results indicate that the shear resistance of biaxial fabrics increased as shear angle increased, although this is not a linear relationship. There appear to be three major factors affecting the shear resistance:-

i) Friction between the yarns - a resistance to the rotation at the yarn intersections.

ii) Tension in the stitch - a resistance to the elongation of the stitch, which causes the stitch to tighten, increasing friction at the yarn intersections.

iii) Compaction of the yarns - as the fibres shear, they become aligned which eventually leads to the transverse compaction of the yarns.

The dominant factor depends upon the type of stitch used, the linear density of the yarns, yarn spacing and the direction of shear relative to the stitch. Shearing the fabric parallel to the stitch required approximately double the force of shearing the fabric perpendicular to the fibres, due to the tension in the stitch.

The forming limit of the fabric, known as the locking angle (defined as the inter-yarn angle beyond which the fabric will not shear), is caused by either locking of the stitch (as seen when testing chain and tricot stitched fabric parallel to the stitch) or yarn compaction (when either stitch type is loaded perpendicular to the stitch). When loaded perpendicular to the stitch (i.e. the stitch does not dominate the shear resistance) the shear rigidity of the fabric is proportional to the area of contact between the two plies of the fabric.

As the KDM assumes zero resistance to shear, it is likely that the predictions will be invalid as the ratio of shear resistances between the stitch and non-stitch direction increases, or the fabric reaches its locking angle. The difference in shear rigidity is likely to cause variable shear in the fabric for the same shear force, thus invalidating the assumption of geodesic paths defining the constraints within the model. A solution to this may be to redefine the constraints within the model based on an adaptation of the energy minimisation constraint as proposed by Bergsma [41], using shear rigidity values determined from in-plane shear tests.

For the chain and tricot stitched fabrics where stitch locking occurred at 12° shear, the imbalance is likely to cause problems in preforms that require high fabric shear. For a more balanced fabric such as Tech Textiles E-BXhd 936, preforming

problems due to the difference in shear rigidity are less likely. The effect of shear rigidity on the preforming of simple shapes is investigated in Chapter 7.

Test results indicated that the shear properties may be dependent on the shear velocity, although this was only noticeable when loading parallel to the stitch. The measured fabric shear resistance appears to be independent of the clamping method.

Fabric Code	Parallel to stitch		Perpendicular to stitch		Stiffness Ratios at 58°
	Shear rigidity at 58° (N/deg)	Locking Angle (deg)	Shear rigidity at 58° (N/deg)	Locking Angle (deg)	
Tech Textiles E-BX 948	6.76	-	2.44	-	2.77
Tech Textiles E-BXhd 936	5.30	-	1.19	-	4.46
Tech Textiles E-bBXhd 892	5.38	-	1.20	-	4.47
Flemmings BUC 403	-	78	0.90	-	-
Flemmings BUC 440	-	78	1.14	-	-
Flemmings BUC 545	-	78	1.92	-	-
Flemmings BUC 600	-	78	2.68	-	-
Flemmings BUC 682	-	78	4.04	-	-
Flemmings BUC 786	-	78	1.60	-	-
Flemmings BUC 800	-	78	3.45	-	-
Flemmings BUC 1200	-	78	5.98	-	-
Flemmings BUC 1600	-	78	-	40	-
FGI Plain weave (840 g/m^2)	15.94	-	-	-	-

Table 4.1 Summary of fabric shear properties (Full details of fabric construction parameters are shown in Appendix 3.1).

(Presented results assume that all fabrics consist of +/- 45° yarns in unsheared position i.e. Locking angle = 90°-shear angle)

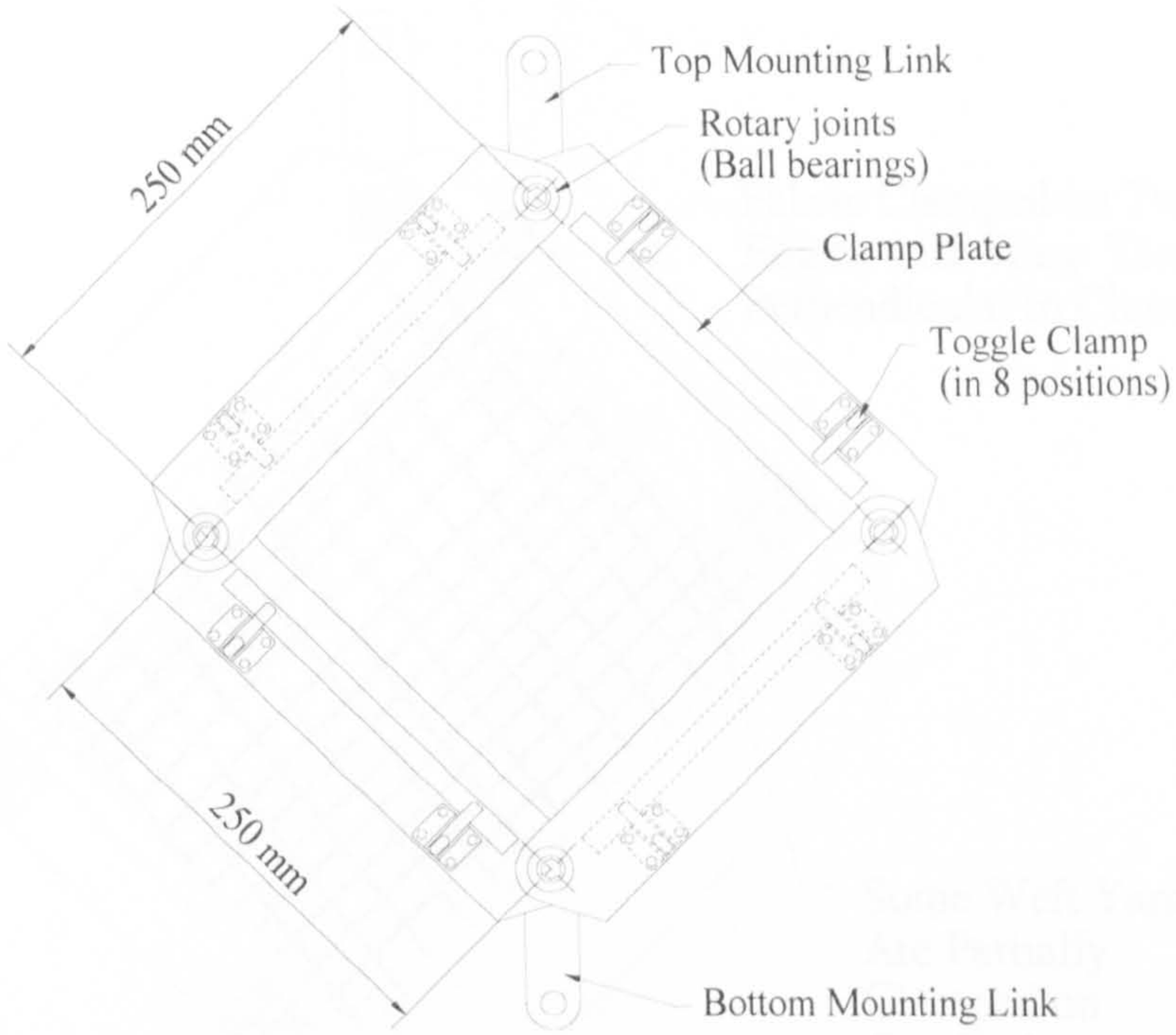

Figure 4.1 Diagram of experimental fabric shear rig used for tests presented in Chapter 4.

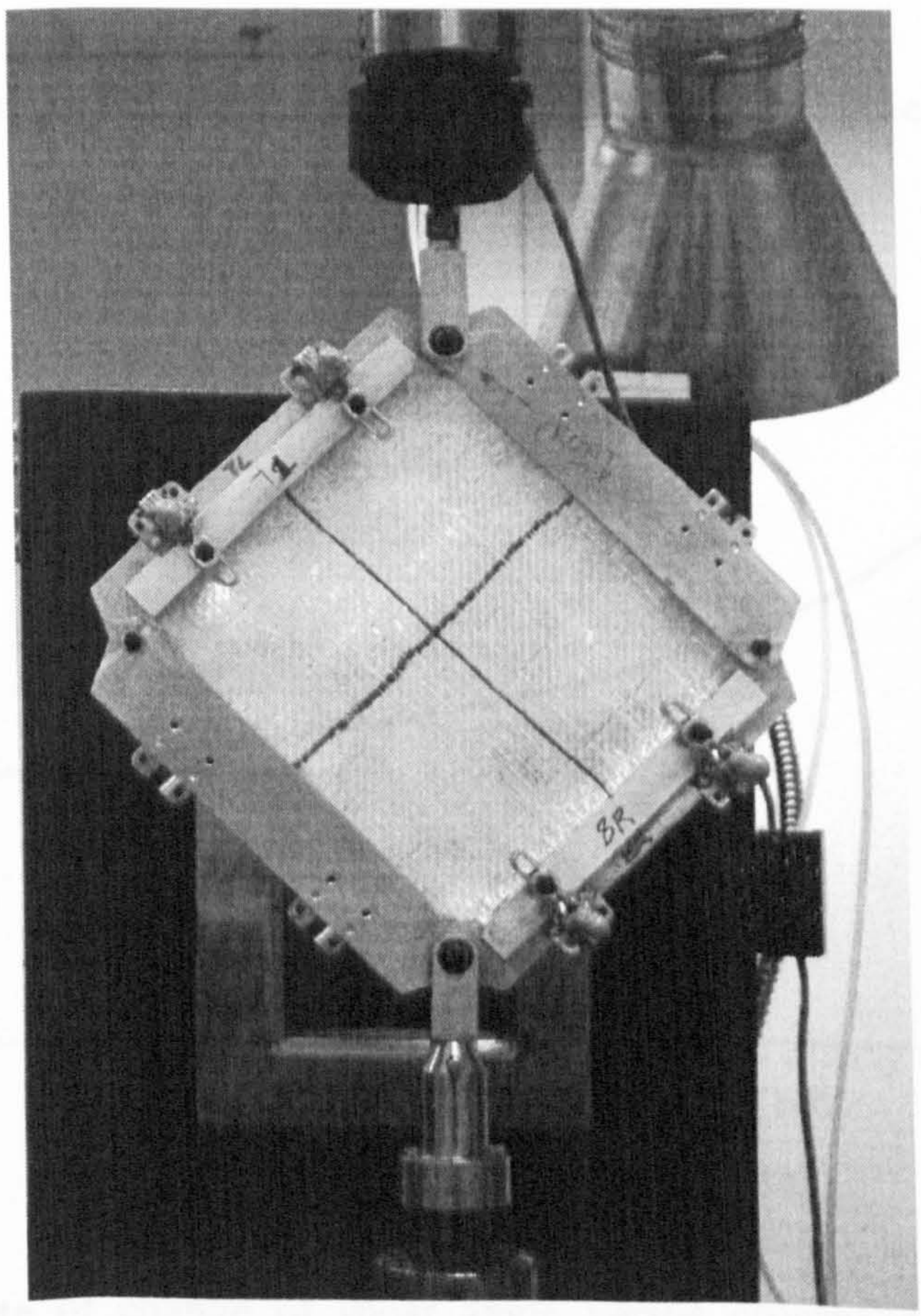

Figure 4.2 Photograph of experimental shear rig loaded with tricot stitch bonded fabric. (Tech Textiles E-BX 948.)

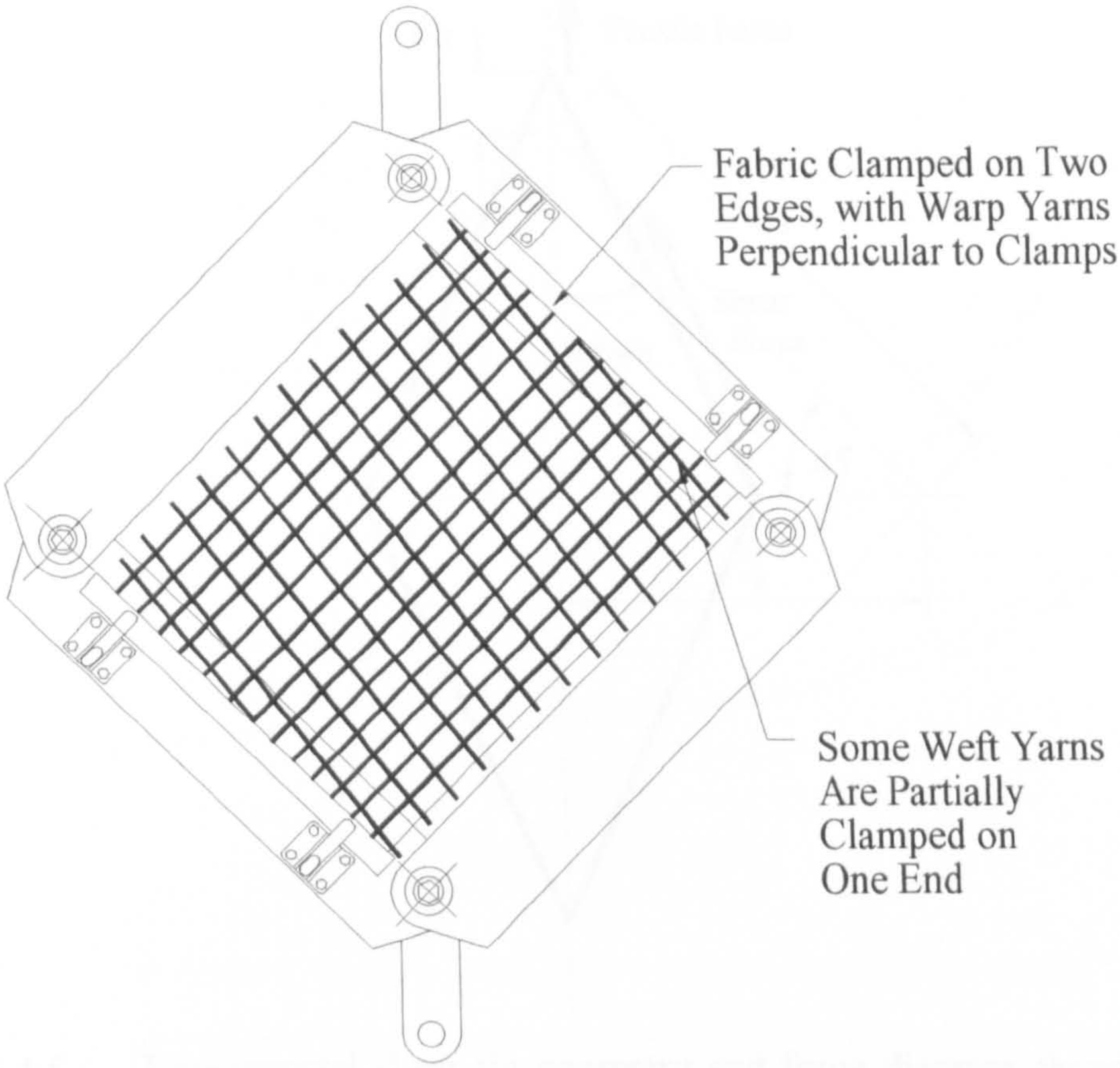

Figure 4.3 Clamping method for non +/- 45° stitch bonded fabrics.

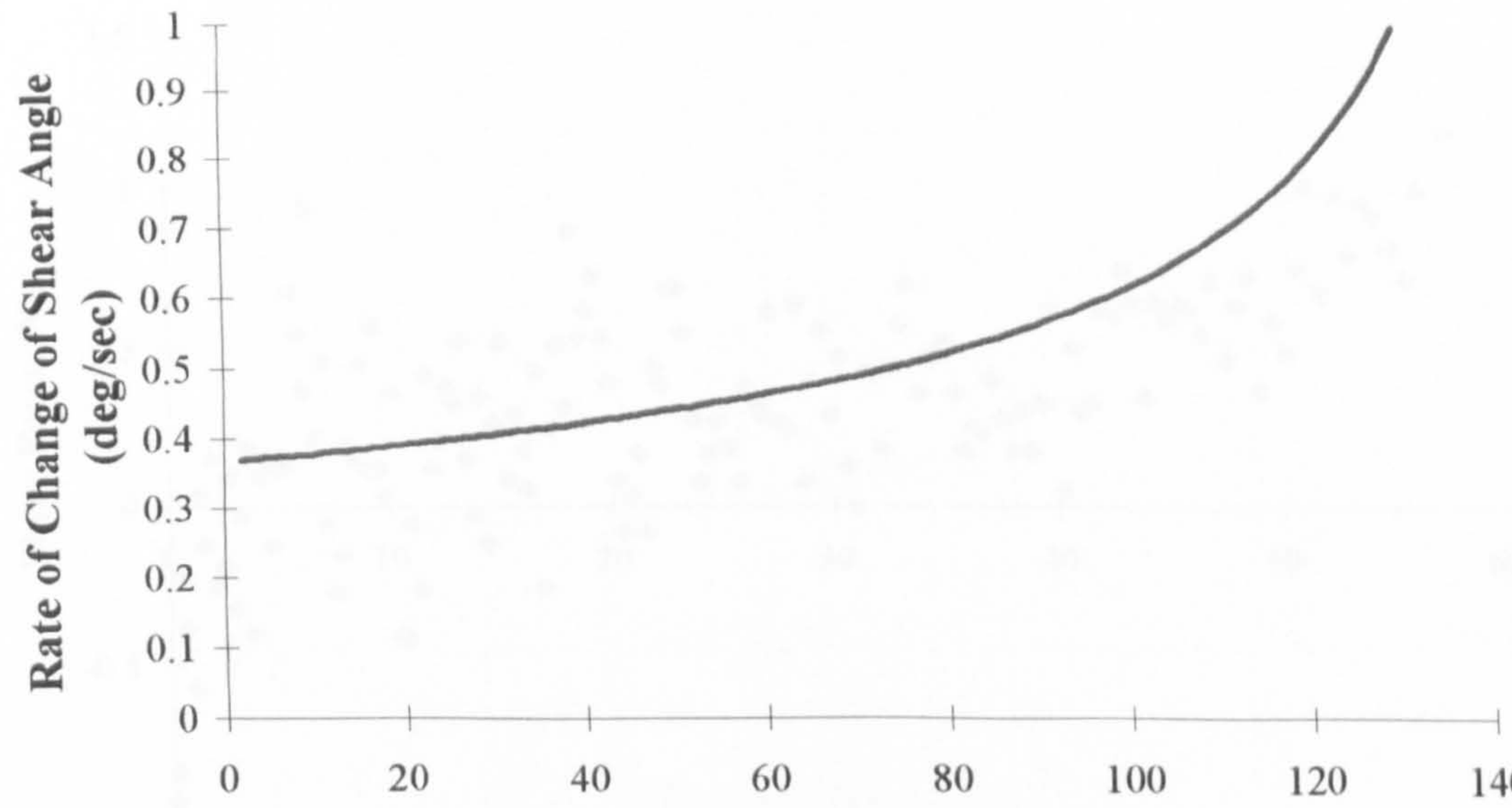

Figure 4.4 Rate of change of shear angle versus crosshead extension through range of travel of experimental shear rig, at 68 mm/min crosshead velocity.

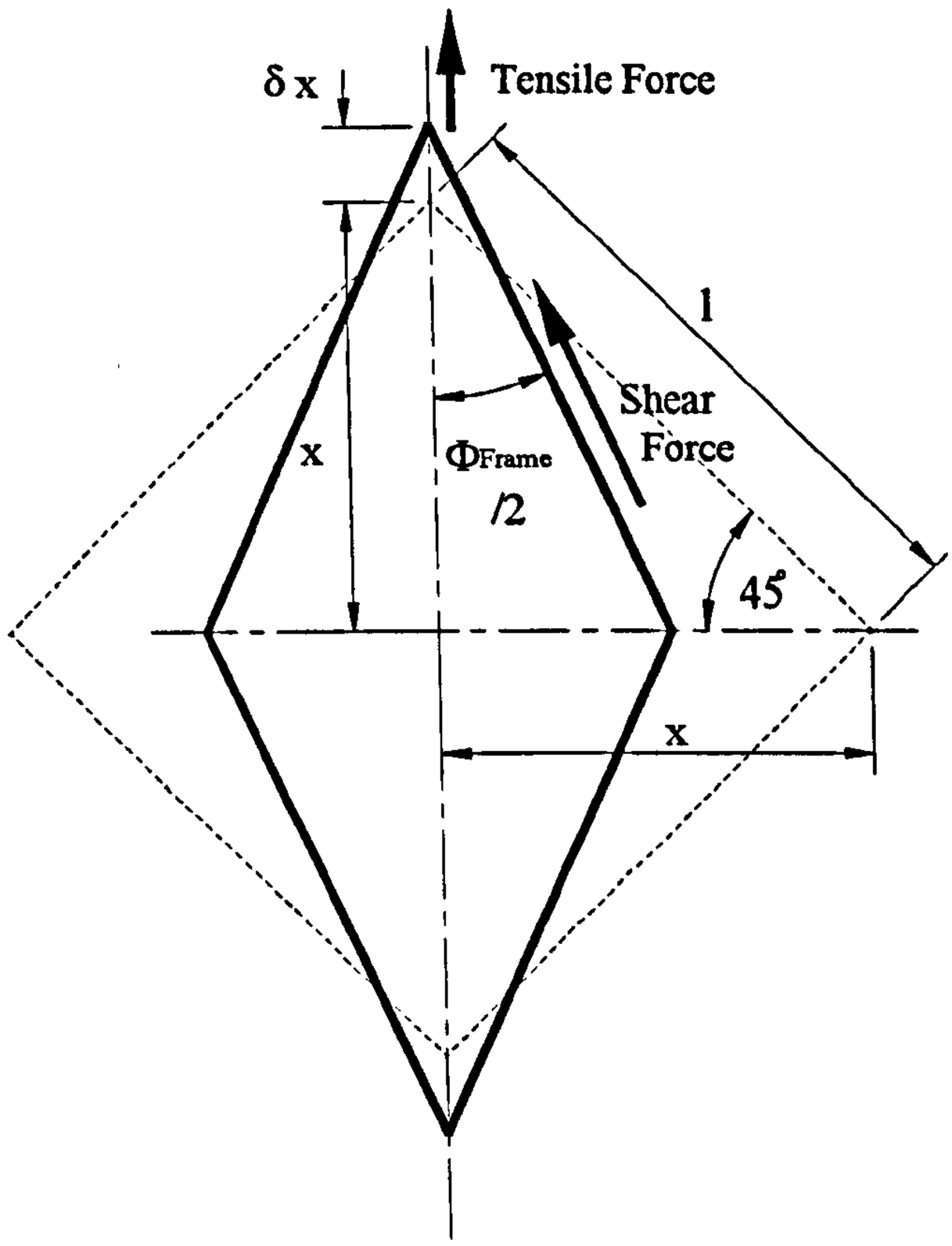

Figure 4.5 Experimental shear rig geometry and force diagram showing zero in-plane shear (indicated by a dotted line) and sheared positions (solid line).

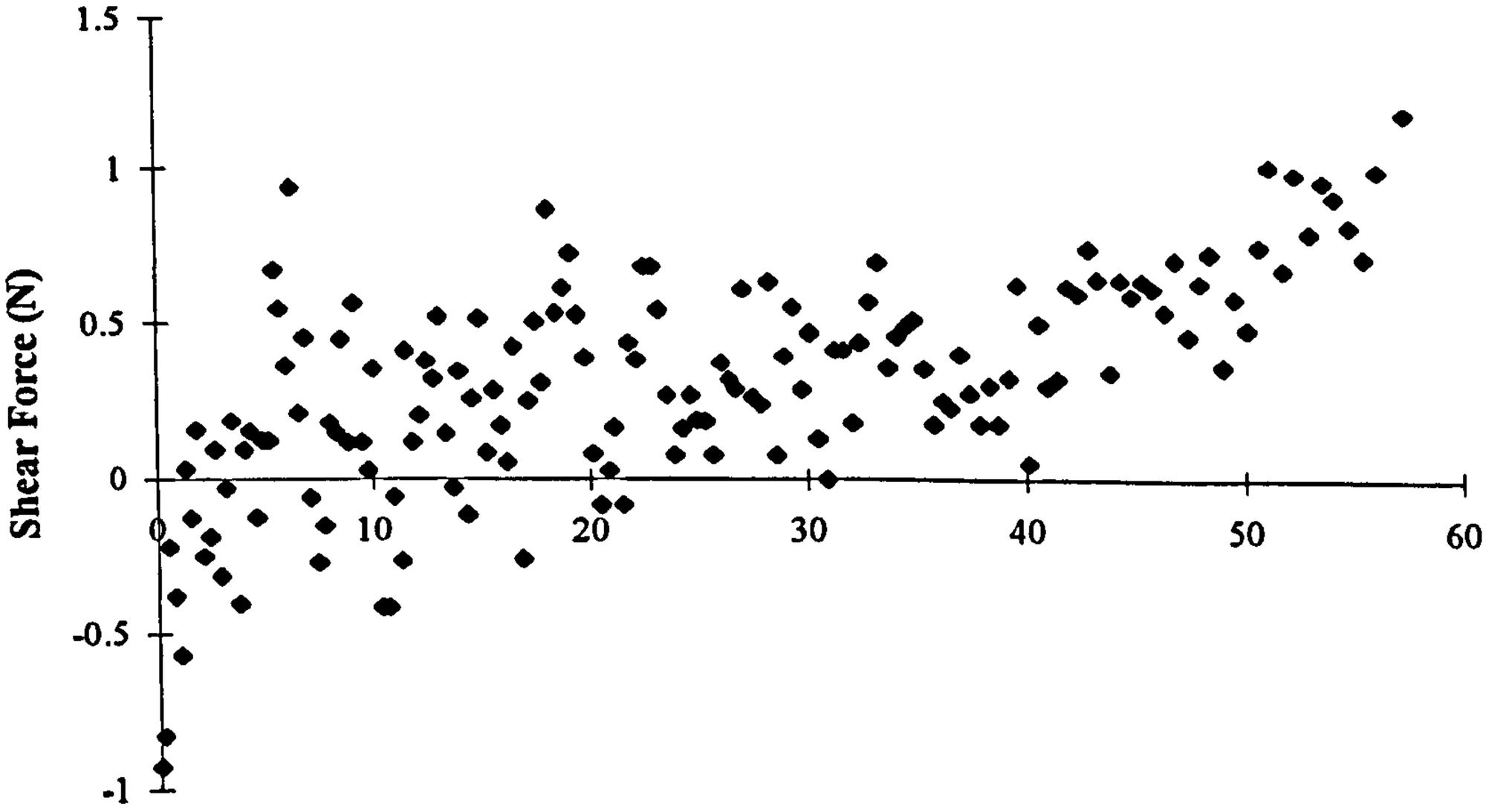

Figure 4.6 Plot of shear force versus shear angle for empty shear rig - 1020 mm/min crosshead velocity.

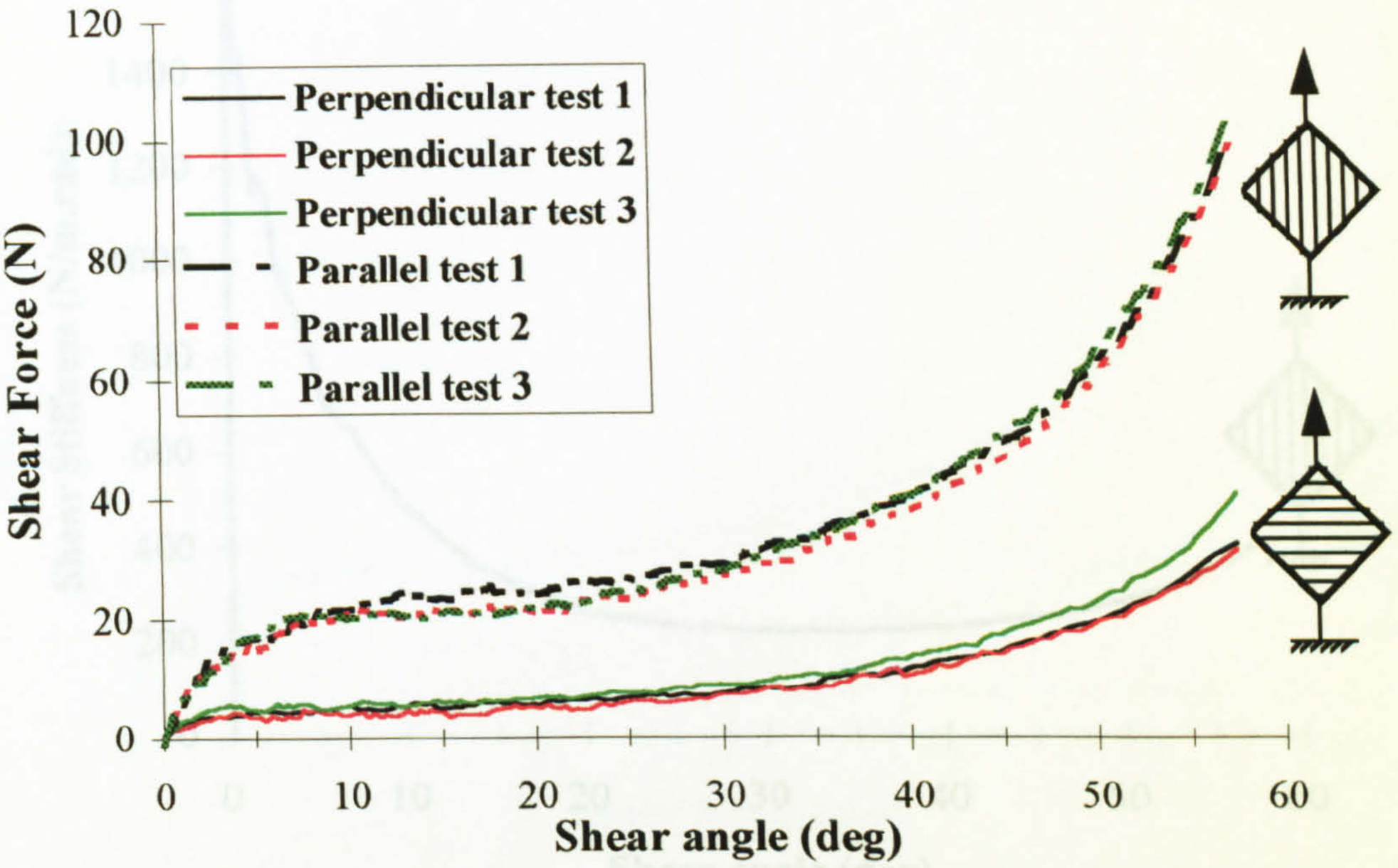

Figure 4.7 Repeated in-plane shear force versus shear angle plots for stitch bonded fabric with stitch orientated perpendicular and parallel to load.
(Tech Textiles E-BX 948 at 68 mm/min crosshead velocity.)

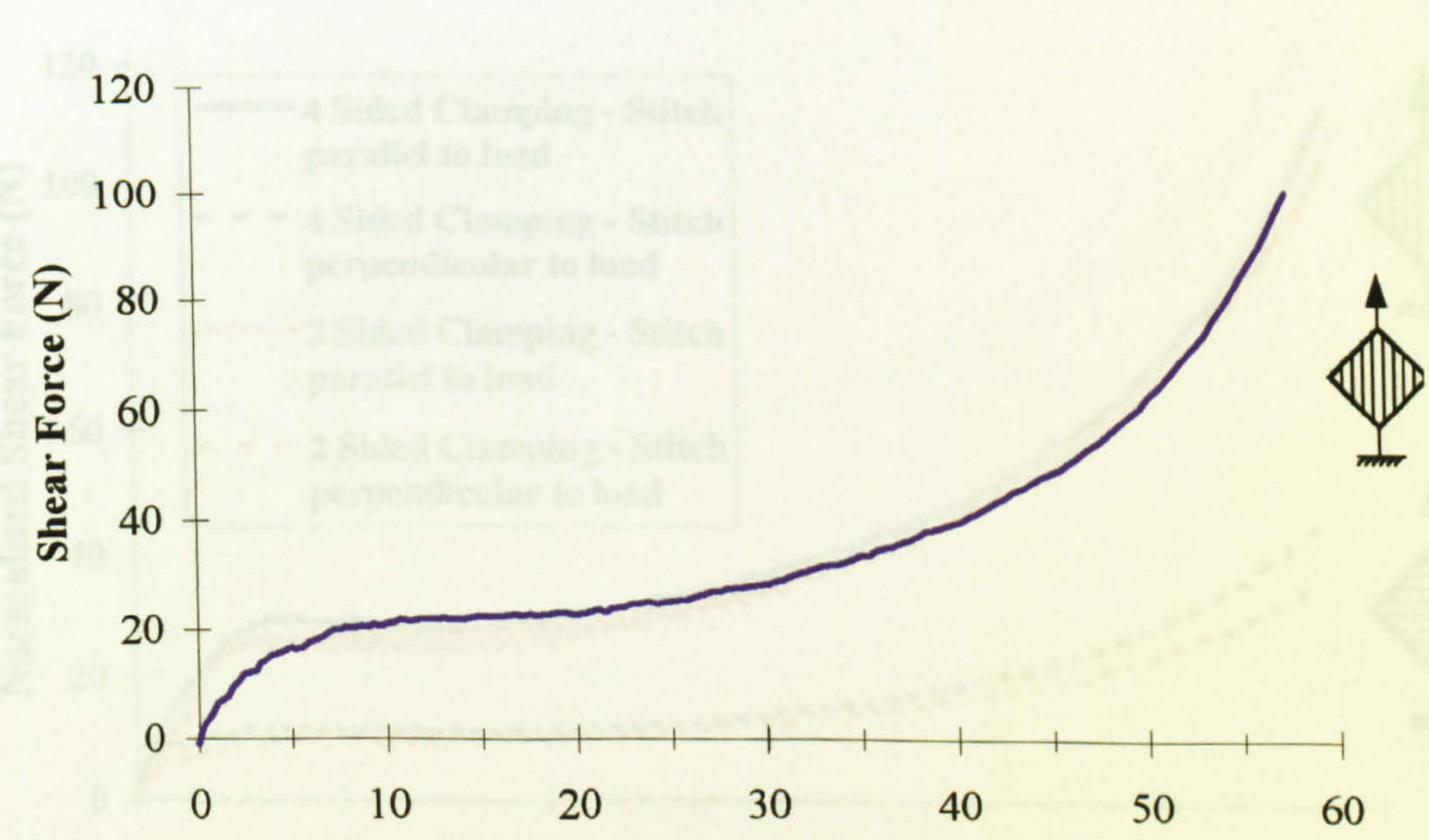

Figure 4.8 Average shear force versus shear angle for stitch bonded fabric, stitch orientated parallel to load. (Tech Textiles E-BX 948 at 68 mm/min crosshead velocity.)

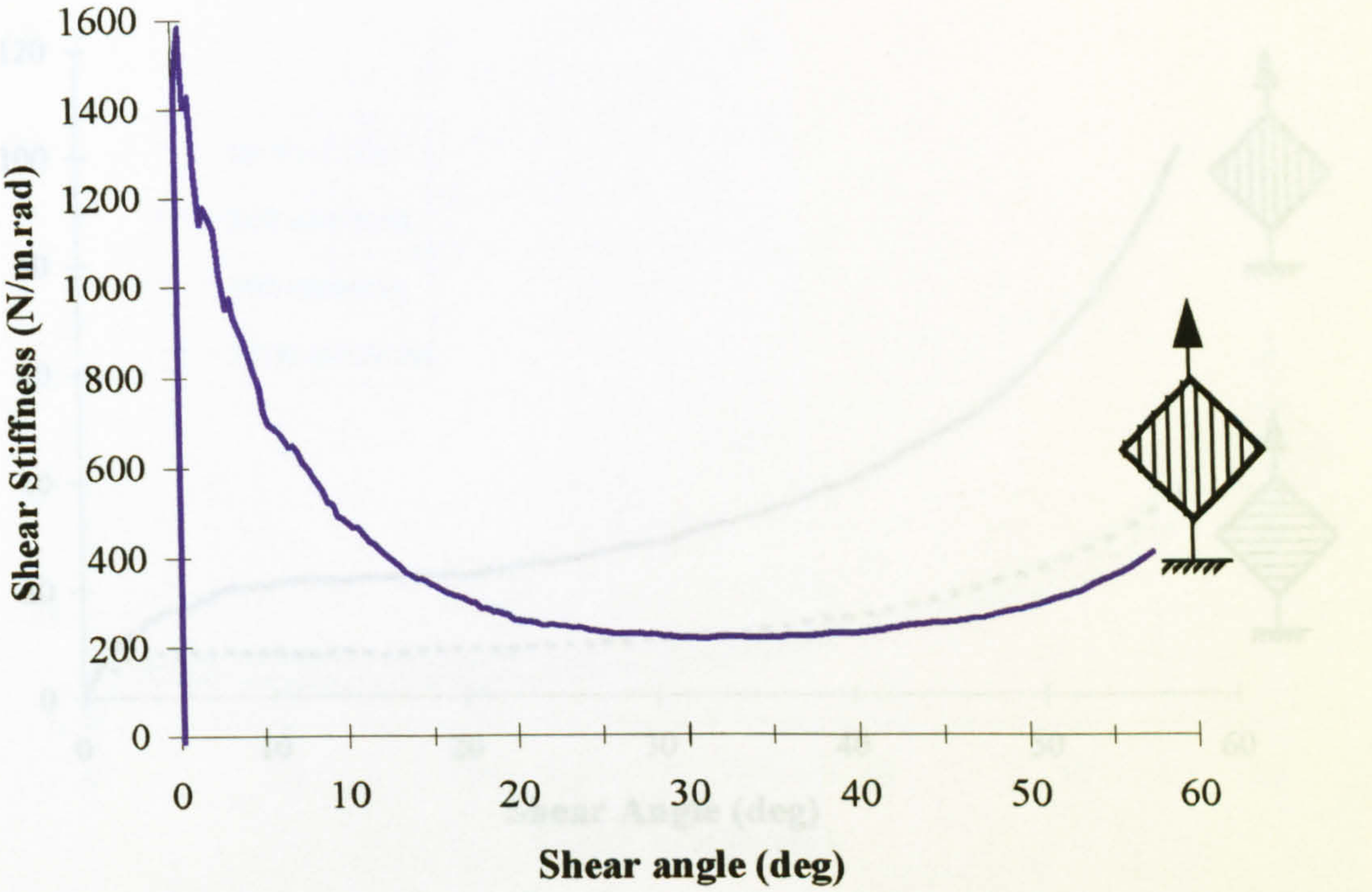

Figure 4.9 Average shear stiffness versus shear angle corresponding to Figure 4.8.

(Tech Textiles E-BX 948 at 68 mm/min crosshead velocity.)

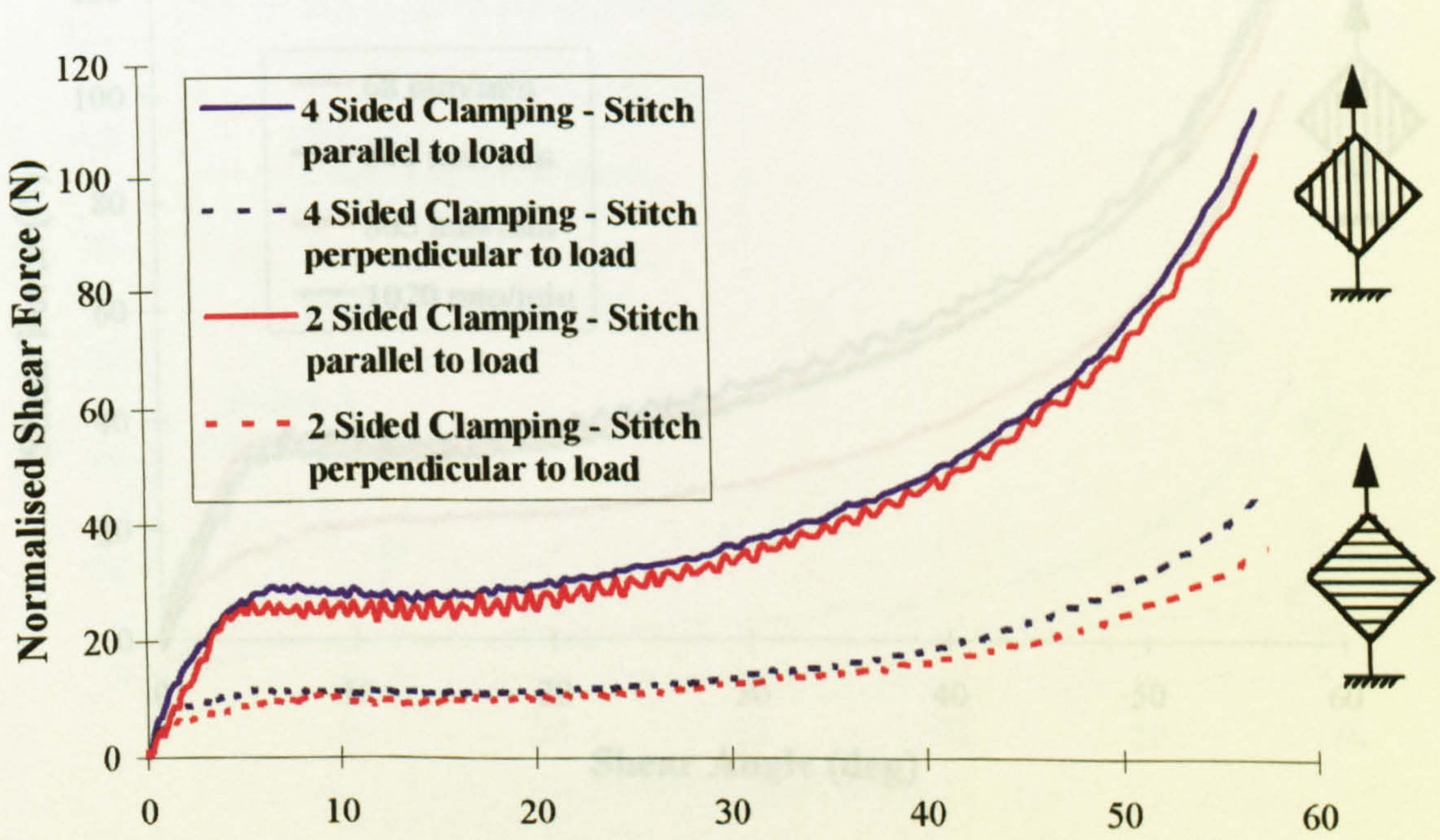

Figure 4.10 Comparison of two and four sided fabric clamping on shear force.

(Tech Textiles E-BX 948 at 1020 mm/min crosshead velocity.)

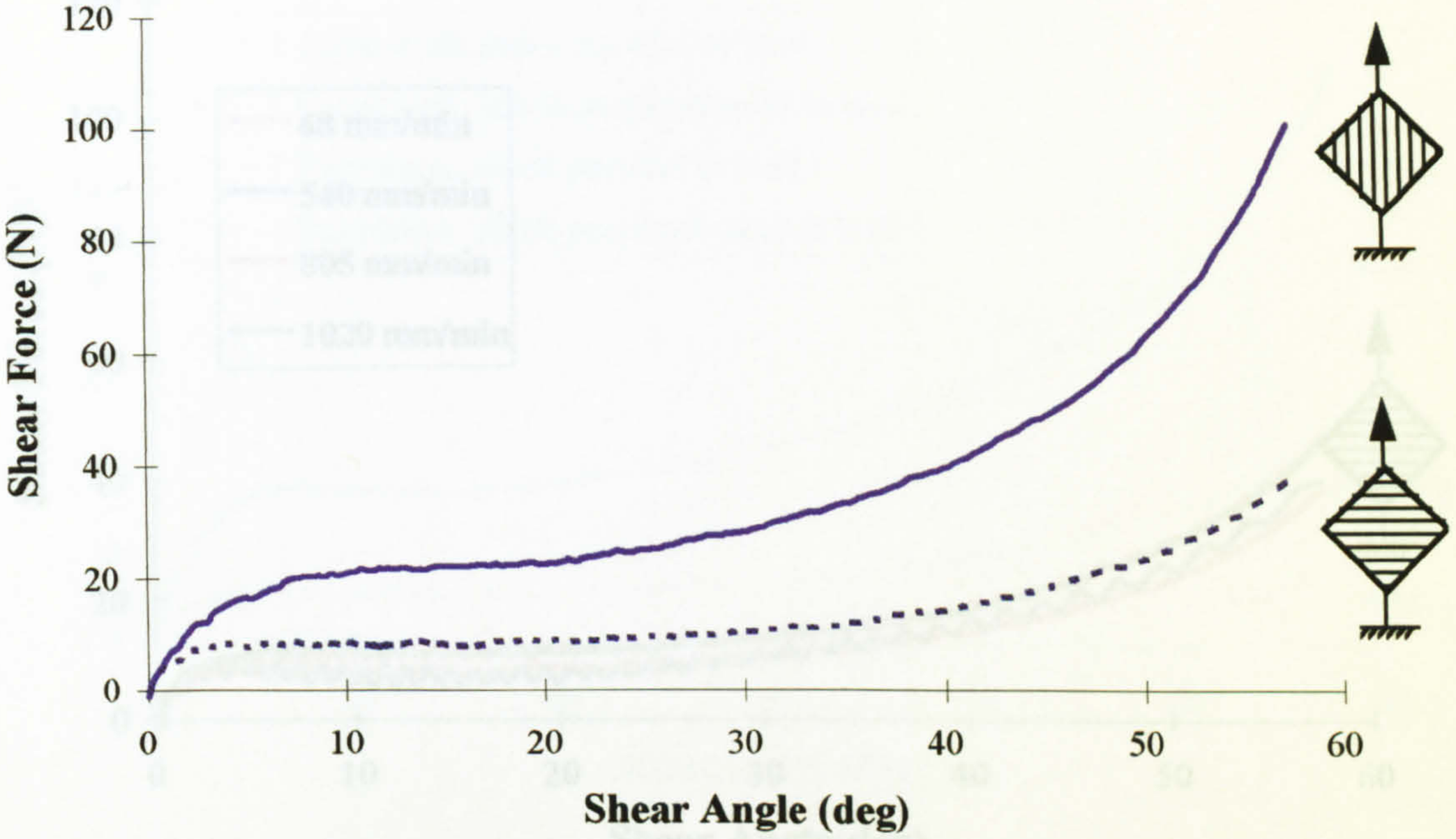

Figure 4.11 In-plane shear force for tricot stitched fabric with the load parallel and perpendicular to the stitch. (Tech Textiles E-BX 948 at 68 mm/min crosshead velocity.)

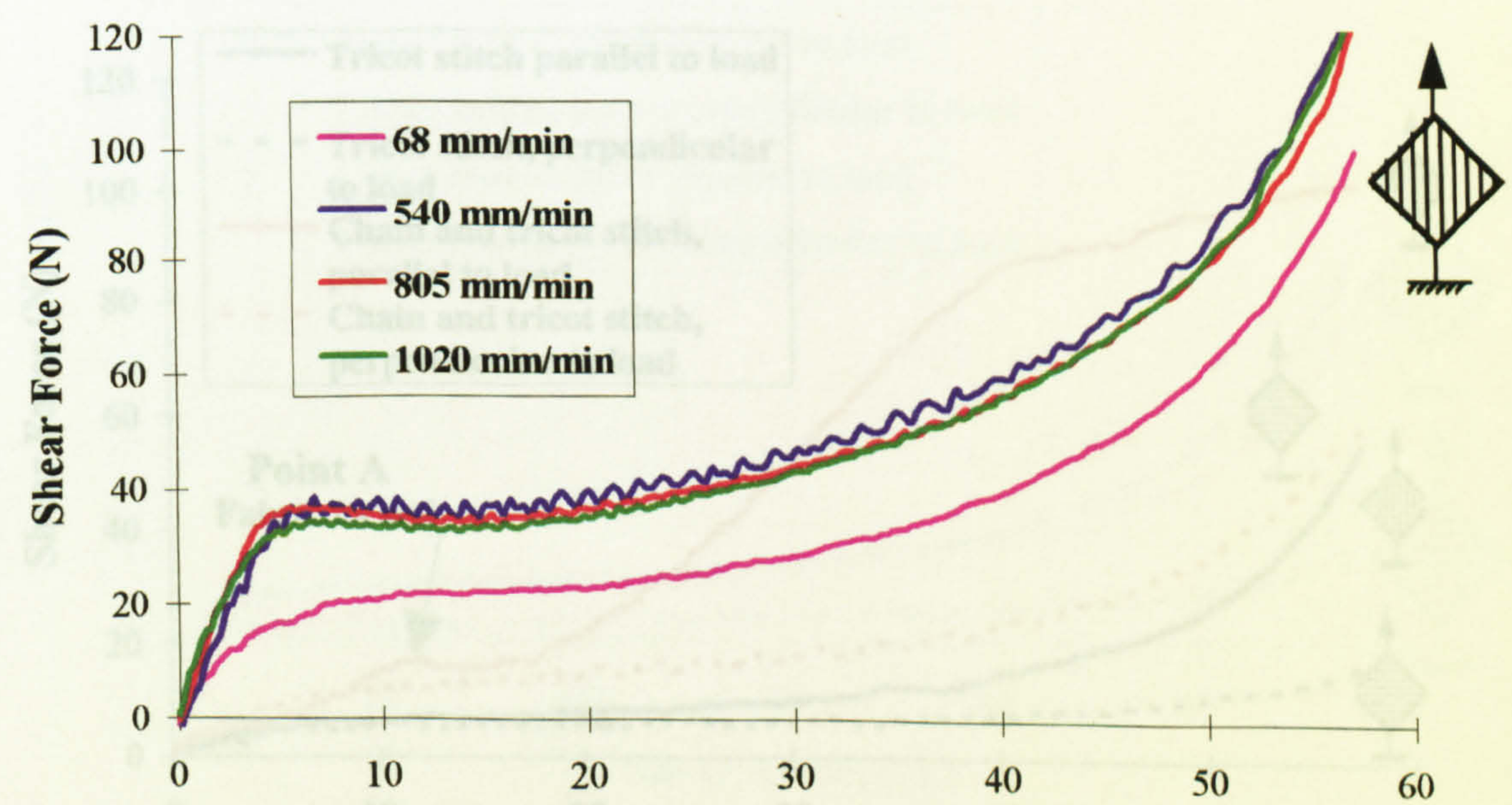

Figure 4.12 Tricot stitched fabric loaded parallel to stitch at various crosshead velocities. (Tech Textiles E-BX 948.)

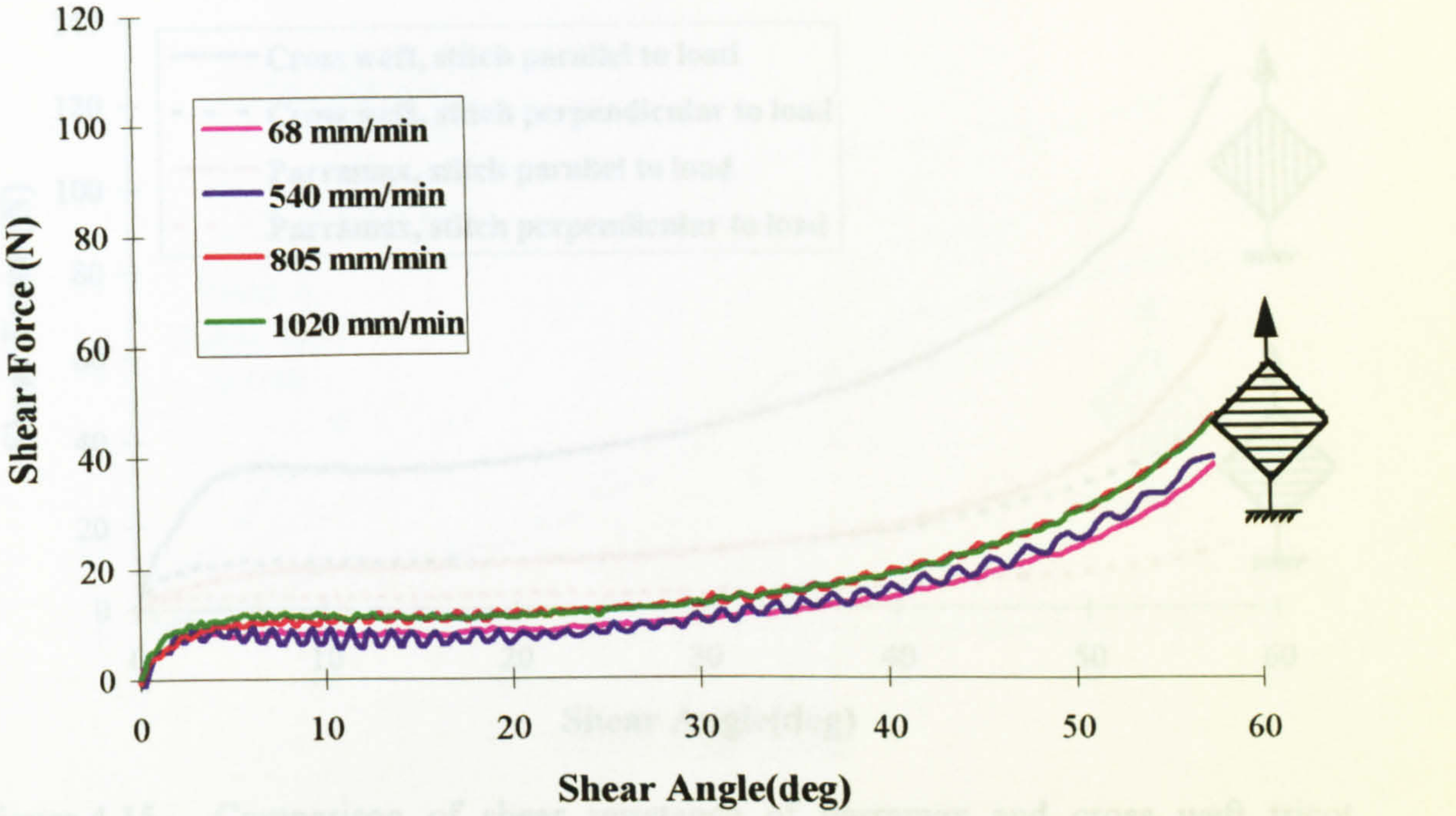

Figure 4.13 Tricot stitched fabric loaded perpendicular to stitch at various crosshead velocities. (Tech Textiles E-BX 948.)

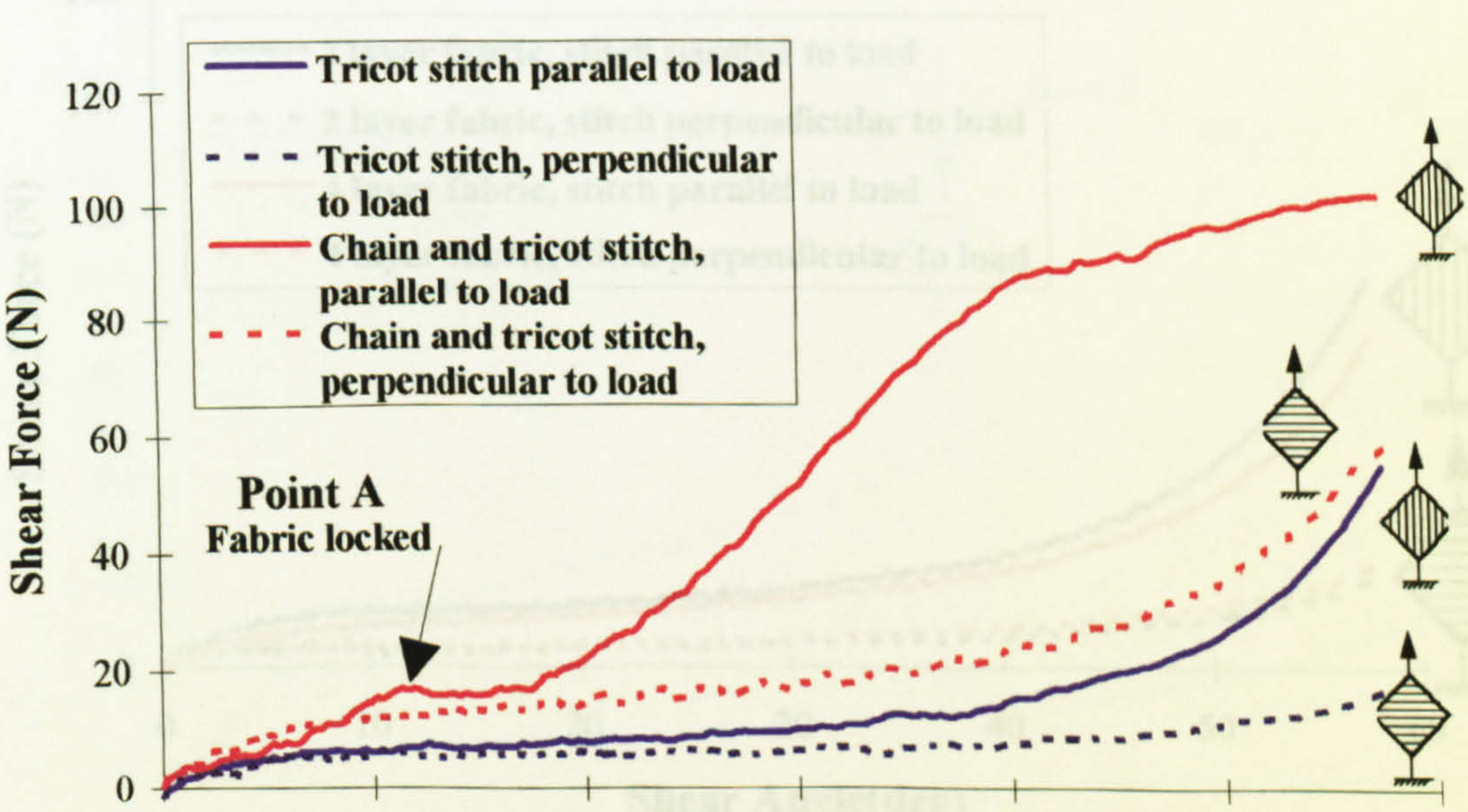

Figure 4.14 Comparison of shear resistance of tricot and tricot and chain stitched fabrics. (Tricot - Tech Textiles E-BXhd 936, Tricot and chain - Flemmings BUC 800, at 68 mm/min crosshead velocity. Note:- Locking (due to stitch) occurred at approximately 12° shear in chain and tricot stitched fabric when loaded parallel to stitch.)

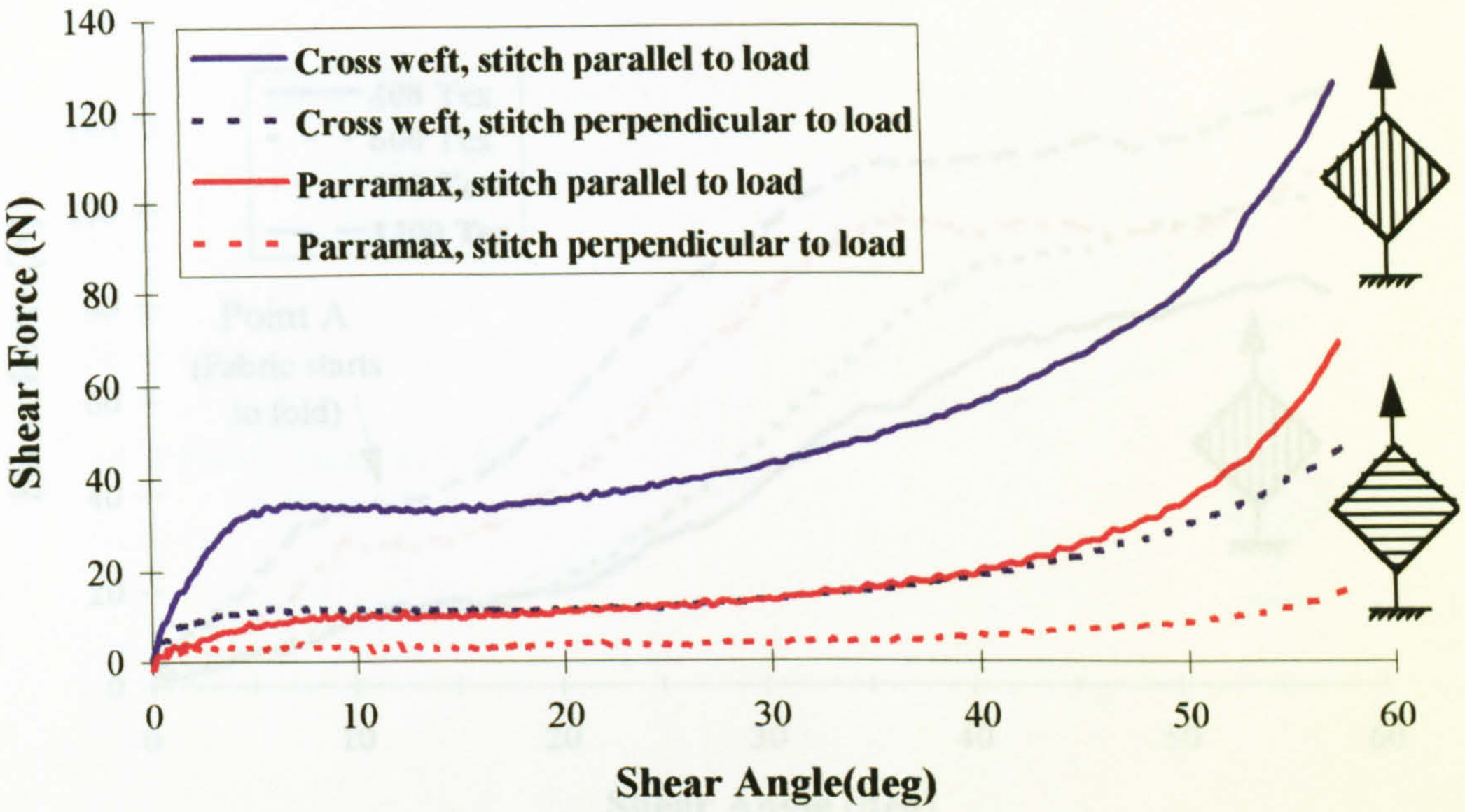

Figure 4.15 Comparison of shear resistance of parramax and cross weft tricot stitched fabrics. (Parramax - Tech Textiles E-BXhd 936, Cross weft - Tech Textiles E-BX 948, at 1020 mm/min crosshead velocity.)

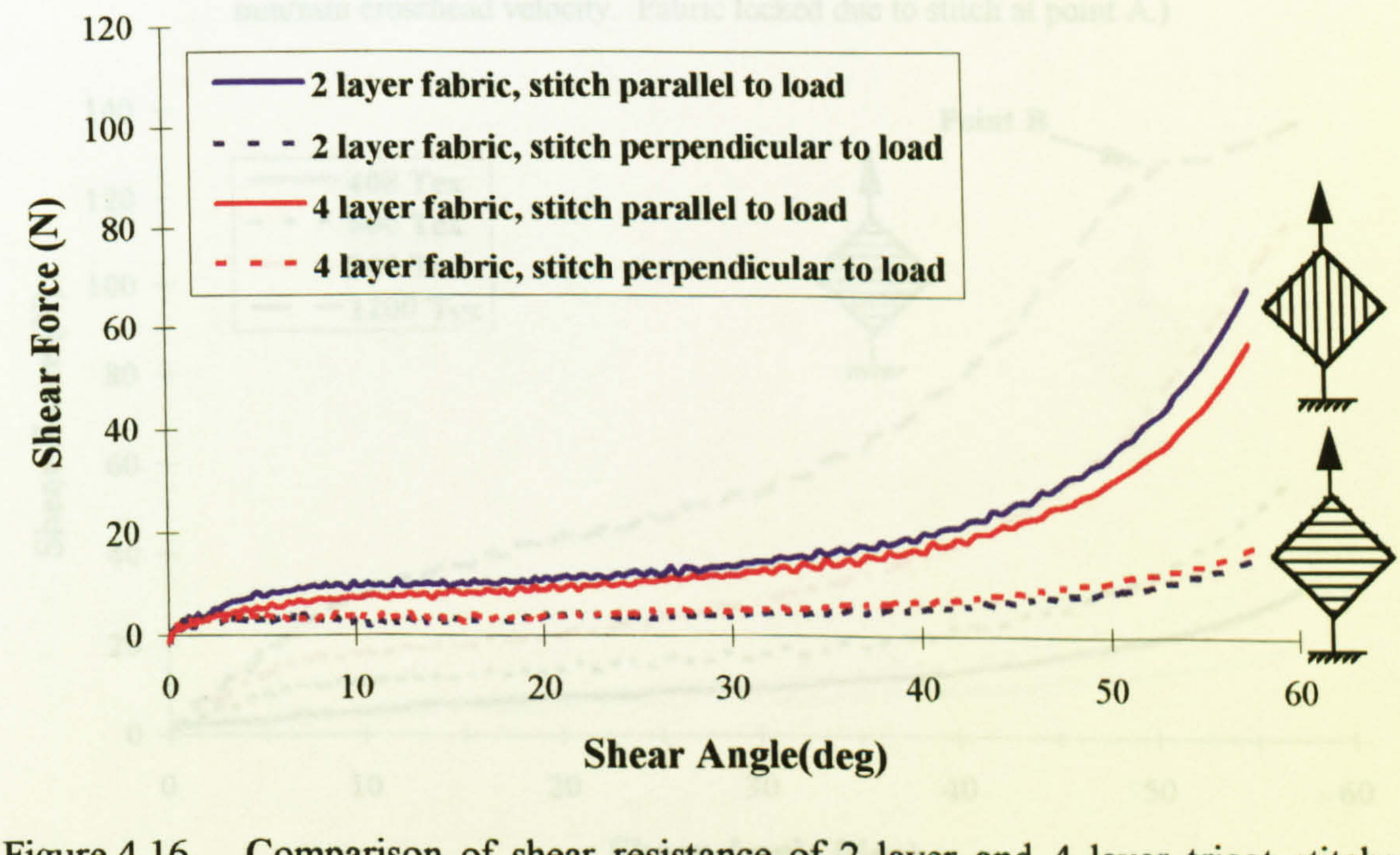

Figure 4.16 Comparison of shear resistance of 2 layer and 4 layer tricot stitched fabrics. (2 layer - Tech Textiles E-BXhd 936, 4 layer - Tech Textiles E-bBXhd 892, at 1020 mm/min crosshead velocity.)

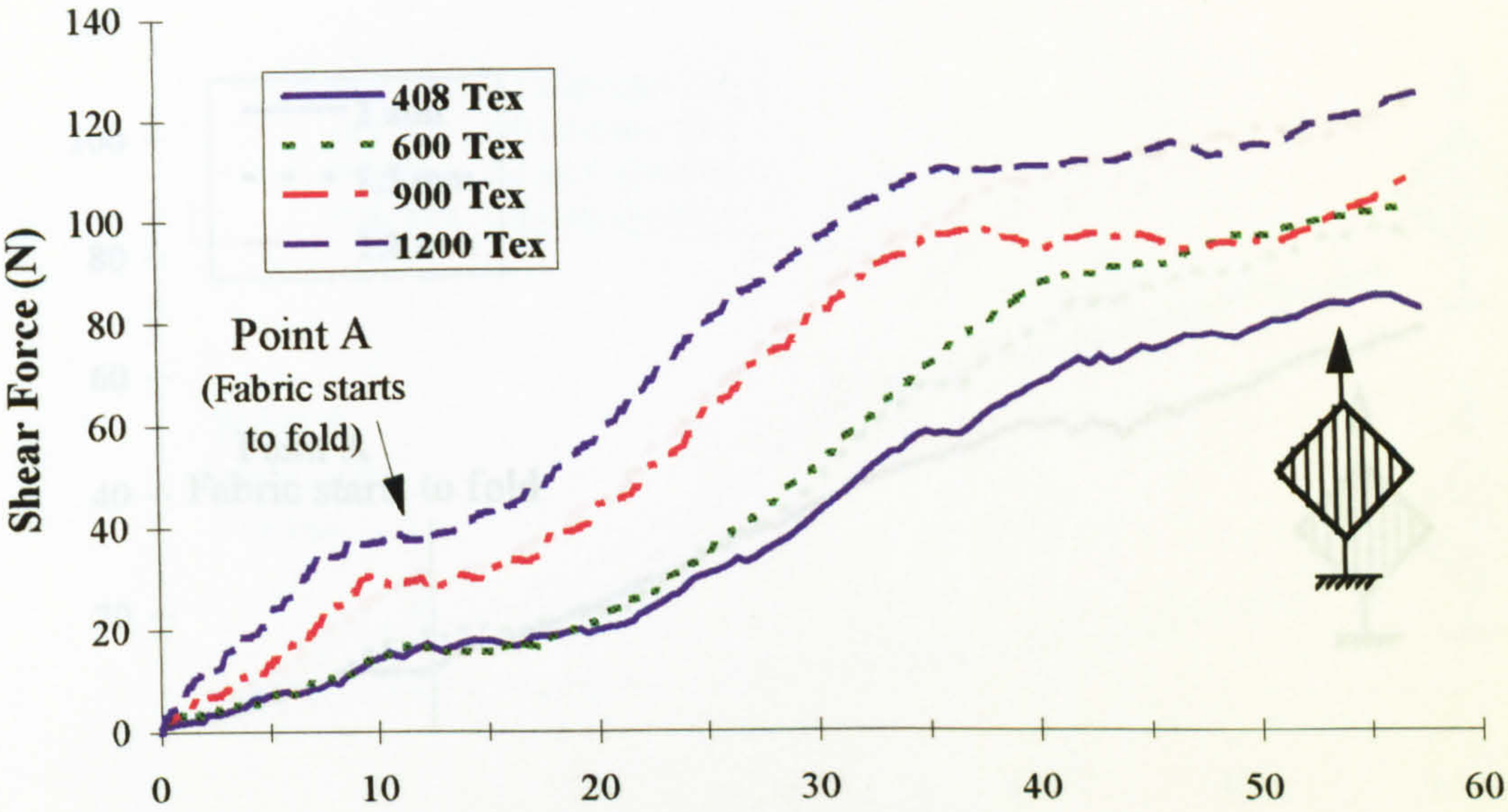

Figure 4.17 Tricot and chain stitched fabric with varying yarn linear density loaded parallel to stitch. (408 Tex: Flemmings BUC 545, 600 Tex: Flemmings BUC 800, 900 Tex: Flemmmings BUC 1200, 1200 Tex: Flemmings BUC 1600, at 68 mm/min crosshead velocity. Fabric locked due to stitch at point A.)

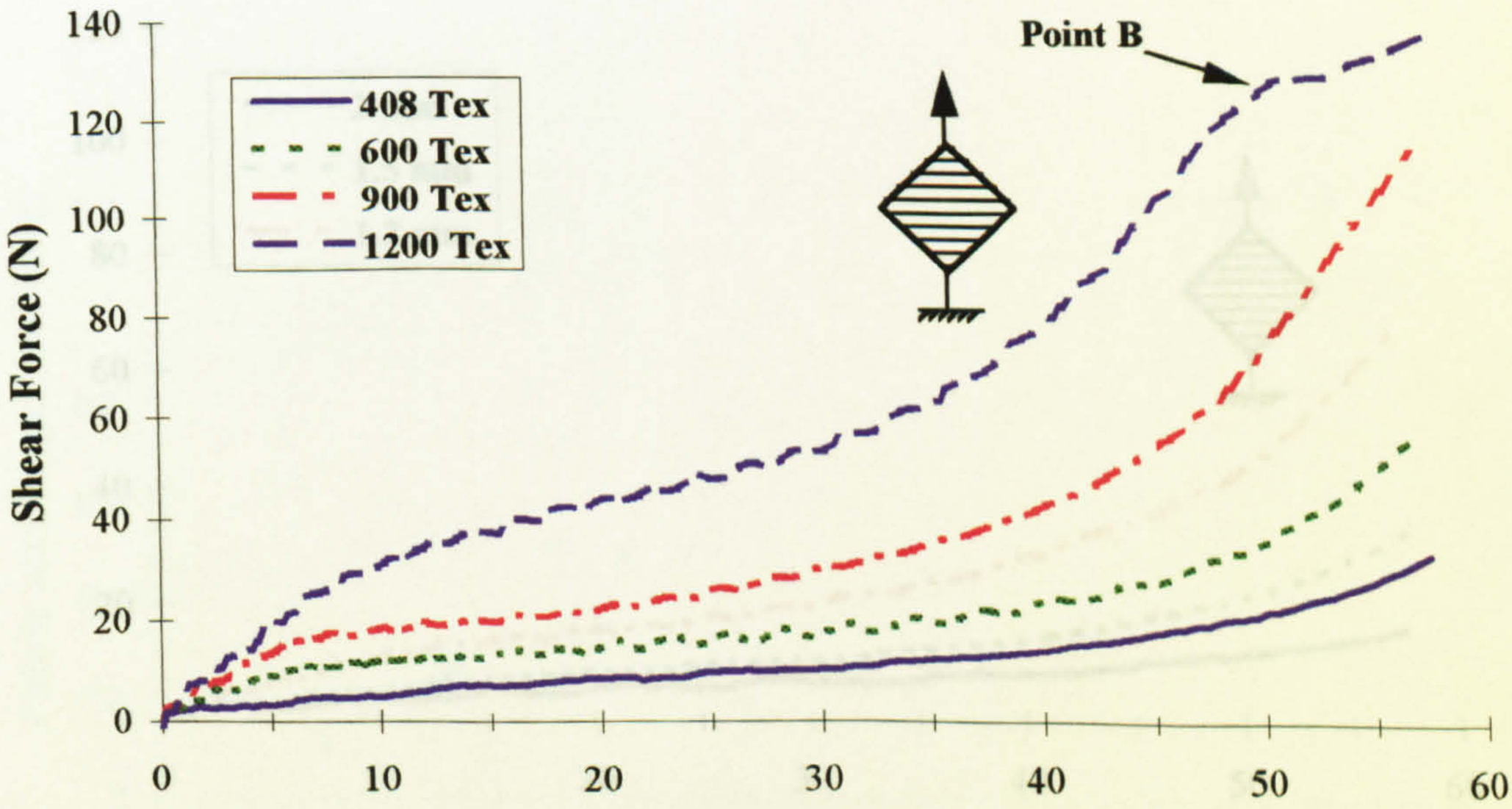

Figure 4.18 Tricot and chain stitched fabric with varying yarn linear density loaded perpendicular to stitch. (408 Tex: Flemmings BUC 545, 600 Tex: Flemmings BUC 800, 900 Tex: Flemmings BUC 1200, 1200 Tex: Flemmings BUC 1600, at 68 mm/min crosshead velocity. Fabric locked due to yarn compaction at point B.)

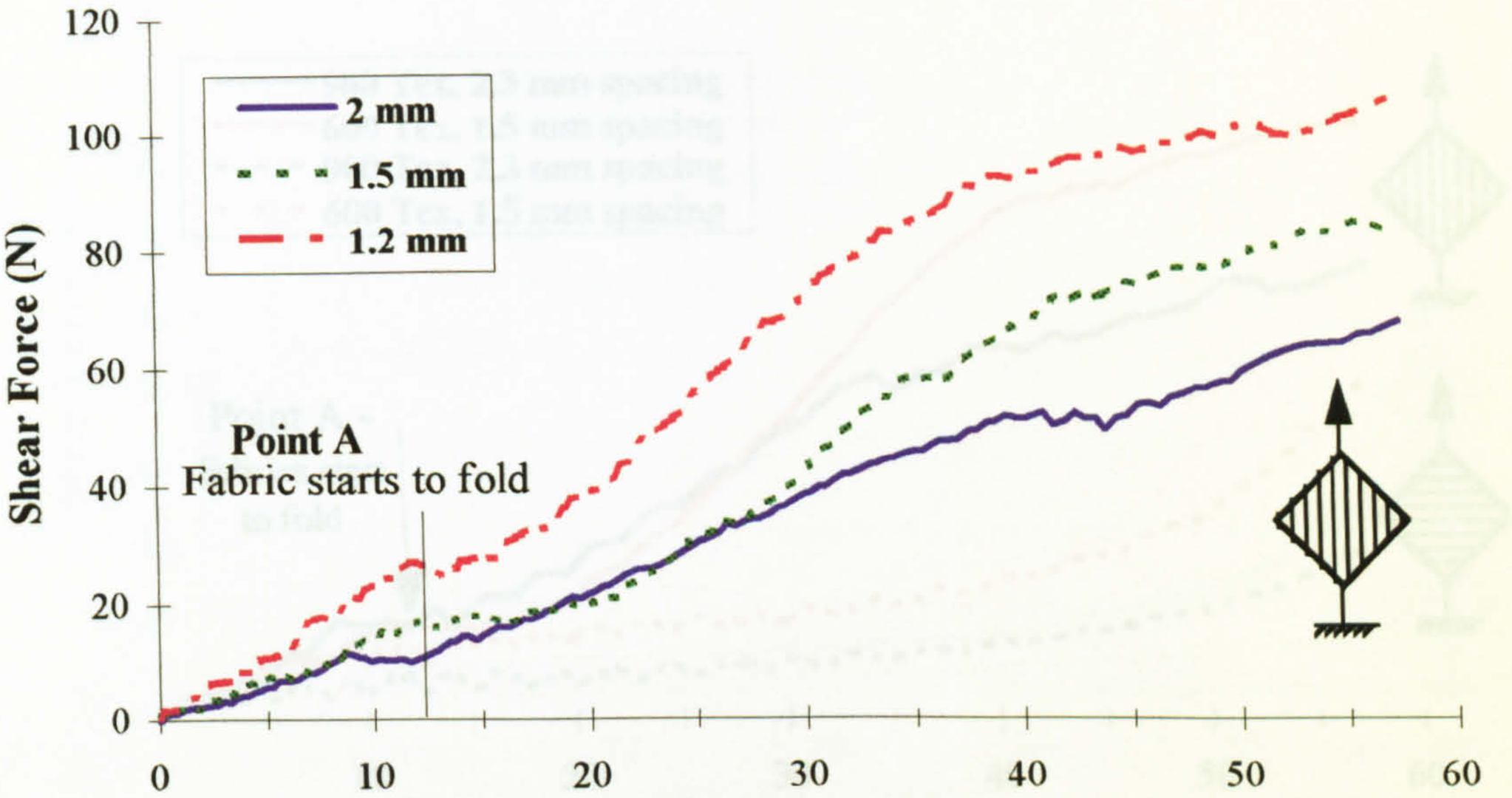

Figure 4.19 Tricot and chain stitch bonded fabric with varying yarn pitch loaded parallel to stitch. (2 mm - Flemmings BUC 403, 1.5 mm - Flemmings BUC 545, 1.2 mm - Flemmings BUC 682, at 68 mm/min crosshead velocity. Fabric locked due to stitch at point A.)

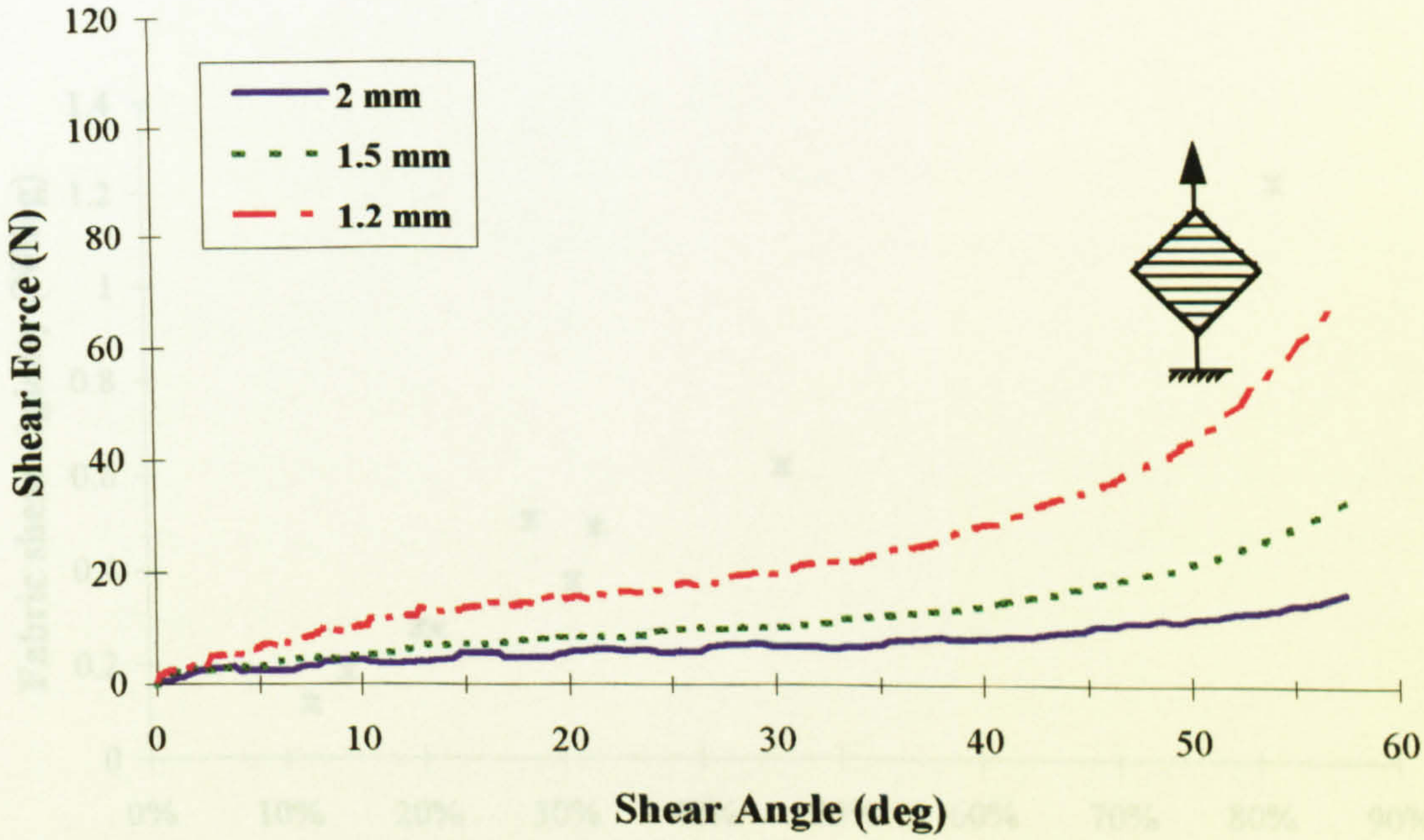

Figure 4.20 Tricot and chain stitch bonded fabric with varying yarn pitch loaded perpendicular to stitch. (2 mm - Flemmings BUC 403, 1.5 mm - Flemmings BUC 545, 1.2 mm - Flemmings BUC 682, at 68 mm/min crosshead velocity.)

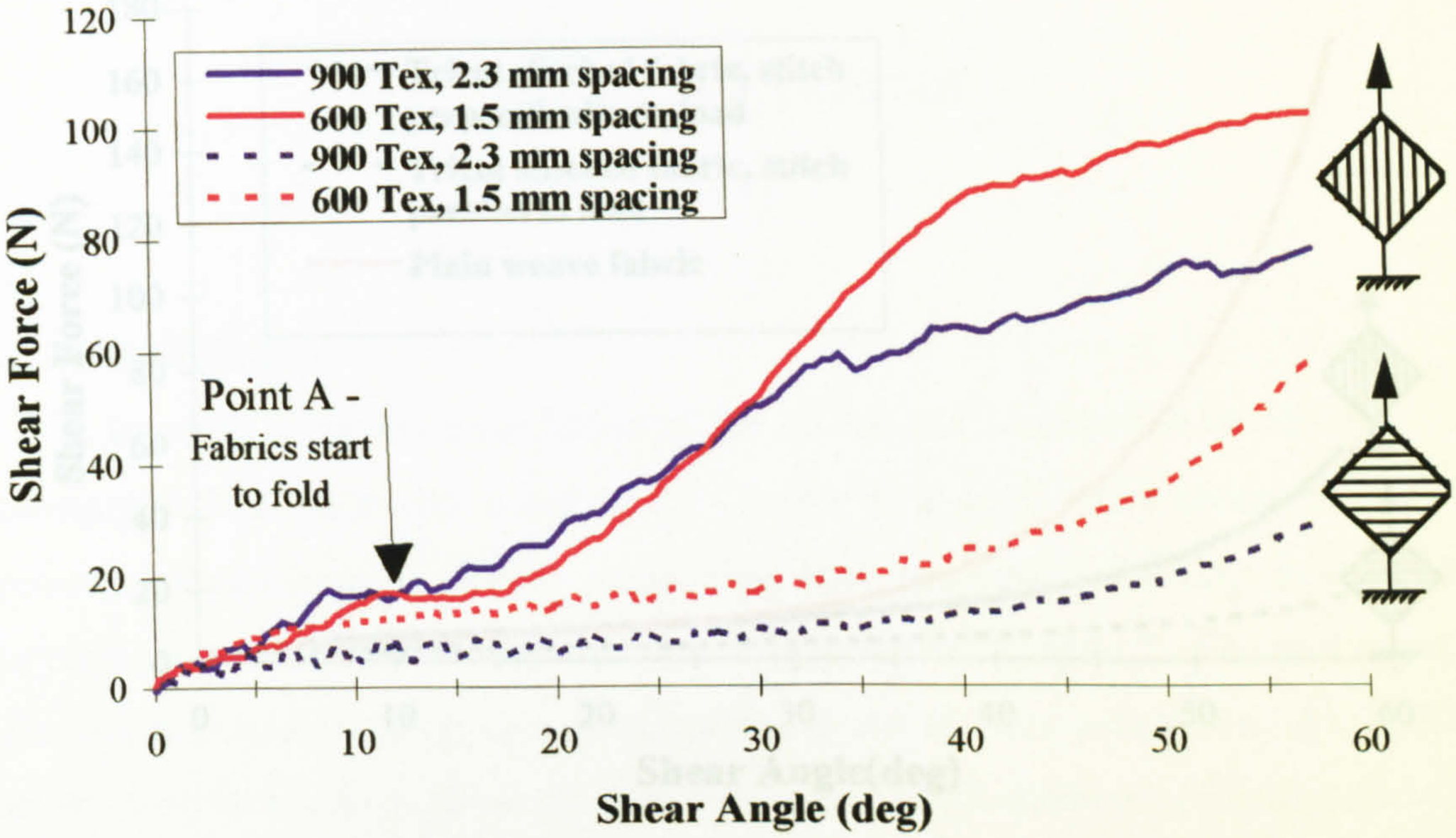

Figure 4.21 Tricot and chain stitched fabric with similar areal density, hence varying yarn pitch and linear density loaded parallel and perpendicular to stitch.
(900 Tex, 2.3 mm pitch - Flemmings BUC 786, 600 Tex, 1.5 mm pitch - Flemmings BUC 800, at 68 mm/min crosshead velocity.)

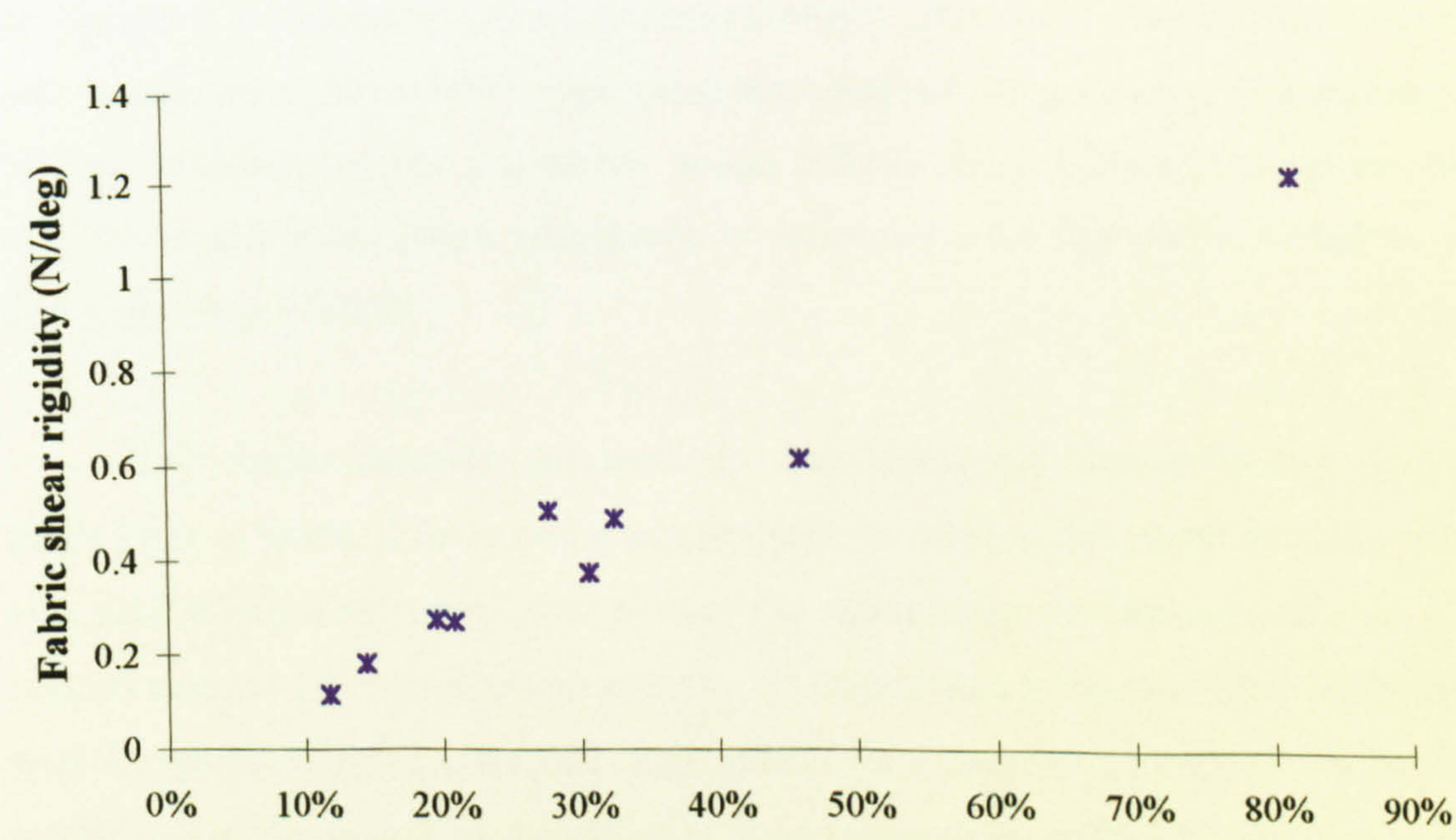

Figure 4.22 Fabric stiffness versus inter layer contact area for tricot and chain stitched fabrics loaded perpendicular to stitch at 68 mm/min crosshead velocity.

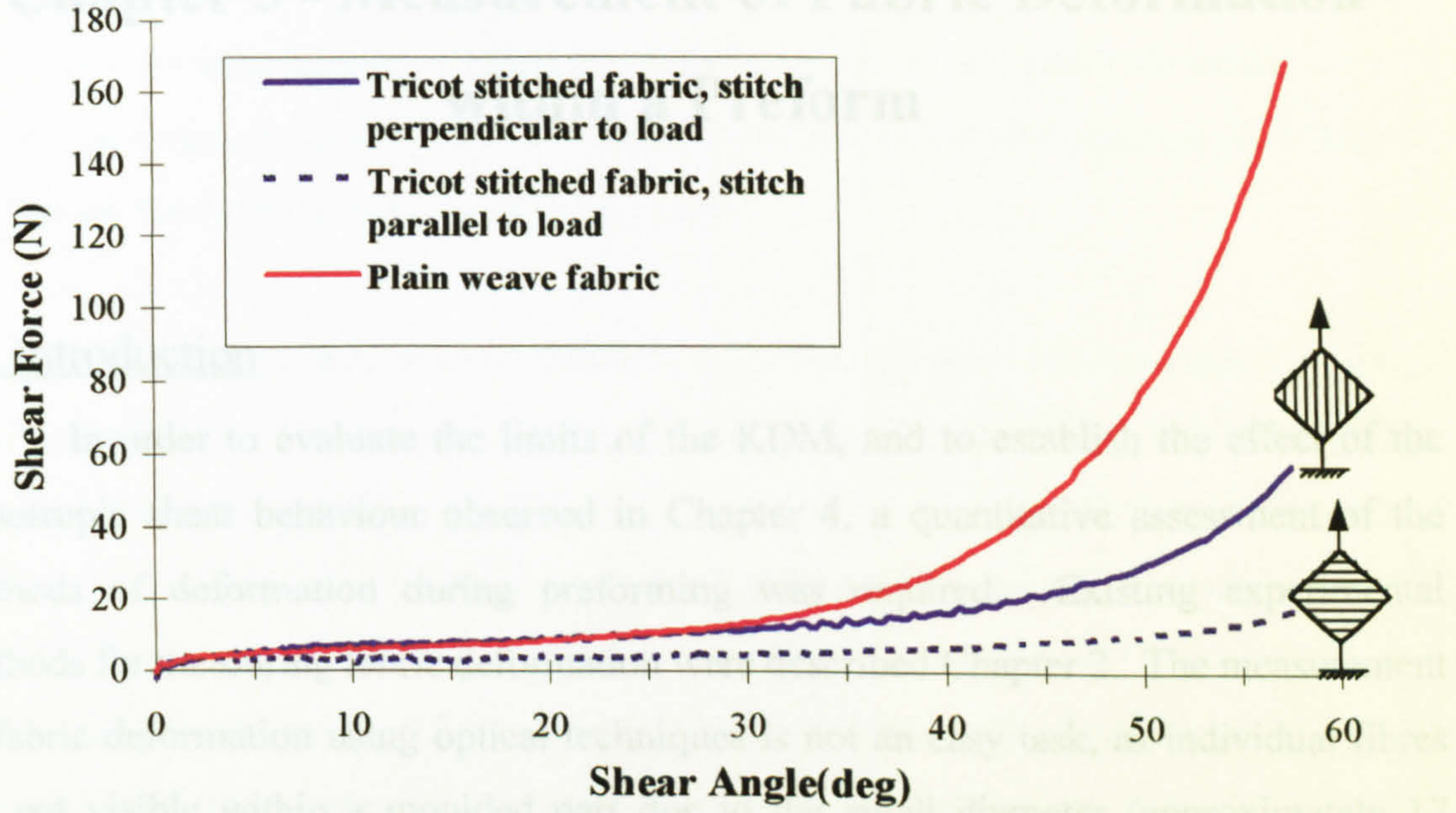

Figure 4.23 Shear force versus shear angle for a stitch bonded fabric and a woven fabric of similar areal density. (Stitched - Tech Textiles E-bBXhd 892, Woven - FGI plain weave (840 g/m^2) at 1020 mm/min crosshead velocity.)

Chapter 5 - Measurement of Fabric Deformation within a Preform

5.1 Introduction

In order to evaluate the limits of the KDM, and to establish the effect of the anisotropic shear behaviour observed in Chapter 4, a quantitative assessment of the methods of deformation during preforming was required. Existing experimental methods for measuring fabric deformation were described Chapter 2. The measurement of fabric deformation using optical techniques is not an easy task, as individual fibres are not visible within a moulded part due to the small diameter (approximately 17 microns) and labour intensity of the process. Therefore previous workers have generally measured properties such as volume fraction and used these along with experimental property data to infer the local fibre orientations.

A test technique was required that would allow direct measurement of fibre positions and orientations within a deformed fabric. This could quantify shear and slip deformation for a known fabric type, orientation and surface geometry. Comparing this with the kinematic model predictions would indicate the validity of the simple shear assumption and provide data with which to characterise the formability of fabrics and their deformation limits.

This chapter describes two methods of measuring the fibre architecture within a single layer of fabric. Firstly grid strain analysis was used to determine the deformation of a grid which was screen printed onto the fabric prior to forming. The grid co-ordinates enabled the deformation at each grid intersection to be calculated. The results were compared with the kinematic drape model for a range of geometries. Secondly a method based on measuring the elliptical aspect ratio of individual fibres from a cross-section of a moulded part was used. This was compared with the grid strain analysis method. The validity of the two techniques and the limits of the simple shear approach are discussed, along with suggestions for improving the experimental and data analysis techniques.

5.2 Grid Strain Analysis

An existing technique based on mapping a deformed grid (see section 2.6.1), which was originally developed to measure the strain in metal stampings, was adapted to measure the deformation of a fabric preform.

Three sets of tests were performed. The first consisted of disc shaped preforms of varying height. The second investigated the effect of initial fabric orientation when draping a truncated pyramid, and the third examined the effect of fabric architecture and forming rate on fabric deformation when formed over a hemispherical punch.

A 6.4 mm square grid was screen printed onto one side of the fabric, along with two red coloured perpendicular paths to allow comparison of a KDM predicted constrained path (see Chapter 3 for further details) for the part and the actual path of the equivalent 'constrained' yarns within the fabric.

5.3 Fabric Forming Techniques

The first two sets of test samples were produced using vacuum forming, while the third was produced using a modified stretch forming technique.

5.3.1 Vacuum Forming Method

A common E-glass biaxial fabric (Tech Textiles E-BXhd 948, Cross weft, tricot stitch) was used throughout the disc, pyramid and S-rail tests. Wooden formers were made to the required geometry and sealed with a varnish. The fabric was placed over the male former with the red grid lines running through the centre of the geometry, and formed using vacuum bag consolidation as follows (Figure 5.1). The fabric was sprayed with Minwax polyurethane varnish applied via an aerosol. A flexible vacuum bagging film was then placed over the tool and fabric, and the edges sealed using a tacky tape. Vacuum hose connection fittings were inserted through the film and attached to a pump. A vacuum was then applied, forcing the fabric to conform to the tool surface, and the varnish was allowed to cure.

Problems were encountered with bridging over sharp corners, as the vacuum tended to clamp the fabric onto the flat base before it could be drawn into the corners.

Initially this caused problems, as the KDM predictions assumed the fabric adhered to the surface geometry. To overcome this, a metal plate was cut to the outline of the male former, and was used to force the fabric into shape prior to vacuum consolidation (Figure 5.2).

5.3.2 Press Forming Technique

A computer-controlled hydraulic press [MTS Systems Corporation] was used to control punch speed as seen in Figure 5.3. A 100 mm diameter hemispherical punch was used to form the fabric as shown in Figure 5.4, with 2 mm clearance between the punch and upper die plate. The gridded fabric was placed in the press with the red lines signifying the constrained paths running through the axis of the punch. An aluminium disc, used to prevent the fabric base from splaying once formed (as seen in Figure 7.1), was placed on top of the fabric and the press platens were closed. The 2 mm clearance was maintained between the platens to ensure the fabric was not clamped, as this would cause the fabric to tear under tensile loads. The clamping force applied by the platens on the fabric could not be maintained to the required accuracy due to the press hydraulic control system being designed for the higher forces required for clamping metal samples. The press was closed to a pre-set stop and the 2 mm gap was adjusted using metal shims. The punch was programmed to provide 65 mm penetration at a range of speeds from 10 mm/s to 110 mm/s. This produced a hemispherical ended cylindrical preform. Once the fabric was formed it was rigidised with Minwax polyurethane varnish and grid strain analysis was used to map the deformed shape.

5.4 The Grid Strain Analysis System

5.4.1 CamSys Automated Strain Analysis and Measuring Environment

Once the fabric was formed and rigidised, the surface grid positions were measured using the CamSys Incorporated Automated Strain Analysis and Measurement Environment (ASAME) equipment. The equipment consisted of a PC based data analysis package linked to a digital image capture system (see Figures 5.5 and 5.6). The preform was placed onto the turntable, the position of which was measured by rotary transducer. A video camera was used to capture the image in digital form. This was positioned under PC control by stepper motor driven lead screws. Proprietary PC

based software stored the position of the camera and turntable, along with the digital image.

Two images were captured from different turntable angles, approximately 45° apart. These were processed by the software to produce a single pixel line grid, which was trimmed by the user to show the same area in each view. These views were then combined to determine a unique co-ordinate for each grid intersection [78]. More detailed information on the process is given in Appendix 5.1. The grid intersection co-ordinate data were output to a text file, which was post-processed to provide fabric deformation data such as inter-yarn shear angle and slip between grid intersections. This is described in Appendix 5.2.

5.4.2 Accuracy of the ASAME System

To aid interpretation of the data, an indication of baseline error was required. CamSys claim an accuracy of +/- 2% strain, if due care was taken in capturing the initial shots. This is likely to be more difficult to achieve with fabric due to the potential deformation induced by cutting and handling of the sample and blurring of the grid edges during the screen printing process. On a typical metal sample the grid (approximately 0.5 mm wide) is etched onto the surface chemically which gives a crisp line definition. The screen printing method used to print the grids onto the fabric produced a wider line (1.5 mm) with lower quality edge definition which was thought likely to decrease the test accuracy.

Two sample areas were chosen at random from a flat, gridded sheet of fabric and scanned. The arising image showed a maximum principal engineering strain of 3.8%. Figure 5.7 shows that the maximum strains occurred at the edges of the sample. This phenomenon also appeared on metal test samples [105], and is due to the way the software smoothes the surface (and hence the grid co-ordinates) to reduce effects of measurement error. It does this using a least squares fitting method [79].

The measurement accuracy could be improved by taking images at 45° to the surface and reducing the size of the area being scanned. In order to allow comparison of the KDM predictions with the experimental data, the imaging of a large grid area of approximately 77 mm square (a 12 x 12 grid) was required. This meant using the

concatenation process within the CAMSYS software to connect the overlapping edges of many small area grids (four 7 x 7 grids) to form one large grid of the area (a 13 by 13 grid). This proved difficult to implement on surfaces that were curved, as large errors could be introduced into the experimental data, due to averaging of the adjoining edge co-ordinates by the software to produce a smooth edge join. Therefore the data for the hemispherical preforms were collected by imaging the area of interest using one grid (approximately 10 by 10 grid elements), which only allowed comparisons of the curved portion of the preform. The disc and pyramid preforms were captured in four sets using up to 12 by 12 grids which were successfully joined using the concatenation technique. Therefore the accuracy of the grids measured by the GSA method will at best correspond to that for the 10 by 10 grid shown in Figure 5.7, but for the larger disc and pyramid preforms it is likely to be worse.

To check the repeatability of the process, an undeformed area of gridded fabric was examined repeatedly, resetting the system between each set of scans. This gave a maximum difference of 2% between the strain readings which was within the manufacturer's claims.

5.4.3 Post Processing of the Strain Data.

The standard ASAME output data was based on either major or minor principal strains. For the present study, these strains need to be presented as fabric shear angles and proportional slip. To extract the data in a form that was applicable to fabrics, a text file was produced containing x, y, z co-ordinates and strains at each grid intersection point.

Inter-yarn angles and slip data were calculated at each grid intersection. The distance between successive grid intersections (L'), was compared to the original grid spacing (L) to provide an estimate of slip in the fabric:

$$Slip(\%) = \frac{L' - L}{L} * 100 \qquad (5.1)$$

The angles between corresponding vectors on each side of a grid intersection were calculated and interpreted as the inter-yarn angle (ϕ) at each point [Appendix 5.2]. From this and knowledge of the initial inter-yarn angle, the inter-yarn shear angle (θ_s) can be calculated as defined in section 2.3.

A graphical representation of the shear and slip deformation was produced using Advanced Visual Systems inc. (AVS) software running on a Silicon Graphics Workstation. The geometric data from the ASAME text file was used to construct an image of the deformed mesh, upon which the inter-yarn angles were represented by a colour scale applied to the surface, and the slip by a colour scale applied to a grid representing the mesh (See Figure 5.8).

The slip and inter-yarn angle data were written to separate AVS format input files to allow graphical inspection of the results as shown in Figure 5.8. The inter-yarn shear angle at each grid intersection point was chosen as the basis for comparison between the KDM and the experiments as the exact ply angle could not be measured for non +/- 45° fabrics. Other comparisons such as grid position within 3 dimensional space were considered but proved to be unsuitable due to the lack of comparable datum points between the experimental results and predicted data.

5.4.4 Possible Errors due to Local Curvature

The method for calculating the experimental slip value from the co-ordinate data assumes the grid follows a straight line between the measured grid intersection points. This may not be true in certain cases. Around small radii the calculated, direct distance between grid intersections can be smaller than the true path across the surface, thereby producing "negative slip" results which are, of course, erroneous (Figure 5.9). This will subsequently be referred to as the experimental edge effect, and taken into consideration when examining the slip distributions. Given an equation for the geometry that was draped, and a common set of vectors between the surface and the measured grid, the true distance between the points across the surface and thereby the error could be calculated. This was not attempted for the data presented here, as a common set of datum points between the measured grid and the model surface geometry could not be established accurately.

The error due to the experimental edge effect is calculated from the actual and vector distances between the points. This varies from 0 % to a maximum -30 % of the original grid spacing (Figure 5.10) depending upon the position of the grid intersections relative to the patch edge (denoted by x1 in Figure 5.9).

$$Error = \frac{D_{Actual} \cdot D_{vec}}{D_{Actual}} \qquad (5.2)$$

This approach is only valid if no slip has occurred in the fabric (as it would be removed from the data) and assumes that the reference point for comparison between the data (in this case the red lines representing the constrained path) passes through the centre of the part.

This effect was most noticeable in the discs of varying heights (section 6.3). This was due to small radii at the upper and lower edges of the cylindrical portions. Due to the handling process, approximately 2 mm error in the positioning of the constrained path intersection may have occurred. This corresponds to a maximum error of 24 % (Figure 5.10), that could be introduced by the incorrect use of a correction factor. Therefore the data in this report have not been corrected to allow for the experimental edge effect.

This same effect will produce smaller errors for curved surfaces, producing a smaller distance between the points than the path of the yarn (Figure 5.11). Again, this may produce erroneous slip values. For uniformly curved surfaces such as a hemisphere, a correction factor can be calculated from the radius and grid size and applied to the slip data. This was calculated for the experimental data obtained from hemispherical preforms presented in Chapters 6 and 7. The precise method is described in Appendix 5.3.

All of the discussion so far assumes that the grid deformation corresponds to that within the fabric. This may be true for the upper surface of the fabric (upon which the grid is printed), but may not hold for the underside. To test this assertion would require the grid to be printed on both sides of the fabric, with both sides being scanned individually. Alternatively printing a set of lines along the yarns on either side of the fabric, or manufacturing a fabric with tracer yarns in both directions, and impregnating the fabric with resin may allow the camera to see both sets of lines as a grid. This would represent the actual yarn movement in the fabric, although it may prove difficult to capture using the ASAME process due to the resin reducing the contrast between the grid and fabric. To produce results for yarn shear would require the assumption that the initial yarn grid was uniform and aligned which may not be true.

5.4.5 Possible Error in Model Predictions at Patch Edges

The assumption within the KDM that the position of the nodes define a sphere about the previous node point (see Chapter 3 for further details) can cause an error in the predicted fibre co-ordinates when the fibre paths change surface orientation such as when crossing patch boundaries. This is similar to the edge effect described in section 5.4.4, and will subsequently be referred to as the patch error. The fibre paths are assumed to follow vectors between the node intersections (Figure 5.12), which may not occur when the fibres change patches (depending upon the relative orientation of the patches). The patch error can affect the orientation prediction (calculated from the node positions), and may therefore appear in subsequent plots comparing experimental and predicted orientations. This patch error will be zero if the patches are in the same plane and is maximised if the patches are perpendicular. The error can be minimised by reducing the fibre spacing used in the model, but this causes large increases in run-time and produces large data files. For the disc and pyramid experiments the model fibre spacing was 2.13 mm (Figure 5.12) and the node positions were output for every third fibre (i.e. every 6.4 mm). For the hemispherical KDM data the patch error is similar to that caused by the edge effect (due to the constant radius of the hemisphere).

5.5 Measurement of Fibre Aspect Ratio to Determine Orientation

The grid strain analysis provided a useful measure of the accuracy of the KDM, as well as estimating the slip occurring in a fabric and the maximum fabric shear (hence fabric locking angle) during preforming. This assumes that the direction of a gridline printed on the surface of the fabric can be related directly to the direction of a fibre within the fabric, and produces average fibre angles at each grid intersection. This has inherent errors as discussed in section 5.4. Another technique which measures fibre angles through a laminate cross section was used for comparison purposes and to study the fabric deformation through the thickness.

5.5.1 Experimental Measurement Technique

A 26 mm high circular disc identical to one used in the ASAME experiments described in section 6.3, was draped with a 2 layer biaxial +/- 45°, Cross weft, stitch bonded fabric with an areal density of 948 g/m^2. The fabric was placed over a wooden former and a vacuum bag was placed over the fabric and evacuated to form the fabric to

the shape. Polyester resin (Cray valley 8345.001) was drawn through an injection port in the centre of the disc and the vacuum held while the resin cured. Samples were cut along the line of maximum inter-fibre shear deformation in the fabric (Figure 5.13) to allow comparison with the grid strain analysis results. The samples were mounted perpendicular to the bottom face of a casting pot, and encapsulated in polyester casting resin. Once cured, the bottom faces were polished, and for each sample the warp and weft fibre layers were photographed using an optical microscope mounted camera. The samples were aligned by eye to be perpendicular to the microscope slide edge, so that the out of plane angle (γ) between the fibre and a known vector (the edge of the sample) was assumed to be zero. The images were scanned into a TIFF format graphics file and examined using a PC based image analysis package [Micrografx Inc., Picture Publisher]. The software allowed the co-ordinates of the major and minor axis boundary points to be measured for each fibre.

Twelve data points were taken from each sample consisting of three groups of four fibres at either side of and centre of the scanned image (shown numbered 1 - 12 in Figure 5.14). The major and minor axis lengths and the angle of the fibre with respect to the plane (Θ) for each data point in the layer were then calculated using the method described in section 2.7.1. The results were averaged for each ply and the inter-fibre angles were calculated from the two planar fibre angles (Θ) at each position as shown in Figure 5.15. The inter-fibre shear angle was calculated from the post forming inter-fibre angle assuming that the fabric was initially +/- 45°.

5.6 Comparison of Ellipse Method with Grid Strain Analysis and Kinematic Drape Model

The results obtained using the method described in section 5.5 were compared with those from the GSA system and the kinematic drape model (Figure 5.16). There was a gap in the ellipse average data at 63 mm from the centre of the disc, as the sample could not be mounted normal to the base of the casting pot due to extreme curvature in the sample as it formed around the edge of the disc. Therefore no data were acquired for the sample at this position. The results show a good correlation between the two experimental methods at radii between 0 mm and 45 mm and from 90 mm to 118 mm. The GSA produced errors at sharp corners due to the method used to calculate the

angles, which is apparent at 63 mm and 81 mm so the GSA data have been omitted at these points. The elliptical method produced local measurements within the reinforcement, whereas the GSA produced an average over the area of the grid.

The results verify the KDM, apart from around corners and in areas where the model predicts inter-fibre shear angles higher than the fabric locking angle (the area between 80 and 100 mm, where 78° shear is predicted). The respective merits of the two techniques are discussed in the following paragraphs.

GSA evaluates the fibre orientation across the entire sample surface. This is valid for most areas, except where the fibre orientations change rapidly, and depart from the average angles measured by the GSA. The data acquisition and processing is fast and repeatable. The method provides fibre orientations and strain data across the grid which can be used to estimate slip between the yarns. Problems occur when processing highly deformed areas, where wrinkling has occurred or where fibres have slipped excessively and obscured the grid lines which prevents complete mapping of the grid.

The elliptical method measures fibre orientations at specific locations within the sample. Acquiring the data proved time consuming (approximately two hours per sample) and required the user to locate visually and measure co-ordinates of the major and minor ellipse axes, which reduces the repeatability of the results. Recent work has automated the image capture and analysis part of the process [87, 88, 106], eliminating problems such as distinguishing individual fibres within the tows at high volume fractions, and improving the speed and accuracy of the results.

The accuracy of the results depends upon the repeatability of cutting the samples, mounting the samples perpendicular to the photographed surface, quality of polishing, number of fibres analysed and accuracy in measuring the major and minor axes of the fibres. Another problem (described in section 2.7.1) is the sensitivity to measurement errors when the fibres are almost perpendicular to the cut, which may require two sets of samples to be examined, each with a different cut plane orientation. Therefore, the best application of the ellipse method in fabric preforms would be in measuring fibre angles in areas where the GSA cannot be applied accurately, such as around sharp corners and in areas where the fabric is close to its locking angle.

5.7 Summary

A method for measuring fibre orientations within a preform was required to evaluate the limits of the KDM. Two methods of measuring fibre orientations within a fabric were evaluated. The relative advantages of each method have been discussed, along with the application of the results derived from such tests. GSA provided a rapid and convenient method but there were several circumstances where the analysis provided invalid data. The measurement of the fibre angle using the ellipse method proved accurate within the boundaries of operator care, but was time consuming, although recent developments in computer software have improved the repeatability and speed of analysis of the results.

GSA was adopted for subsequent work, due to the facility for the measurement of slip and the amount of data that could be collected. As the KDM assumed simple shear to be the only mode of deformation, a measure of slip within the grid would indicate the validity of this assumption. It also allowed investigation of the relationship between slip and inter-fibre shear for various geometries and fabrics.

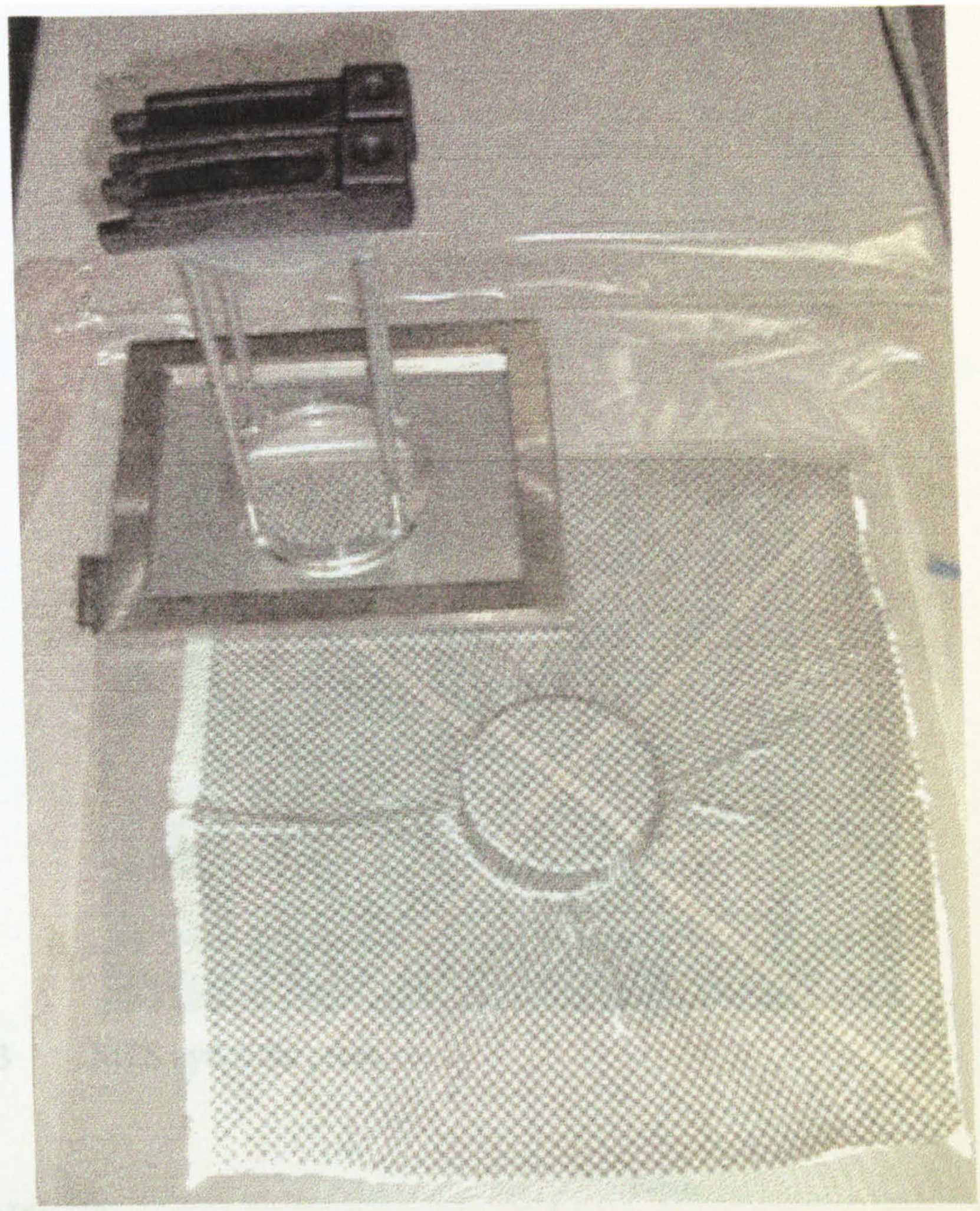

Figure 5.1 Vacuum assisted preforming equipment for disc geometry.

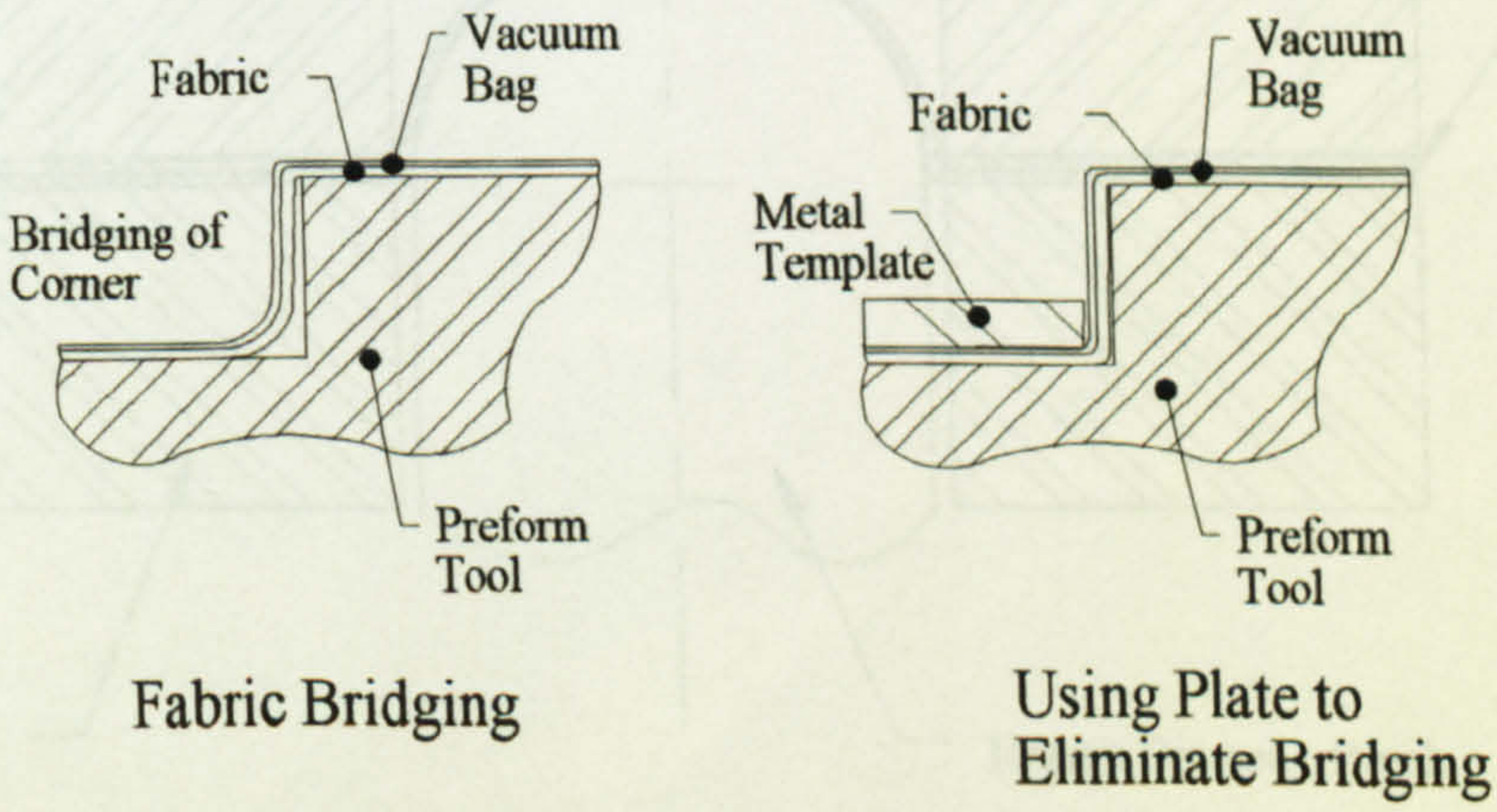

Figure 5.2. Fabric bridging problem and solution.

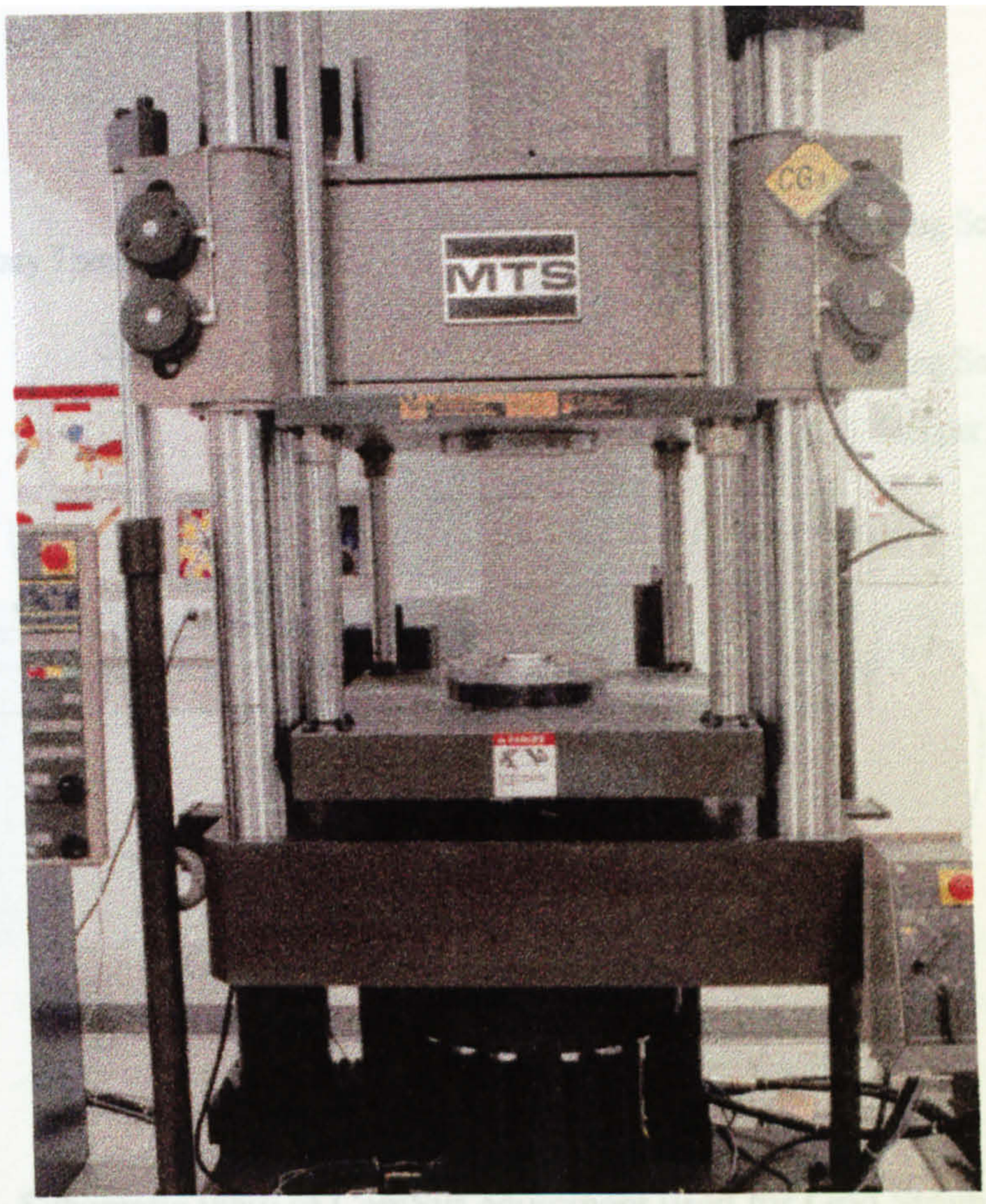

Figure 5.3 MTS hydraulic press.

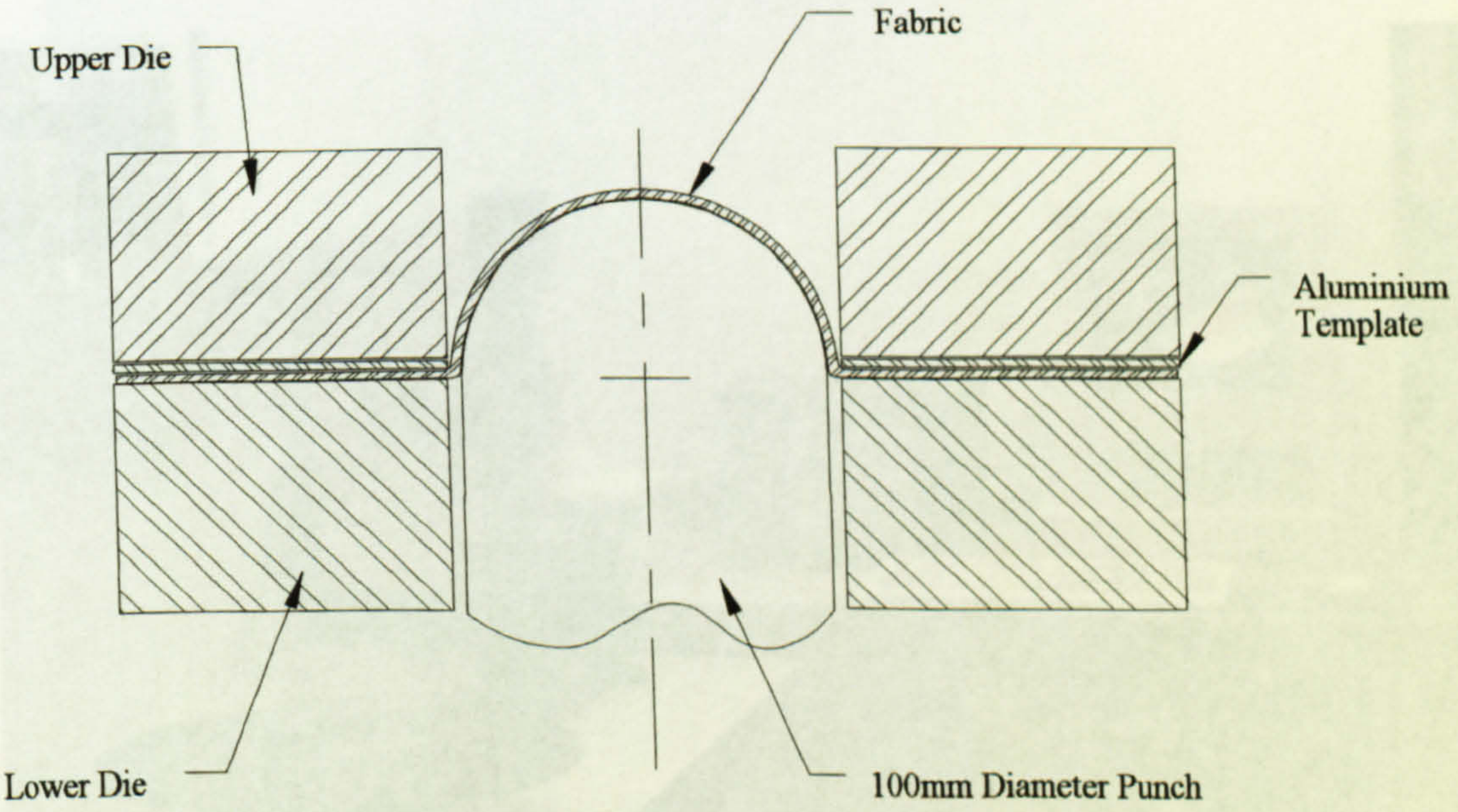

Figure 5.4 Schematic view of press forming equipment.

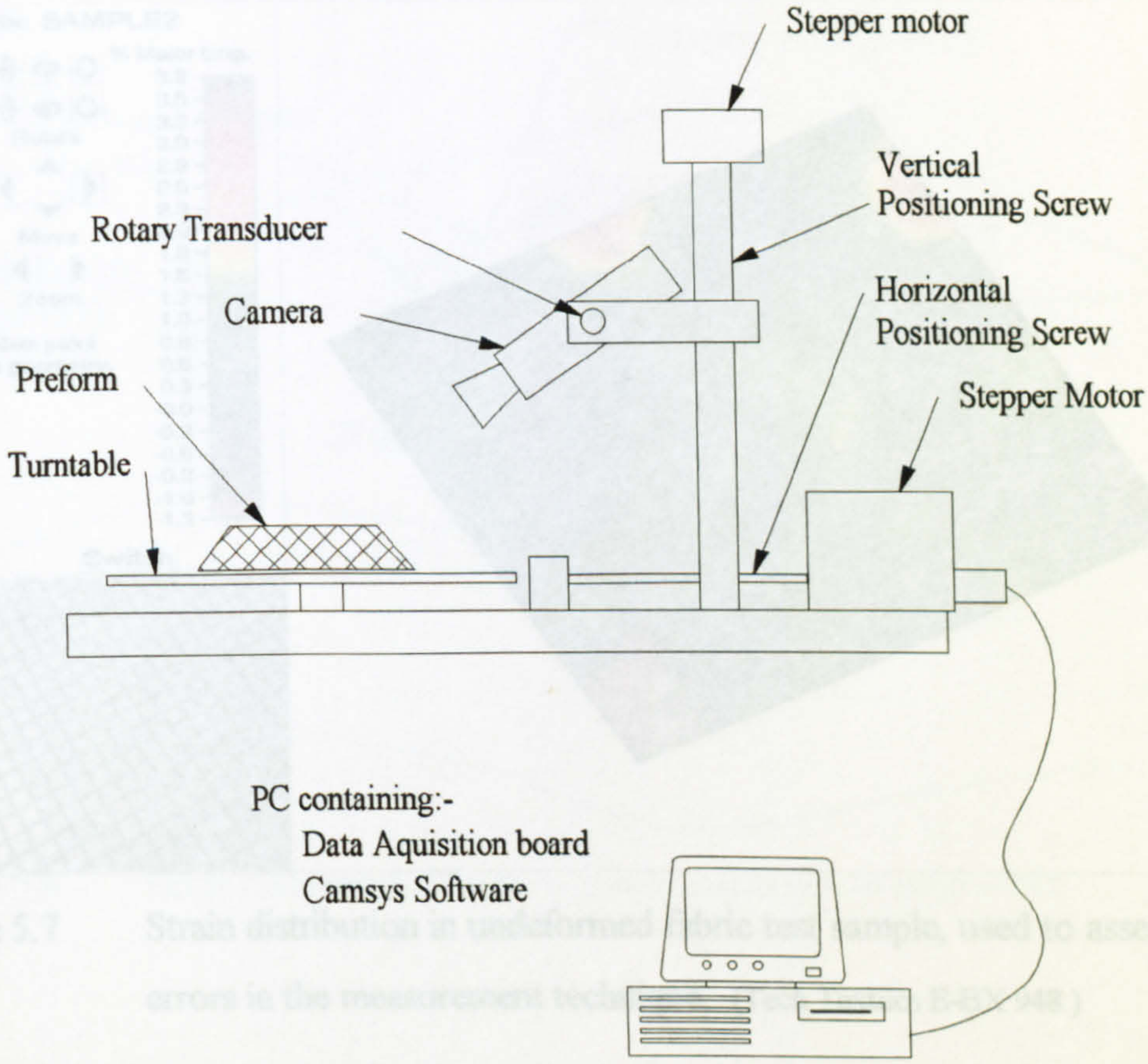

Figure 5.5 Schematic view of CamSys equipment used for Grid Strain Analysis of the fabric preforms.

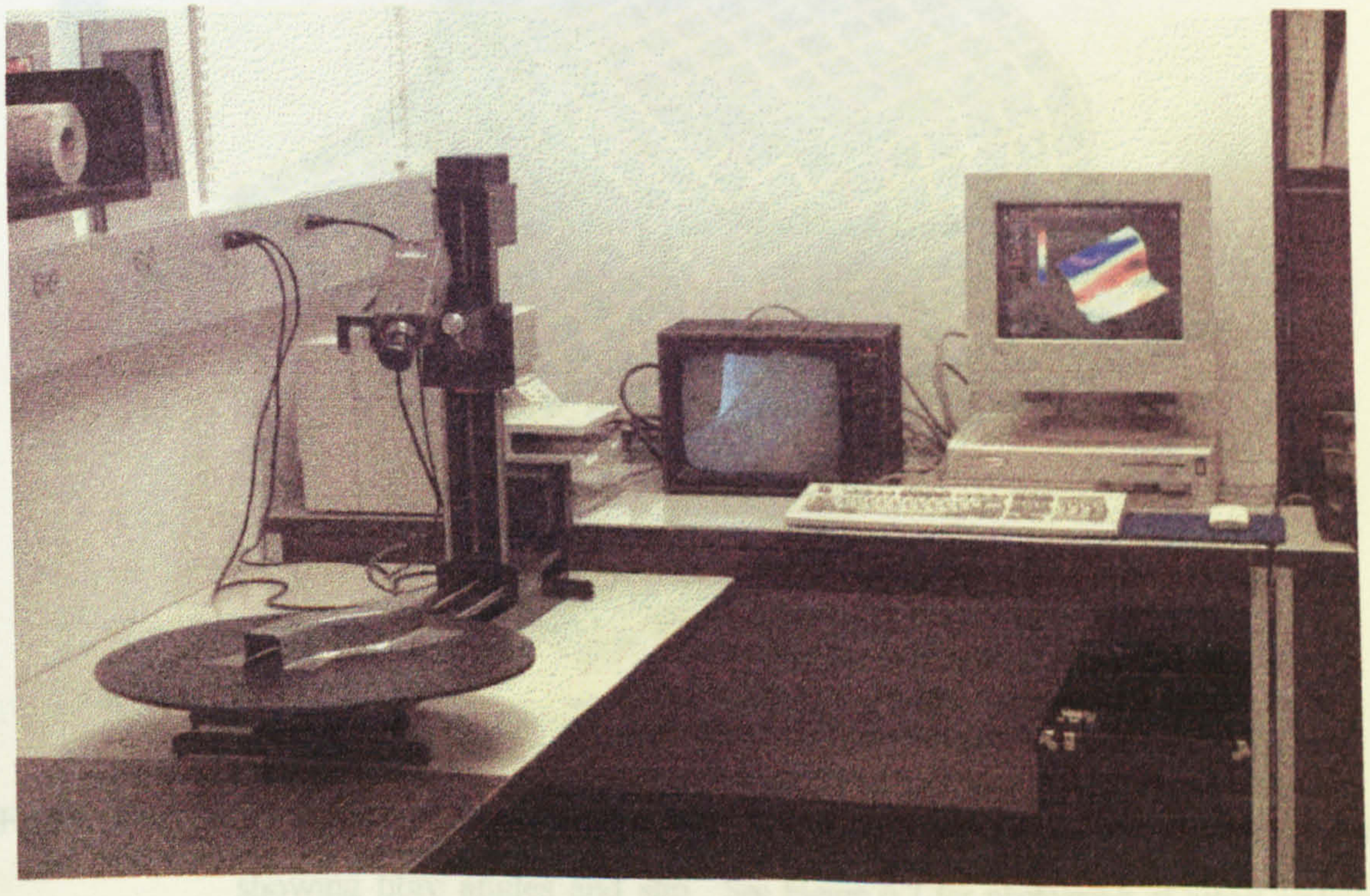

Figure 5.6 CamSys equipment.

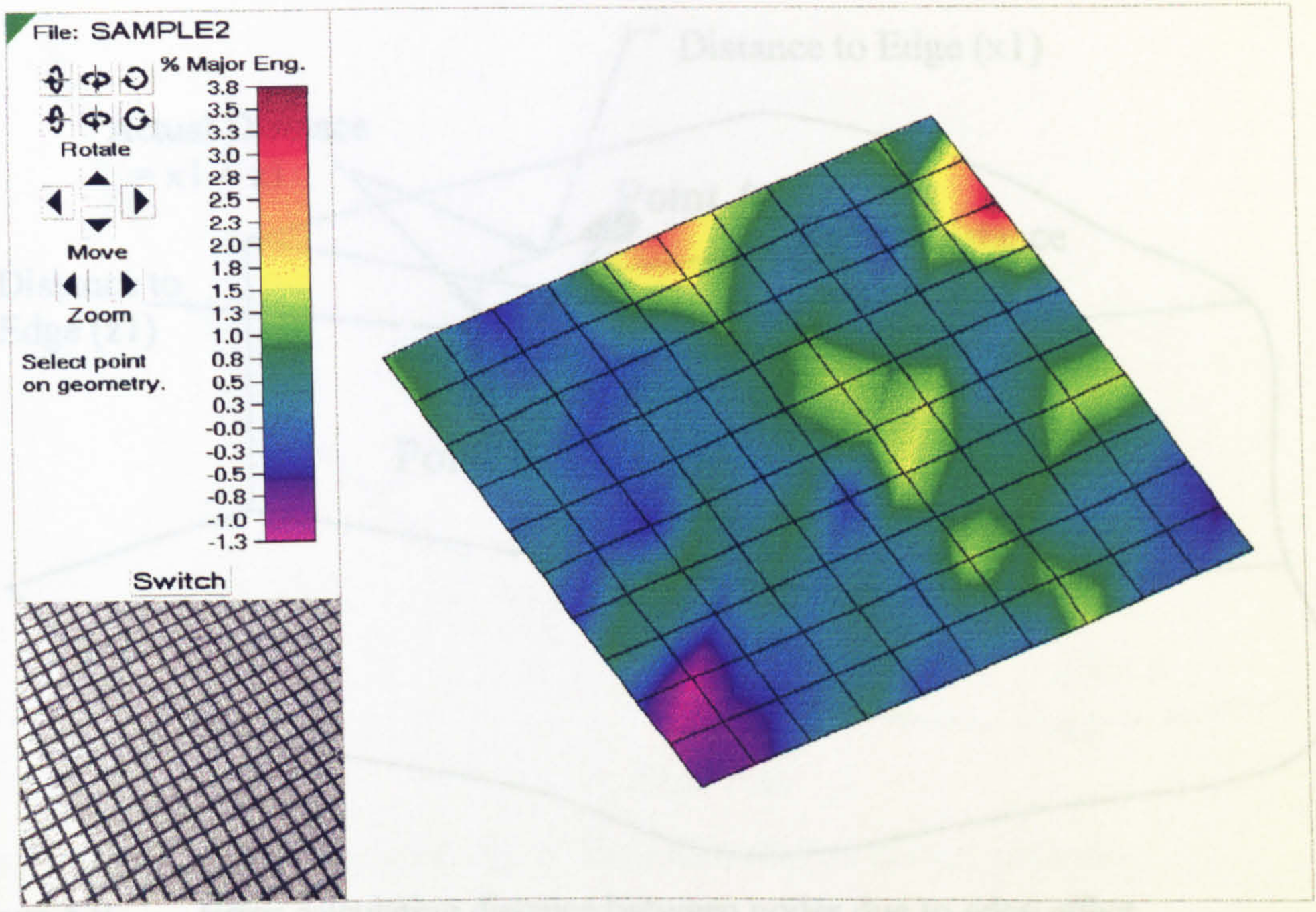

Figure 5.7 Strain distribution in undeformed fabric test sample, used to assess baseline errors in the measurement technique. (Tech Textiles E-BX 948.)

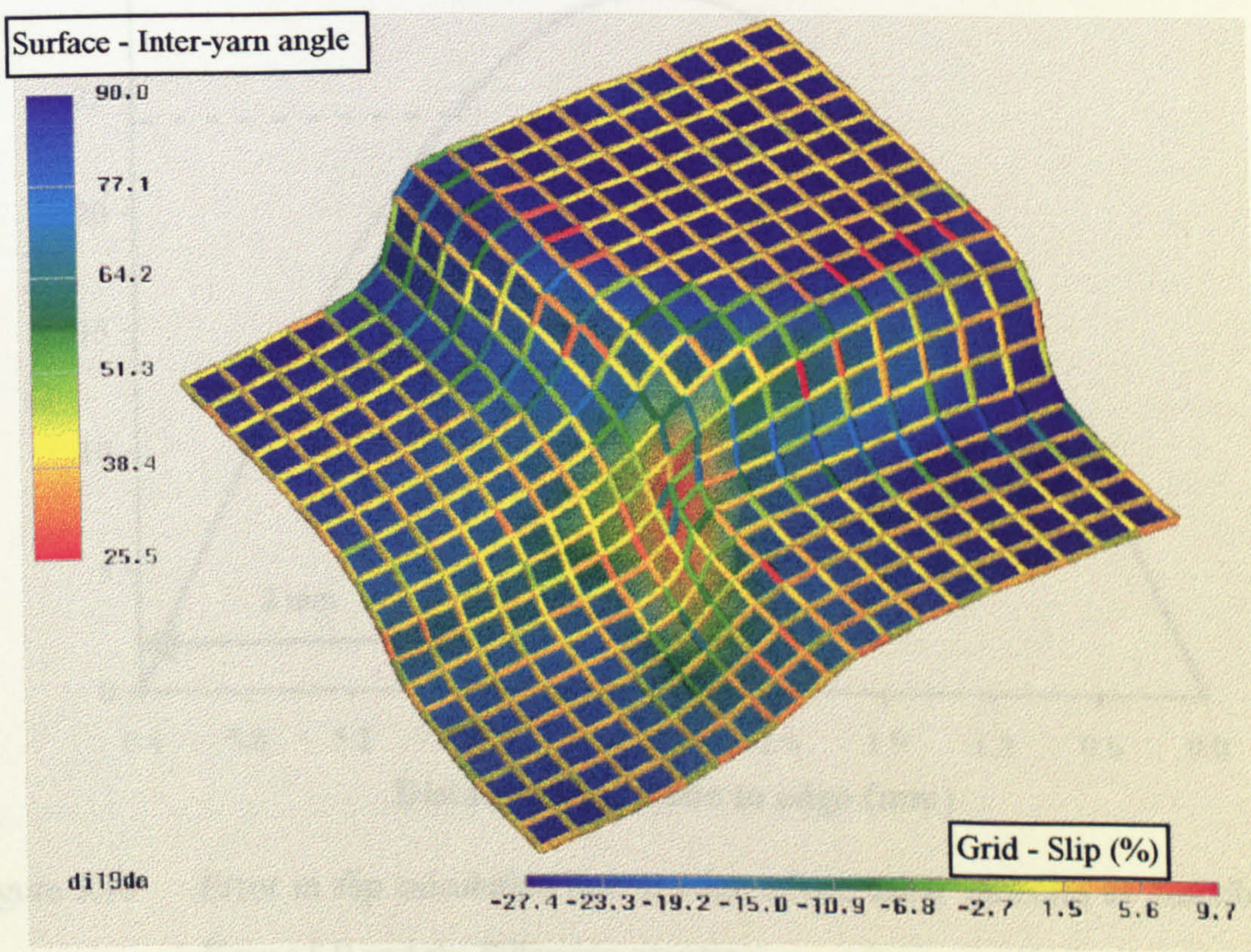

Figure 5.8 AVS plot of experimental data for one quadrant of 19 mm deep disc showing fibre angles and slip. See Figure 6.7 for photograph of actual preform. (Tech Textiles E-BX 948, vacuum formed.)

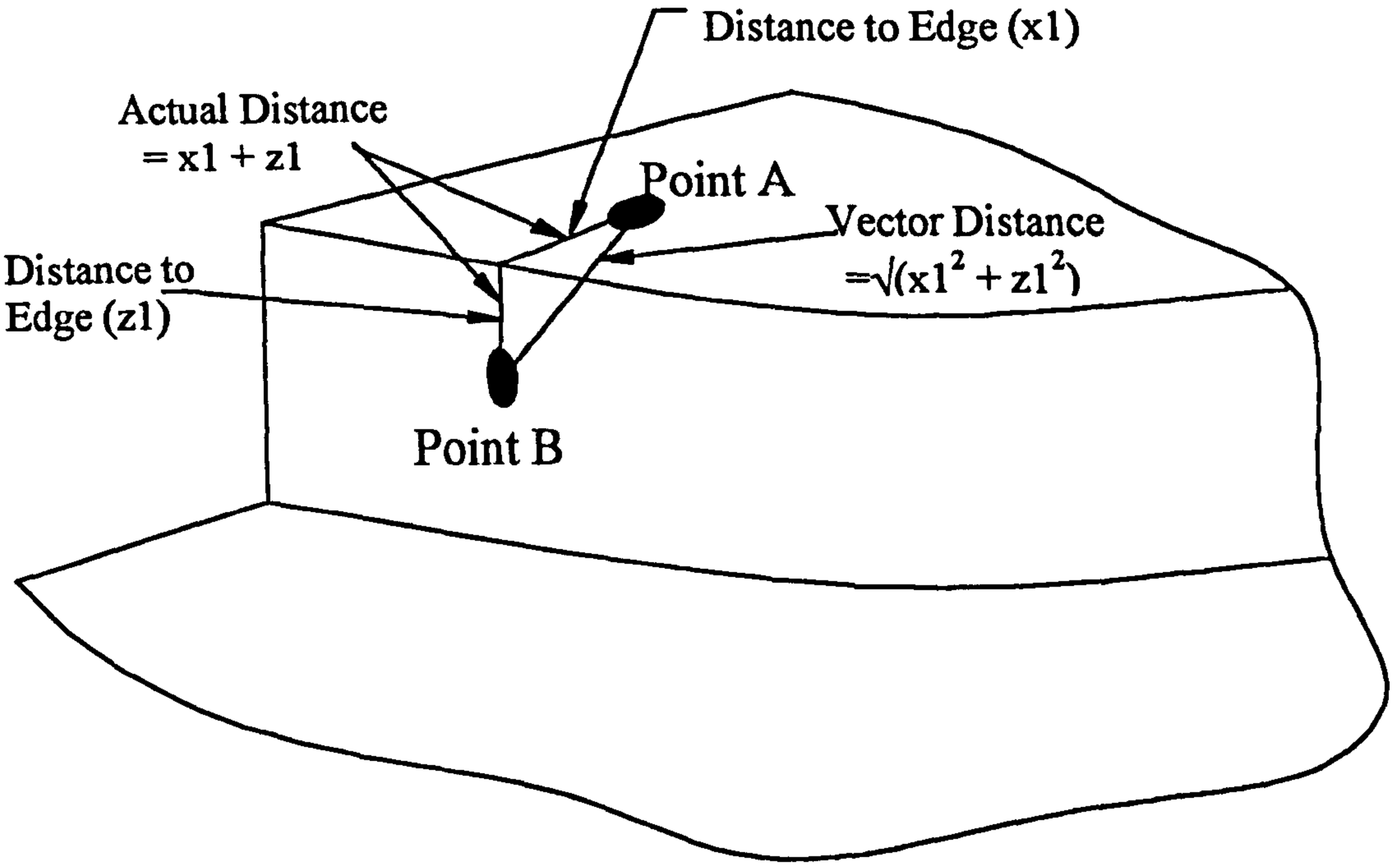

Figure 5.9 Error calculating distance between nodes due to edge effect.

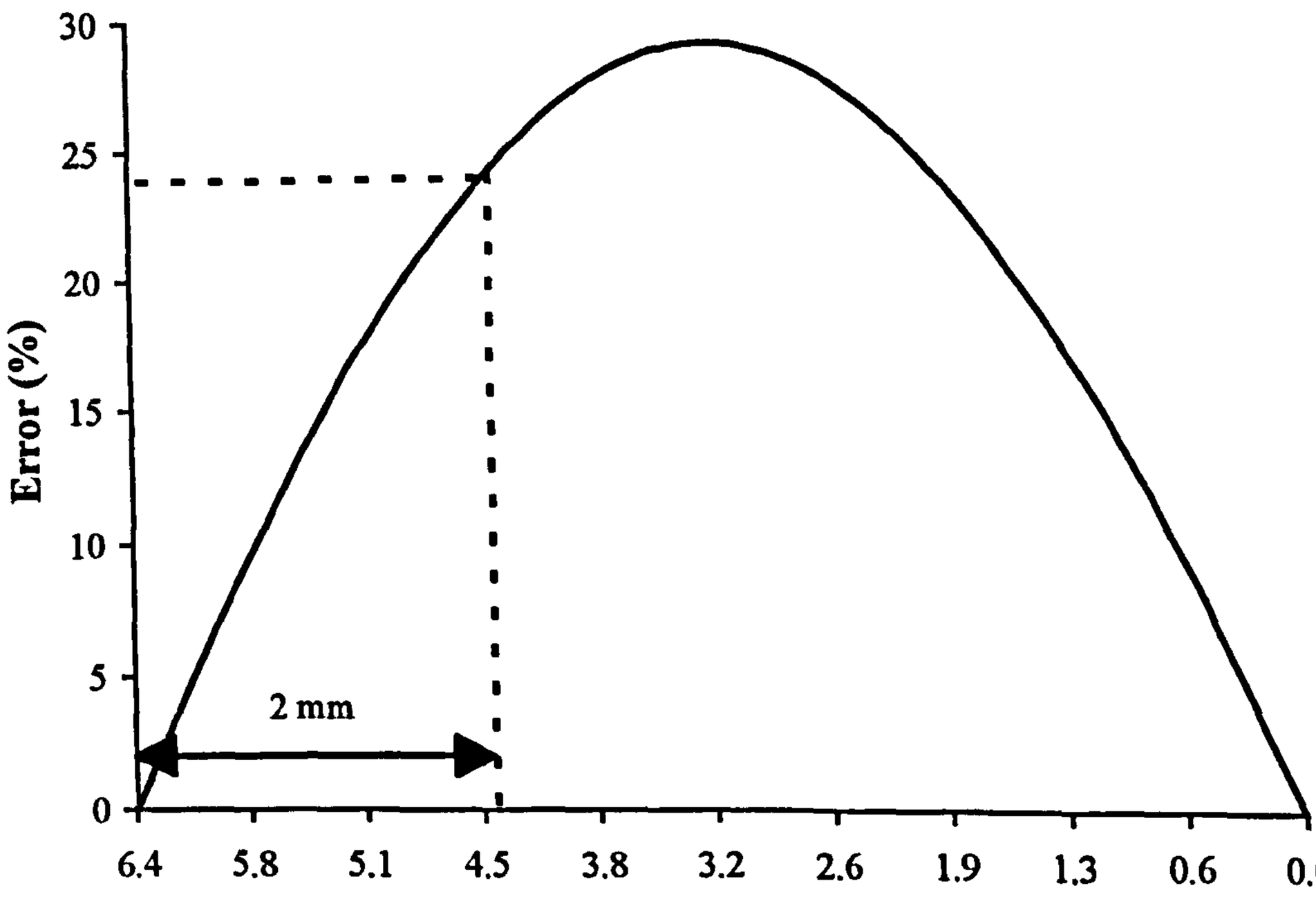

Figure 5.10 Error in slip calculation due to edge effect, using variables as described in Figure 5.9 and the following equation:-

$$Error(\%) = \frac{(x1+z1) - \sqrt{x1^2 + z1^2}}{(x1+z1)} \cdot 100$$

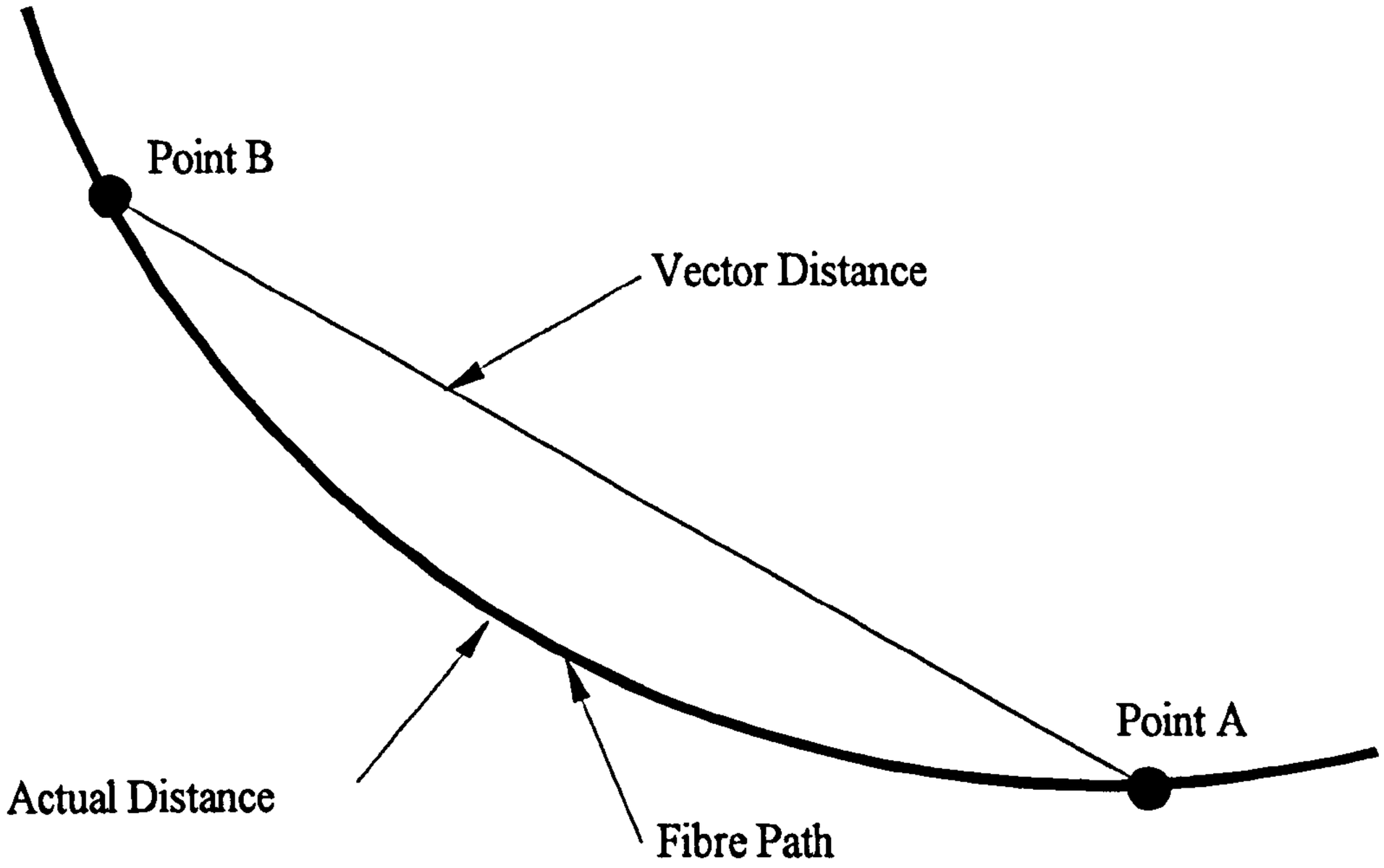

Figure 5.11 Error calculating slip in fibres formed over curved surfaces.

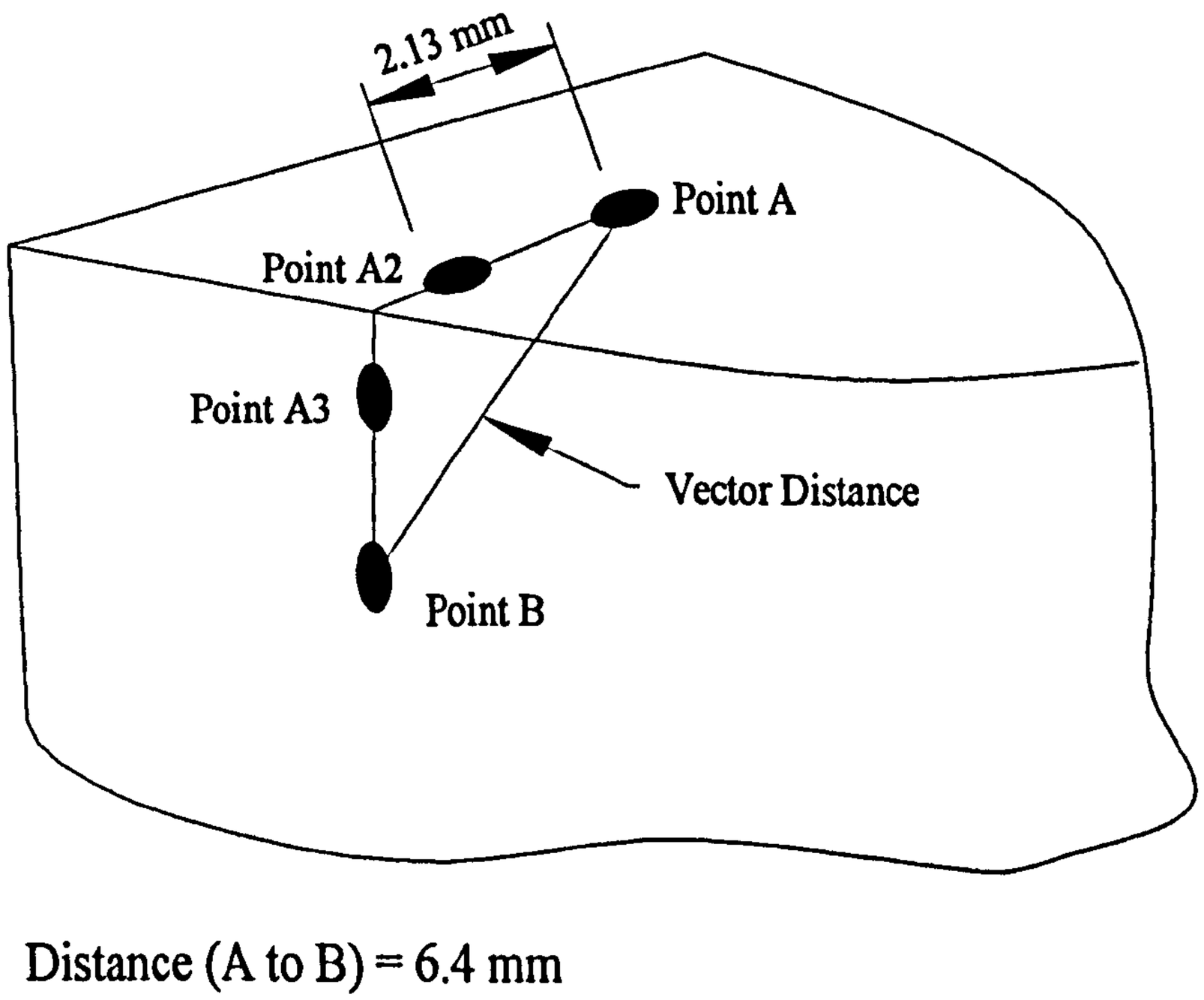

Figure 5.12 Error in model calculation at patch edges.

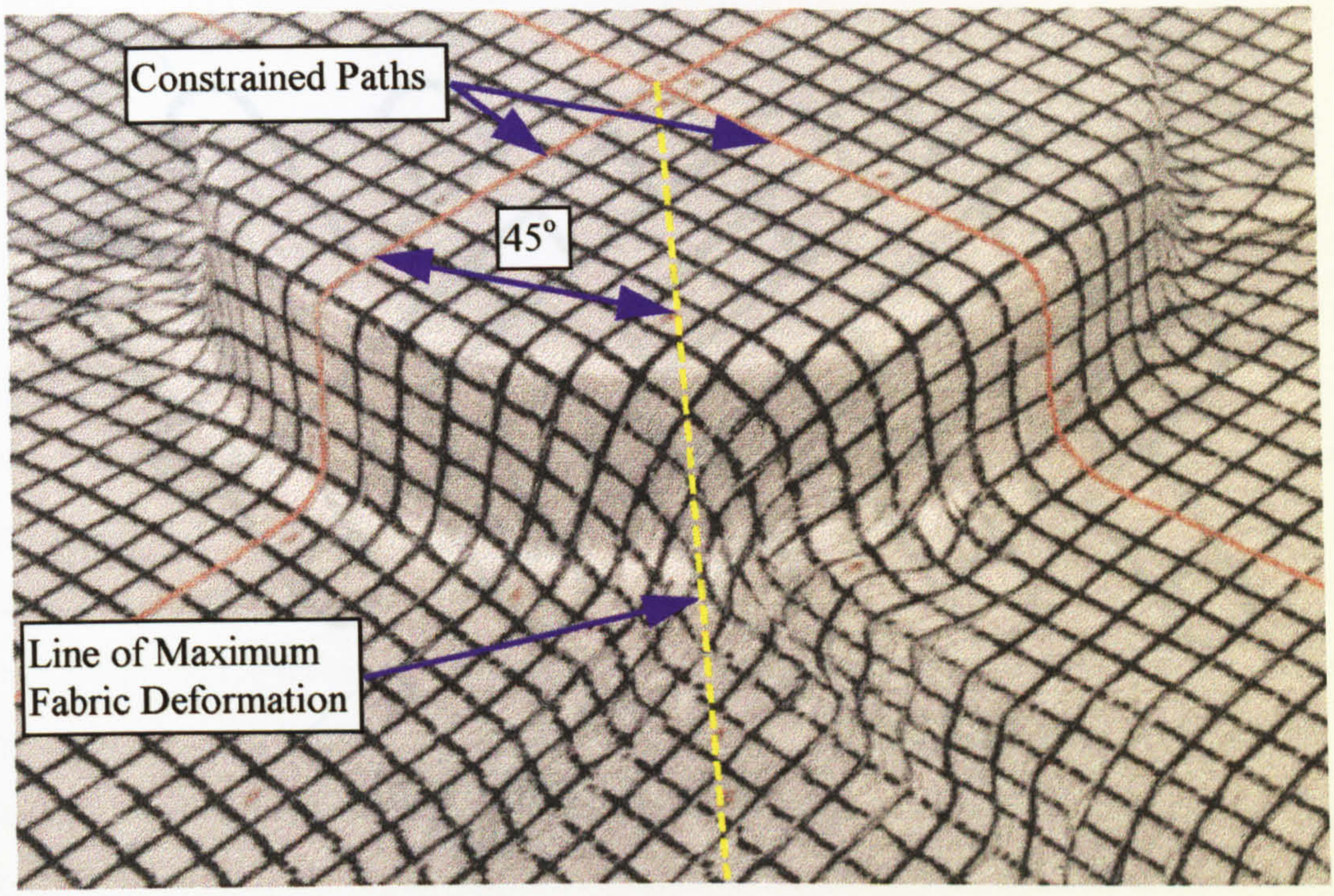

Figure 5.13 Line of maximum fabric shear deformation across 26 mm high disc.

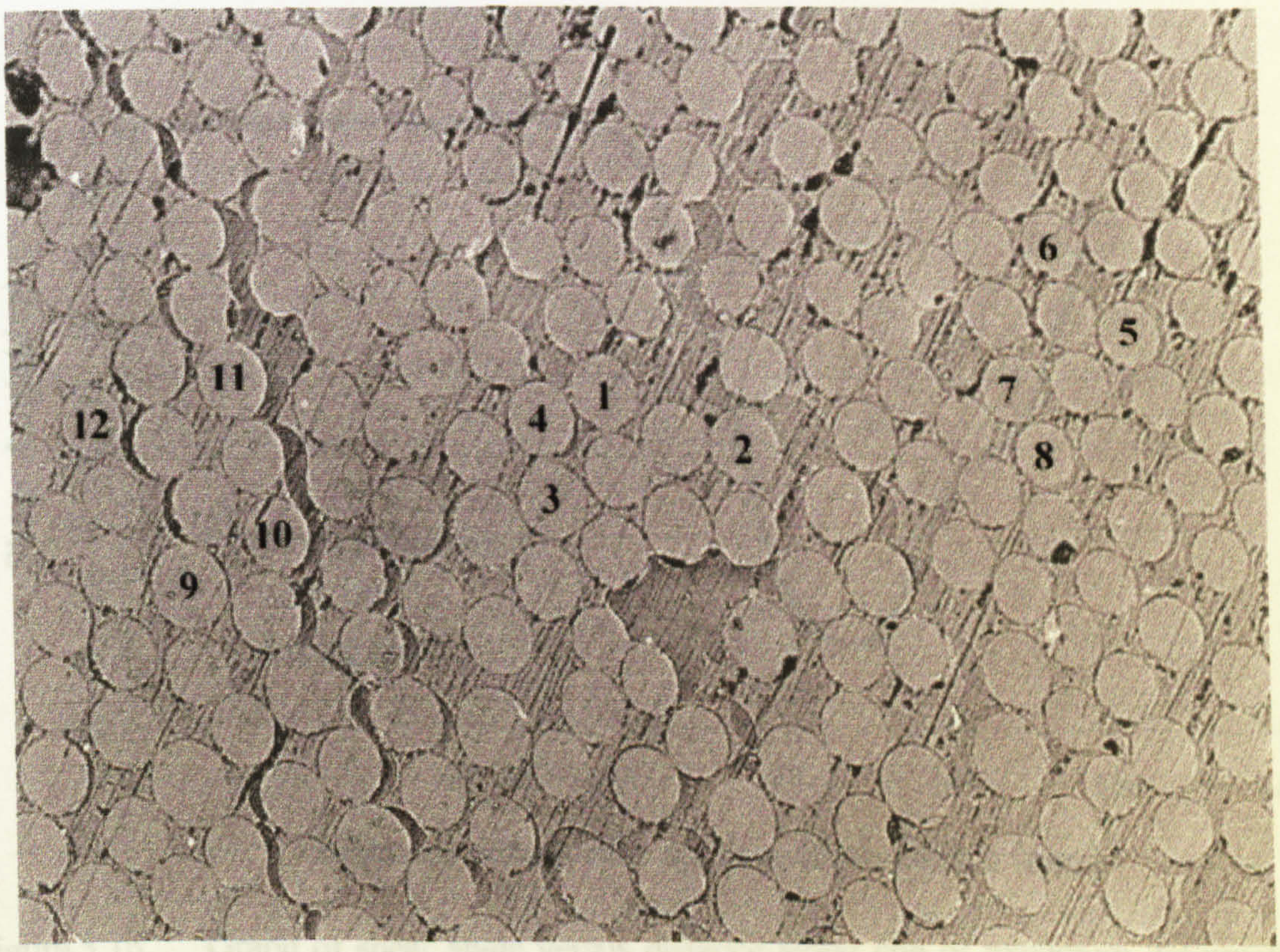

Figure 5.14 Scanned image of polished sample showing elliptical section of fibres when cut through an off-axis plane.

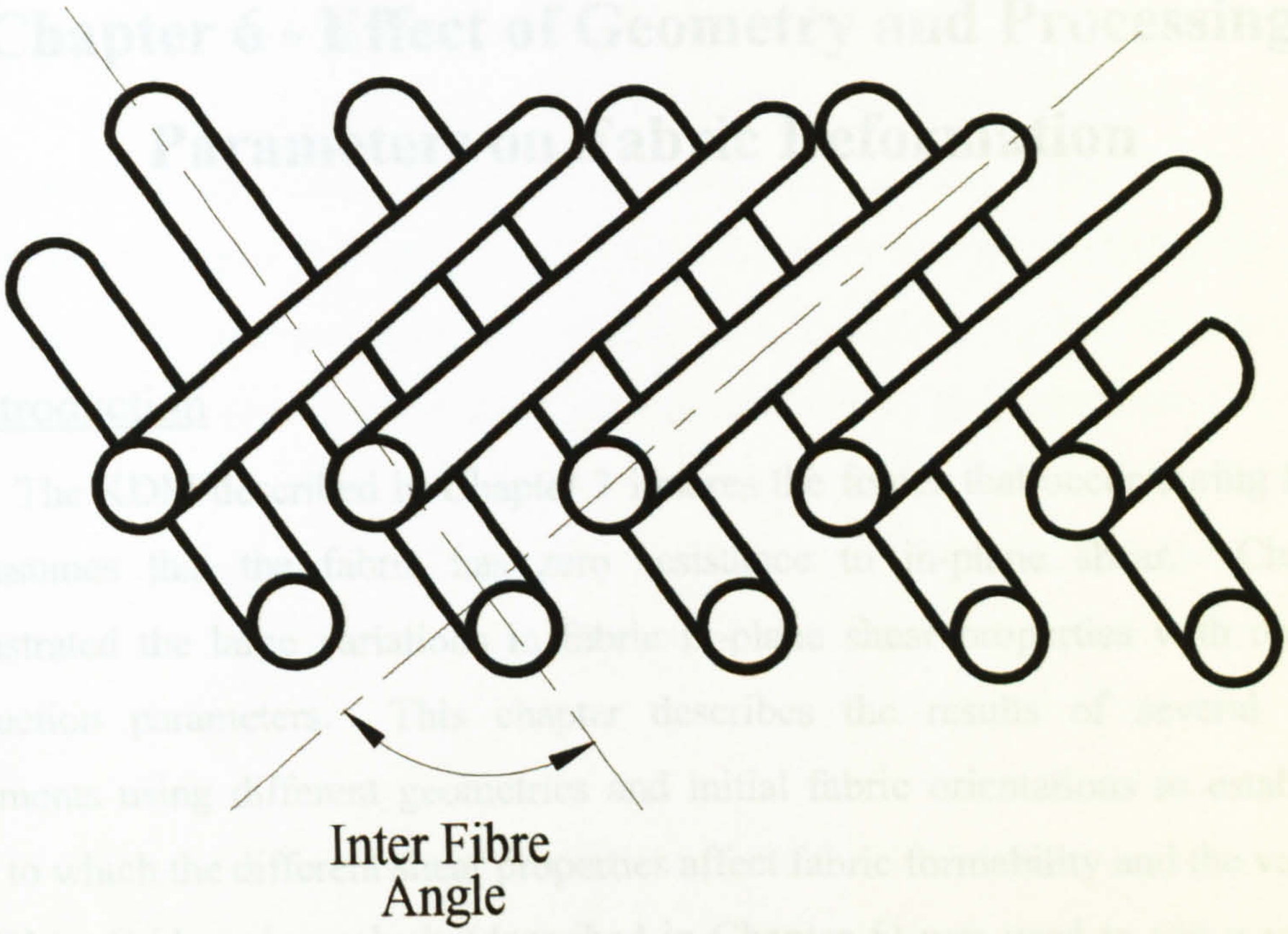

Figure 5.15 Definition of inter-fibre angle for samples cut using ellipse process.

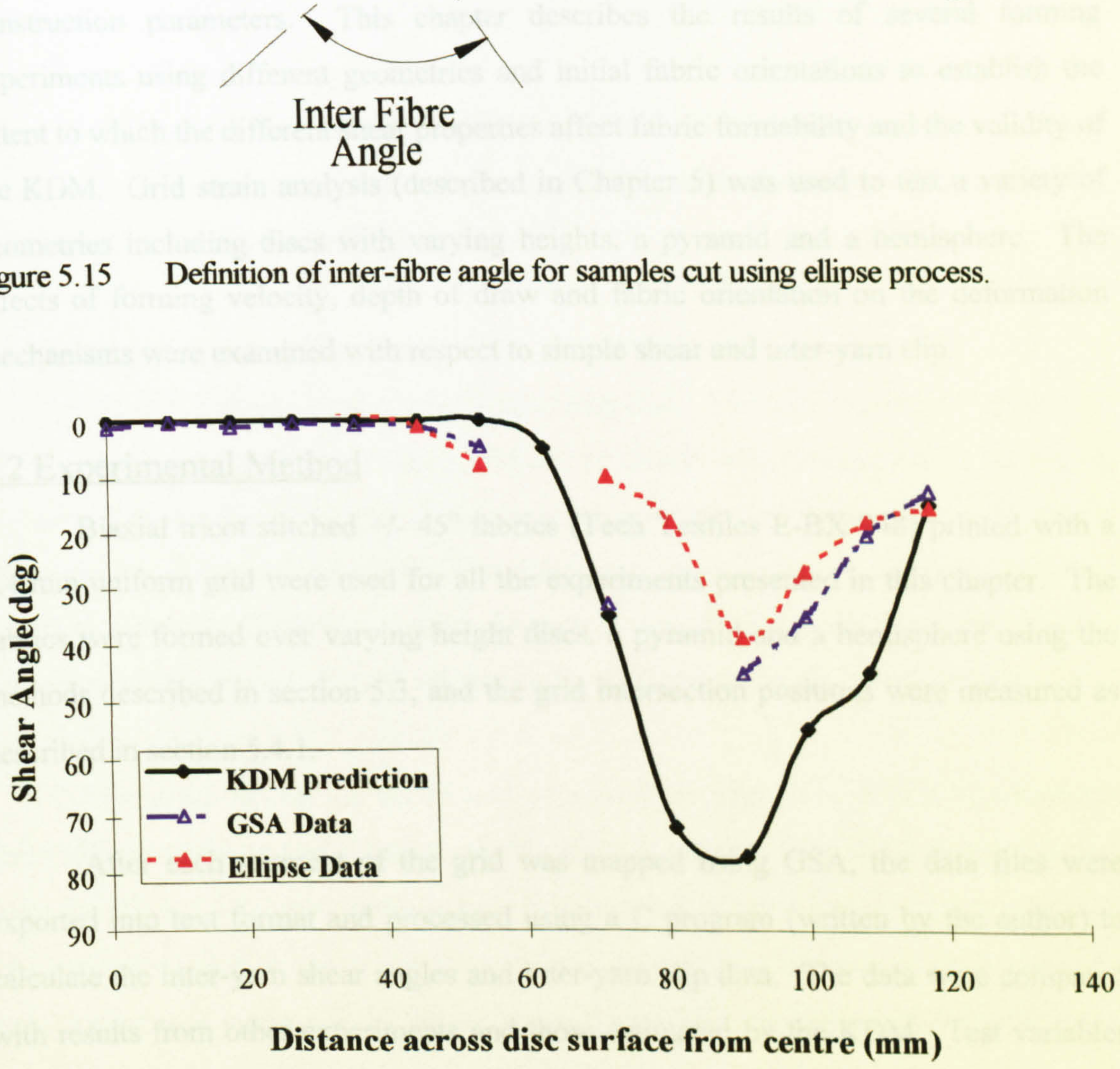

Figure 5.16 Graph of shear angle versus distance along line of maximum deformation (see Figure 5.13) for both experimental methods and KDM across the surface of a 26 mm high disc.

Chapter 6 - Effect of Geometry and Processing Parameters on Fabric Deformation

6.1 Introduction

The KDM described in Chapter 3 ignores the forces that occur during forming and assumes that the fabric has zero resistance to in-plane shear. Chapter 4 demonstrated the large variations in fabric in-plane shear properties with respect to construction parameters. This chapter describes the results of several forming experiments using different geometries and initial fabric orientations to establish the extent to which the different shear properties affect fabric formability and the validity of the KDM. Grid strain analysis (described in Chapter 5) was used to test a variety of geometries including discs with varying heights, a pyramid and a hemisphere. The effects of forming velocity, depth of draw and fabric orientation on the deformation mechanisms were examined with respect to simple shear and inter-yarn slip.

6.2 Experimental Method

Biaxial tricot stitched +/- 45° fabrics (Tech Textiles E-BX 948) printed with a 6.4 mm uniform grid were used for all the experiments presented in this chapter. The fabrics were formed over varying height discs, a pyramid and a hemisphere using the methods described in section 5.3, and the grid intersection positions were measured as described in section 5.4.1.

After each segment of the grid was mapped using GSA, the data files were exported into text format and processed using a C program (written by the author) to calculate the inter-yarn shear angles and inter-yarn slip data. The data were compared with results from other experiments and those estimated by the KDM. Test variables included forming speed, fabric orientation and depth of draw. The experimental data were also processed to allow visual comparison with the kinematic model predictions using AVS imaging software as described in section 5.4.3.

6.3 Effects of Disc Height on Fabric Deformation

To study the effects of the geometry height on fabric deformation, five discs of identical diameter but varying height were draped with the same fabric. Each disc had a diameter of 120 mm with heights varying from 7 mm to 38.6 mm. During the draping of each disc, the intersection of the two coloured lines denoting the constrained path used in the model were positioned as close to the centre of the disc as possible (Figure 6.1). The fabric was located using the printed grid and a hole running through the center of each disc as a guide. It was estimated that up to 2 mm error in the positioning of the lines could occur due to the manual positioning and relatively coarse grid spacing of 6.4 mm.

For comparison of the predicted and measured fabric deformation the inter-yarn shear angle and percentage slip were examined along lines of maximum shear deformation (as indicated in Figure 6.1).

6.3.1 Draping of a 7 mm Disc

Figure 6.2 shows a preformed 7 mm deep disc. The red lines denoting the path of the constrained fibres used in the KDM can be clearly seen running across the centre. Figure 6.3 shows the AVS plot of the same surface quadrant with experimental local ply angle and slip data displayed. The maximum shear occurs at the base, on a line running diagonally from the centre. The shear angles along this line were used in subsequent comparisons. Figure 6.4 shows the KDM result for the same surface.

Figure 6.5 shows the KDM and experimental data along a line of maximum shear (the principal axis of shear) across the disc. Relatively little shear was required to form the fabric. The experimental data show approximately 5° more shear occurred at maximum deformation (approximately 80 mm from centre) in the quadrants where the deformation was perpendicular to the stitch than when sheared parallel to the stitch. This supports the findings described in section 4.4.2, i.e. the fabric is approximately twice as stiff at 15° shear when loaded parallel to the stitch. The KDM data are generally close to the experimental values, apart from at 80 mm from the centre where a 'patch error' occurs in the calculation (as described in section 5.4.5) due to the sudden change in surface orientation at the edge of the disc. This causes an over-estimation of

the shear angle, therefore the KDM predicted data in the following figures have been isolated where this occurs. The shear in the fabric is generally well below the maximum shear angle (i.e. less than 58°) tested in section 4.4.2 and has therefore not locked, and it appears that the KDM is accurate at this level of shear deformation.

Figure 6.6 shows the inter-yarn slip occurring along the same path as above. Since the KDM does not predict slip, no such plot from the model is included. Errors between 55 mm and 81 mm caused by the experimental edge effect described in section 5.4.4, indicating erroneous negative slip have been removed. The accuracy of GSA technique is approximately +/- 3.8 % so most of the slip data in Figure 6.6 must be ignored. However, as there is a lack of measurable slip in the experiments, inter-fibre shear would appear to be the most important deformation method for low draw shapes.

6.3.2 Draping of a 19 mm Disc

Figure 6.7 shows the 19 mm deep disc draped with a gridded fabric. Figure 6.8 shows the corresponding AVS plot which was imaged from the front quadrant. The maximum shear deformation occurs in the same area as that for the 7 mm deep disc, but larger shear occurs. A view of the KDM prediction for the same geometry can be seen in Figure 6.9, showing the area of highest shear in the same place as the draped fabric. The shear data (Figure 6.10) shows that the model is accurate up to approximately 70 mm from the centre. There may be an error in the KDM at 80 mm due to the 'patch error' so the data have been isolated in the following figures. At 90 mm from the centre the KDM predicts 60° shear which is close to the estimated 'locking angle' for the Tech Textiles E-BX 948 fabric (section 4.4.5). As shown in Figure 6.7 the fabric has limited the amount of shear deformation it has undergone by deforming using alternate mechanisms. In quadrants where the fabric was sheared parallel to the stitch, the fabric has wrinkled and lifted off the surface reducing the maximum shear in Figure 6.10 to approximately 35°. In the quadrant where the fabric was sheared perpendicular to the stitch, the yarns have buckled and the maximum shear angle is 50°. As the deformation was not symmetric within the quadrant the experimental data shown (along the line of predicted maximum shear) may not be the true maximum shear that the fabric underwent. The yarn buckling can be seen as approximately -12 % slip in Figure 6.11. Figure 6.11 shows that apart from yarn buckling, the measured slip levels were within the error of the GSA.

6.3.3 Draping of a 38 mm Disc

Figures 6.12 shows the 38 mm high disc draped with a gridded fabric. Severe wrinkling occurred in the fabric starting on the vertical surface. Figure 6.13 shows the corresponding AVS plot of the inter-yarn angle and slip for the same quadrant. The GSA could not map the entire grid due to the wrinkling problem.

The KDM result is shown in Figures 6.14. Extreme shear deformation was predicted on the vertical and lower surfaces and this is compared with the experimental data in Figure 6.15. Close agreement was evident up to 75 mm from the centre where a maximum of 40° shear occurs. Beyond this the KDM predicts up to 87° shear, which is clearly beyond the fabric locking angle. There are no data for the experiments in this region due to the wrinkling problem discussed previously.

Figure 6.16 show that minimal slip occurred in the fabric. The folding of the fabric can be seen at approximately 90 mm from the centre, where the figure shows 25% negative slip.

6.3.4 Comparison of Maximum Shear Angles for Varying Depth of Disc

The KDM results are compared with experimental data for all quadrants and all depths of disc in Figure 6.17. The data shows the maximum measured shear angle in the samples, which is not necessarily along the line of maximum predicted shear due to folding and non-symmetry in the preform. The KDM results suggest that as the disc depth increases the minimum ply angle approaches 0°. Clearly, due to physical limitations this is impossible and the maximum measured shear angle is approximately 60°. This value is slightly beyond the limits of the uniaxial tests described in Chapter 4, but demonstrates the dominance of the locking angle.

In high shear deformation results (such as the 14 and 19 mm high discs), a 25° higher shear angle occurred in quadrants where the fabric was sheared perpendicular to the stitch than when sheared parallel to the stitch. One of the major causes of this is the imbalance in shear stiffness of the fabric due to the stitch type as described in section 4.4.2. This caused asymmetry in the quadrants of the 19 mm deep disc reported in section 6.3.2. A factor which occurred when the fabric locked was the formation of folds in the fabric, which absorbed excess fabric locally, thus reducing the shear

required elsewhere. This was seen in the 38 mm high disc (section 6.3.3), where the fabric locked at 60° shear and the fabric folded. The accuracy of the measured maximum shear angle in these cases depended upon the proximity of the grid points to the fold, or how much buckling occurred across the fabric surface, as this obscured or blurred the grid definition. Therefore manual editing of the image to join the lines and remove erroneous shaded areas was occasionally required, introducing errors into the digital image and hence the shear and slip data.

6.4 Effect of Fabric Orientation on Deformation

To study the effect of fabric orientation (with respect to the geometry axes) on formability, a truncated pyramid was modelled and draped with the intersecting red lines representing constrained paths running through the centre of the pyramid, and the initial fabric orientation at 0°, 15°, 30°, 45° to the axes (Figure 6.18).

Figure 6.19 shows the pyramid draped at 0° to the axis of symmetry and the KDM result for the same geometry. Wrinkling can be seen along the vertical edge with minimal shear deformation on the surfaces of the pyramid. The area of wrinkling corresponds to the area of high shear (89° shear) predicted by the model. Similar comparisons can be made for pyramids draped at 15° and 30° respectively (Figures 6.20 and 6.21). When draped at 45° to the axes (Figure 6.22), a similar deformation pattern to that of the 19 mm discs occurred. Although the predicted maximum shear angle is slightly less than that predicted at the other orientations (85° as opposed to 89°) it was still beyond the fabric locking limit, and wrinkling occurred away from the base of the pyramid.

A comparison of the maximum shear for each fabric orientation can be seen in Figure 6.23. In each case the fabric wrinkled due to the locking limit being reached. The large scatter and lower locking angles which are evident were attributed to the wrinkling and the associated mapping problems described earlier. Re-orientation of the fabric reduced the severity of the wrinkling, and the optimal orientation of the fabric was 45° to the pyramid edge which corresponded to the sample with the least wrinkling. This coincided with the lowest maximum shear angle predicted by the KDM. It would be expected that repeating the tests with a shallower pyramid would allow a more

conclusive result. Due to a limitation in the availability of the ASAME equipment this was not studied further.

6.5 Effect of Forming Speed on Fabric Deformation

To examine the effect of forming speed on fabric deformation, the same stitch bonded fabric as used for the in-plane shear rate tests described in section 4.4.3 (Tech Textiles E-BX 948) was press formed into a hemisphere (Figure 6.24) at three different punch velocities (10 mm/sec, 65 mm/sec, 110 mm/sec), using the method described in section 5.3.2.

Figure 6.25 shows the KDM predictions, where the area of highest shear is predicted at the base of the hemisphere. Figures 6.26 and 6.27 compare the inter-fibre shear angles along the line of maximum predicted shear deformation between the KDM predictions and the three test samples. There is a close correlation between the experimental and predicted shear angles when sheared perpendicular to the stitch (Figure 6.27). The effect of differences in shear stiffness due to stitch orientation discussed earlier can be seen by the reduced shear in quadrants where the fabric was sheared parallel to the stitch (Figure 6.26). There appears to be no noticeable effect of forming speed on the shear deformation.

6.6 Modelling of Non-Symmetric Shapes

The use of gridded fabric to allow observation of fabric deformation in more complex preforms such as a square section 'S' rail was attempted This highlighted a problem in the method used for constrained path definition within the KDM. The geodesic paths used by the model for a square section 'S' rail geometry, with an initial fabric orientation parallel to the outer channel edge, are shown in Figure 6.28. It appeared that the surface area between the paths in one quadrant (Quadrant A) was much larger than that in another (Quadrant B). This would suggest that the fabric has to shear in opposite directions in each quadrant, which had not been observed during the draping of previous male geometries, suggesting the paths were invalid.

Subsequent draping of the geometry confirmed the constrained path prediction to be invalid (Figure 6.29). The constrained path algorithm is based on geodesic

principles, which assume that the path crosses the boundary between two planar surface at a constant angle of incidence, as described in section 3.4.2. The red lines representing the constrained path across the preform followed a route that minimised differences in fabric shear between the four quadrants.

The co-ordinates of the red lines representing the constrained path on the formed fabric were manually measured, using the centre of the geometry as a datum, and used to define the constrained path co-ordinates for the model. Visual comparison between the formed part (Figure 6.29) and the KDM predictions based on the modified constrained paths (Figure 6.30) showed a good correlation between the predicted and the experimental grid patterns. A quantitative assessment using the ASAME process was more difficult due to the large surface areas involved and the problems associated with joining smaller grids described in section 5.4.2, so this was not attempted.

6.7 Conclusions

An automated grid strain analysis system was used to measure fabric deformation over a variety of geometries. These were compared with results from the kinematic drape model described in Chapter 3.

The effect of altering the height of a disc showed that the KDM provides a good approximation of fabric drape at low shear angles. As shear increased, the effect of stitch alignment on the deformation was also observed. This agreed with the in-plane shear stiffness tests described in Chapter 4, which showed the shear stiffness of a tricot stitched fabric increased when the loading was aligned with the stitching. The shear stiffness of the fabric used in the forming tests was approximately double when sheared in direction of the stitch as perpendicular to it. However, the difference in shear between the quadrants within the preforms did not occur in the same ratio. There appears to be no effect of preforming velocity on the drape of a hemispherical preform, suggesting the results of the shear velocity tests reported in section 4.4.3, are not significant to preforming.

For taller discs where the KDM predicted higher shear angles than the fabric could conform to, the KDM provided accurate results up to the onset of fabric locking

where wrinkling occurred. The shear data shown in Figure 6.10 indicate that an imposed locking angle within the KDM would increase the accuracy in areas of large deformation. Since locking is fabric dependent, the limiting values need to be specified for each particular fabric. This type of modification cannot be done using the existing drape algorithms which assumes a constant fibre spacing. The fibre spacing would need to be altered locally within the equations to allow for fibre buckling at high shear angles.

There was no evidence of a relationship between slip and shear angle. This suggests that the slip model reported by Laroche and Vu-Khanh [74] is not valid for SBFs. At high shear angles yarn buckling was evident, which indicates that compressive forces are created in the fabric.

The application of the KDM to more general shapes such as an 'S' rail indicated problems in the conventional approach for calculating the constrained paths using geodesic principles. From inspection of the data, the constraints should be applied using a minimisation of shear force approach. This would require information of the shear stiffness of the fabric being modelled, which as reported in Chapter 4 is directional.

An investigation into the effect of initial fabric orientation on the draping of a pyramid, indicated that problems such as wrinkling and extreme fabric shear can be minimised by optimising the original fabric orientation with respect to the geometry. The KDM indicated which was the optimum fabric orientation, although the fabric folded when formed at all four orientations. The results indicated that for the draping of a less extreme geometry, the KDM can be used to optimise the geometry profile and fabric lay-up prior to manufacture.

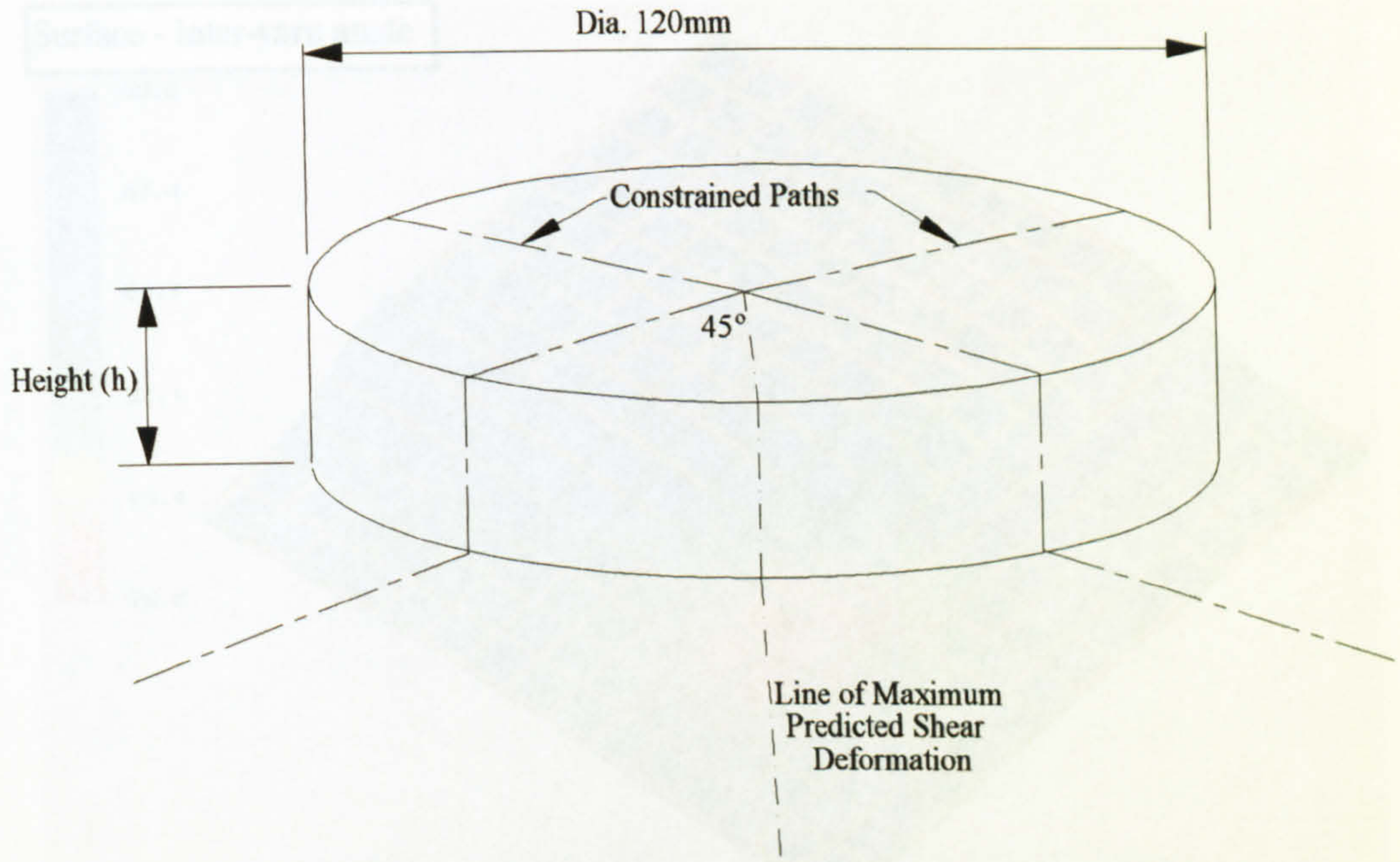

Figure 6.1 Disc geometry showing constrained paths (used in KDM) and line of maximum predicted shear deformation (used for comparison of data). (Disc height (h) varied from 7 mm to 38 mm.)

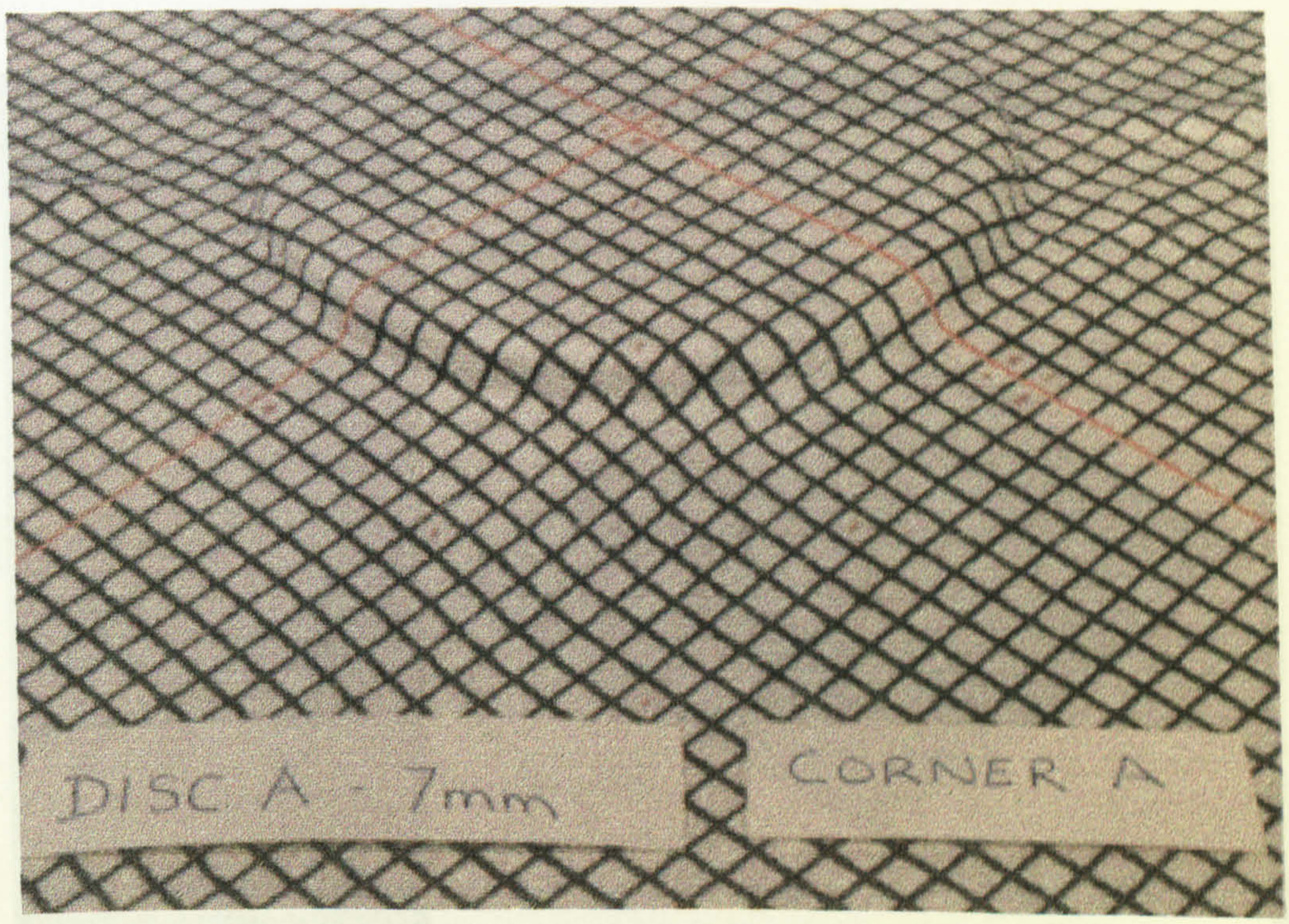

Figure 6.2 7 mm high disc preformed with gridded fabric. Note: The red lines defining constrained yarns run through the centre of the fabric defining four preform quadrants. (Fabric - Tech Textiles E-BX 948, vacuum formed.)

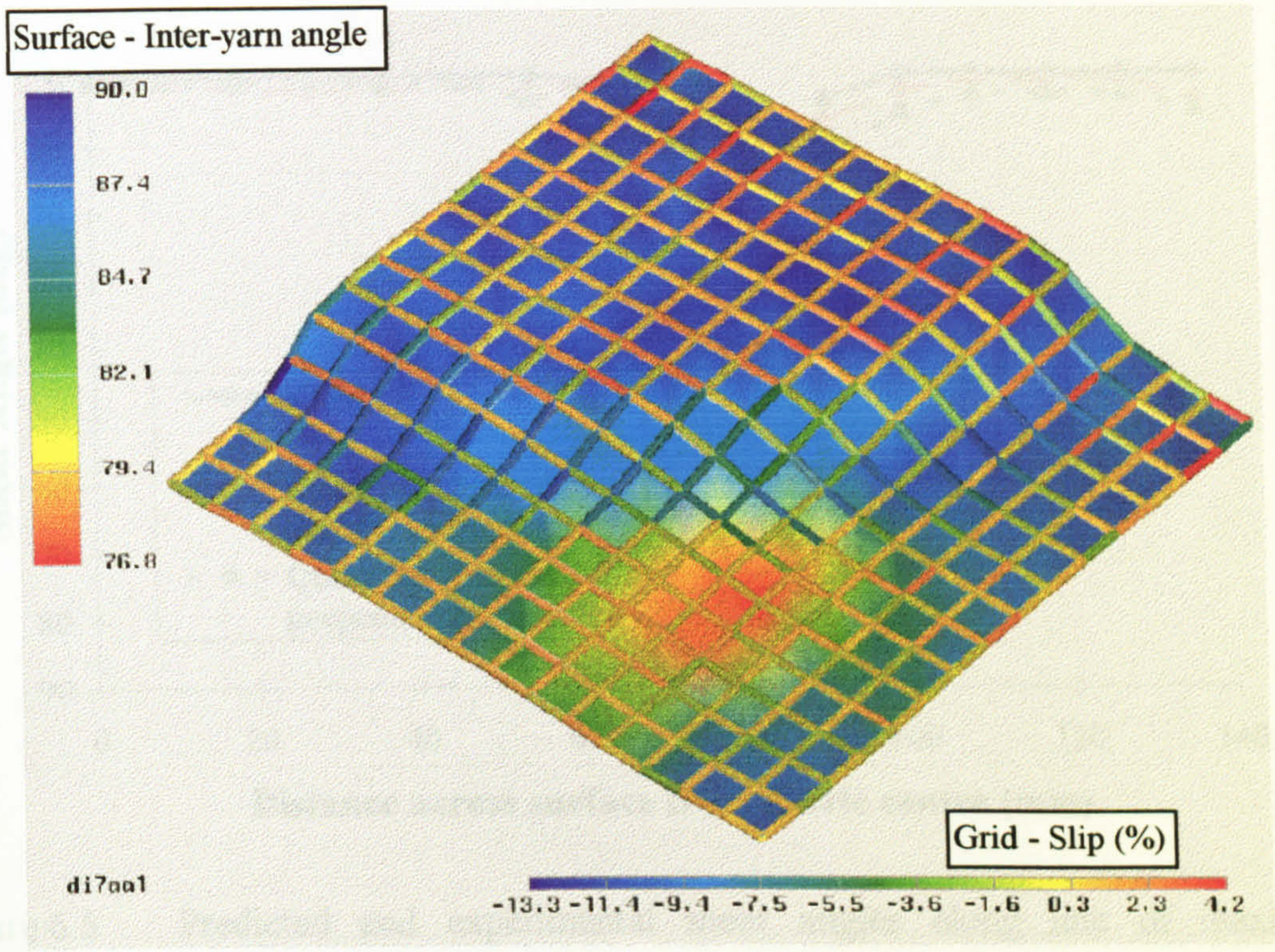

Figure 6.3 AVS plot of experimental shear and slip data for a 7 mm high disc, corresponding to front quadrant in Figure 6.2. Surface colour represents ply angle and grid colour defines slip. (Tech Textiles E-BX 948, vacuum formed).

Figure 6.4 KDM estimated fabric drape for a 7 mm high disc. Note: Low levels of shear are required to drape the fabric. (2.13 mm grid spacing provides more accurate results than 6.4 mm.)

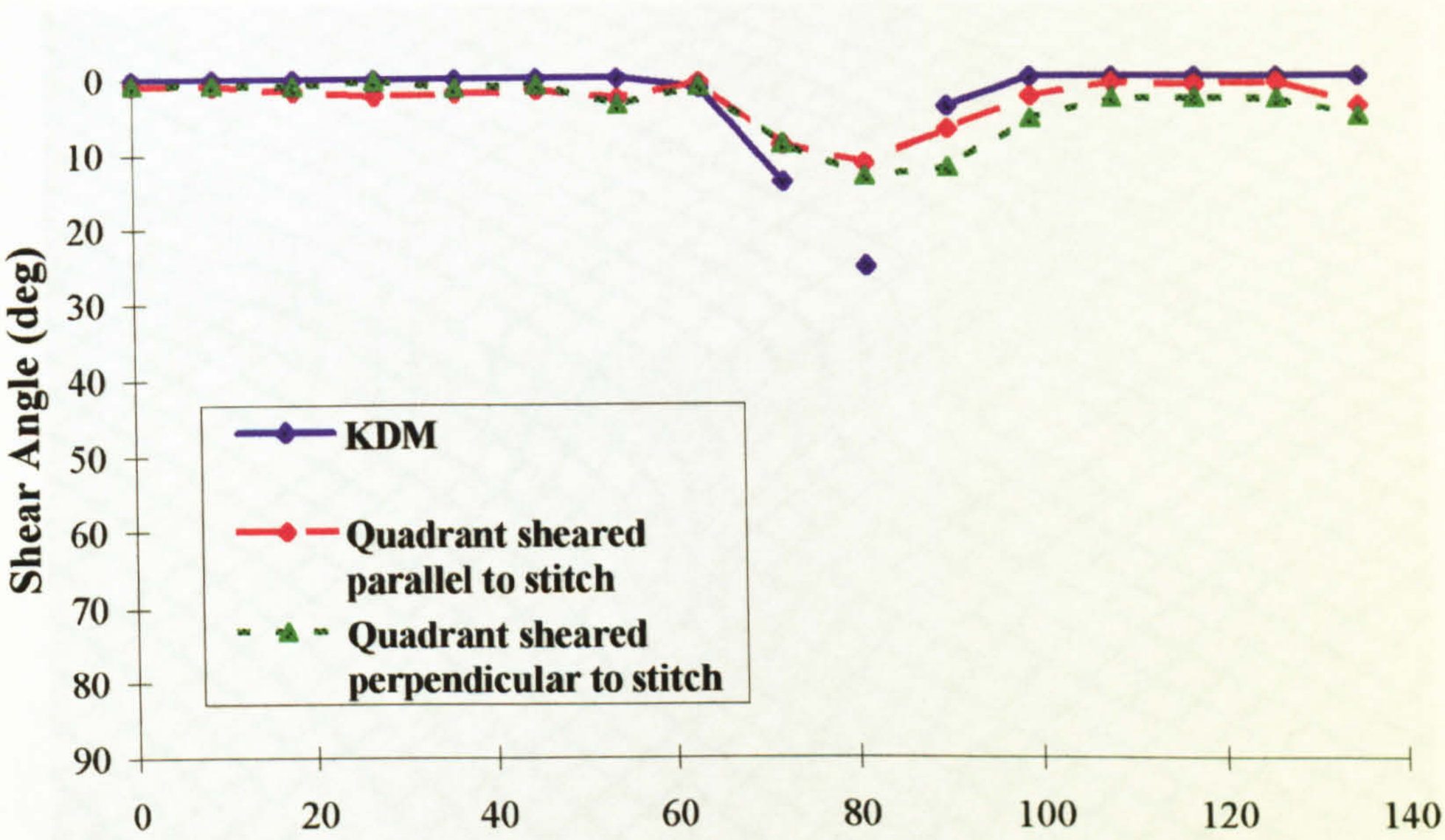

Figure 6.5 Predicted and experimental shear angles along line of maximum deformation for a 7 mm high disc. (Tech Textiles E-BX 948, vacuum formed.)

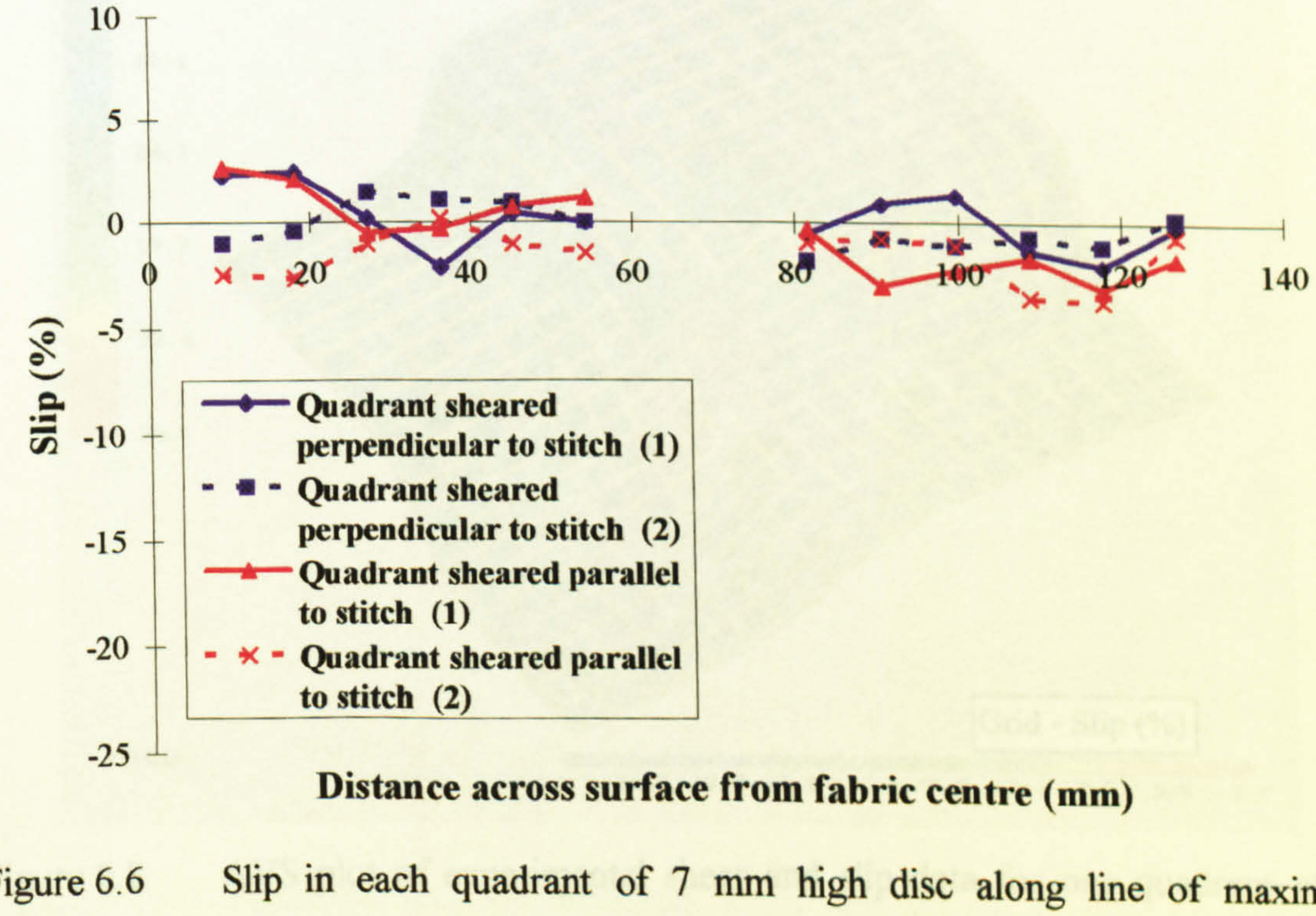

Figure 6.6 Slip in each quadrant of 7 mm high disc along line of maximum deformation. (Tech Textiles E-BX 948, vacuum formed.)

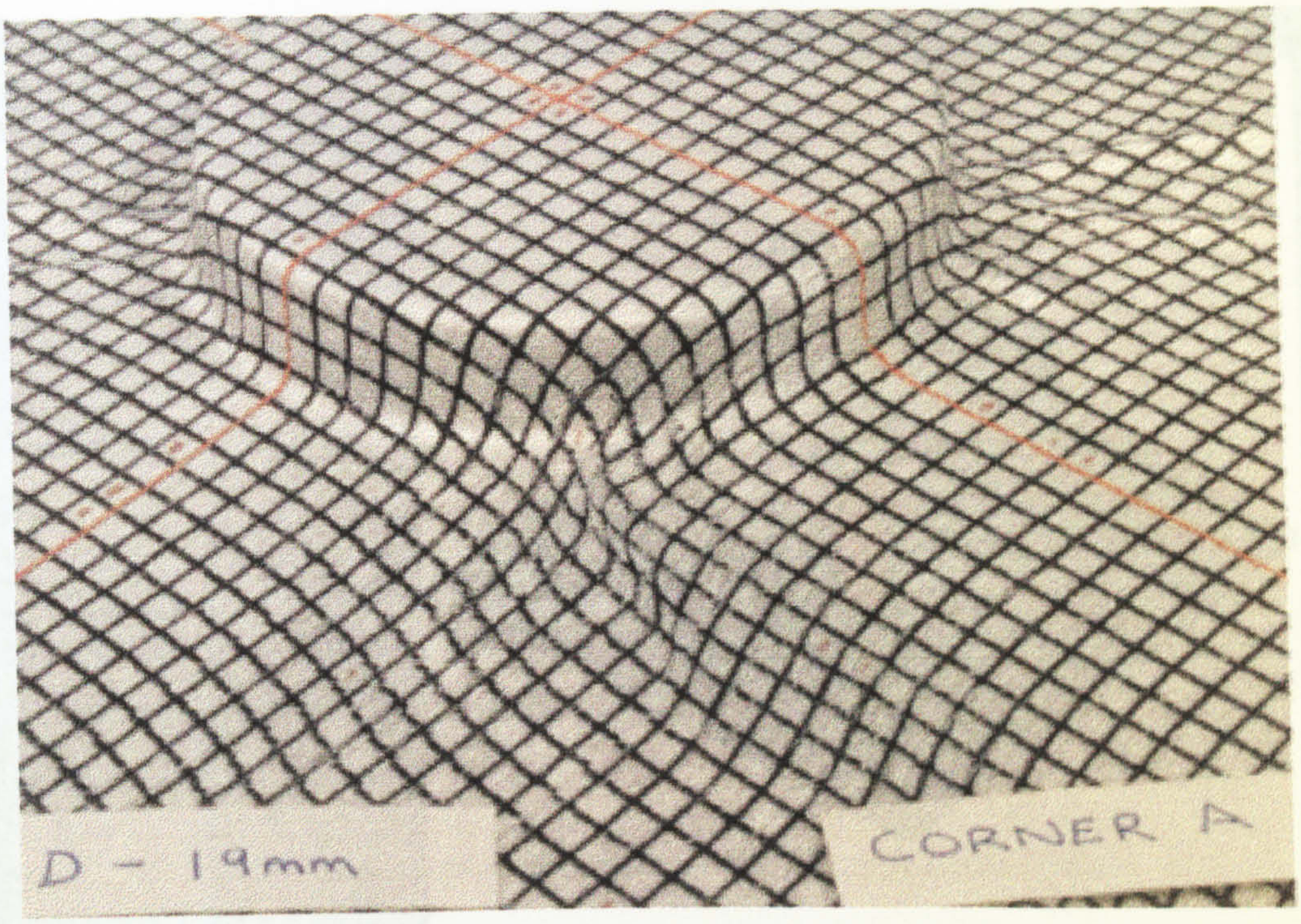

Figure 6.7 19 mm high disc preform. Note: the fibres are buckling in the plane of the fabric in the front quadrant (denoted Corner A in photo) and wrinkling in the two quadrants to the left and right. (Fabric - Tech Textiles E-BX 948, vacuum formed.)

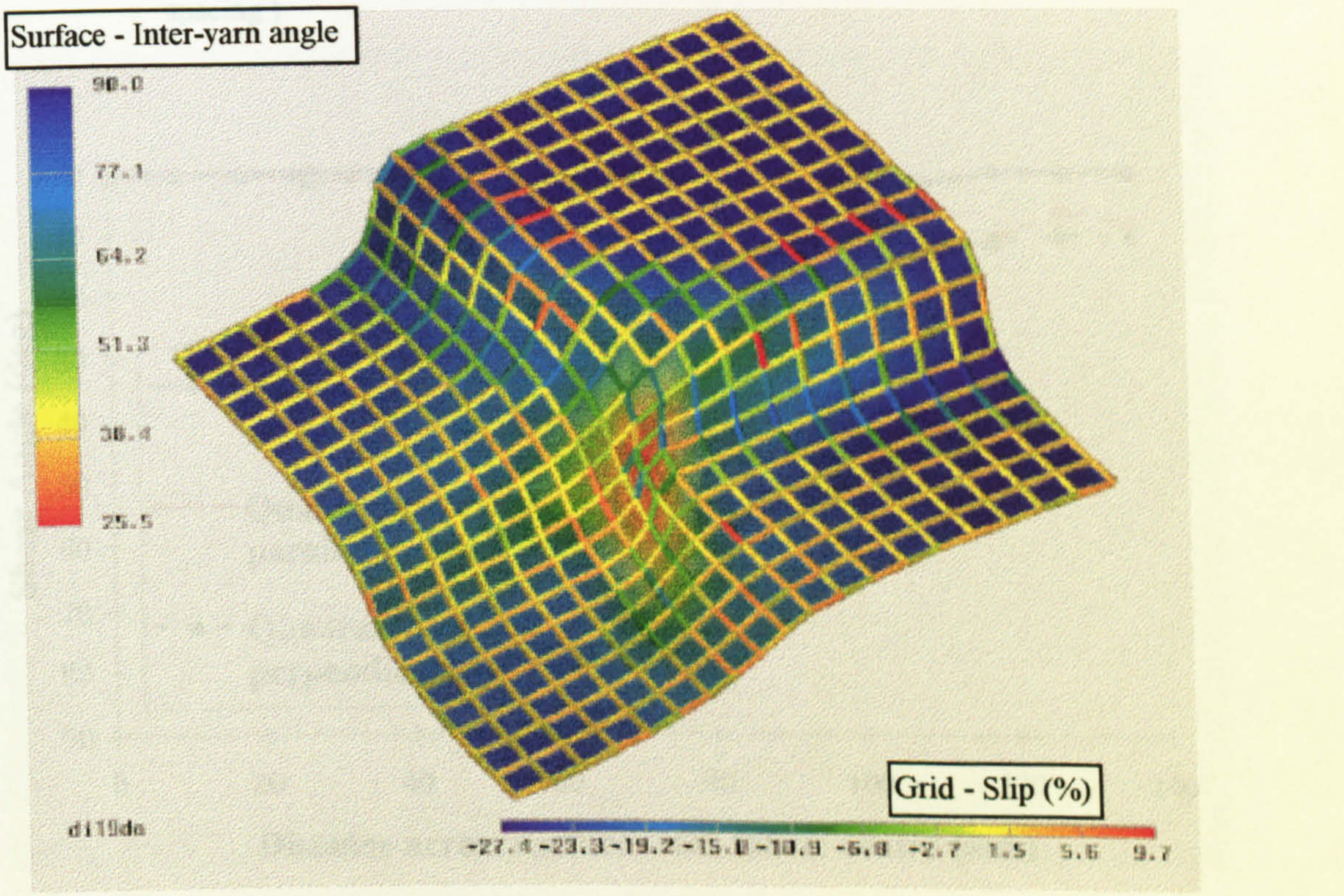

Figure 6.8 AVS plot of experimental shear and slip data for one quadrant of 19 mm high disc. Note: The buckling of the fibres can be seen as negative slip (denoted by the colour of the grid bars) in the area of highest shear. (Fabric - Tech Textiles E-BX 948, vacuum formed.)

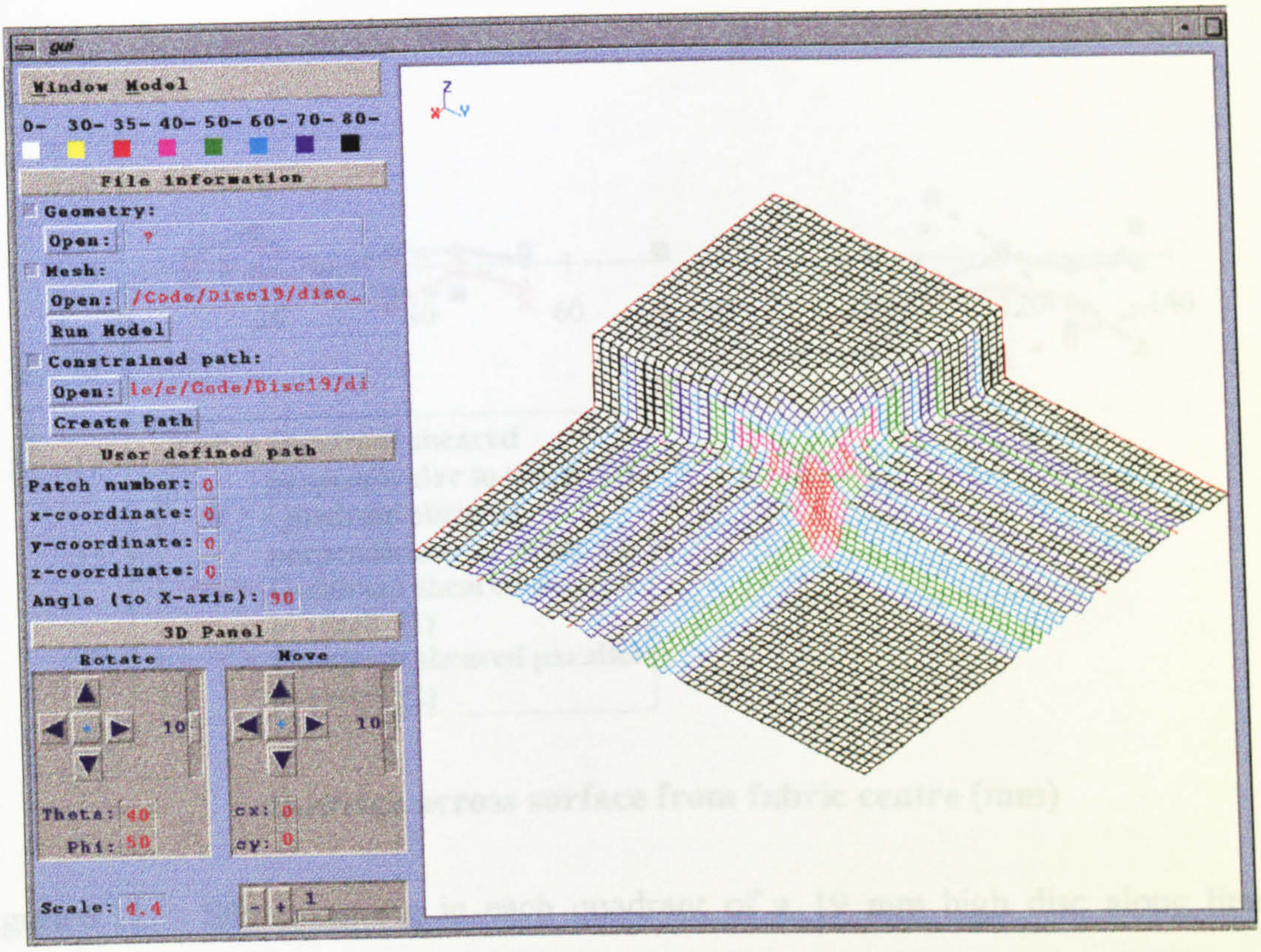

Figure 6.9 KDM estimated fabric drape for a 19 mm high disc. (2.13 mm grid spacing.)

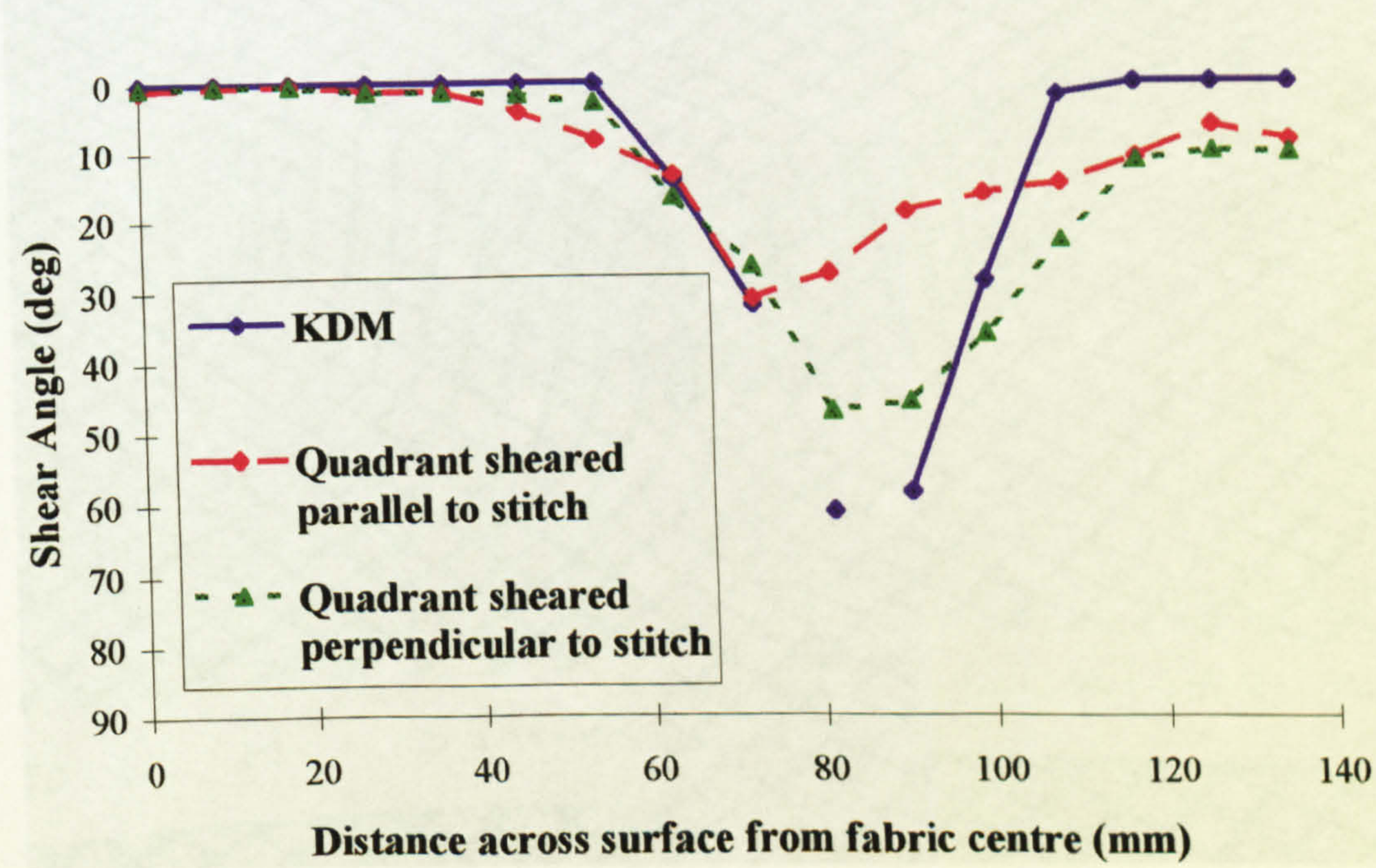

Figure 6.10 Predicted and experimental shear angles along line of maximum deformation for a 19 mm high disc. (Tech Textiles E-BX 948, vacuum formed.)

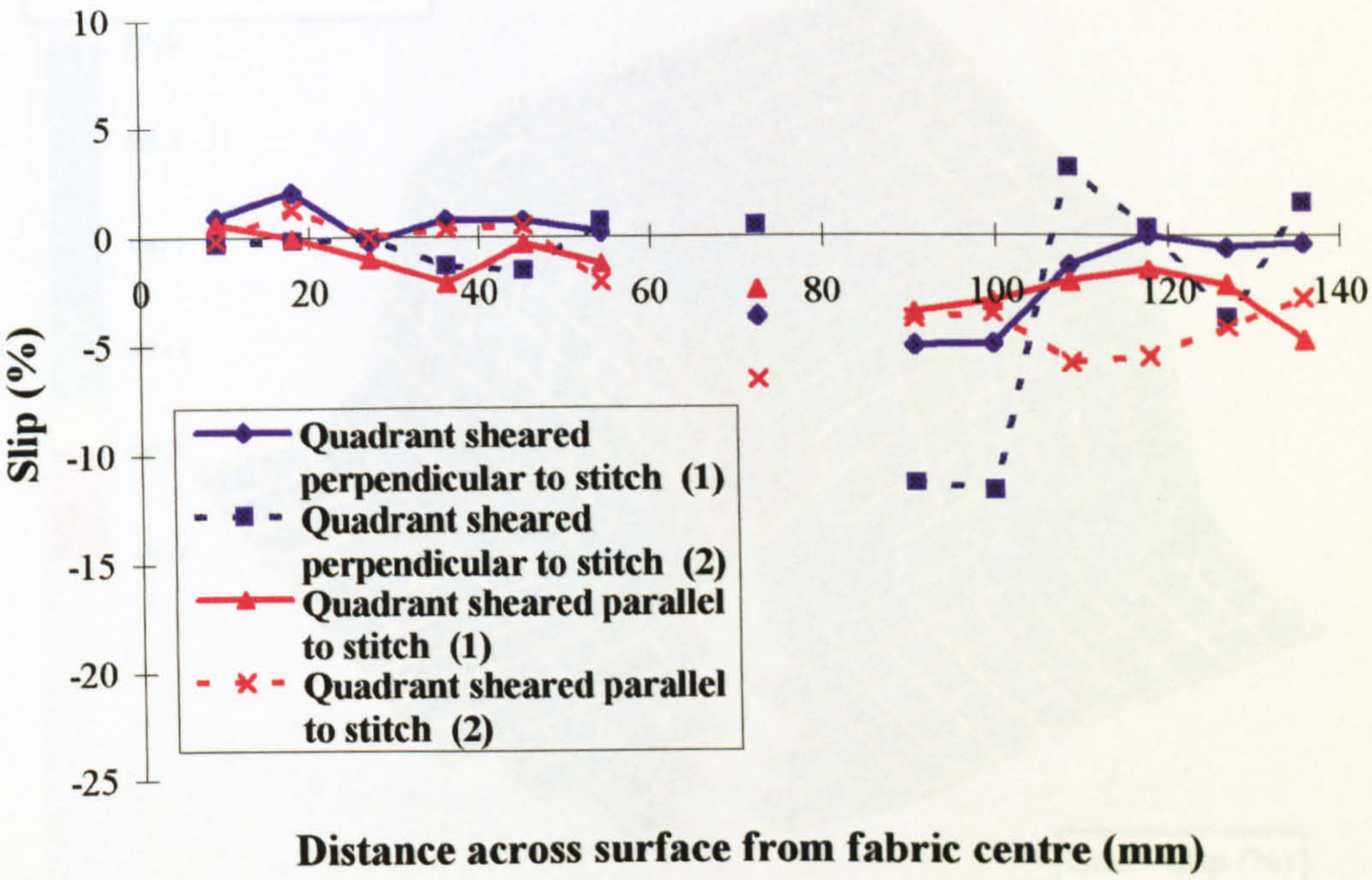

Figure 6.11 Slip occurring in each quadrant of a 19 mm high disc along line of maximum deformation. (Fabric - Tech Textiles E-BX 948, vacuum formed.)

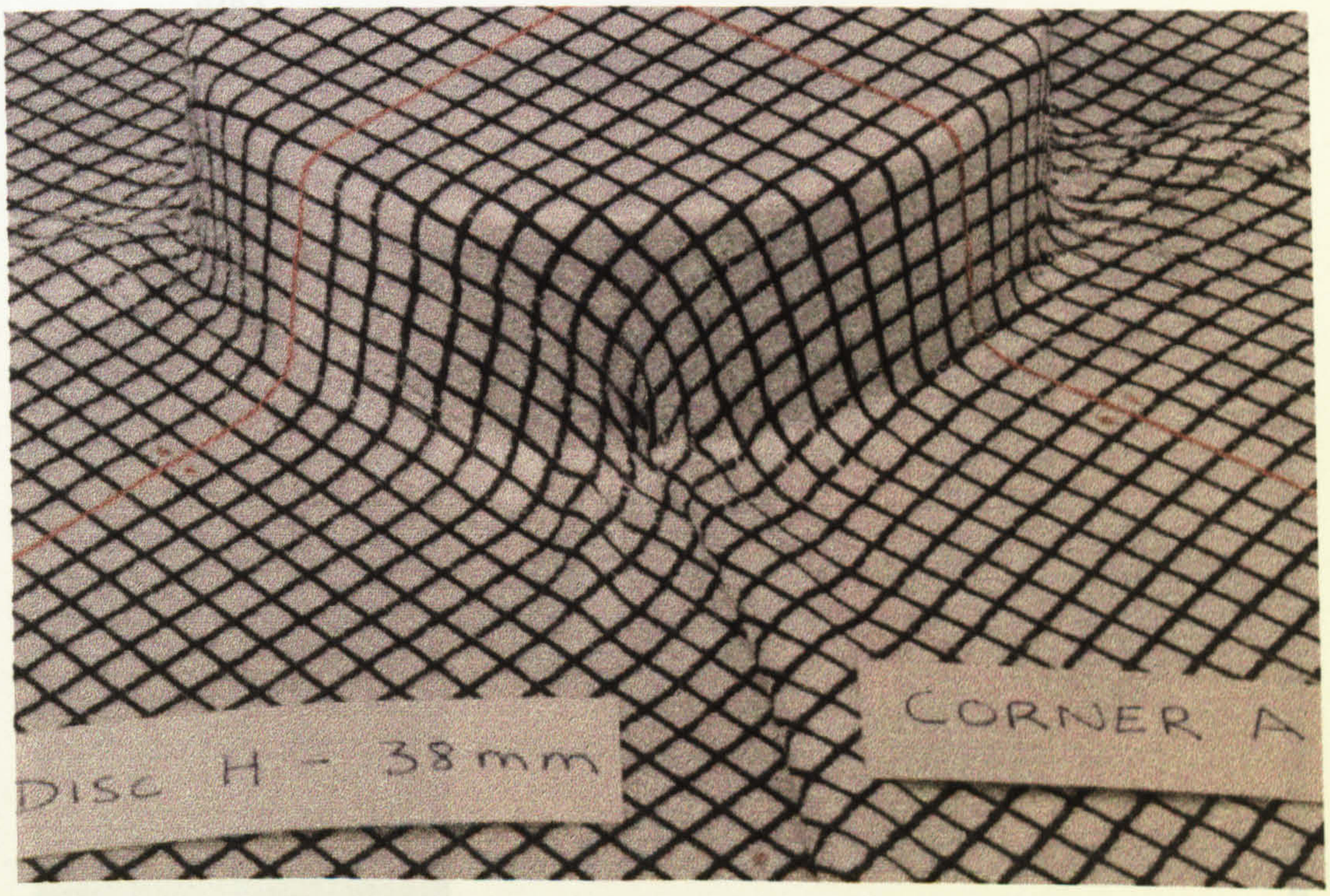

Figure 6.12 38 mm high disc preform. Note: Wrinkling occurred due to fabric locking which prevented complete mapping of grid. (Tech Textiles E-BX 948, vacuum formed.)

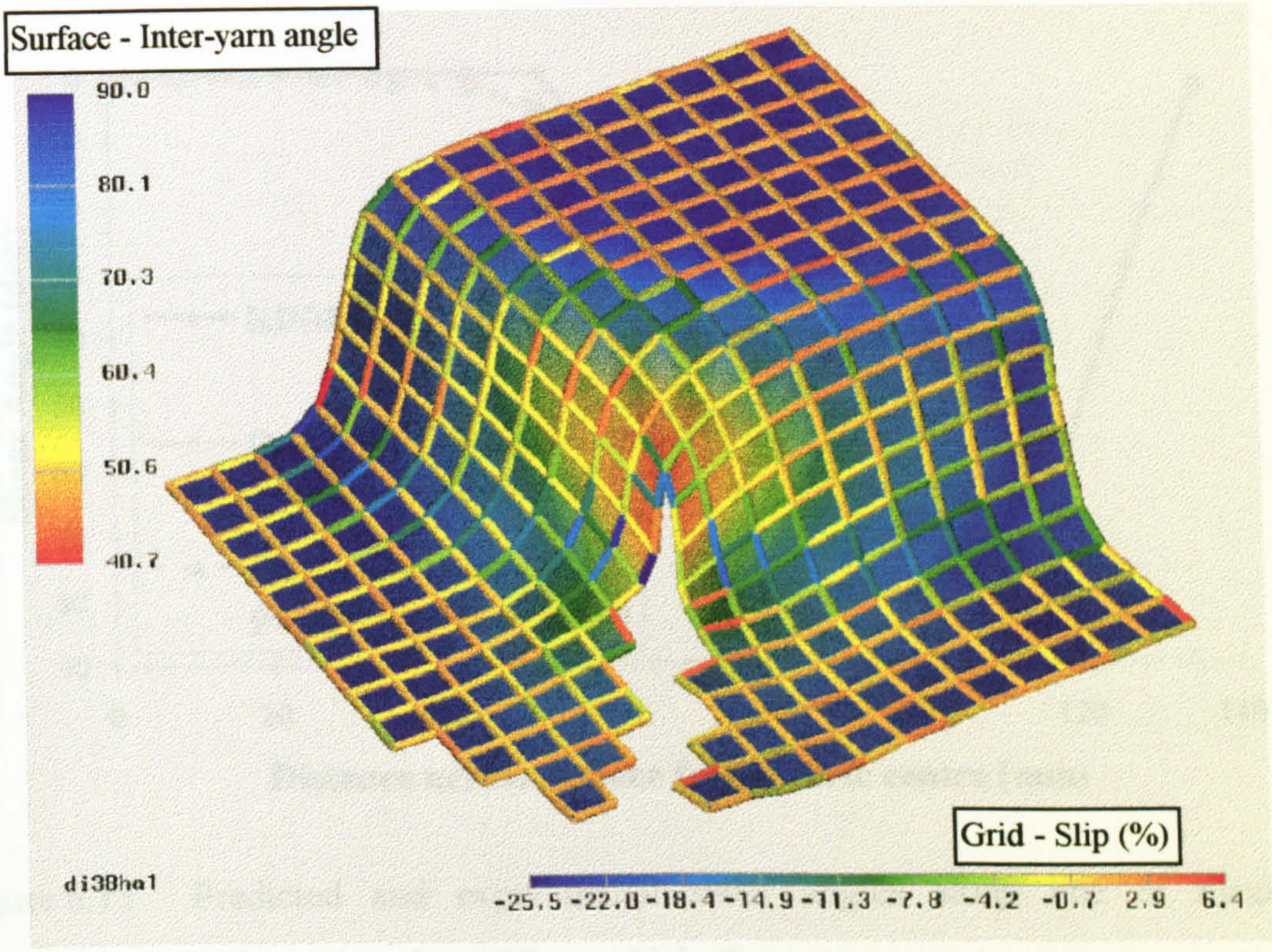

Figure 6.13 AVS plot of experimental shear and slip data for one quadrant of 38 mm high disc. (Note: Missing data due to fabric wrinkling, Tech Textiles E-BX 948.)

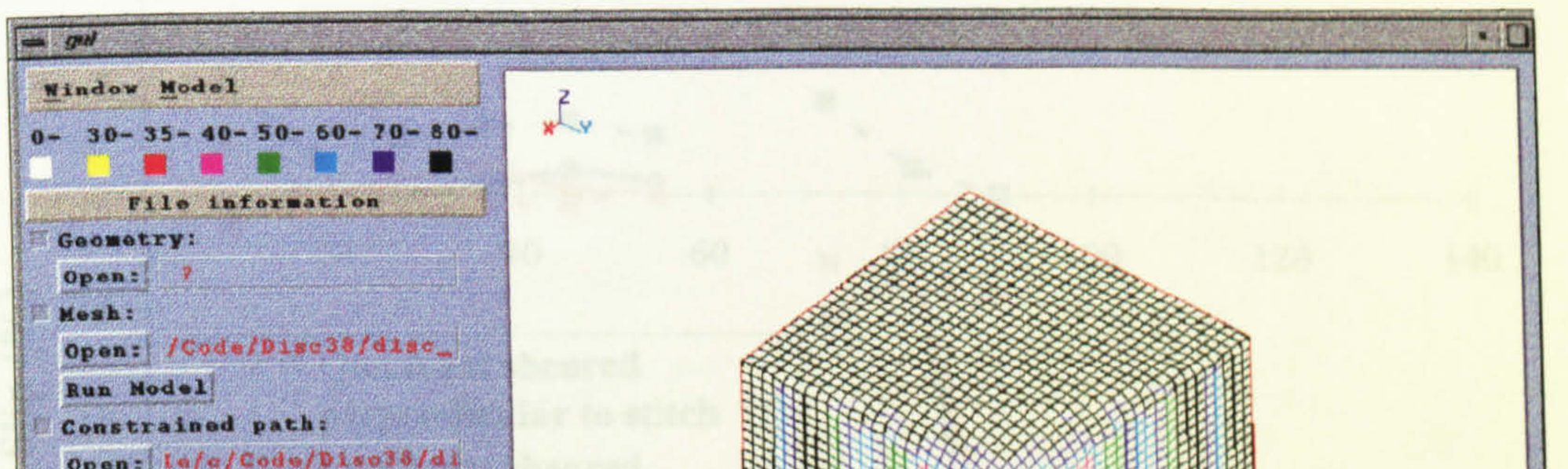

Figure 6.14 KDM estimated fabric drape for a 38 mm high disc. (2.13 mm grid spacing).

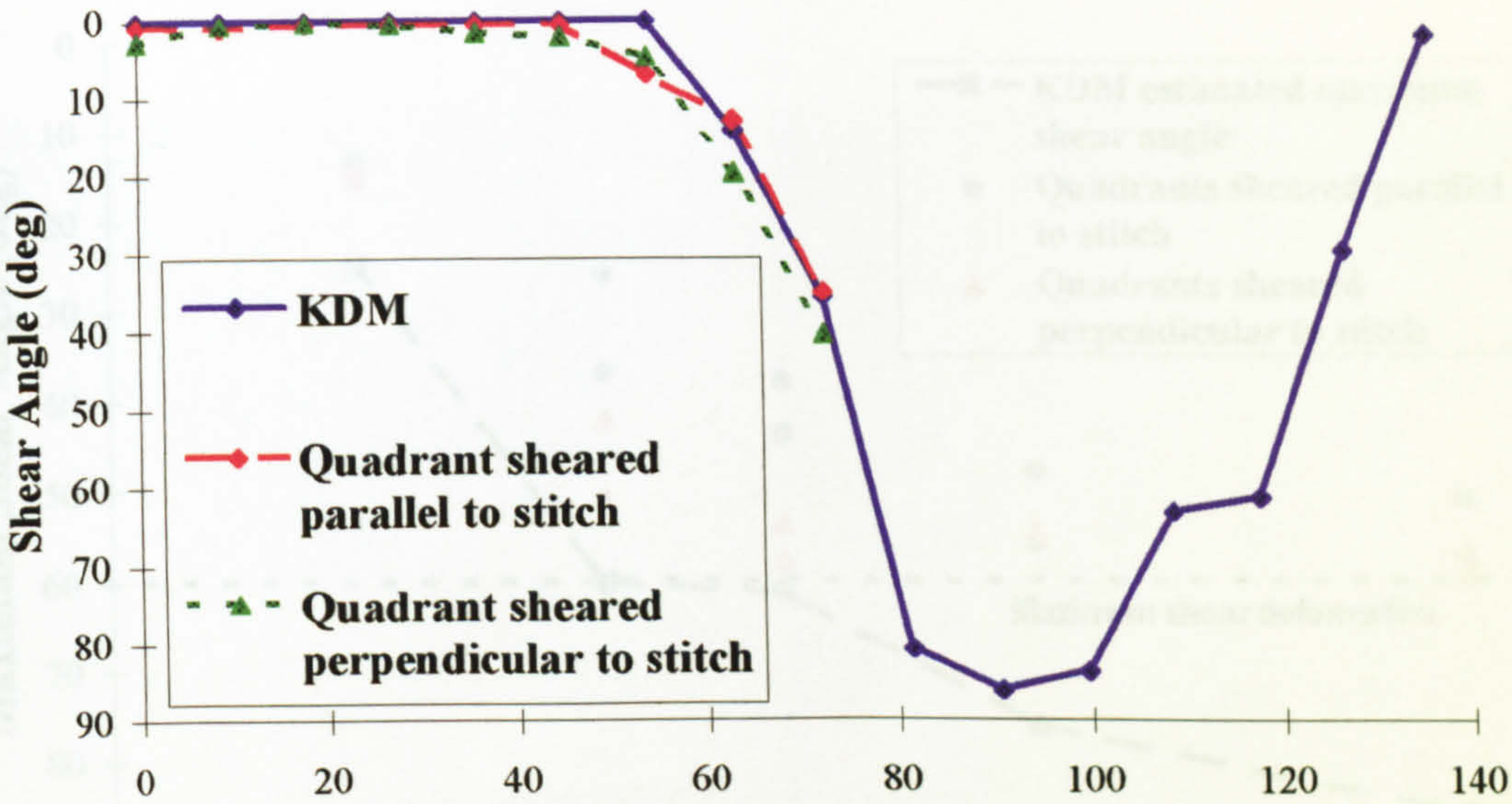

Figure 6.15 Predicted and experimental shear angles along line of maximum deformation for a 38 mm high disc. Note: missing data due to wrinkling, (Fabric - Tech Textiles E-BX 948, vacuum formed.)

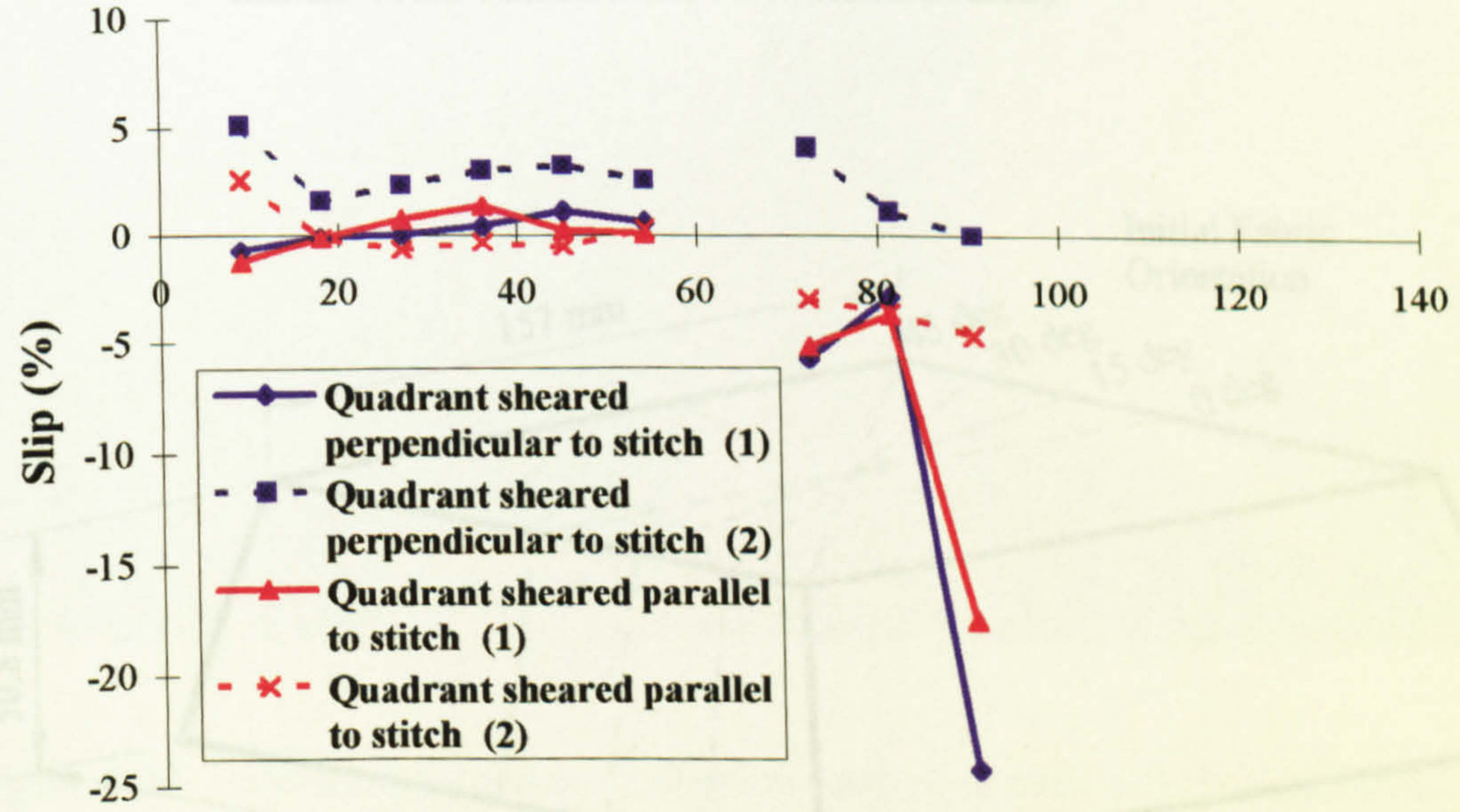

Figure 6.16 Slip in each quadrant of a 38 mm high disc along line of maximum deformation. Note: Missing data due to edge effects and wrinkling in the fabric, (Fabric - Tech Textiles E-BX 948, vacuum formed.)

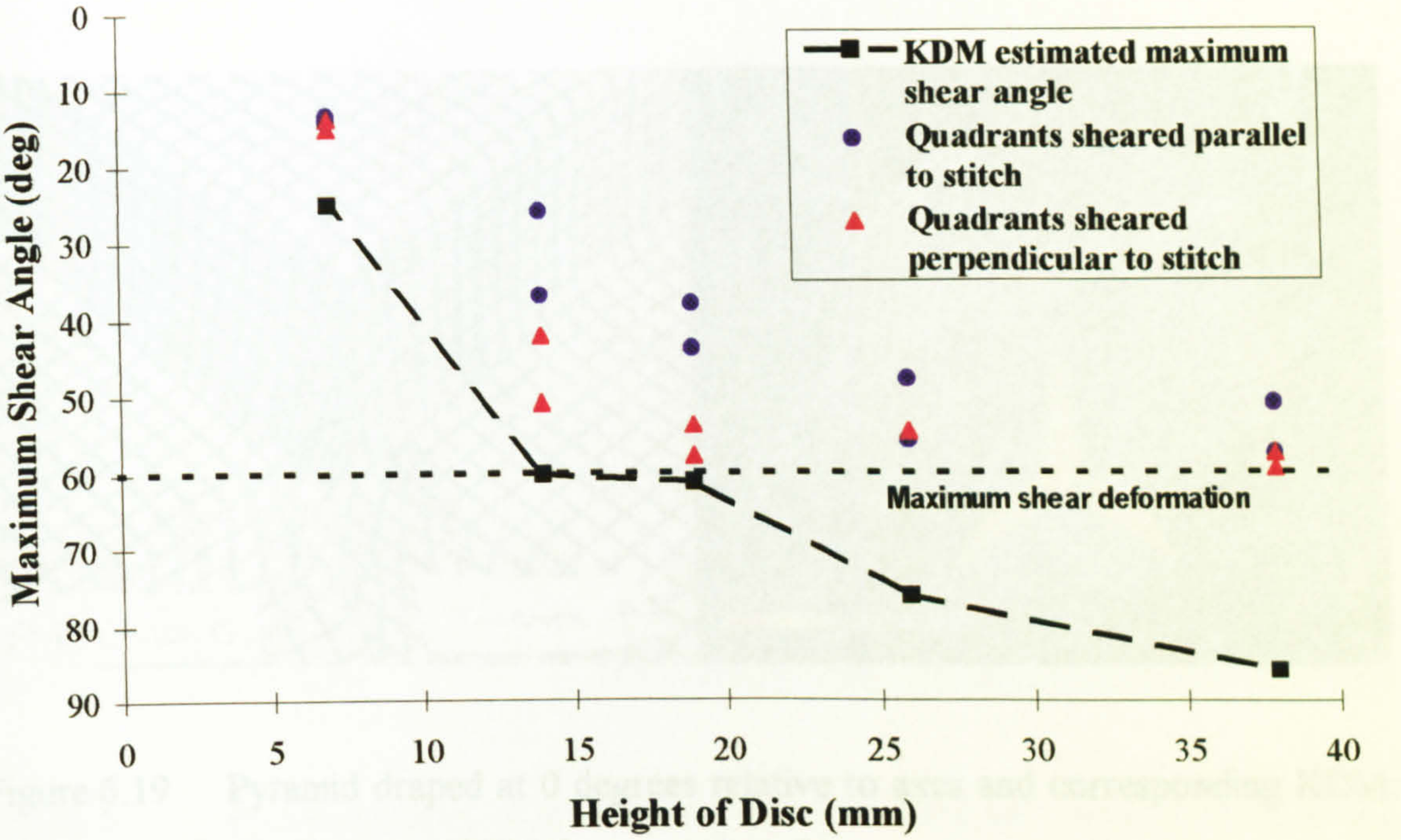

Figure 6.17 Maximum measured shear angle for varying heights of disc. Note: Higher shear occurs in quadrants sheared perpendicular to the stitch due to stitch tension. (Tech Textiles E-BX 948, vacuum formed.)

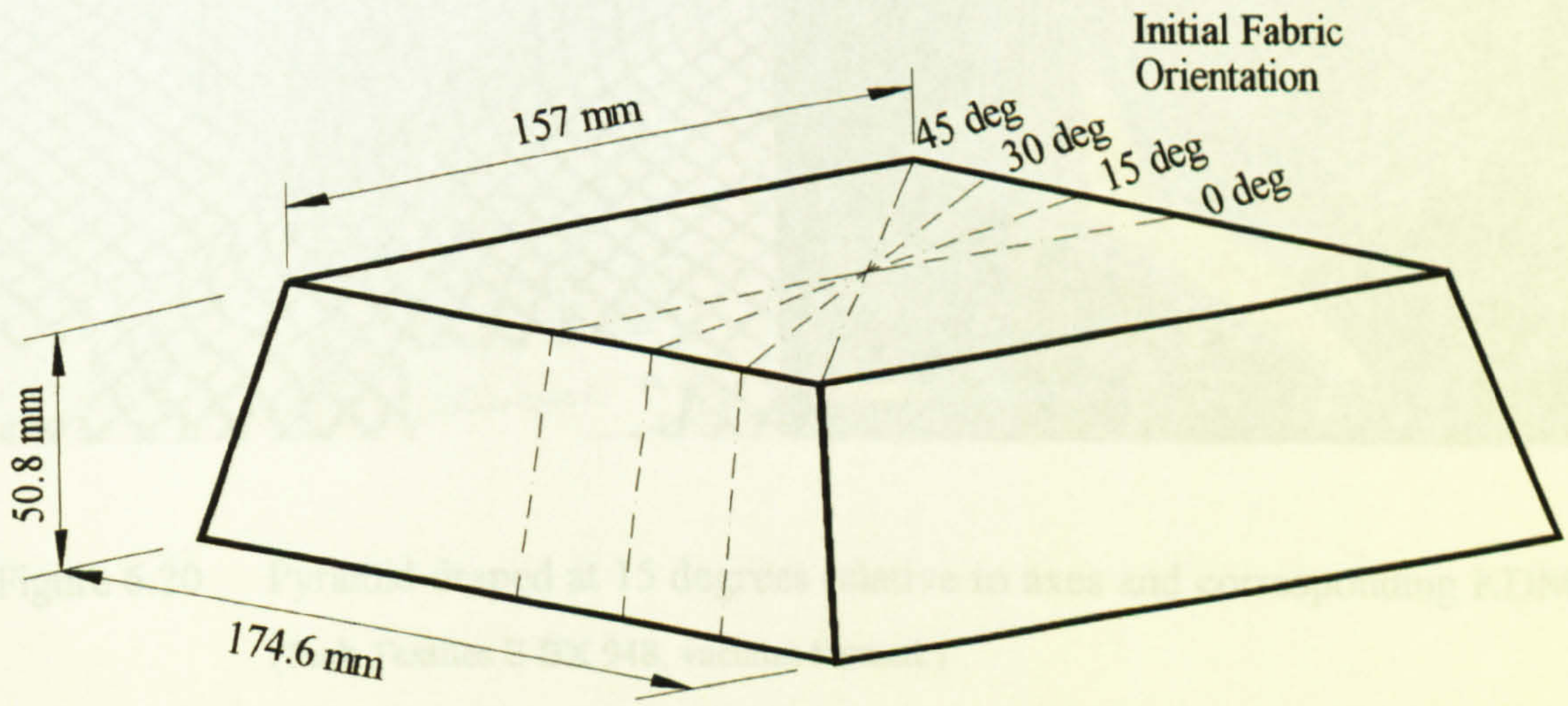

Figure 6.18 Details of pyramid dimensions and initial fabric orientation with respect to pyramid centreline.

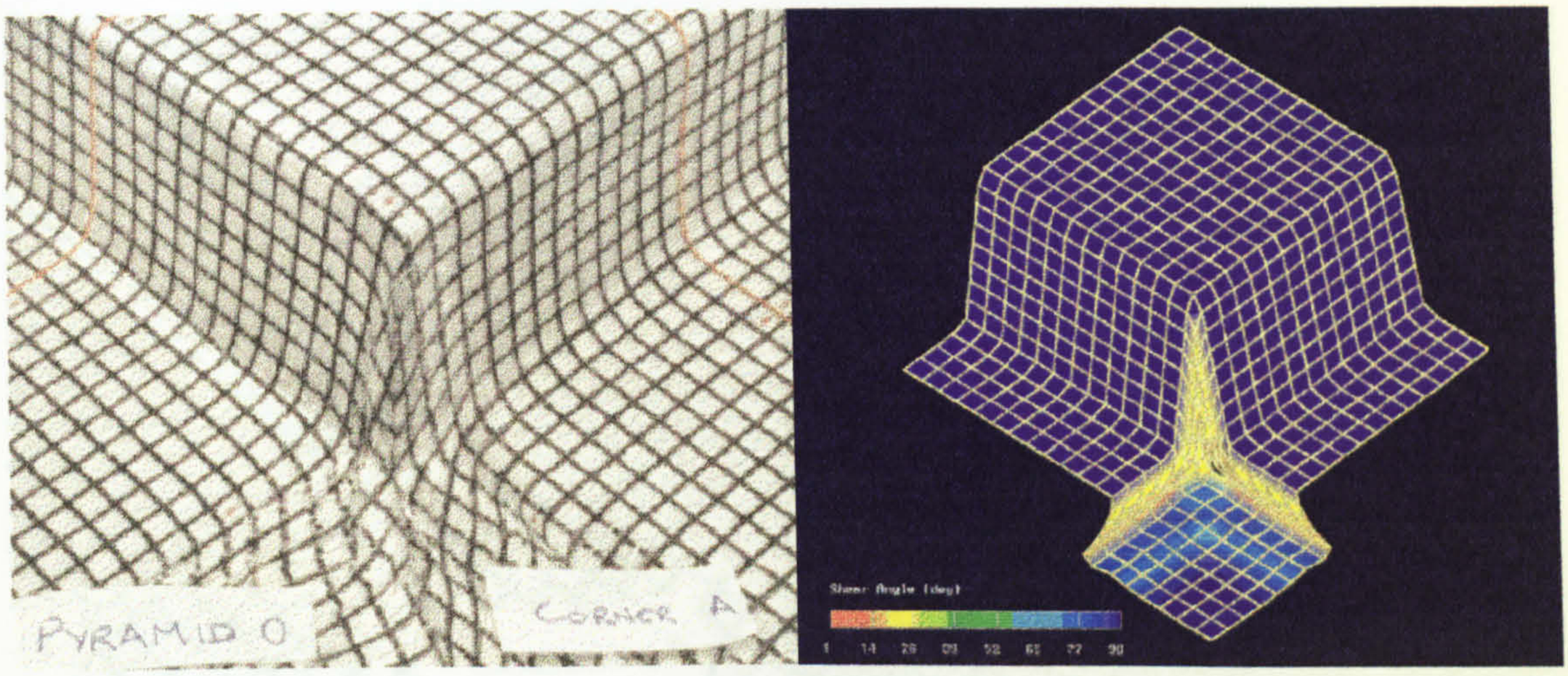

Figure 6.19 Pyramid draped at 0 degrees relative to axes and corresponding KDM.

(Tech Textiles E-BX 948, vacuum formed.)

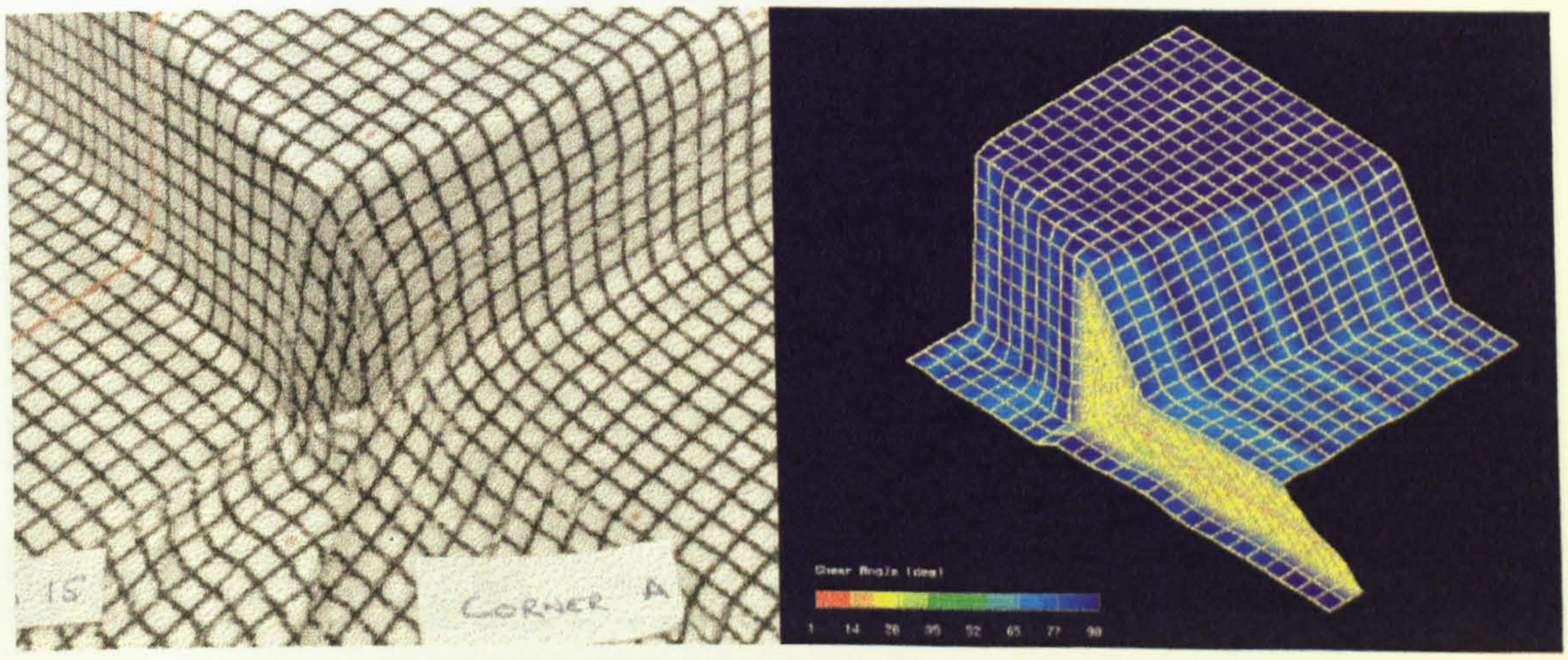

Figure 6.20 Pyramid draped at 15 degrees relative to axes and corresponding KDM.

(Tech Textiles E-BX 948, vacuum formed.)

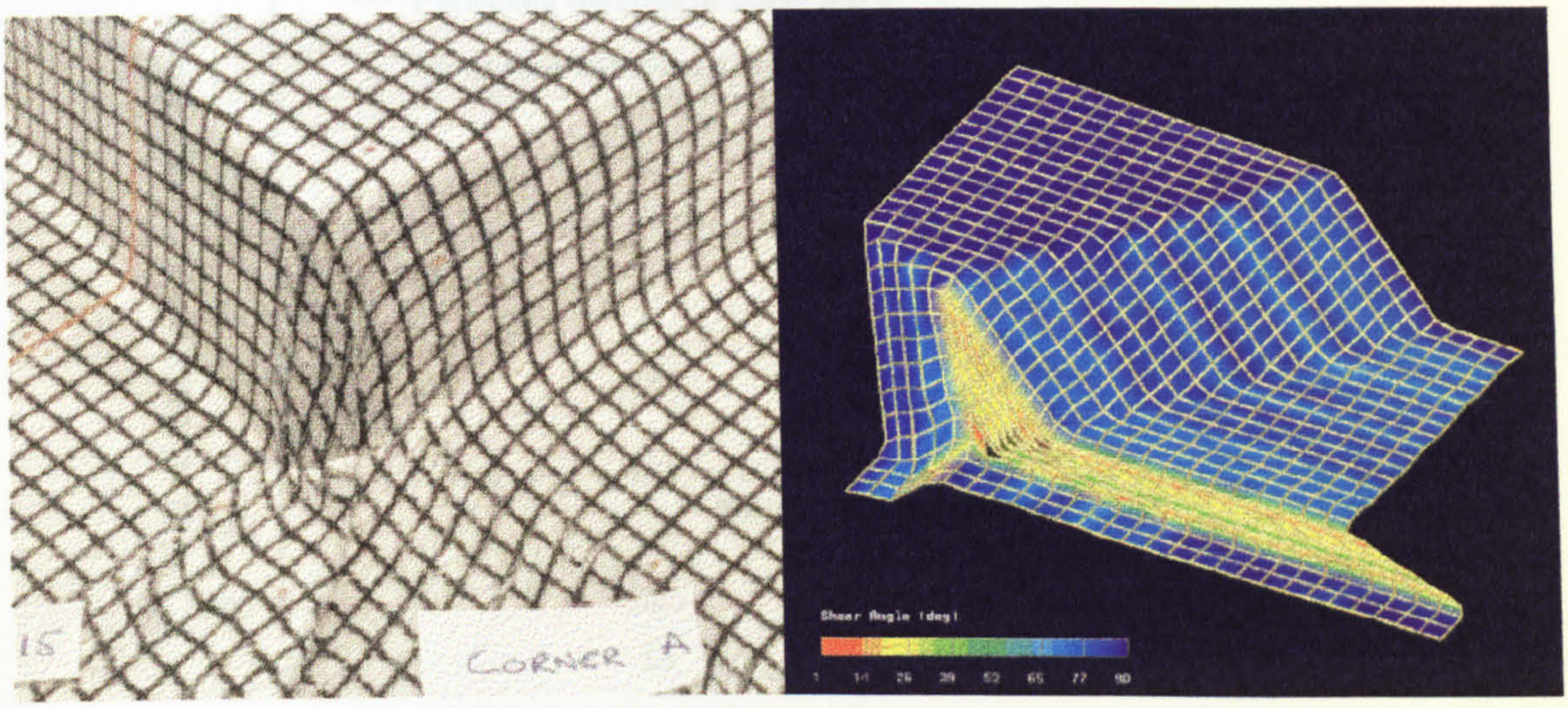

Figure 6.21 Pyramid draped at 30 degrees relative to axes and corresponding KDM.

(Tech Textiles E-BX 948, vacuum formed.)

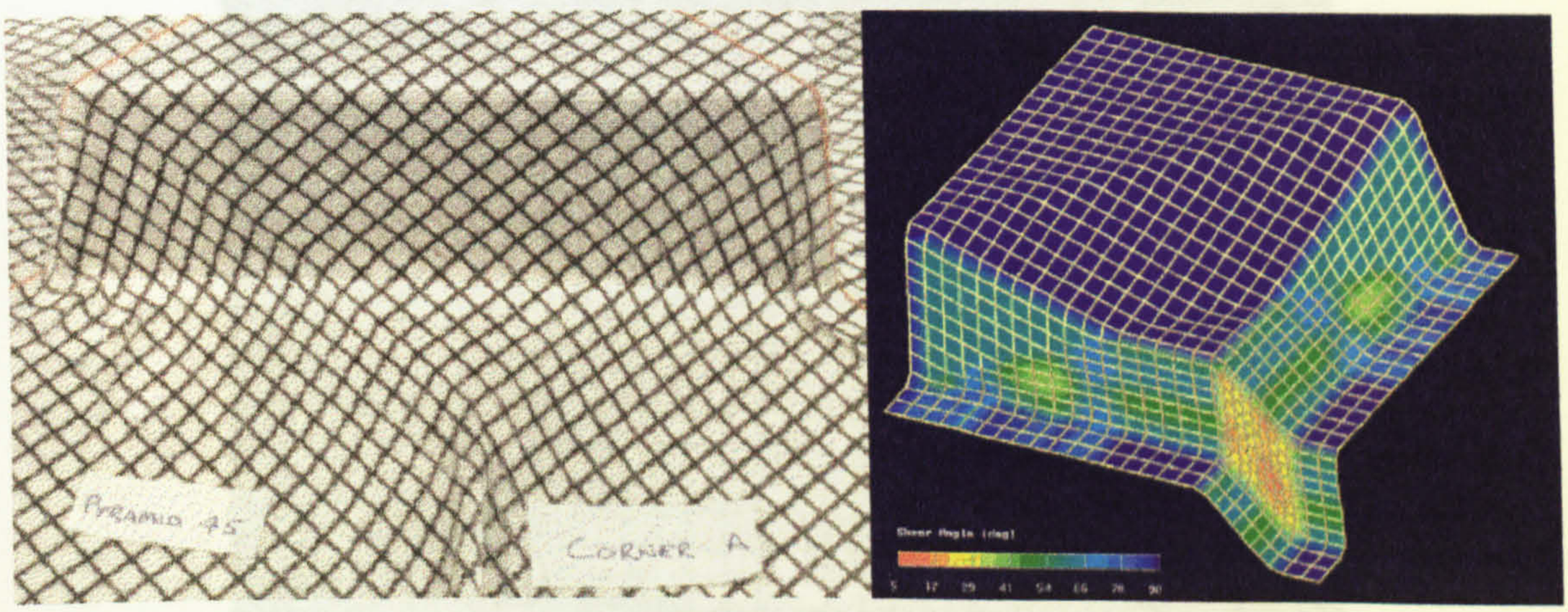

Figure 6.22 Pyramid draped at 45 degrees relative to axes and corresponding KDM.

(Tech Textiles E-BX 948, vacuum formed.)

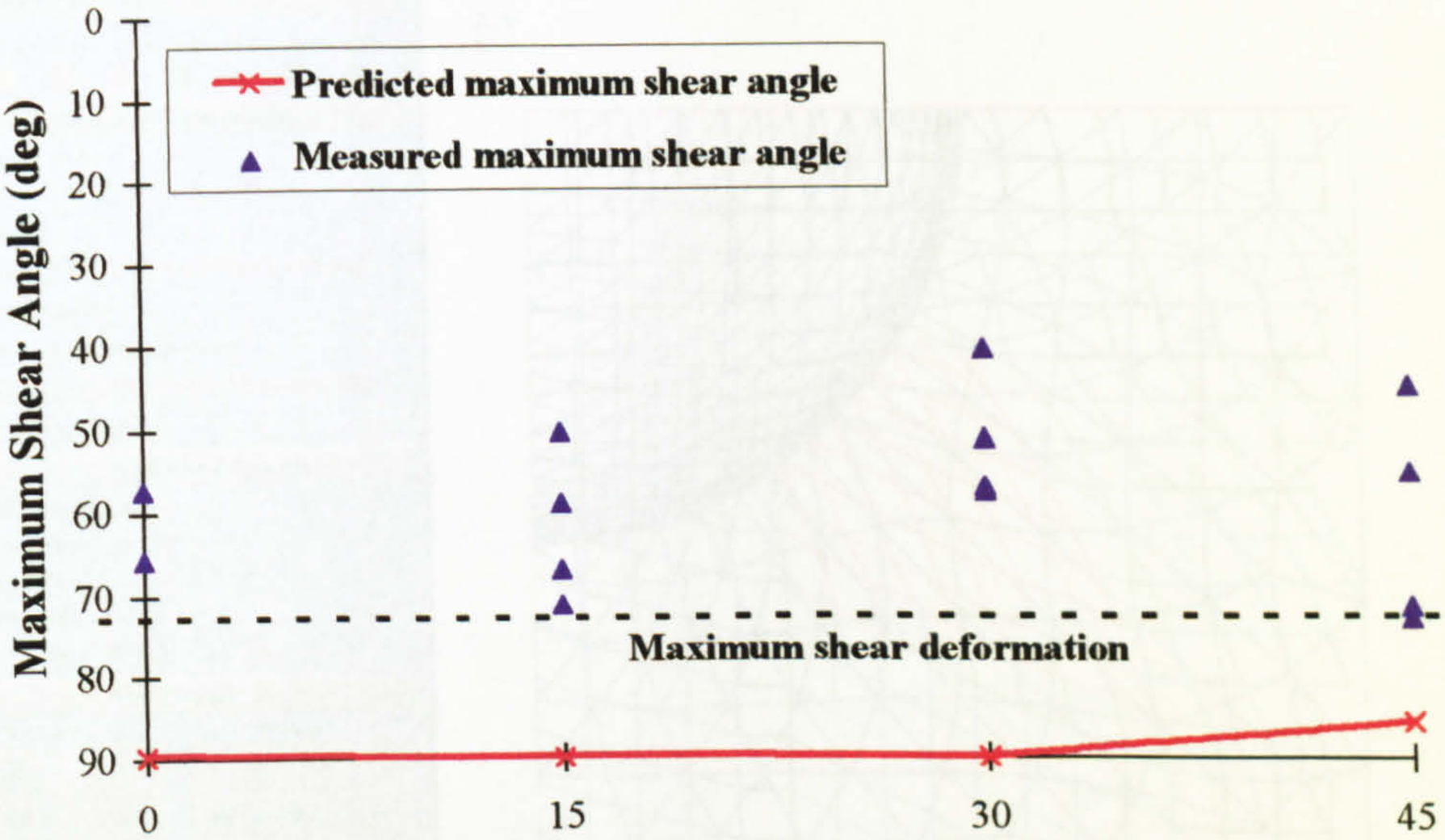

Figure 6.23 Comparison of maximum shear angle for a pyramid draped at different orientations with respect to pyramid axes. (Tech Textiles E-BX 948, vacuum formed.)

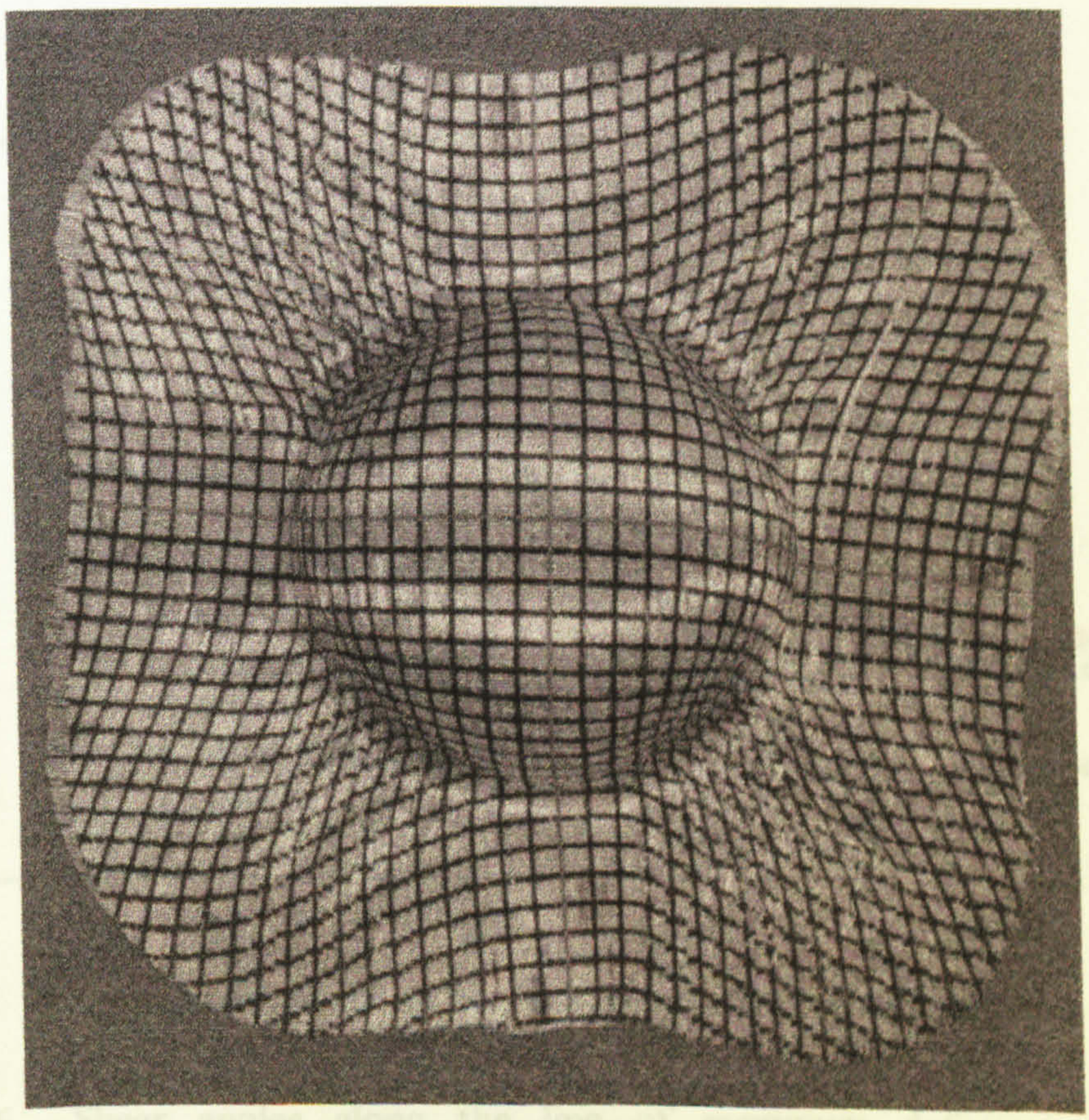

Figure 6.24 Fabric formed into a hemispherical preform. Note: The shear deformation is not symmetric between the quadrants (Tech Textiles E-BX 948, press formed at 65 mm/min.)

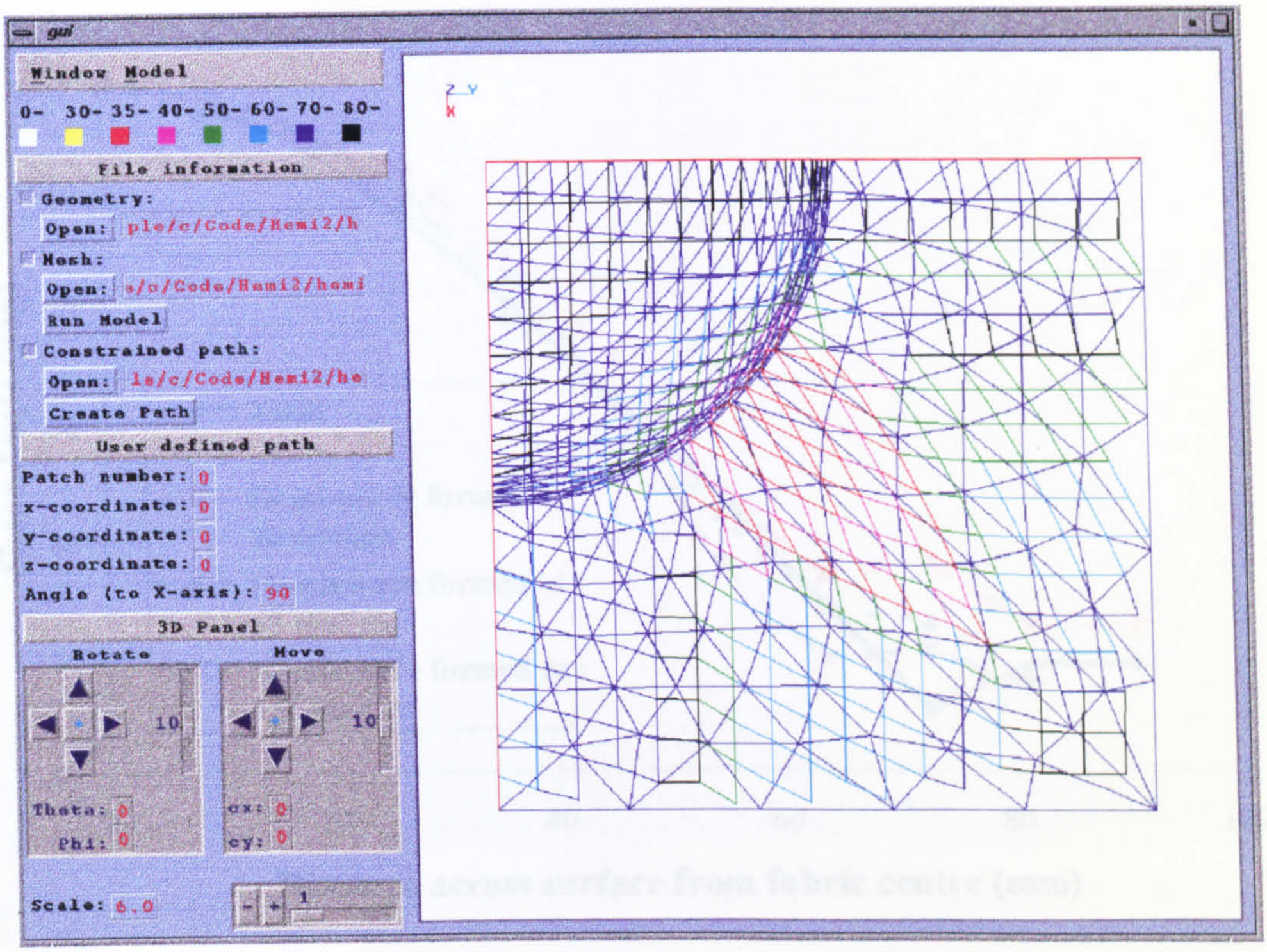

Figure 6.25 KDM estimate for hemispherical quadrant (6.4 mm grid spacing).

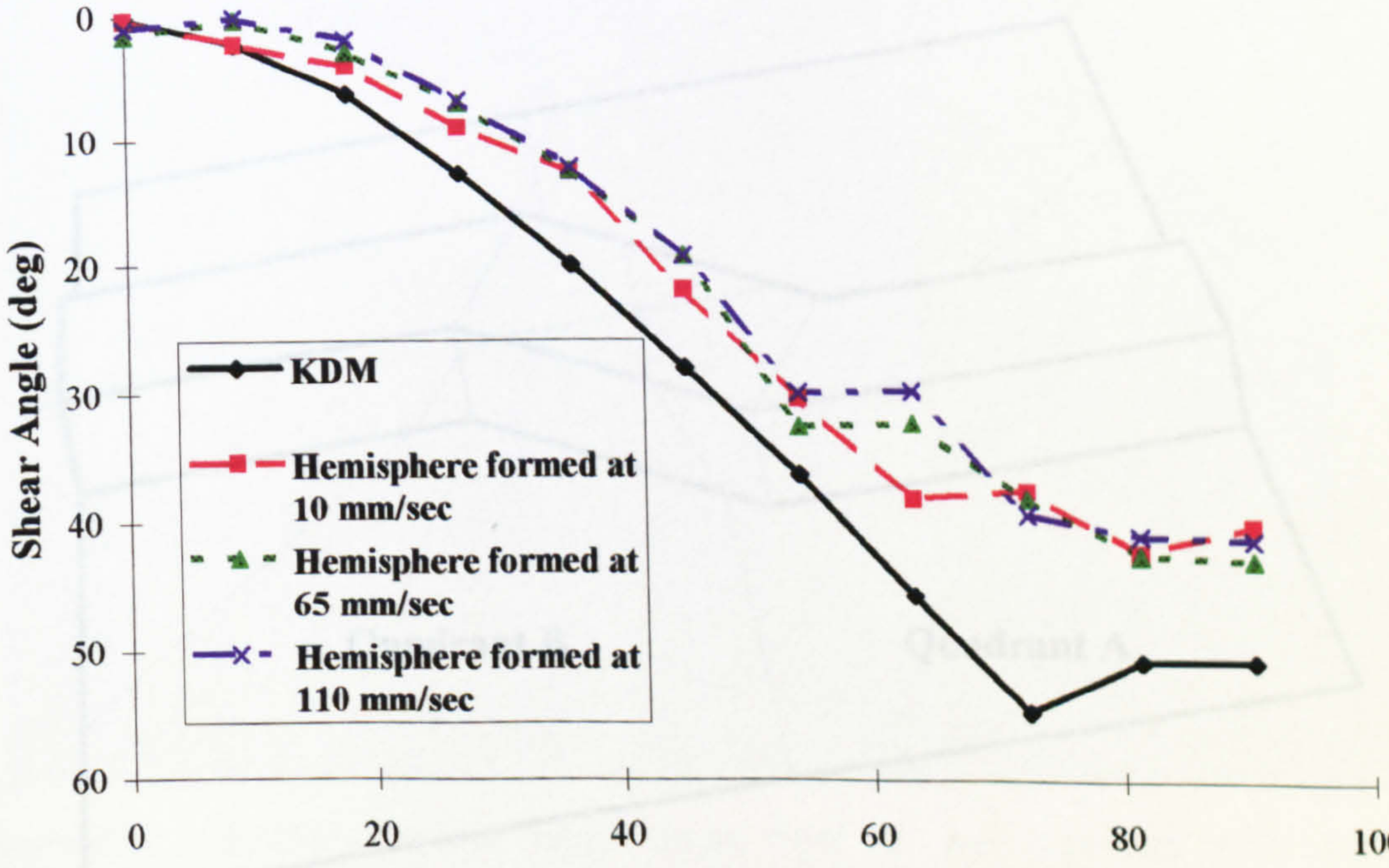

Figure 6.26 Shear angles along the line of maximum deformation across a hemisphere, in quadrants with stitch parallel to shear direction. (Tech Textiles E-BX 948, press formed at various speeds.)

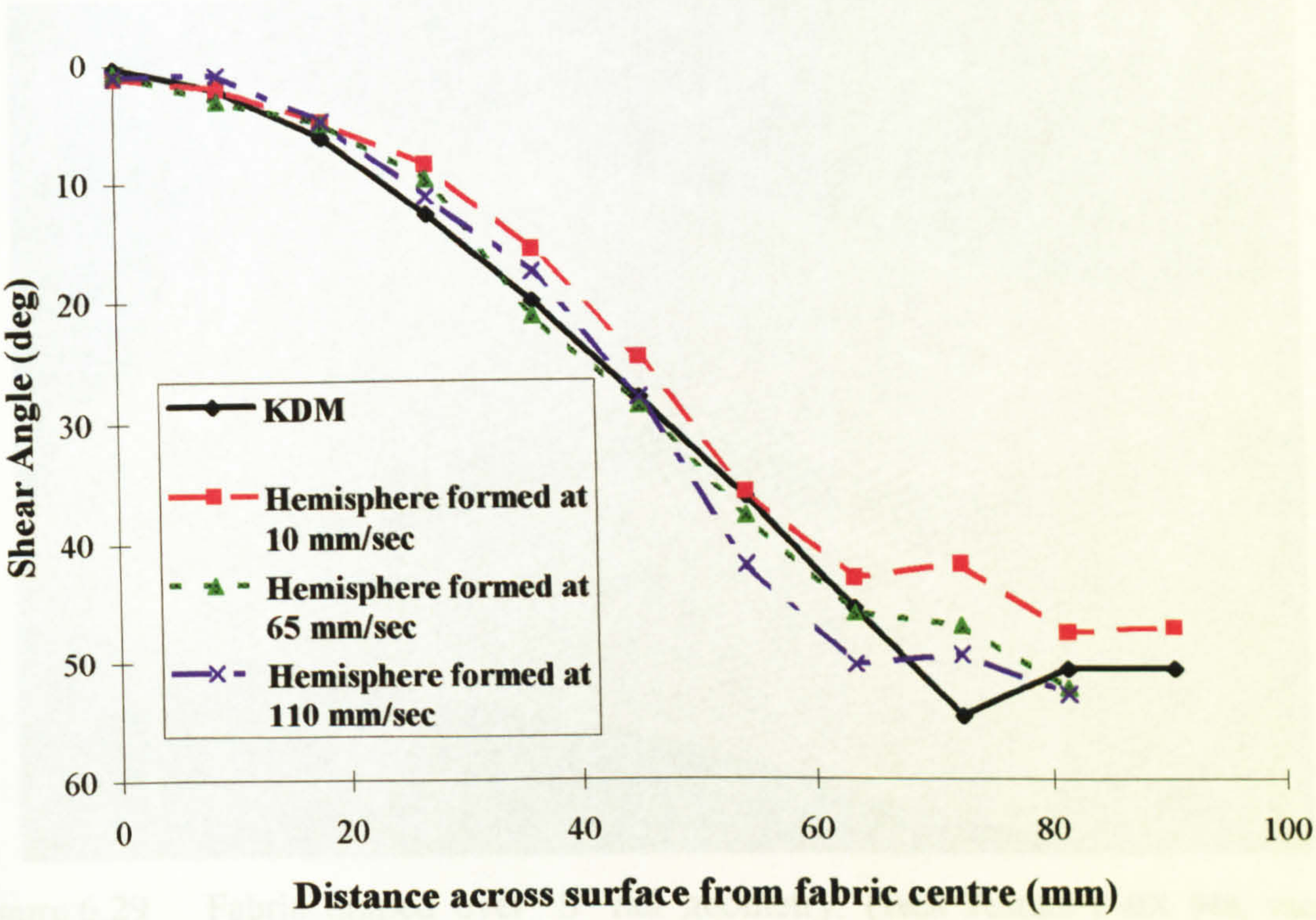

Figure 6.27 Plot of shear angles along the line of maximum deformation across a hemisphere, in quadrants with stitch perpendicular to shear direction. (Tech Textiles E-BX 948, press formed at various speeds.)

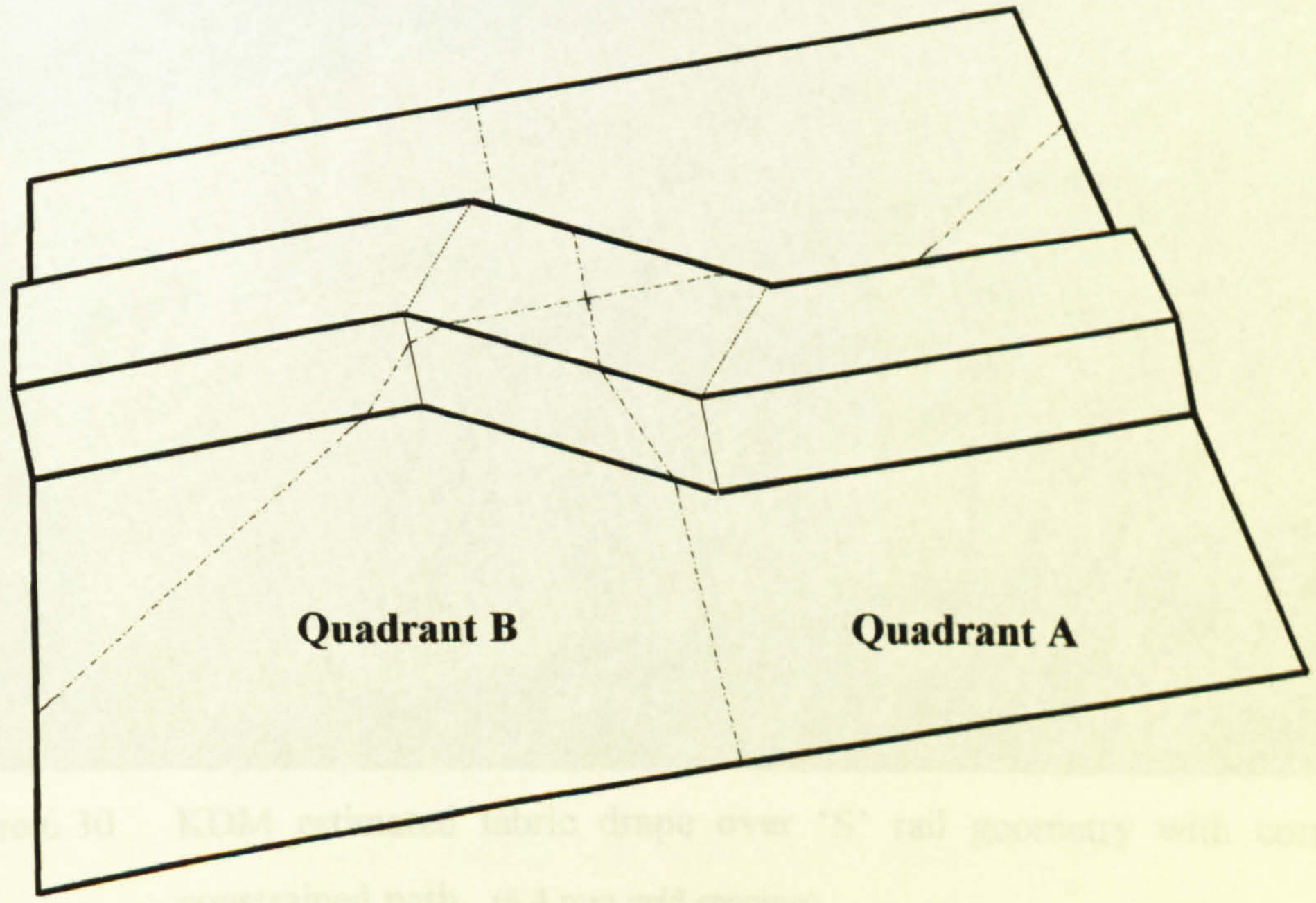

Figure 6.28 Predicted paths across an 'S' rail geometry using geodesic principles.

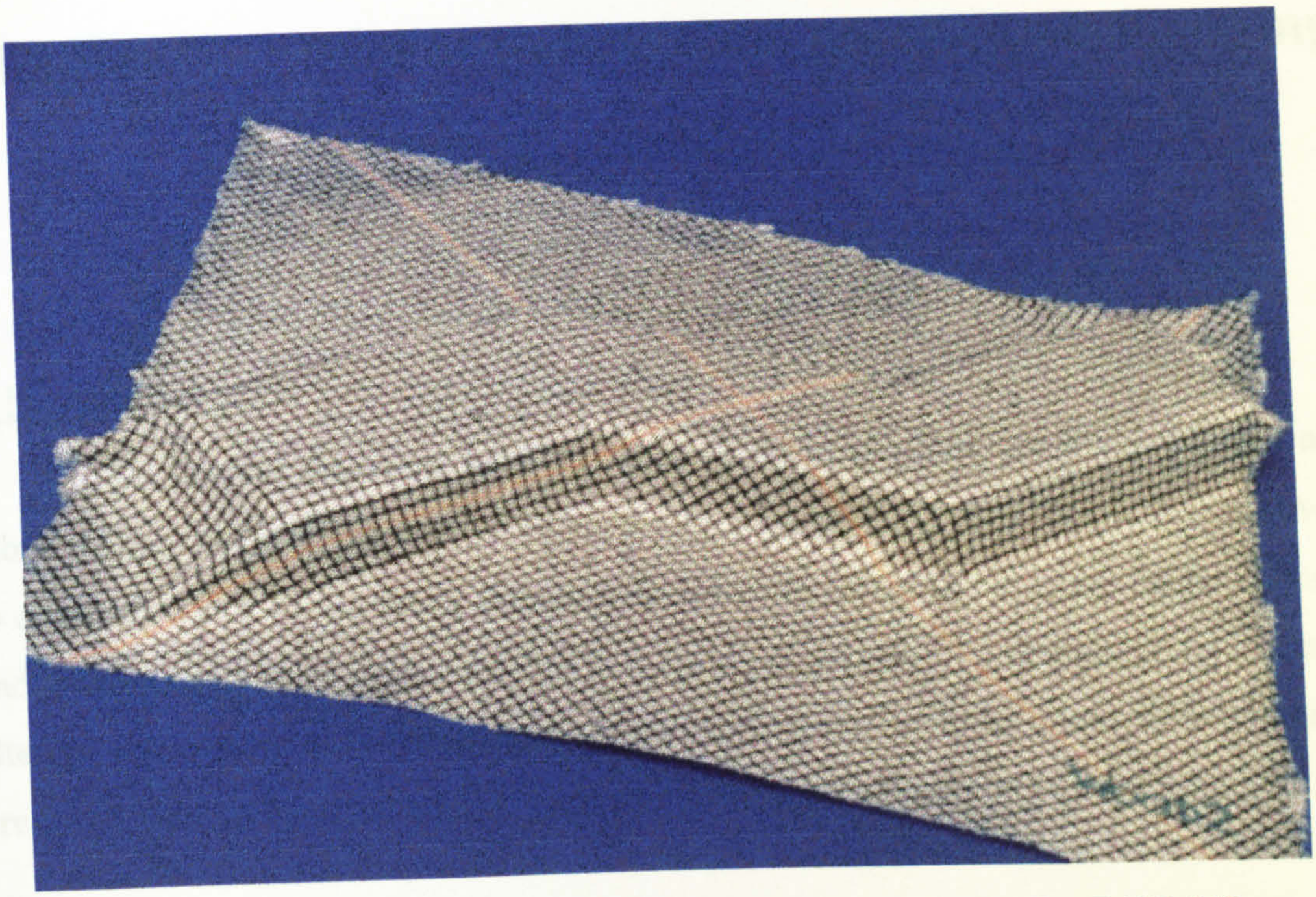

Figure 6.29 Fabric draped over 'S' rail geometry. (Tech Textiles E-BX 948, vacuum formed.)

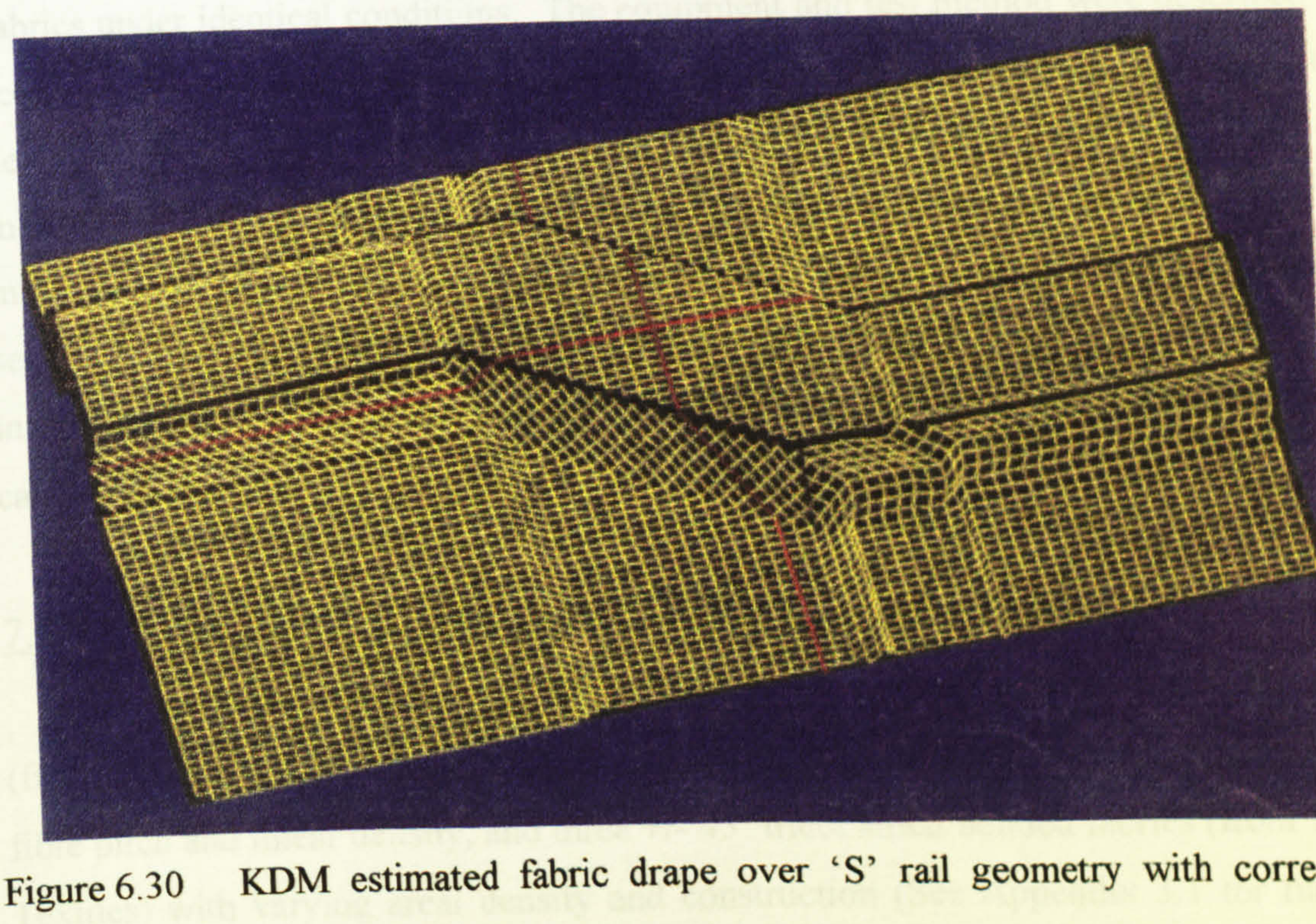

Figure 6.30 KDM estimated fabric drape over 'S' rail geometry with corrected constrained path. (6.4 mm grid spacing).

Chapter 7 - Effect of Fabric Construction on Forming Properties

7.1 Introduction

This chapter describes how the differences in in-plane shear compliance and fabric locking angle measured in Chapter 4 affect formability. The aim of the work was to establish which of the fabric parameters shown to affect the in-plane shear stiffness and locking angle were relevant to the formability of fabrics. To determine the effect of altering the construction parameters, a hemispherical punch mounted in a hydraulic press was used to form the fabrics, with the preform architecture measured using GSA.

7.2 Experimental Method

A hemispherical punch mounted in a hydraulic press was used to form various fabrics under identical conditions. The equipment and test method were described in section 5.3.2 and the fabrics correspond to those tested using the in-plane shear rig described in Chapter 4. All tests were performed with a constant punch velocity of 65 mm/sec. A 280 mm diameter disc of fabric was deformed through its centre by a 100 mm diameter hemispherical punch to a depth of 65 mm (Figure 7.1) as described in section 5.3.2. The fabric was rigidised and the grid mapped using GSA as described in section 5.4.1. The deformation of the grid (and hence of the fabric) was then calculated from the grid intersection co-ordinates.

7.3 Effect of Fabric Construction Parameters on Formability

The fabrics consisted of nine +/- 49° chain and tricot stitch bonded fabrics (from Flemmings Industrial Fabrics) with different constituent parameters such as fibre pitch and linear density, and three +/- 45° tricot stitch bonded fabrics (from Tech Textiles) with varying areal density and construction (See Appendix 3.1 for further details). The following paragraphs compare the formability of fabrics with different constituent parameters to determine the dominant parameters. The formability results are also compared to those obtained from the in-plane shear tests discussed in Chapter 4.

7.3.1 Effect of Stitch Type and Orientation on Forming Properties

A photograph of a typical press formed fabric (Tech Textiles E-BXhd 936) is shown in Figure 7.2. The path of two initially perpendicular lines representing the initial centre line of the fabric over the centre of the punch can be seen running vertically and horizontally from the centre of the specimen to the edge. These paths are equivalent to the 'constrained' paths that are generated by the KDM. The paths are not rotationally-symmetrical as would be expected for an orthotropic material over a symmetrical surface. The in-plane shear tests described in Chapter 4 indicated that stitch bonded fabrics are stiffer when loaded parallel to the stitching than when loaded perpendicular due to the resistance to elongation of the stitch. Therefore for the same in-plane shear force, less deformation would occur in the quadrants where the stitch is running parallel than when the stitch is running perpendicular to the shear direction. This difference in shear deformation between the quadrants can be seen in the outline of the initially round fabric. The larger fabric shear deformation in the top left and lower right quadrants where the stitch runs perpendicular to the direction of shear has produced a more prominent 'ear' in the outline.

Figure 7.3 shows the average inter-yarn shear angle in quadrants sheared parallel and perpendicular to the stitch for the fabric sample shown in Figure 7.2. The data were taken along the line of maximum deformation across the fabric surface, and plotted for quadrants when the stitch direction runs parallel and perpendicular to the shear direction respectively. The shear deformation was approximately 13° less than that predicted using the KDM, and 10° higher when the stitch ran parallel and perpendicular to the shear direction respectively. When loaded parallel to the stitches the higher stiffness reduced the fabric movement. This explains the imbalance which is evident in adjacent quadrants. Figure 7.3 shows the maximum shear deformation in the fabric is 53° occurring at 72 mm from the fabric centre. This is close to the estimated fabric locking angle of 58° obtained in Chapter 4. The large deformations in quadrants loaded perpendicular to the stitch had distorted the grid such that data beyond that point could not be measured reliably, hence there are no shear data beyond 72 mm. Figure 7.4 shows the inter-yarn slip along the same path. The data at 72 mm from the centre of the fabric has been removed as the change in surface plane between the punch and base plate causes errors in the slip calculation as explained in section 5.4.4.

The slip data plotted in Figure 7.4 show little evidence of slip occurring. Most of the data falls within the GSA error band, so little can be deduced from the data. However, at 81 mm from the centre of the fabric in-plane buckling of the fibres due to high shear deformation occurs, denoted by up to -12% slip occurring. This suggests that the fabric is near its formability limit, although how close is difficult to deduce.

Figure 7.5 shows the same tool geometry formed with a chain and tricot stitched fabric of similar areal density (Flemmings BUC 800). The large differences in the fabric deformation between adjacent quadrants, are due to locking of the fabric when loaded parallel to the stitch direction. When the fabric within quadrants sheared parallel to the stitching locks, the fabric must shear further in the other quadrants to allow the fabric to conform to the surface. The fabric outline shows a larger 'ear' effect than that seen in the tricot stitched fabric (Figure 7.2) and wrinkles can be seen running radially from the edge of the hemisphere along the flat outer ring, in the top left and lower right quadrants where the fabric has reached its locking angle.

The in-plane shear tests (Chapter 4) indicated that the chain stitched fabrics lock at approximately 12° shear when sheared parallel to the stitch and at above 58° shear when sheared perpendicular to the stitch (the fabric shear range exceeded that of the test equipment in this direction). This is confirmed by the plots of shear angle with the stitch running parallel and perpendicular to the shear direction as seen in Figure 7.6. The fabric locked at approximately 12° shear in quadrants where the stitch ran parallel to the shear direction. Therefore larger shear deformation has occurred in quadrants where the stitch is running perpendicular to the shear direction, where there is a maximum shear angle of approximately 53° . This is higher than that predicted by the KDM but at least 5° lower than the fabric locking angle.

In fabrics with high areal density and hence high in-plane shear stiffness such as the Flemmings BUC 1600, severe wrinkles formed in areas of high deformation as the fabric could not conform to the surface by simple shear alone. The fabric was forced to leave the surface and forms wrinkles, which result in a defective moulding. This can be seen in Figure 7.7 as wrinkles on the edge of the hemispherical preform in the top left and lower right quadrants.

7.3.2 Effect of Fabric Construction on Forming Characteristics

The effect of altering the fabric manufacturing method and construction on the in-plane shear stiffness of fabric was shown in Section 4.4.5. To establish whether this affected the fabric formability, three fabrics with differing construction methods but similar stitch patterns and areal densities were tested. They consisted of a tricot bonded two layer Parramax constructed fabric (Tech Textiles E-BXhd 936), a four layer tricot stitched Parramax constructed fabric (Tech Textiles E-bBXhd 892), and a two layer cross weft tricot stitched fabric (Tech Textiles E-BX 948). The fabrics were formed under the same test conditions at a punch velocity of 65 mm/sec.

Figures 7.8(a) and 7.8(b) show plots of inter-yarn shear angles along the line of maximum deformation for the three fabrics representing quadrants with the stitch running perpendicular and parallel to the shear direction respectively. For the quadrants where the stitch runs perpendicular to the shear direction the data are similar for all the fabrics. There is up to 4° difference between the shear deformation of the cross weft fabric and the Parramax fabrics, although each follows a similar trend. A comparison of shear deformation between the kinematic drape model predictions and experimental results shows up to 10° higher experimental shear results than predicted when loaded perpendicular to the stitch (Figure 7.8a) and up to 16° lower experimental shear than predicted when loaded parallel to the stitch (Figure 7.8b). This corresponds to the higher in-plane shear stiffness of the fabrics when loaded parallel to the stitch. The difference in shear rigidity between the fabric types reported in Table 4.1 suggest that the more balanced fabric (Tech Textiles E-BX 948 had a shear stiffness ratio of 2.8) would form more symmetrically than less balanced ones (Tech Textiles E-BXhd 936 had a shear stiffness ratio of 4.5). However, it appears that the difference in the shear stiffness caused little difference in their formability over this geometry as they all conformed to the surface. However, there was some evidence of fibre buckling occurring so the fabrics may be nearing their locking angle.

A comparison of inter-yarn slip for the same experiments can be seen in Figures 7.9(a) and 7.9(b). Again, apart from buckling of the fibres at high shear deformation at 81 mm from the centre, the data is within the GSA error band.

7.3.3 Effect of Altering Yarn Parameters on Fabric Formability

Chain and Tricot stitched fabrics of varying constructions were formed under identical test conditions. The in-plane shear stiffness tests (Chapter 4) indicated that the major limit when forming chain stitched fabrics such as the Flemmings BUC range was locking of the stitch at approximately 12° shear (78° ply angle) when loaded parallel to the stitch direction. The KDM indicated that the shear limit of these fabrics would be reached when formed into a hemispherical geometry, so it would be expected that there would be little difference in preform architecture between different areal densities as the stitch locking would dominate forming. Because the fabrics were approximately +/- 49° rather than the +/-45° of the tricot stitched fabrics, the grids were printed with opposite corners following the stitch direction. Hence the printed grids did not correspond to the fibre directions and therefore only fabric shear could be calculated from the data. Therefore no slip data could be produced from the following experiments.

Figures 7.10(a) and 7.10(b) shows the effect of varying the yarn linear density on shear deformation along the line of maximum deformation. Figure 7.10(a) shows that the shear deformation perpendicular to the stitch is higher than predicted using the KDM and that the fabrics exhibit similar deformation until higher shear angles are reached at approximately 63 mm from the centre. At this point the fabrics with a lighter yarns (hence lower areal density) show higher shear suggesting that fabrics with lower areal densities can shear further before locking. Figure 7.10(b) shows that, as indicated by the in-plane shear tests, the deformation in stitch-limited quadrants is dominated by locking of the stitch at approximately 12° shear for all fabrics. In this case the effect of varying tow linear density would appear to be negligible.

The effect of varying the tow spacing while maintaining a constant yarn linear density can be seen in Figures 7.11(a) and 7.11(b). Figure 7.11(a) shows the shear deformation perpendicular to the stitch is higher than that predicted using the KDM and similar for all fabrics in packing limited quadrants. The maximum shear deformation is approximately 63° at 91 mm from the centre for all fabrics suggesting that the lighter fabrics were more formable than the heavier fabrics (BUC 800 and BUC 1200) shown in Figure 7.10(a). The deformation in stitch-limited quadrants (Figure 7.11(b)) has stitch locked at approximately 15° shear for all the fabrics. This

is 3° higher than that exhibited by other chain stitched fabrics, and may be due to variations in the stitch tension.

The deformation of fabrics with similar areal densities but different yarn linear density (hence different tow spacing) with the stitch running perpendicular and parallel to the shear direction can be seen in Figures 7.12(a) and 7.12(b) respectively. The fabric constructed from the heavier yarn (900 Tex, 2.3 mm tow spacing) was less stiff than that using light yarn (600 Tex, 1.5 mm tow spacing) when loaded perpendicular to the stitch in previous tests (see section 4.4.5). This does not appear to have affected the formability of the fabric as the traces follow the same trend. Figure 7.12(a) shows that the deformation is similar for both fabrics and up to 11° higher than predicted by the KDM. In Figure 7.12(b) the fabric locking can be seen in both traces at about 12° shear which is similar to that measured by the in-plane shear test.

7.4 Conclusions

The effect of fabric construction on formability for simple hemispherical geometry was established for various stitch bonded fabrics. The type and tension of stitch dominated the forming properties. The effects of fabric areal density were more difficult to determine as the deformation of the fabrics used were dominated by stitch locking at low shear angles (approx. 12°) and differences in shear stiffness which were both due to the stitch type.

Fabrics constructed using a chain stitch had a limited shear range when loaded parallel to the stitch direction. This premature locking forced more deformation into other areas as the fabric formed to the geometry, and caused large differences in the in-plane shear induced in initially symmetric quadrants when formed over a symmetric part. This effect was not seen using a tricot stitched fabric which had a similar shear compliance in both directions (described in Chapter 4). This confirmed that the differences in the fibre locking angle caused by stitching produced by the in-plane shear results described in Chapter 4 were relevant to the forming of fabrics. Therefore the fabric stitch is a major consideration when selecting a fabric for high

drape applications or in laminates where symmetry of the preform architecture is important.

The orientation of the tricot stitch relative to the shear direction affected the formability of the fabric. There was up to 14° less deformation in the quadrants where the stitches were parallel to the shear direction than those where the stitches ran perpendicular. The in-plane shear test results described in Chapter 4 showed that stitch bonded fabrics were stiffer when loaded parallel to the stitch direction than when loaded perpendicular, which would explain the lower levels of shear deformation which were measured in the former case.

The effects of changing tow spacing, yarn linear density or areal density on fabric formability were uncertain for chain stitched fabrics since the deformation (and hence locking angle) was dominated by the stitching. Some correlation between the areal density and the maximum shear angle was evident when comparing the heaviest (1600 g/m^2) and lightest (403 g/m^2) fabrics in fibre packing-limited situations, with the lighter fabrics undergoing more shear deformation.

The slip calculated in tricot stitch bonded fabrics was negligible. However, when high shear angles occurred at the base of the hemispheres, fibre buckling (shown as negative slip on the graphs) resulted indicating that the fabric was beyond its shear forming limit. Local fibre buckling would cause a reduction in laminate stiffness and a variation in preform permeability. Slip data for chain stitch bonded fabrics could not be determined due to problems mapping a square grid onto a non uniform fabric architecture.

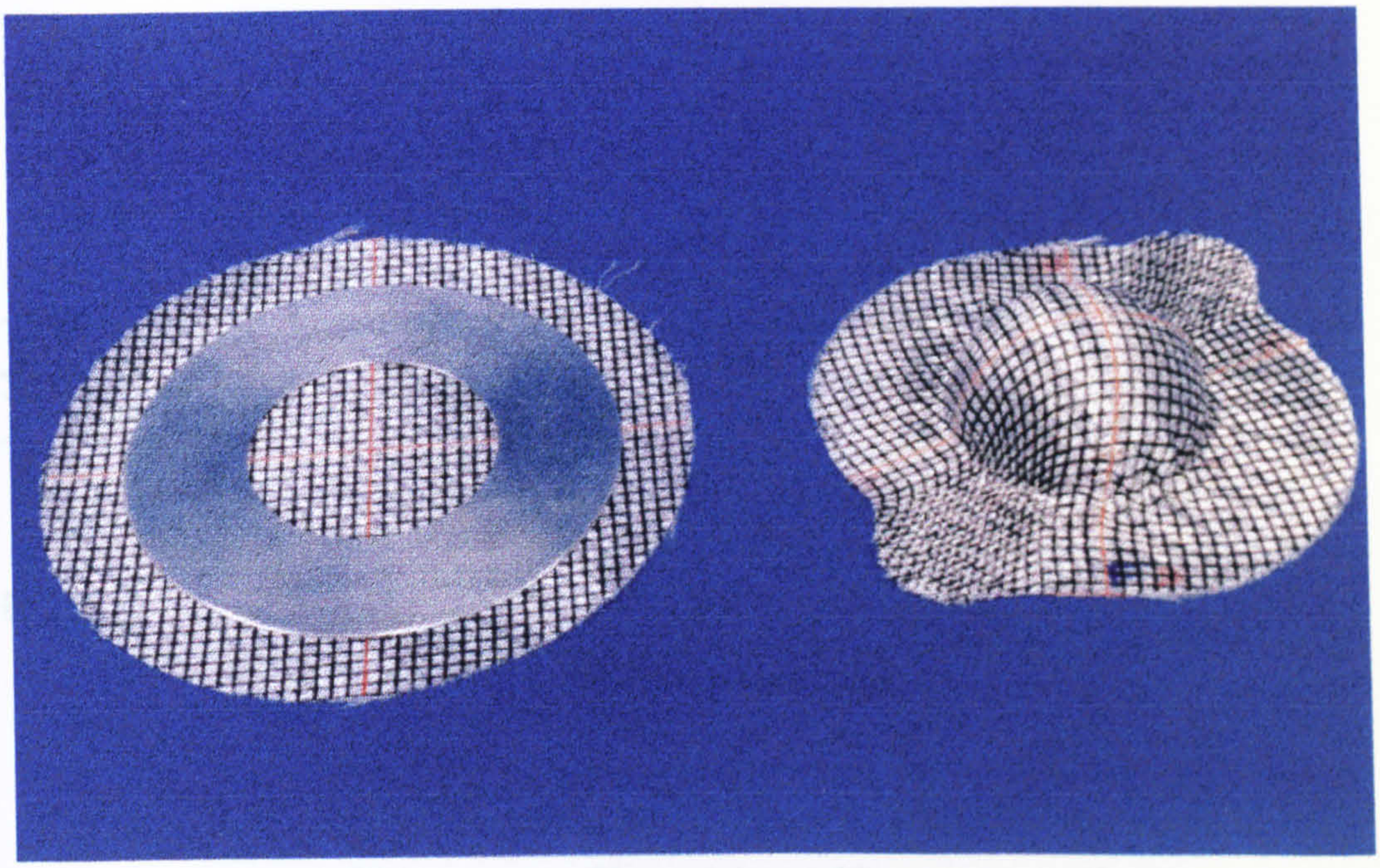

Figure 7.1 Gridded fabric before and after forming into a hemispherical preform. (Flemmings BUC 800, 65 mm/sec punch velocity.)

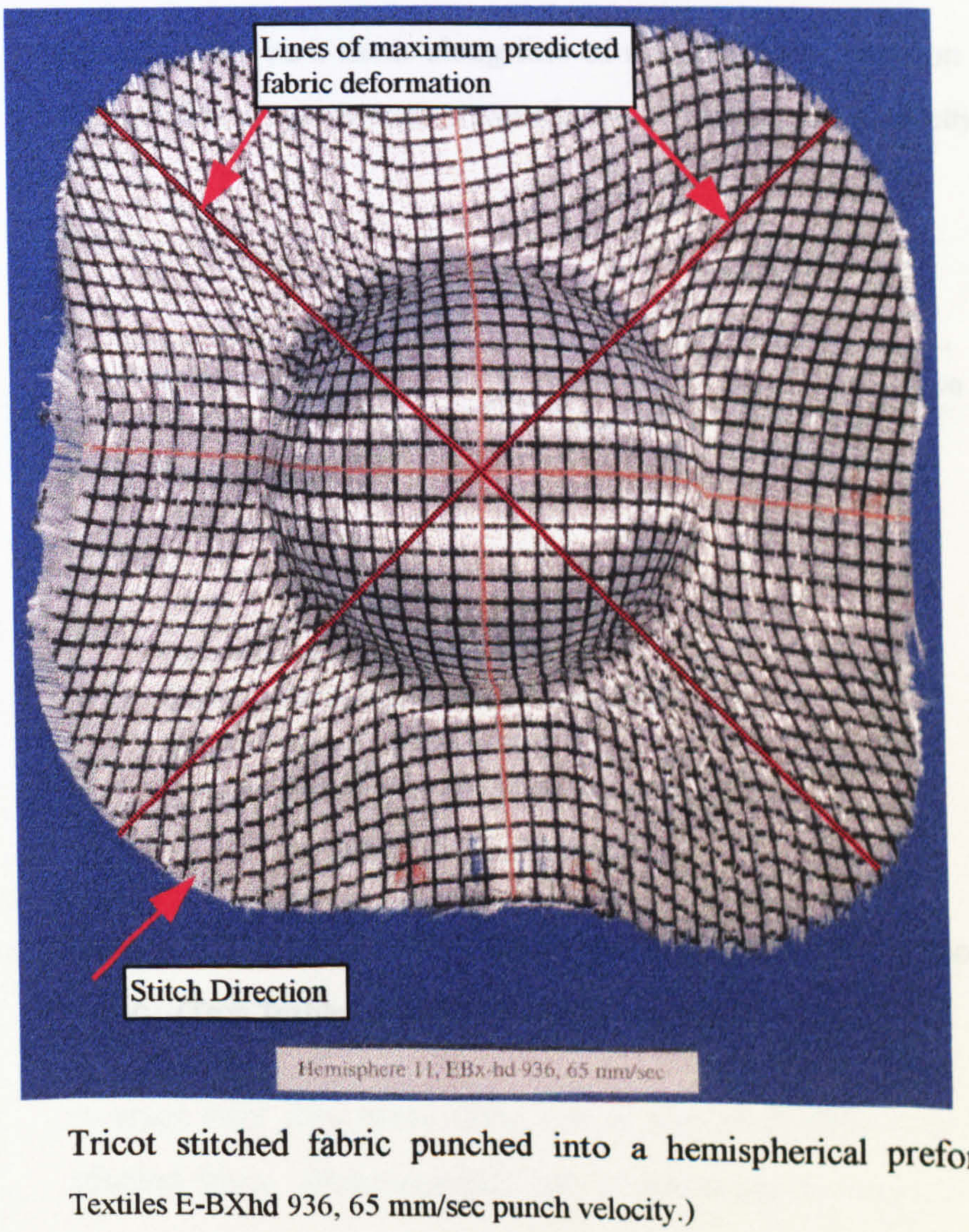

Figure 7.2 Tricot stitched fabric punched into a hemispherical preform. (Tech Textiles E-BXhd 936, 65 mm/sec punch velocity.)

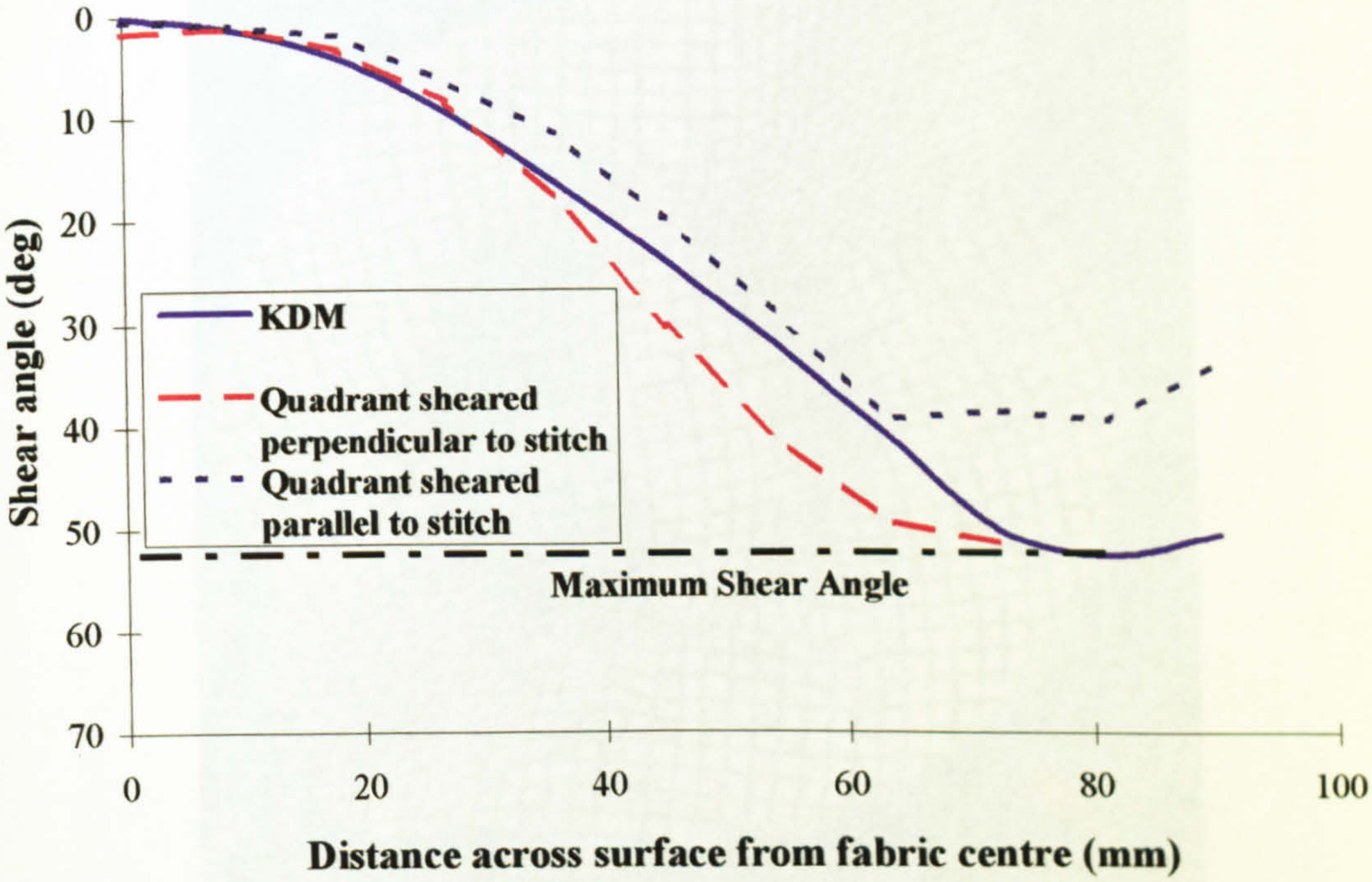

Figure 7.3 Average inter yarn shear along line of maximum deformation for tricot stitched fabric. (Tech Textiles E-BXhd 936, 65 mm/sec punch velocity.)

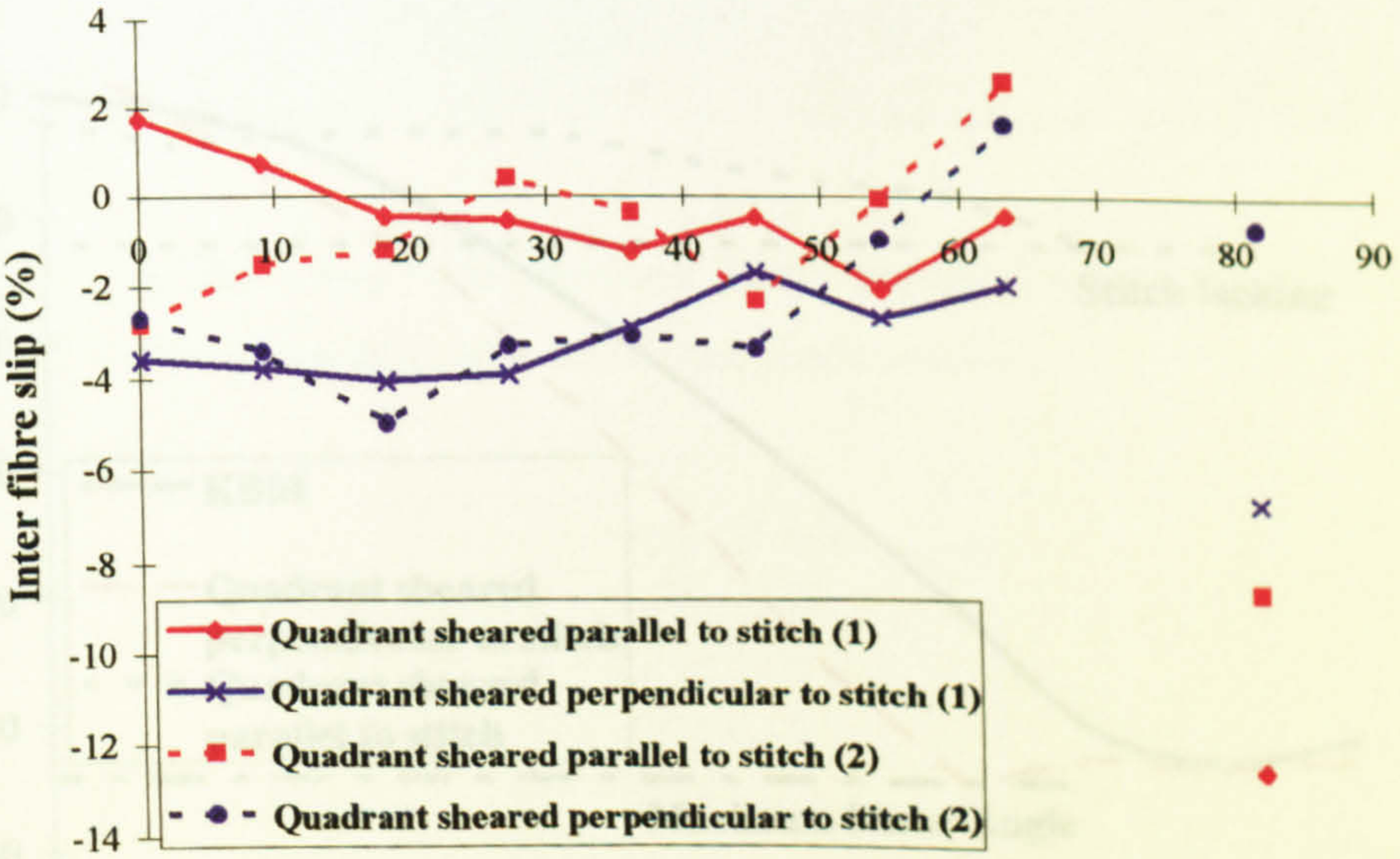

Figure 7.4 Inter yarn slip along line of maximum deformation for a tricot stitched fabric. (Tech Textiles E-BXhd 936, 65 mm/sec punch velocity.)

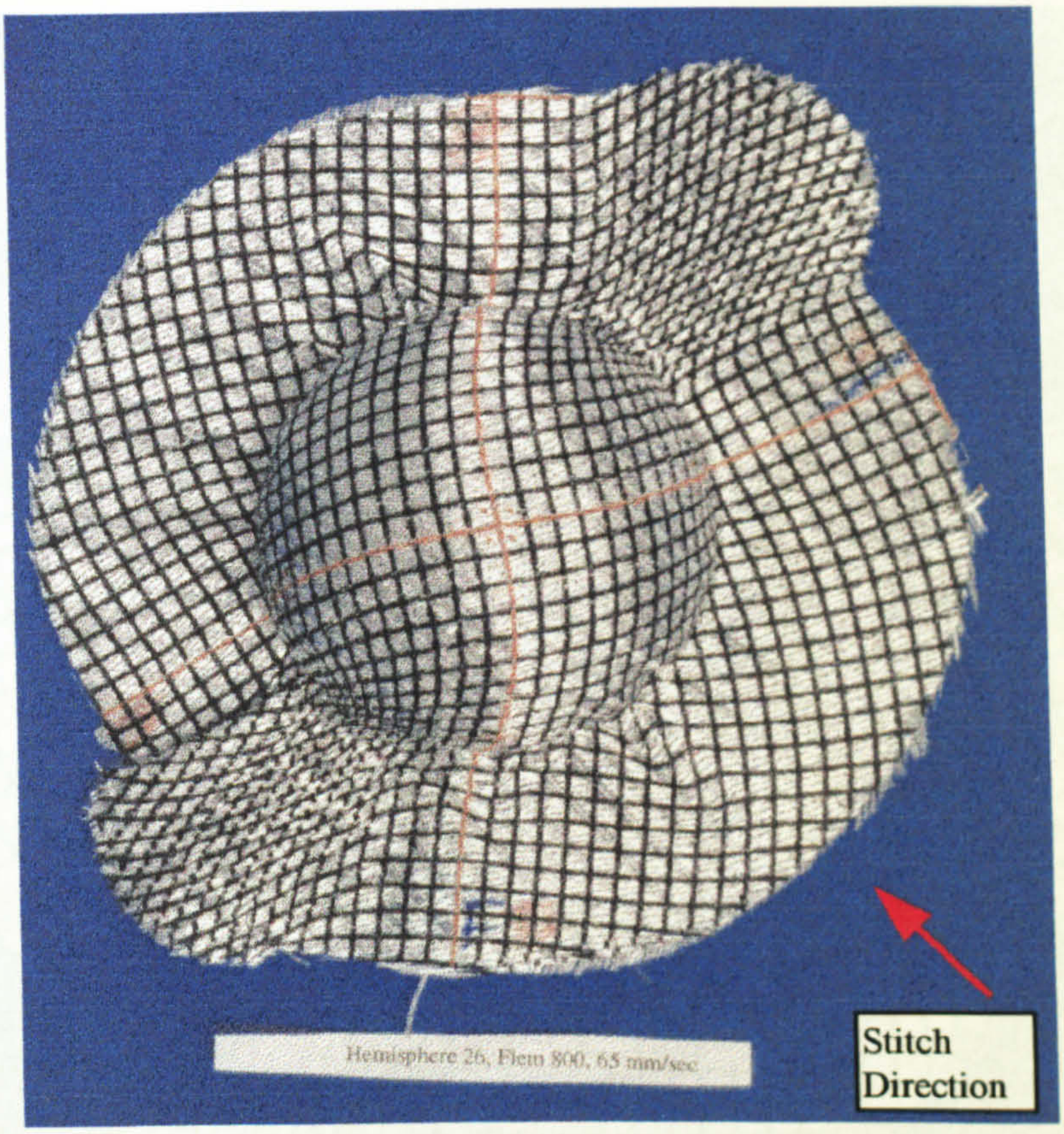

Figure 7.5 A tricot and chain stitched fabric punched into a hemispherical preform. (Flemmings BUC 800, 65 mm/sec punch velocity.)

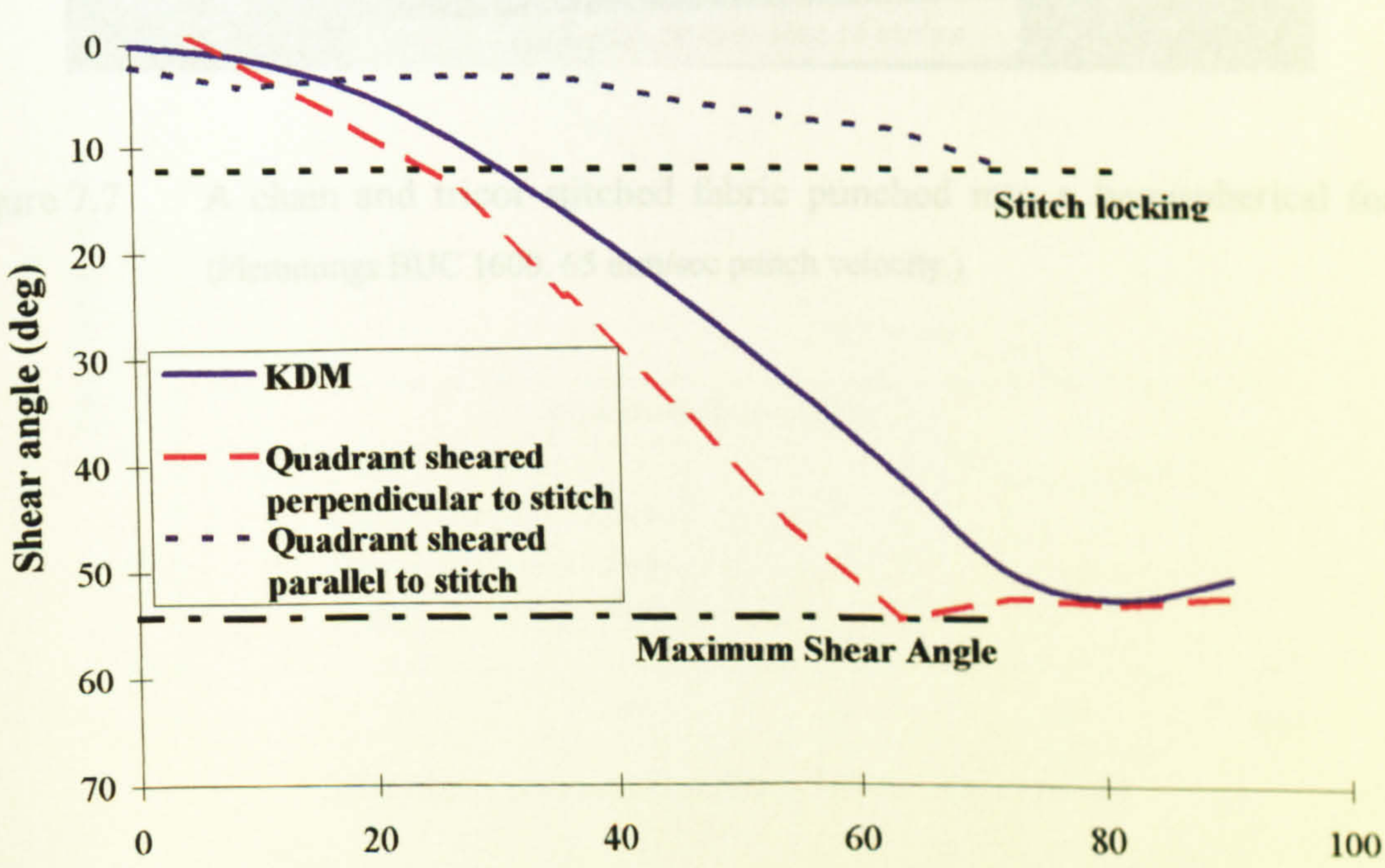

Figure 7.6 Average inter yarn shear along line of maximum deformation for chain stitched fabric. (Flemmings BUC 800, 65 mm/sec punch velocity.)

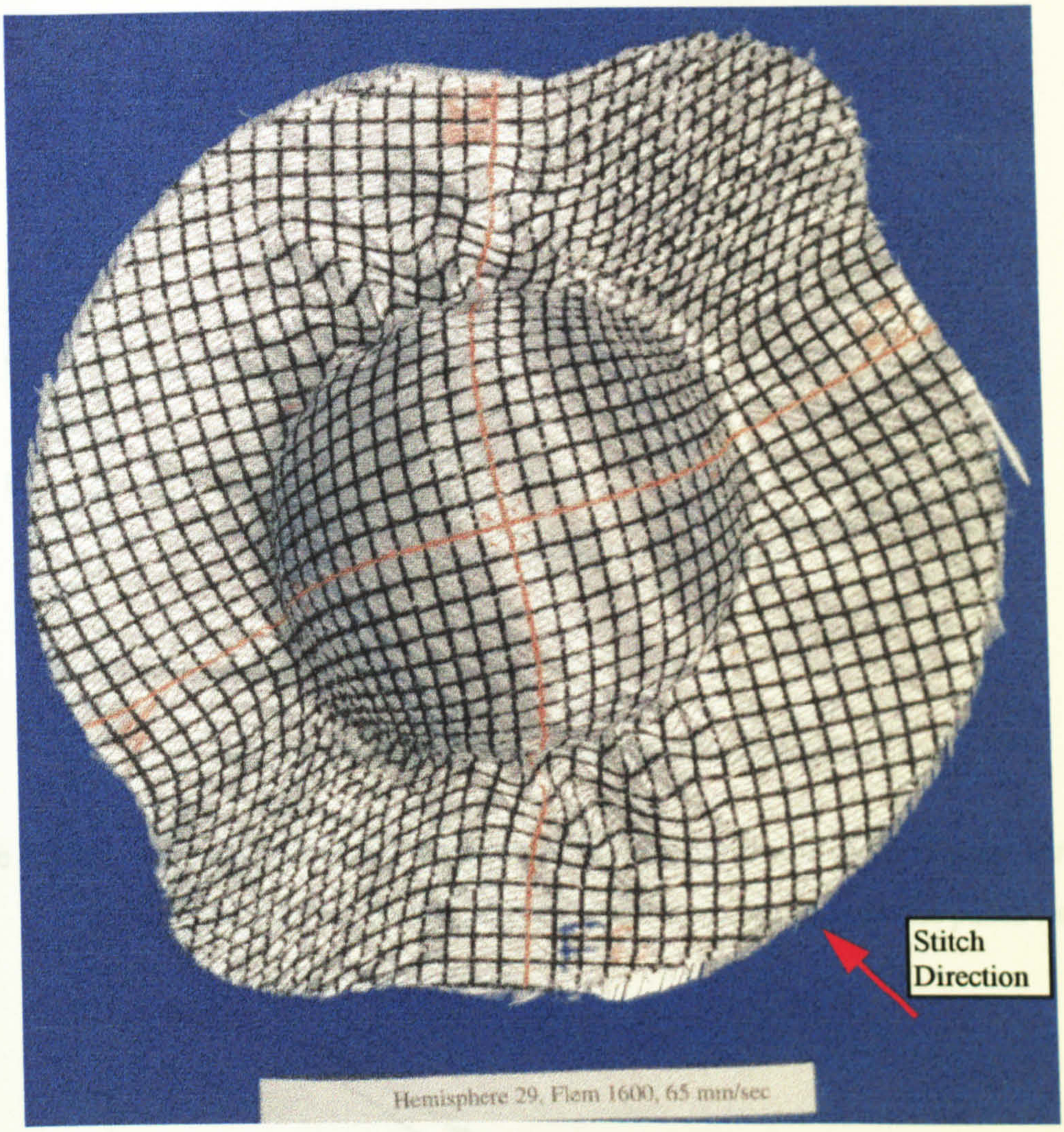

Figure 7.7 A chain and tricot stitched fabric punched into a hemispherical form. (Flemmings BUC 1600, 65 mm/sec punch velocity.)

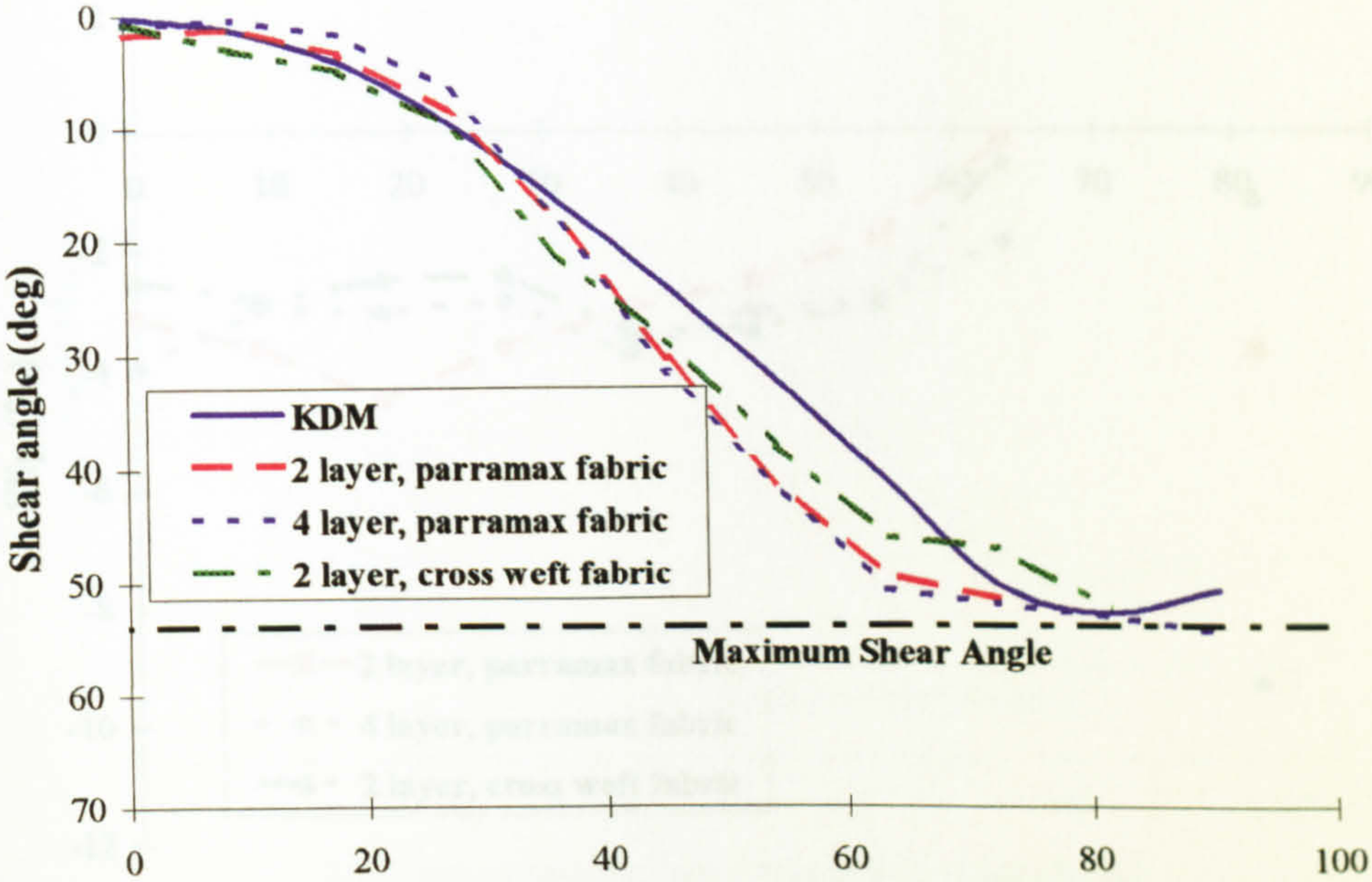

Figure 7.8(a) Average inter fibre yarn along line of maximum deformation for tricot stitched fabrics formed perpendicular to stitch. (65 mm/sec punch velocity.)

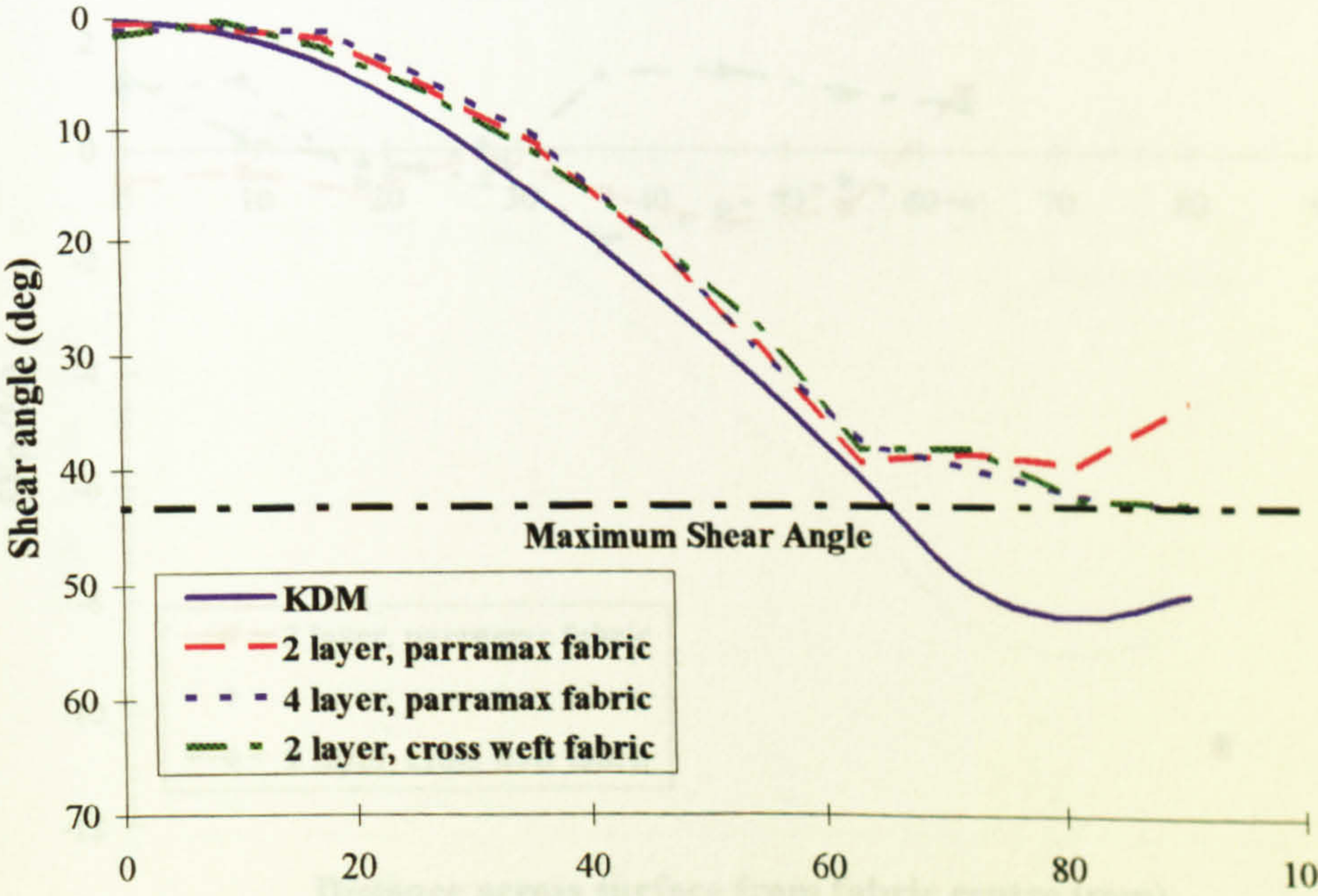

Figure 7.8(b) Average inter yarn shear along line of maximum deformation for tricot stitched fabrics formed parallel to stitch (65 mm/sec punch velocity.)

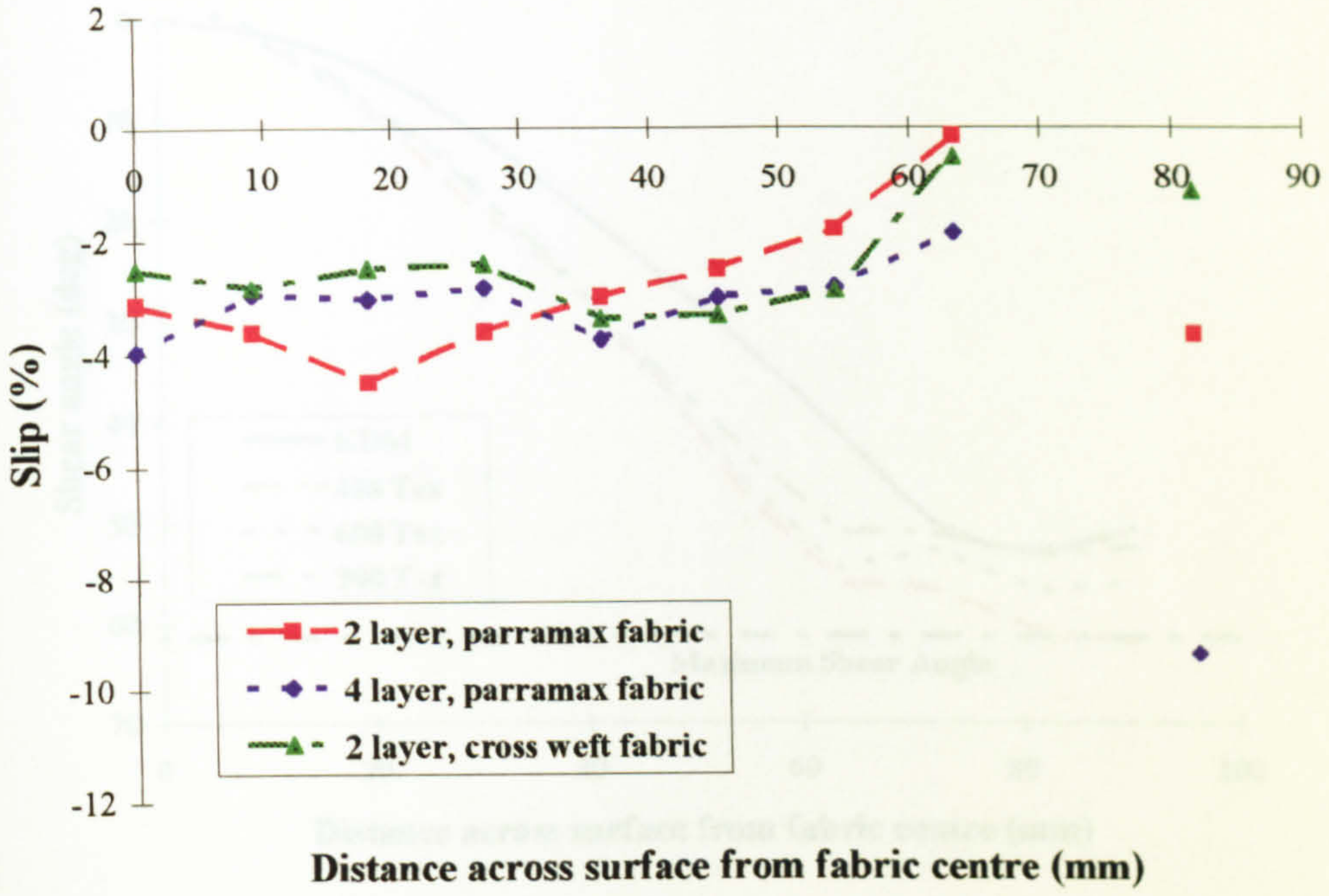

Figure 7.9(a) Inter yarn slip along line of maximum deformation for tricot stitched fabrics formed perpendicular to stitch. (65 mm/sec punch velocity.)

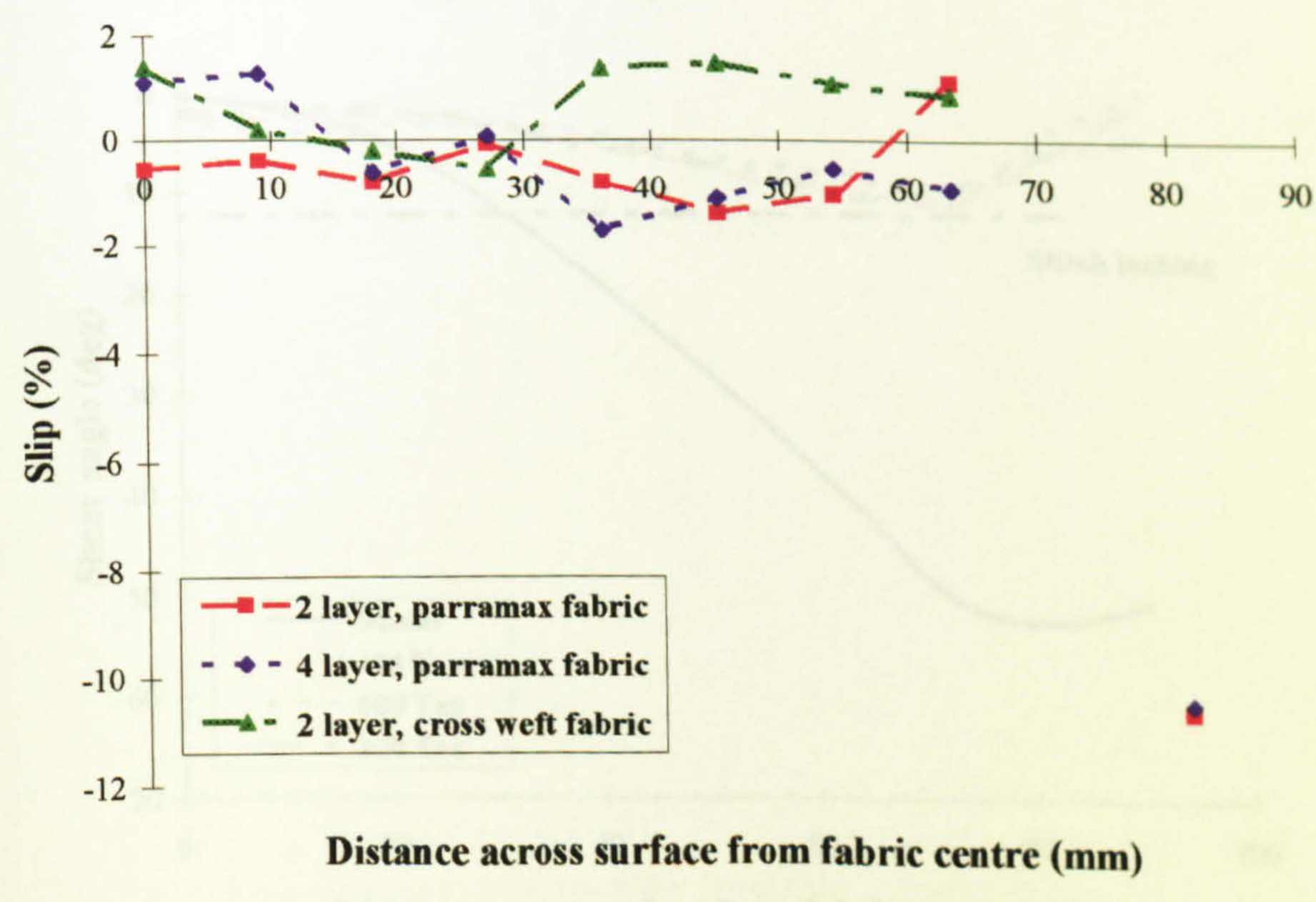

Figure 7.9(b) Inter yarn slip along line of maximum deformation for tricot stitched fabrics formed parallel to stitch. (65 mm/sec punch velocity.)

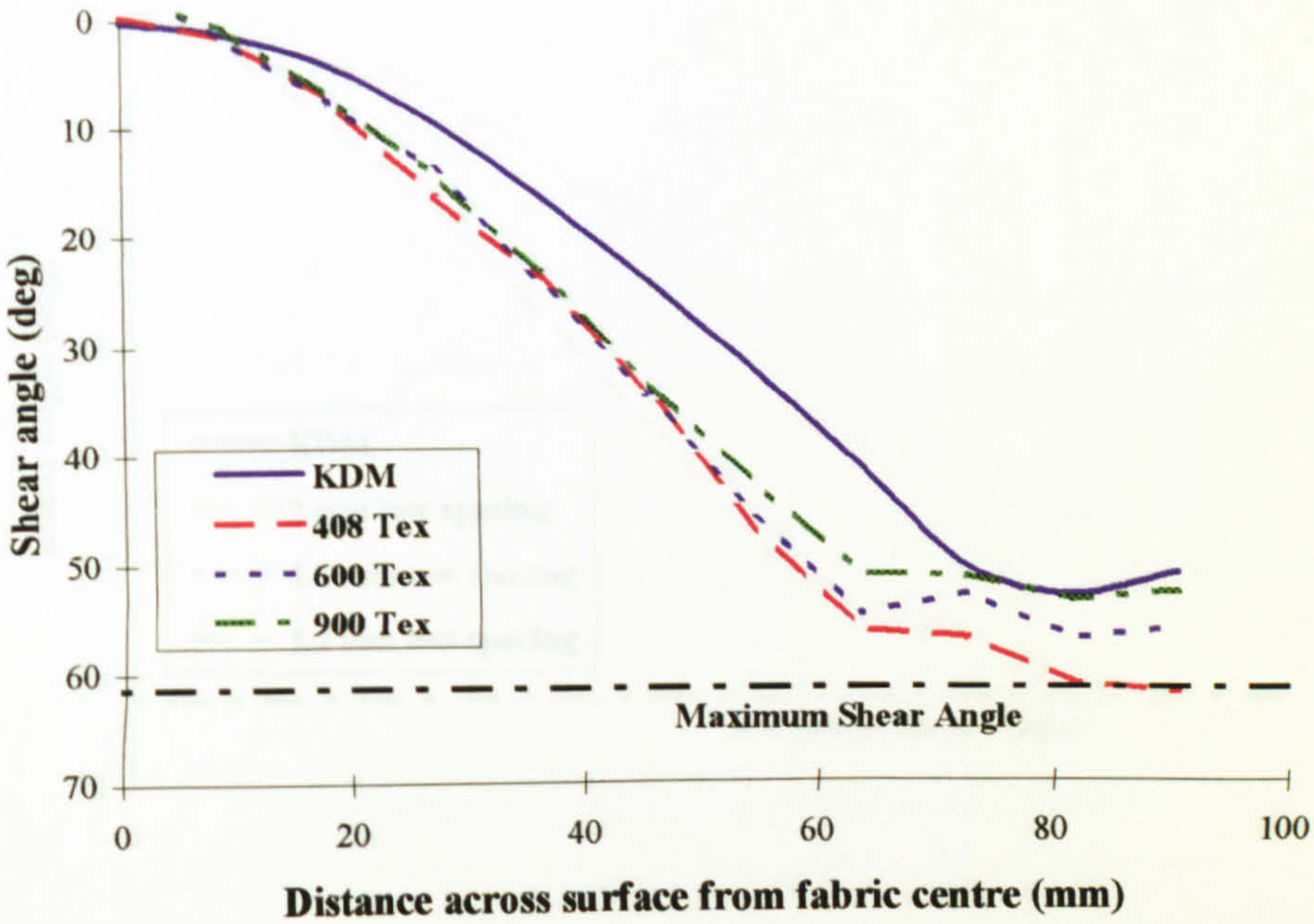

Figure 7.10(a) Inter yarn shear along line of maximum deformation for chain stitched fabrics with varying linear fibre density formed perpendicular to stitch. (Flemmings BUC fabrics, 408 Tex - BUC 545, 600 Tex - BUC 800, 900 Tex - BUC 1200. 65 mm/sec punch velocity.)

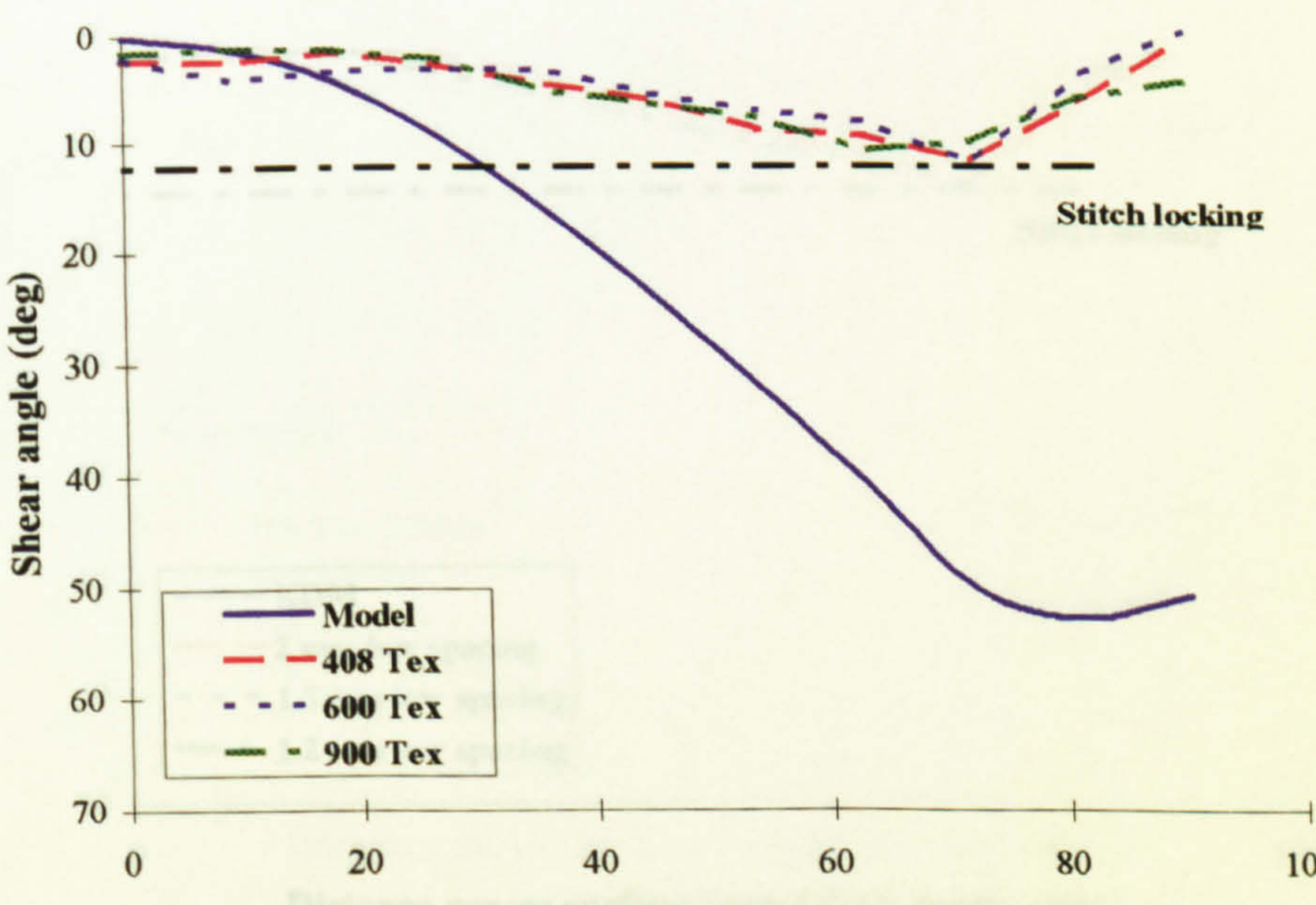

Figure 7.10(b) Inter fibre shear along line of maximum deformation for chain stitched fabrics with varying linear fibre density formed parallel to stitch. (Flemmings BUC range, 408 Tex - BUC 545, 600 Tex - BUC 800, 900 Tex - BUC 1200, 65 mm/sec punch velocity.)

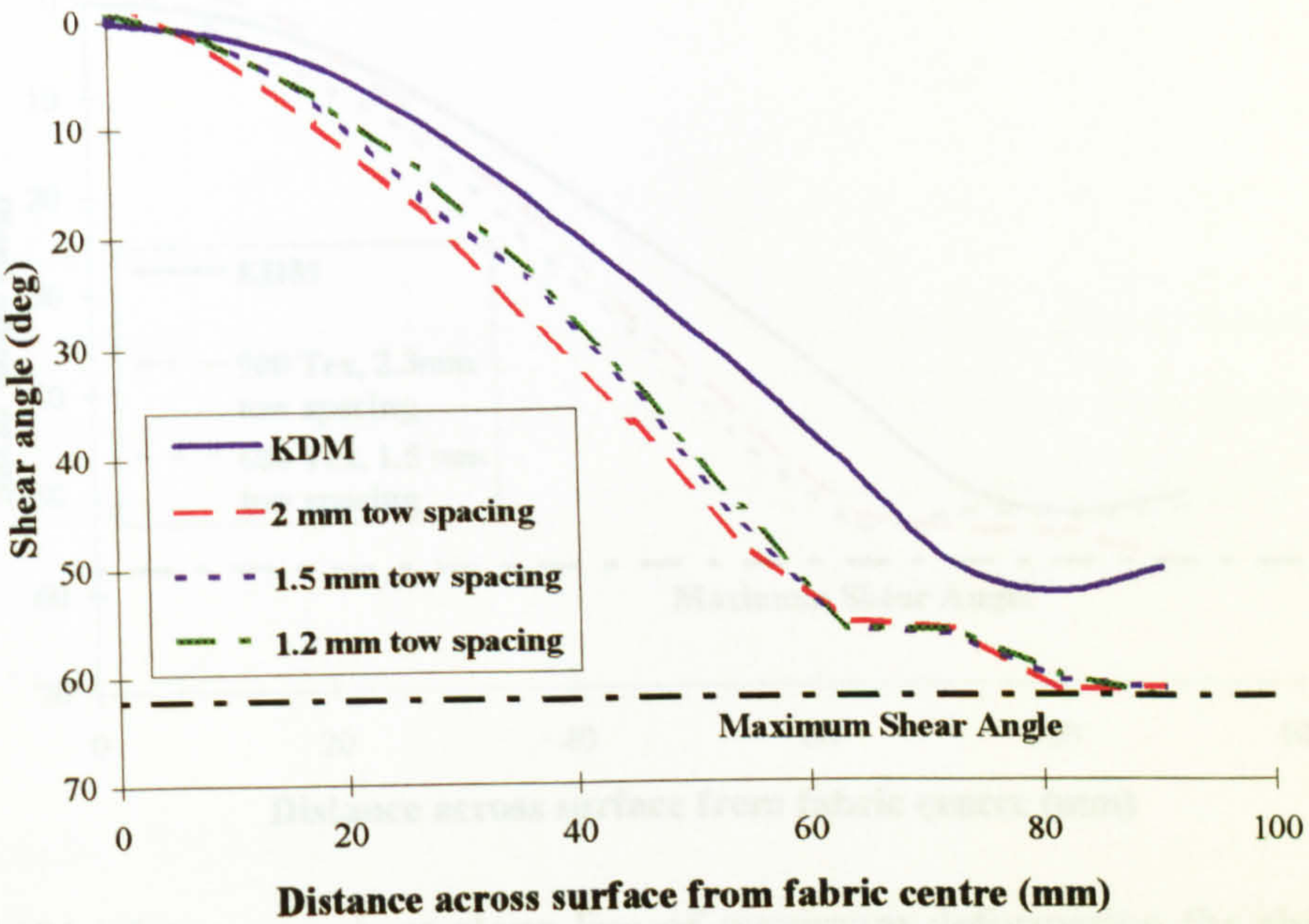

Figure 7.11(a) Inter fibre shear along line of maximum deformation for chain stitched fabrics with varying fibre tow spacing formed perpendicular to stitch. (Flemmings BUC range: 2 mm - BUC 403, 1.5 mm - BUC 545, 1.2 mm - BUC 682, 65 mm/sec punch velocity.)

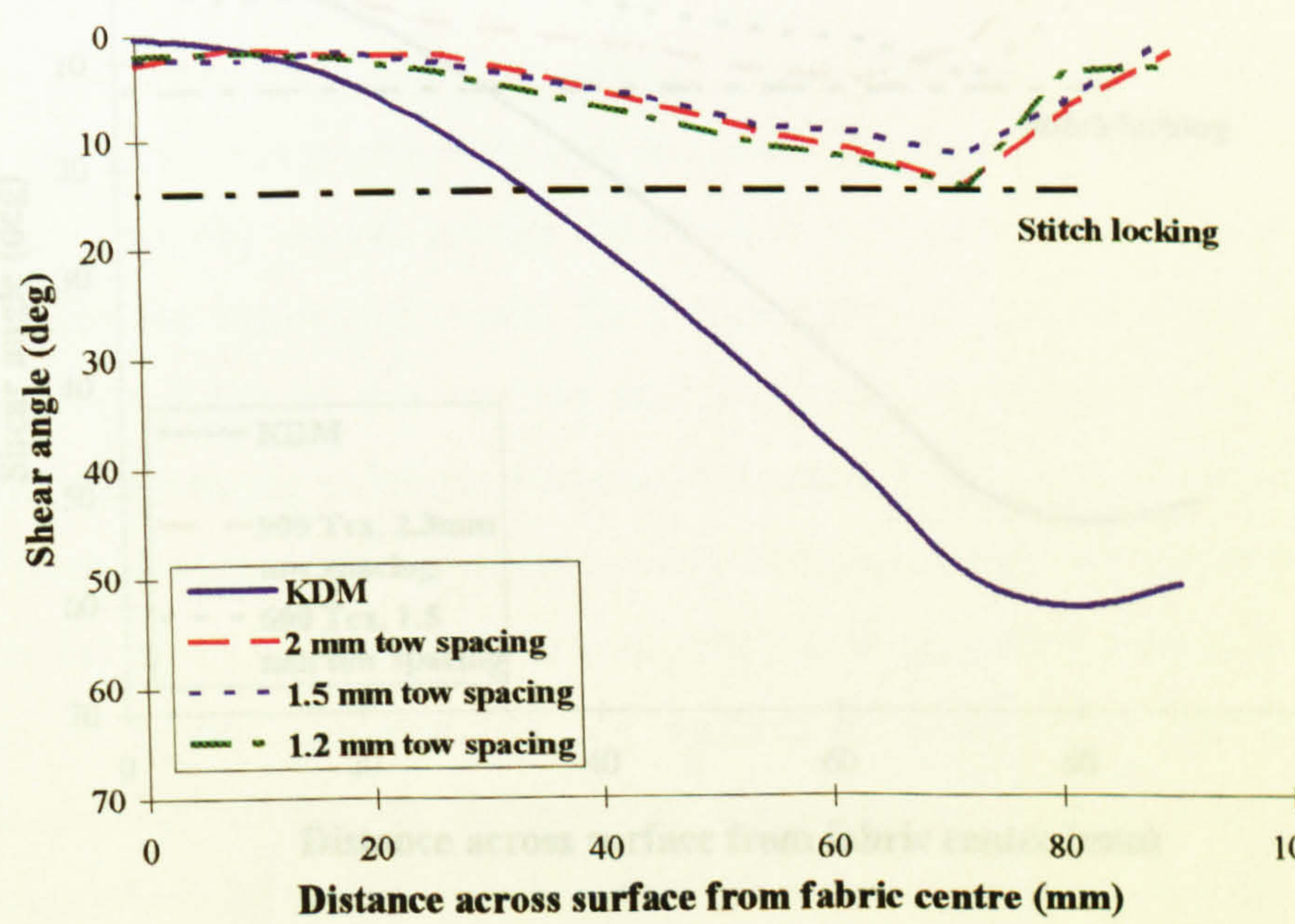

Figure 7.11(b) Inter fibre shear along line of maximum deformation for chain stitched fabrics with varying fibre spacing formed parallel to stitch. (Flemmings BUC range: 2 mm - BUC 403, 1.5 mm - BUC 545, 1.2 mm - BUC 682 65 mm/sec punch velocity.)

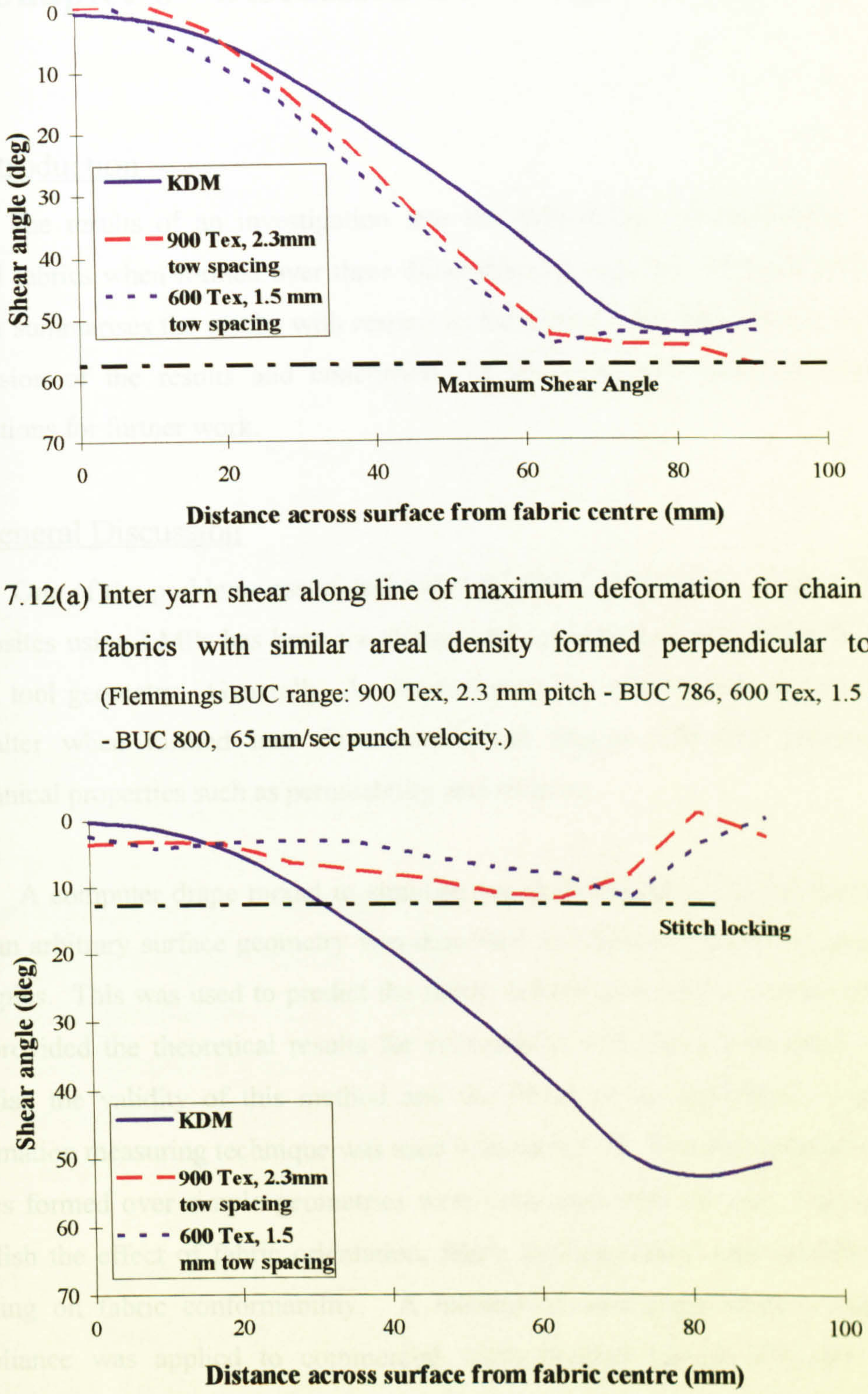

Figure 7.12(a) Inter yarn shear along line of maximum deformation for chain stitched fabrics with similar areal density formed perpendicular to stitch. (Flemmings BUC range: 900 Tex, 2.3 mm pitch - BUC 786, 600 Tex, 1.5 mm pitch - BUC 800, 65 mm/sec punch velocity.)

Figure 7.12(b) Inter yarn shear along line of maximum deformation for chain stitched fabrics with similar areal density formed parallel to stitch. (Flemmings BUC range: 900 Tex, 2.3 mm pitch - BUC 786, 600 Tex, 1.5 mm pitch - BUC 800, 65 mm/sec punch velocity.)

Chapter 8 - Discussion and Major Conclusions

8.1 Introduction

The results of an investigation into the deformation characteristics of stitch bonded fabrics when formed over three dimensional geometries were presented. This chapter summarises the results with respect to the project aims described in Chapter 1. Discussion of the results and conclusions of the work are presented along with suggestions for further work.

8.2 General Discussion

One of the problems associated with high speed production of fibre reinforced composites using LMPs has been the design and optimisation of preform lay-ups and mould tool geometry. Generally, the internal structure of a biaxial engineered fabric will alter when formed into three-dimensional shapes, affecting processing and mechanical properties such as permeability and stiffness.

A computer drape model to simulate the deformation of biaxial fabric formed over an arbitrary surface geometry was described in Chapter 3 based on simple shear principles. This was used to predict the fabric deformation over a number of surfaces and provided the theoretical results for comparison with the experimental data. To establish the validity of this method and the limits of its application a grid based deformation measuring technique was used [Chapters 5-7]. The deformation of gridded fabrics formed over simple geometries were compared with the model predictions to establish the effect of fabric orientation, fabric locking, fabric type and the effect of stitching on fabric conformability. A method of measuring fabric in-plane shear compliance was applied to commercial stitch bonded fabrics [Chapter 4]. The parameters which affect in-plane shear properties were compared with the results of the fabric forming experiments to determine the important parameters for fabric selection.

8.3 Modelling Fibre Deformation within an Engineered Fabric Preform

The literature review presented in section 2.5 suggested a KDM as the basis for modelling fabric forming. This assumes that the fibres rotate about their intersection points (simple shear) so that the fabric can be modelled as a pin-jointed net. A kinematic drape model based on pure shear principles was produced based on work published by Long [26]. The advantage of this method was the use of general surface geometries similar to those created by finite element pre-processors. To provide a unique solution to the drape equations a set of constraints representing the paths of two initially perpendicular fibres was required. These were calculated using geodesic principles across the surface geometry from a user specified point.

The experimental results showed that the KDM provided a reasonable approximation of the fabric architecture when draped over a surface until the deformation limit of the fabric was reached. As the model assumed the fabric has no resistance to shear deformation, an alternative method would be required to model fabric specific deformation allowing for fabric properties such as shear resistance. The fabric shear properties can be measured using the equipment described in Chapter 4. It may be possible to incorporate fabric specific data into the model through the use of a mechanistic approach as described by Bergsma [41], but would not provide the quick solution provided by the kinematic method. A simpler method would be to use an iterative constraint method, where the constraints are redefined using a minimisation of shear energy approach during the drape process. This would overcome the problems associated with the geodesic constraints method when applied to non-symmetric surfaces as shown by the S-rail preform described in section 6.6.

8.4 Measuring Deformation of Engineered Fabrics

The KDM is based on unrestricted shear deformation, and is therefore fabric independent. An investigation into the in-plane shear properties was performed to establish which factors affect fabric shear. An experimental rig was developed to measure and compare the shear stiffness of fabrics under various forming conditions.

The results suggested that the stitch used to bind the fabric had a major effect on the shear properties. Two types of stitching were used. Chain stitching caused the

fabric to lock at lower shear angles compared with tricot stitching. When the fabric has locked no further shear deformation can occur, causing the fabric to deform by other methods such as wrinkling, which would be detrimental to subsequent properties. The orientation of the stitch with respect to the shear direction had a major effect on the fabric shear resistance. The fabrics using chain stitch locked at approximately 12° shear when loaded parallel to the stitch, but could undergo more than 58° shear (a limit of the test machine) when loaded perpendicular to the stitch. The effect of using tricot stitching was less severe, with the in-plane shear stiffness approximately twice as high when loaded parallel to the stitch as opposed to perpendicular loading. This caused an imbalance in the shear deformation of the fabric which cannot be represented using a KDM.

Increasing the linear density or pitch of the yarns within the fabric increased the fabric areal density, which caused an increase in the in-plane shear resistance of the fabrics. However an investigation into two fabrics of comparable areal density but differing fibre linear density showed the fabric made with lower linear density fibres was stiffer. For fabrics formed perpendicular to the stitch (where effects of stitching on shear properties are not dominant), the shear resistance is related to the area of fibre contact between the two fabric layers.

8.5 Measurement of Fabric Deformation within a Preform

To investigate the deformation of the fabric structure within a preform, two methods of measuring fabric orientation were assessed. GSA was applied to measure fabric shear and slip within a preform. The other method involved cutting sections from moulded parts and examining the aspect ratio of the fibre sections to indicate inter-fibre shear. The most effective method was GSA which was relatively fast, automated (and hence repeatable) and provided results for both inter-fibre shear and slip deformation. The basis of the method was to measure the deformation of a grid printed onto the fabric prior to forming. A PC based software package (CamSys ASAME) was used to measure the co-ordinates of the grid intersections from digital images of the preform. The co-ordinate data were processed to provide measurements of the fabric shear and slip at each intersection across the grid, proving that fabric shear was the most dominant deformation mechanism. In-plane fibre buckling occurred as the shear angle

approached the fabric locking angle, where the fabric reaches the limit of pure shear deformation. Fabric wrinkling occurred in areas where the KDM predicted shear angles beyond the forming limit of the fabric.

The GSA method proved suitable for measuring fabric deformation. Large areas of fabric could be measured quickly and repeatably, producing both shear and slip data. The results assume that the deformation of the grid printed on the fabric was the same as that of the fabric. This may not be the case for loosely stitched fabrics where each fabric layer can move easily, or multiple layer preforms where inter ply slip is likely. The results did not show large amounts of slip occurring, which may be due to the relative coarseness of the printed grid when compared to the yarn spacing.

The effects of altering fabric construction parameters such as yarn linear density, pitch and stitch type on fabric formability were investigated. The parameter that caused the largest effect was stitch type, as locking of the stitch occurred, which preventing further shear in the fabric. This was a major problem with chain stitch bonded fabrics when loaded parallel to the stitch. The shear stiffness imbalance caused by the stitch, which was noticed in the in-plane shear compliance tests presented in Chapter 4, was also noticed in the forming tests. The fabrics with the largest ratio between in-plane shear stiffness also showed the largest variation in shear deformation between quadrants where the stitch ran parallel and perpendicular to the shear direction. Other parameters such as forming speed did not affect the architecture of the preform significantly.

8.6 Wider Implications

The results of this work indicate that simple shear based drape models are a useful starting point for preform design. They allow the designer to optimise the fabric orientation and surface geometry for a worst case scenario (i.e. unlimited shear). Therefore the results must be interpreted to provide an indication of whether the preform could be formed successfully. However, the next stage would be to incorporate fabric properties such as in-plane shear stiffness and stitch locking into the model to increase the types of fabric and geometries that can be modelled accurately. This must also be performed in conjunction with research into processing properties to

establish whether other fabric parameters, such as permeability at high volume fractions, limit the useful formability of a fabric.

For the larger more complex preforms such as those required by the automotive industry it is likely that a large amount of fabric deformation is required. Therefore careful selection of the fabric is required to prevent forming problems, such as wrinkling due to fabric locking. The imbalance in fabric shear properties due to the stitch could cause problems in large preforms, and knowledge of the shear properties of a fabric would allow such problems to be minimised.

8.7 Recommendations for Future Work

The following suggestions for future research are a result of questions that arose during this project. Most are further investigations into the important parameters in fabric forming, and how they can be optimised to increase the application of stitch bonded fabrics. Assumptions that were inherent in the experimental method could also be validated with further research.

- *Investigate methods of defining constraints for kinematic based models.* The method for defining the constraints of the kinematic drape model based on geodesic principles used in this thesis has been shown to be invalid for predictions based on a non-axi-symmetric geometry and where the fabric has an in-plane shear stiffness bias due to the stitching. Other methods of applying constraints such as the minimisation of energy method suggested by Bergsma [41], could be adapted to use fabric shear stiffness data for each direction. Therefore the variation in fabric deformation due to directional shear properties could be included in the model.

- *Implement mechanics based drape model* - A limitation of the kinematic approach is the assumption that fabrics have zero resistance to shear. The results are therefore a worst case scenario. To allow the modelling of larger more complex shapes, the effect of fabric forming properties must be included. Modelling fabric parameters, such as shear stiffness and fabric locking, would provide a more accurate prediction of fibre architecture and allow investigation

of processing methods such as edge clamping. This would require a force based approach similar to that proposed by Bergsma [41]. An alternative approach based on a modification to the commercial PAM-STAMP code (thermoplastic sheet forming model), incorporating fabric shear properties instead of resin flow resistance could be used to include fabric forming data into a drape model.

- *Study methods of optimising fabric clamping to minimise problems during preforming* - Edge restraint applied to the fabric in the form of clamping can eliminate problems such as bridging and wrinkling in preforms. Knowledge of how to design edge restraint to influence stitched fabric forming is required. Research by de Luca *et al* [53] used the PAM-STAMP code to show that blank holder pressure has a large effect on thermoplastic sheet forming. This approach could be adapted to model biaxial stitched fabrics.

- *Incorporate drape model into a composite processing design system* - Maximum use of the fibre orientation predicted by the model would be made by combining the model output with a resin flow and mechanical property prediction package to provide a complete preform and laminate design and optimisation package. This would reduce problems at each stage of the laminate manufacture and therefore avoid costly tooling modifications.

- *Improve the accuracy of the GSA technique* - The analysis of the GSA results assumed that the deformation of the grid printed on the fabric was the same as that of the fabric. This could be proven by constructing a fabric with black fibres running parallel in each ply which would form a grid within the fabric when cast in resin.

- *Determine effect of fabric construction parameters on fabric locking angles* - The experimental method for measuring fabric in-plane shear properties presented in this thesis did not record locking angles for all the fabrics due to limitations in the range of the test equipment. A parallelogram based shear rig with a wider shear range than that used in this research would confirm the results suggested in this thesis.

- *Develop a model for fabric shear properties* – The research presented in this thesis suggests that fabric shear properties are related to the area of intersection between the layers. To prevent the preform designer from having to test each fabric, a model to predict fabric shear properties such as stiffness and locking angle could be developed. This could be based on the area of intersection assumptions along with a model of rotational resistance due to friction and the resistance of the stitch to extension. This could be derived from empirical data or a model of stitch deformation.

- *Investigate effect of altering stitch parameters on fabric formability* - The stitch type has been shown to have a major effect on the fabric in-plane shear stiffness and locking angle. An investigation into the effect of parameters such as stitch type, pitch, stitch tension and material on shear characteristics would permit the optimisation of forming properties of fabrics.

8.8 Major Conclusions

The major conclusions arising from the research described in this thesis are:-

i) The simple shear based kinematic drape model provides a worst case estimation of fabric architecture, which can be used to estimate problems in preform design. The model assumptions become invalid if the limit of the fabric shear deformation is reached during forming.

ii) The geodesic based constrained path algorithm is invalid for complex geometries and when applied to fabrics with a large in-plane shear resistance bias due to the stitching. A method based on the minimisation of shear energy within the fabric would seem to be more suitable.

iii) The limit of fabric in-plane shear deformation can be either due to locking of the stitch or packing of the fibres, depending upon the direction of the stitch with respect to the shear direction. A chain stitch causes the fabric to lock at relatively low shear angles, whereas a tricot stitch allows higher shear before locking.

iv) Fabric in-plane shear properties and locking angles can be measured and compared using the force versus shear angle plots obtained from a simple test fixture.

v) The in-plane shear stiffness of the fabric is dependent upon the direction of the stitch relative to the direction of shearing. When the fabric is sheared parallel to the stitch direction, the stitch is the major factor defining in-plane shear stiffness.

vi) When the stitching is not dominating the in-plane shear properties i.e. the fabric is sheared perpendicular to the stitch direction, the in-plane shear resistance is related to the area of intersection between the yarn layers. For the biaxial tricot stitch bonded fabrics presented in this thesis the in-plane shear resistance when loaded perpendicular to the stitch is approximately a factor of two lower than when loaded parallel to the stitch.

vii) The in-plane shear resistance and subsequent preform fibre architecture of the fabrics tested in this thesis were not velocity dependent.

viii) A method of measuring fabric deformation within a fabric preform has been established. The deformation of a grid printed onto the fabric surface is measured and processed to provide in-plane shear and slip data.

ix) When the maximum shear deformation has been reached within the fabric, in-plane fibre buckling can occur. This could be modelled within the existing kinematic drape model by shortening the fibre spacing locally within the equations.

References

1. *Engineered Materials Handbook.* Vol. 1 'Composites', ASM International, 1987.
2. *Fuel Economy for Motor Vehicles*, Corporate Average Fuel Efficiency Report, Part 600, United States Environmental Protection Agency, 1997.
3. Flynn M.S. and Belzowski B.M. *Barriers to Automotive Structural Composites: Concerns, Competition, and Competence.* Advanced Composites Proceedings of 11th ESD ACCE, Dearborn, MI, USA, 6-9 Nov 1995, pp. 517-534.
4. Harrison A. *Driving Composites - Weighting for Improved Vehicle Fuel Economy?* Proceedings of 5th International Conference on Automated Composites (ICAC 97), Glasgow, UK, 4-5 Sept 1997, pp 3-12.
5. Wlosinski R.K. and Kniveton T.W. *Design and Manufacturing Pilot of an SRIM Composite Crossmember.* Proceedings of the 10th Annual ASM/ESD Advanced Composites Conference, Dearborn, MI, USA, 7–10 Nov 1994, pp 77-82.
6. Johnson C.F., Chavka N.G., Jeryan R.A., Morris C.J. and Babbington D.A. *Design and Fabrication of a HSRTM Crossmember Module.* Proceedings of Third Annual Conference on Advanced Composites, Detroit, MI, USA, 15-17 Sept 1987, pp 197-217.
7. Owen M.J., Middleton V. and Rudd C.D. *Fibre reinforcement for high volume resin transfer moulding (RTM).* Composites Manufacturing, June 1990, Vol 1(2): pp 74-78.
8. Smith P. *Structural Preform Design for Low Cost Composite Processing* , PhD Thesis, 1998, University of Nottingham.
9. McGeehin P. *Preform Manufacture for Liquid Moulding Processes* , PhD Thesis, 1994, University of Nottingham.
10. Turner M.T., Rudd C.D., Long A.C. and Middleton V. *Computer Integrated Design and manufacture of Structural Preforms.* Proceedings of 5th International Conference on Automated Composites (ICAC 97), Glasgow, UK, 4-5 Sept 1997, pp 245-252.

11. Drummond T. *A Totally Automated Near Net Dry Fiber Preform Manufacturing Process for the Composite Industry.* Proceedings of 56th Annual Technical Conference (ANTEC 98), Atlanta, GA, USA, 26-30 Apr 1998, pp 2296-2305.

12. Soh S.K. and Kordyban E. *Orientated Fiber Preforms with Slurry Process.* Advanced Composites Proceedings of 11th ESD ACCE, Dearborn, MI, USA, 6-9 Nov 1995, pp 221-232.

13. Johnson R.W. and Landon M.D. *Simulation and Optimisation of a Slurry-Based Fiberglass Preform Manufacturing Process.* Advanced Composites Proceedings of 11th ESD ACCE, Dearborn, MI, USA, 6-9 Nov 1995, pp 233-245.

14. Morales A. and Brosius D. *Engineered Textile Preforms for RTM.* Proceedings of Composites in Manufacturing 10, Anaheim, USA, 7-10 Jan 1991, pp 1-14.

15. Chavka N.G. and Johnson C.F. *Critical Preforming Issues for Large Automotive Structures.* Proceedings of 6th ASM/ESD Advanced Composites Conference, Detroit, MI, USA, 8-11 Oct 1990, pp 413-422.

16. Buckley D.T. *Manufacturing Automation Components for Net Shape, High Volume, Complex Preforms.* Proceedings of 5th International Conference on Automated Composites (ICAC 97), Glasgow, UK, 4-5 Sept 1997, pp 263-262.

17. Mazzoni B. and Riley J. *Update for Glass Mat Preformers.* Proceedings of 6th ASM/ESD Advanced Composites Conference, Detroit, MI, USA, 8-11 Oct 1990, pp 423-427.

18. Bland R.J. Harper A.R. and Grove S.M. *Cost Effective Automation for Low to Medium Volume RTM Production.* Proceedings of 50th Composites Institute Annual Conference, 30 Jan-1 Feb 1995, Session 3-B pp 1-6.

19. Hill D.J. *Microwave Preheating of Thermoset Resin for Resin Transfer Moulding,* PhD Thesis, 1993, University of Nottingham.

20. Johnson M.S. *The Application of Microwave Preheating to Resin Transfer Moulding,* PhD Thesis, 1996, University of Nottingham.

21. Blanchard P.J. *High Speed Resin Transfer Moulding of Composite Structures,* PhD Thesis, 1995, University of Nottingham.

22. Kendall K.N., Mangin C. and Ortiz E. *Dynamic Manufacturing Simulation of an Automotive LCM Component.* Proceedings of 5th International Conference

on Automated Composites(ICAC 97), Glasgow, UK, 4-5 Sept 1997, pp 329-336.

23. Rudd C.D. *Preform Processing for High Volume Resin Transfer Moulding (RTM),* PhD Thesis, 1989, University of Nottingham.

24. Bulmer L.J. *In-Plane Permeability of Reinforcements for Liquid Moulding Processes,* PhD Thesis, 1994, University of Nottingham.

25. Kendall K.N. *Mould Design for High Volume Resin Transfer Moulding,* PhD Thesis, 1991, University of Nottingham.

26. Long A.C. *Preform Design for Liquid Moulding Processes,* PhD Thesis, 1994, University of Nottingham.

27. Rice E.V. *Computer Aided Engineering Techniques for Resin Transfer Moulding,* PhD Thesis, 1993, University of Nottingham.

28. Potter K.D. *The influence of accurate stretch data for reinforcements on the production of complex structural mouldings. Part 1: Deformation of aligned sheets and fabrics.* Composites, 1979(July): pp 161-167.

29. Long A.C. and Rudd C.D. *A simulation of reinforcement deformation during the production of preforms for liquid moulding processes.* Proceedings of the Institution of Mechanical Engineers, Part B: Journal of Engineering Manufacture, 1994, Vol 208: pp 269-278.

30. Robertson R.E., Hsiue E.S., Sickafus E.N. and Yeh G.S.Y. *Fiber Rearrangement During the Moulding of Continuous Fiber Composites. 1. Flat cloth to a Hemisphere.* Polymer Composites, 1981. Vol 2(July): pp 126-131.

31. Van West B.P., Keefe M. and Pipes R.B. *The Draping of Bi-directional Fabric Over Three-Dimensional Surfaces.* Proceedings of the American Society for Composites, 4th Technical Conference, Bladisbury, Virginia, October 1989, pp 463-472.

32. Rudd C.D., Morris D.J., Chick J.P. and Warrior N.A. *Material Characterisation for SRIM.* Proceedings of 4th International Conference on Automated Composites (ICAC 95), Nottingham, UK, 6-7 Sept 1995, pp 211-218.

33. Daillo M.L., Gauvin R. and Trochu F. *Experimental Analysis of Flow through Multi-layer Fiber Reinforcements in Liquid Composite Moulding.* Proceedings of 4th International Conference on Automated Composites (ICAC 95), Nottingham, UK, 6-7 Sept 1995, pp 201-210.

34. Trochu F., Audet M., Gauvin R. and Beguin Y. *Non-Isothermal Analysis of Mold Filling in Liquid Composite Molding.* Proceedings of 5th International Conference on Automated Composites (ICAC 97), Glasgow, UK, 4-5 Sept 1997, pp 215-222.

35. Long A.C., Blanchard P.J., Rudd C.D. and Smith P. *Combined Drape and Flow Modelling for Liquid Composite Moulding.* Proceedings of 5th International Conference on Automated Composites (ICAC 97), Glasgow, UK, 4-5 Sept 1997, pp 51-58.

36. Chan A.W. and Morgan R.J. *Application of Computer Simulation to Liquid Composite Moulding Design.* Proceedings of ESD Advanced Composites Conference (*ACCE 97)*, Detroit, MI, USA, April 1997, pp 229-237.

37. Massey B.S. *Mechanics of Fluids.* Van Nostrand Reinhold (International).

38. Bickerton S., Simacek P., Gugielmi S.E. and Advani S.G., *Investigation of Draping and its Effects on the Mold Filling Process during Manufacturing of a Compound Curved Composite Part.* Composites Part A, 1997, Vol 28A: pp 801-816.

39. Krenchel H. *Fibre Reinforcement.* Akademisk Forlag (Copenhagen).

40. Rudd C.D., Middleton V., Owen M.J., Long A.C. and McGeehin P. *Design Processing and Performance of Structural Preforms.* Proceedings of 2nd Canadian International Conference on Composites (CANCOM 93), Ottawa, Canada, September 1993, pp139-152.

41. Bergsma O.K. *Computer Simulation of 3D Forming Processes of Fabric Reinforced Plastics.* Proceedings of 9th International Conference on Composite Materials (ICCM/9), Madrid, Spain, July 1993, pp 560-567.

42. Mack C. and Taylor H.M. *The Fitting of woven cloth to surfaces.* Journal of Textile Institutes (Transactions), 1956, Vol 47: pp 477-488.

43. Chen B. and Govindaraj M. *A Physically Based Model of Fabric Drape Using Flexible Shell Theory.* Textile Research Journal, 1995, Vol 65(6): pp 324-330.

44. Breen D.E., House D.H. and Wozny M.J. *A Particle-Based Model for Simulating the Draping Behaviour of Woven Cloth.* Textile Research Journal, 1994, Vol 64(11): pp 663-685.

45. Taylor C.A. *Finite Element Simulation of Thermoforming - Experiments and Analyses.* Proceedings of 46th Annual Technical Conference (ANTEC 89), New York, 1989, pp 435-437.

46. O Bradaigh C.M. *Sheet Forming of Composite Materials*, Flow and Rheology in Polymer Composites Manufacturing, Edited by S.G. Advani, Elsevier Science, pp 517-569.

47. Pipkin A.C. and Rogers T.G. *Plane deformations of incompressible fibre-reinforced materials.* Journal of Applied Mechanics, 1971, Vol 38: pp 634-640.

48. Spencer A.J.M. *Deformations of Fibre Reinforced Materials.* Clarendon Press (Oxford).

49. O Bradaigh C.M. and Pipes R.B. *Finite element analysis of composite sheet-forming process.* Composites Manufacturing, 1991, Vol 2(3/4): pp 161-169.

50. O Bradaigh C.M., McGuinness G.B. and Pipes R.B. *Numerical analysis of stresses and deformations in composite materials sheet forming: central indentation of a circular sheet.* Composites Manufacturing, 1993, Vol 4(2): pp 67-82.

51. Smiley A.J. and Pipes R.B. *Fiber Placement During the Forming of Continuous Fiber Reinforced Thermoplastics.* Proceedings of Composites in Manufacturing 6, Ananheim, California, 19-22 Jan 1987, pp129(1-13).

52. Cogswell F.N. *The processing science of thermoplastic structural composites.* International Polymer Processing, 1987, Vol 1(4): pp 157-165.

53. Murtagh A.M. and Mallon P.J. *Shear Characterisation of unidirectional and fabric reinforced thermoplastic composites for pressforming applications.* Proceedings of 10th International Conference on Composite Materials (ICCM/10), Whistler, B.C., Canada, August 1995, pp 373-380.

54. de Luca P., Lefebure P. and Pickett A.K. *Numerical and Experimental Investigation if Some Press Forming Parameters of Two Fibre Reinforced Thermoplastics: APC2-AS4 and PEI-CETEX.* Proceedings of 4th International Conference on Flow Processes in Composite Materials, Aberystwyth, UK, 9-11 Sept 1996, pp 1-15.

55. McEntee S.P. and O'Bradaigh C.M., *Large Deformation Finite Element Modelling of Single-Curvature Composite Sheet Forming with Tool Contact.* Composites Part A, 1998, Vol 29A: pp 207-213.

56. Johnson A.F. *Rheological Model for the Forming of Fabric Reinforced Thermoplastic Sheets.* Proceedings of Flow Processes in Composites Materials, Galway, Ireland, 1994, pp 145-158.

57. de Luca P., Pickett A.K., Queckborner T. and Johnson A.F. *Development Validation and first Industrial Numerical Results of a Finite Element Code to Simulate the Thermoforming Process.* Proceedings of 4th International Conference on Automated Composites (ICAC 95), Nottingham, UK, 6-7 Sept 1995, pp 183-193.

58. Canavan, R.A., Simon, E.R., O`Braidaigh, C.M. and Standley, D. *Hop Drape Forming of Thermoset Composite Materials for Aerospace Applications.* Proceedings of 5th International Conference on Automated Composites (ICAC 97), Glasgow, UK, 4-5 Sept 1997, pp 281-291.

59. Blanlot R. *Simulation of the Shaping of Woven Fabrics.* Proceedings of 11th International Conference on Composite Materials (ICCM-11), Gold Coast, Australia, 14-18 July 1997, Vol V: pp 160-170.

60. St. John, C. *High Strength Thermoplastic Composites Automotive Opportunities.* Proceedings of the 11th Annual ESD/ACCE Advanced Composites Conference, Dearborn, MI, USA, 6-9 Nov 1995, pp 437-449.

61. Johnson C.F., Wilks C.E., Rudd C.D. and Long A.C. *Thermoplastic Stamping of Structural Composites, A Preliminary Assessment.* Proceedings of 5th International Conference on Automated Composites (ICAC 97), Glasgow, UK, 4-5 Sept 1997, pp 61-73.

62. Wakeman M.D., Cain T.A., Rudd C.D., Long A.C. and Brooks R. *Optimisation of the Compression Moulding of Continuous Aligned Glass Reinforced Polypropylene Composites.* Proceedings of 4th International Conference on Automated Composites (ICAC 95), Nottingham, UK, 6-7 Sept 1995, pp 325-332.

63. Seo J.W. and Lee W.I. *A Model of the Resin Impregnation in Thermoplastic Composites.* Journal of Composite Materials, 1991, Vol 25(September): pp 1127-1142.

64. Cain, T.A., Wakeman, M.D., Brooks, R., Long, A.C. and Rudd, C.D. *Isothermal Consolidation of a Co-mingled Thermoplastic Composite.* Proceedings of 7th European Conference on Composite Materials (ECCM-7), London, UK, 14-16 May 1996, pp 1-6.

65. Connor M., Toll S., Manson J.A.E. and Gibson A.G. *A Model for the Consolidation of Aligned Thermoplastic Powder Impregnated Composites.*

Journal of Thermoplastic Composite Materials, 1995, Vol 8(April): pp 138-162.

66. Van West B.P., Pipes R.B., Keefe M. and Advani S.G., *The draping and consolidation of commingled fabrics.* Composites Manufacturing, 1991, Vol 2(1): pp 10-22.

67. Potter K.D. *The influence of accurate stretch data for reinforcements on the production of complex structural mouldings. Part 2: Deformation of random mats.* Composites, 1979(July): pp 168-173.

68. Van Der Ween F. *Algorithms for Draping Fabrics on Doubly-Curved Surfaces.* International Journal for Numerical Methods in Engineering, 1991, Vol 31: pp 1415-1426.

69. Trochu F., Hammami A. and Benoit Y. *Application of Dual Kriging to the Prediction of Fibre Arrangement During the Forming of Complex Composites Parts.* Proceedings of 4th International Conference on Automated Composites (ICAC 95), Nottingham, UK, 6-7 Sept 1995, pp 383-390.

70. MSC/PATRAN, *Composites Modelling for Design, Analysis and Manufacture - Course Notes*, European Engineering Services, 1st edition, 1995.

71. Forster B., *Sikorsky simulation*, in *CADCAM*, Jan 1998, pp 21-24.

72. Prodromou A.G. and Chen J. *On the Relationship between Shear Angle and Wrinkling of Textile Composite Preforms.* Composites Part A, 1997, Vol 28A: pp 491-503.

73. Boisse P., Cherouat A., Gelin J.C. and Sabhi H. *Experimental study and Finite Element Simulation of a Glass Fiber Fabric Shaping Process.* Polymer Composites, 1995, Vol 16(1): pp 83-95.

74. Laroche D. and Vu-Khanh T. *Forming of Woven Fabric Composites.* Journal of Composite Materials, 1994, Vol 28(18): pp 1825-1839.

75. Wang J., Page J.R. and Paton R. *Experimental Investigation into the Draping Properties of Reinforcement Fabrics. Proceedings of 2nd International Symposium on Aeronautical Science and Technology (ISASTI 96)*, Jakarta, Indonesia, 24-27 Jun 1996, pp 1-15.

76. Kobayashi S., Oh S.O. and Altan T. *Metal forming and the finite-element method*, Oxford University Press (Oxford).

77. Fukui S., Kudo H., Yoshida K. and Okawa H. *A Method for Testing of Deep-Drawability of Sheet Metals,* Report of the Institute of Science and Technology, University of Tokyo, 1952, pp 351.

78. Keeler S.P. and Backofen W.A. *Plastic Instability and fracture in Sheets Stretched Over Rigid Punches.* Transcripts of the American Society of Metals, 1963, Vol 56: pp 25.

79. Vogel D.H. and Lee D. *An automated two-view method for determining strain distributions on deformed surfaces.* Journal of Material Shaping Technology, 1989, Vol 4(4): pp 205.

80. Vogel D.H. and Lee D. *The automated measurement of strains from three dimensional deformed surfaces.* Journal of Metals, 1990(February): pp 8-13.

81. Vogel J.H., Lee D., Kapij M.I., Moleski J., Ohwue T. *Comparison of Different Surface Strain Measurement Methods Used for Deformed Sheet Metal Parts.* Proceedings of SAE, International Congress and Exposition, Detroit, MI, USA, 24-28 Feb,1992, pp 73-85.

82. Manthey D.W. and Farhat J.P. *Comparison Between Steel and Aluminium Strain Rate Effects.* Proceedings of SME\FMA Presstech Conference, Rosemont, IL, USA, 18-21 Oct 1993, pp 224/1-9.

83. Breuer U., Neitzel M., Ketzer V. and Reinicke R. *Deep Drawing of Fabric-Reinforced Thermoplastics: Wrinkle Formation and Their Reduction.* Polymer Composites, 1996, Vol 17(4): pp 643-648.

84. Martin T.A., Bhattacharyya D. and Pipes R.B. *Deformation Characteristics and Formability of Fibre-Reinforced Thermoplastic Sheets.* Composites Manufacturing, 1992, Vol 3(3): pp 165-172.

85. Laroche D. and Vu-Khanh T. *Modelling of the Forming of Complex Parts from Fabric Composites. Proceedings of 1st Canadian International Composites Conference and Exhibition (CANCOM 91)*, Montreal, Canada, 4-6 Sept 1991, pp 2C3/1-8.

86. Hull D. *An Introduction to Composite Materials*, Cambridge Press, 1981, pp 71-75.

87. Yang H. and Colton J.S., *Quantitative image processing analysis of composite materials.* Polymer Composites, 1994, Vol 15(1): pp 46-54.

88. Brooks R., Fan J.Y.H. and Hsu J.C.Y. *Computer-integrated design for short fibre-reinforced thermoplastics*. Proceedings of 10th International Conference

on Composite Materials (ICCM/10), Whistler, B.C., Canada, August 1995, pp 119-126.

89. Hine P.J., Davidson N., Duckett R.A., Clarke A.R. and Ward I.M. *Hydrostatically Extruded Glass-Fiber-Reinforced Polyoxymethylene, 1: The Development of Fiber and Matrix Orientation.* Polymer Composites, October 1996. Vol 17(5): pp 720-729.

90. Kawabata S., Niwa M. and Kawai H. *The finite-deformation theory of plain weave fabrics.* Journal of the Textile Institute, 1973, Vol 62(2): pp 21-85.

91. Kutz J.J., *Development of a Process for the Evaluation of Directional Fabric Formability,* MSc Thesis, 1990, Drexel University.

92. Kutz J.J. and Ko F.K. *Evaluation of Fabric Preforms for High Volume Manufacture of Automotive Composites.* Proceedings of 5th ASM/ESD Advanced Composites Conference, Dearborn, MI, USA, 25-28 Sept 1989, pp 291-300.

93. Yu J., Cai Z. and Ko F.K. *Formability of textile preforms for composite applications. Part 1: characterization experiments.* Composites Manufacturing, Jun 1994, Vol 5(2): pp 113-122.

94. Cai Z., Yu J.Z. and Ko F.K. *Formability of textile preforms for composite applications. Part 2: evaluation experiments and modelling.* Composites Manufacturing, Jun 1994. Vol 5(2): pp 123-132.

95. Dreby E.C. *The Planoflex, a simple device for evaluating the pliability of fabrics.* American Dyestuff Reporter, 1941, Vol 30: pp 651-666.

96. Behre B. *Mechanical properties of textile fabrics. Part 1: Shearing.* Textile Research Journal, 1961, Vol 31(2): pp 87-93.

97. Robroek L.M.J. *The Development of Rubber Forming as a Rapid Thermoforming Technique for Continuous Fibre Reinforced Thermoplastic Composites* , PhD Thesis, 1994, Delft University of Technology.

98. Treloar L.R.G. *The effect of test-piece dimensions on the behaviour of fabrics in shear.* Journal of the Textile Institute, 1965, Vol 56: pp T553-T550.

99. Culpin M.F. *The shearing of fabrics, a novel approach.* Journal of the Textile Institute, March 1979, Vol 70(3): p. 81-88.

100. Skelton J. *Fundamentals of Fabric Shear.* Textile Research Journal, 1976(December): pp 862-869.

101. Chavka N.G., Johnson C.F., Stender M.W. and Lipinski P.L. *Development of Lower Cost Preforming for Automotive Structures.* (Extended outline only in:-) Proceedings of ESD Advanced Composites Conference (*ACCE 97)*, Detroit, MI, USA, April 1997, pp 481-496.

102. Hutson K. *High Performance Composite Preform Design.* Proceedings of the 2nd Conference on Advanced Composites, Dearborn, MI, USA, 18-20 Nov 1986, pp 229-239.

103. Spooner M., *Personal Communication with Author,* 1998.

104. Boisse P., Gelin J.C. and Sabhi H. *Forming of Glass Fiber Fabrics into Complex Shapes - Experimental and Computational Aspects.* Annals of the CIRP, 1992, Vol 41(1): pp 327-330.

105. Manthey D. *Personal Communication with Author,* 1996.

106. Hsu C.Y. *Experimental Determination of Fibre Orientation Distribution and Prediction of Stiffness in Short Fibre-Reinforced Thermoplastics,* PhD Thesis, 1997, University of Nottingham.

107. Carter D., *Personal Communication with Author,* 1998.

Appendix 1.1 - Research Publications

The following papers have been published on the work presented in this thesis:-

1) Long, A.C., Rudd, C.D., and Blagdon, M. *A Computer Aided Engineering approach to Preform Design.*, Proceedings of IoM International Conference on Automated Composites (ICAC '95), Nottingham, UK, 6-7 Sept. 1995.

2) Long, A.C., Rudd, C.D., Blagdon, M., Kendall, K.N., and Demeri, M.Y. *Deformation Mechanisms of Engineered Fabrics during Preform Manufacture*, Proceedings of ICCM '95, Whistler, Canada, 14-18 Aug 1995.

3) Long, A.C., Rudd, C.D., Blagdon, M. and Smith, P. *Fibre Movements and Associated Property Changes during Preform Manufacture*, Proceedings of ASM/ESD Advanced Composites Conference, Detroit, MI, USA, 6-8 November 1995, pp 263-273. ISBN 1-56378-023-2.

4) Long, A.C., Rudd, C.D. and Blagdon, M. *Characterising the Processing and Performance of aligned Reinforcements during Preform Manufacture*, Composites Part A - Applied Science and Manufacturing, 1996, Vol. 27A(4), pp 247-255.

5) Long, A.C., Rudd, C.D., Blagdon, M., Kendall, K.N. and Demeri, M.Y. *Simulation and Measurement of Reinforcement Deformation during Preform Manufacture*, Polymers and Polymer Composites, 1996, Vol. 4(5), pp 335-341.

6) Long, A.C., Rudd, C.D., Johnson, M.S. and Blagdon, M. *Experimental Analysis of Fabric deformation Mechanisms During Preform Manufacture*, Proceedings of 11th International Conference on Composite Materials (ICCM 11), Gold Coast, Australia, 14-18 July 1997.

Appendix 3.1 - Fabric Specifications and Manufacturer Details

Summary of Fabric Specifications

A summary of the fabric constituent properties is shown in Table 3.1.1. A comparison of the manufacturers quoted (nominal) and actual areal densities can be seen in Figure 3.1.1.

Table 3.1.1 – Summary of fabric construction parameters.

Fabric Type	Nominal Areal Density (g/m^2) *	Actual Aerial Density (g/m^2) **	Nominal Yarn Linear Density (Tex) *	Yarn Spacing (mm) *	Stitch Pitch (mm) (1) **	Stitch Spacing (mm) (2) **
Tech Textiles E-BXhd 936	936	972	600	1.41	1.93	4.27
Tech Textiles E-BX 948	948	927	740	1.60	2.2	4.9
Tech Textiles E-bBXhd 892	892	865	305	1.41	1.94	4.3
Flemmings 440 (Standard)	440	453	408	1.80	-	-
Flemmings 600 (Standard)	600	569	408	1.30	-	-
Flemmings 800 (Standard)	800	825	600	1.50	-	-
Flemmings 1200 (Standard)	1200	1130	900	1.50	-	-
Flemmings 545 (Custom)	545	553	408	1.50	-	-
Flemmings 1600 (Custom)	1600	1460	1200	1.50	-	-
Flemmings 403 (Custom)	403	424	408	2.00	-	-
Flemmings 682 (Custom)	682	680	408	1.20	-	-
Flemmings 784 (Custom)	786	778	900	2.30	-	-
FGI Plain Weave	840	821	2200	5.2	N\A	N\A

(1) Stitch pitch defined as length of smallest repeating stitch pattern.

(2) Stitch spacing defined as distance across fabric between parallel stitch rows.

* Denotes manufacturers data.

** Denotes data measured by author.

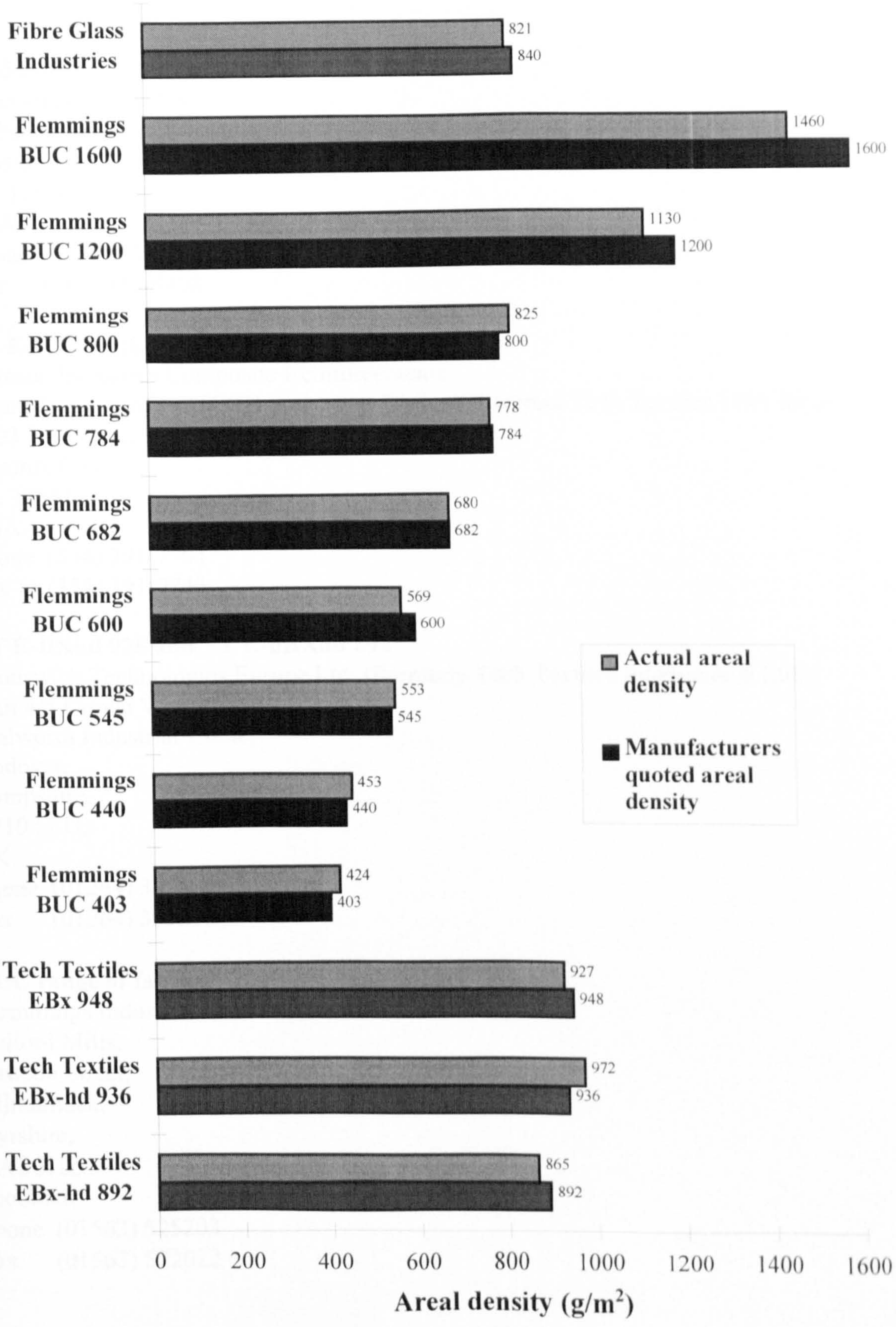

Figure 3.1.1 Summary of fabric nominal and actual areal density

Fabric Manufacturers Addresses

#2454 - 50" RovCloth (840 g/m^2)
Fiber Glass Industries
69 Edson Street,
Amsterdam,
NY 12010,
USA.
Phone (518) 842-4000
Fax (518) 842-4408

TT E-BX 948 (US ref. E-BX 2800)
Johnson Industries Composite Reinforcements
(Manufacturers of COTECH non crimp fabrics for former Tech Textiles USA Inc.)
3503 Lakewood Drive,
Pheonix City,
AL 36867,
USA.
Phone (334) 291-7704
Fax (334) 291-7743

TT E-BXhd 936 and TT E-bBXhd 892
Brunswick Technologies Europe Ltd. (Formerly Tech Textiles International Ltd.)
Unit 4/5 Crown Way,
Walworth Industrial Estate,
Andover,
Hampshire,
SP10 5LU,
UK.
Phone (01264) 333400
Fax (01264) 359610

BUC range of fabrics
Flemmings Industrial Fabrics
Belford Mills,
Lawson Street,
Kilmarnock,
Ayrshire,
KA1 3HZ ,
Scotland.
Phone (01563) 525203
Fax (01563) 522022

Appendix 3.2 - Modified AVS File Format

The modified AVS file format used to describe the surfaces in the kinematic drape model is as follows:-

Header Information:-
No. of nodes,
No. of patches.

Corner Point Information:-

Corner No.,
x,y,x.

Patch Description Information:-

Patch No.,
Unused,
Patch type,
Corner Nos.

```
466 396 0 0 0
1 0.000000 0.000000 0.000000
2 -175.963242 0.000000 12.196870
3 0.000000 0.000000 0.000000
4 -196.208282 0.000000 115.000000
5 0.000000 0.000000 0.000000
6 0.000000 0.000000 0.000000
7 0.000000 0.000000 0.000000
8 0.000000 0.000000 0.000000
9 0.000000 0.000000 0.000000
10 0.000000 0.000000 0.000000
11 0.000000 0.000000 0.000000
12 0.000000 0.000000 0.000000
13 0.000000 0.000000 0.000000
14 0.000000 0.000000 0.000000
15 0.000000 0.000000 0.000000
.
.
.
.
465 -0.000003 18.526081 0.000000
466 -0.000005 30.876814 0.000000
1 1 quad 25 34 79 78
2 1 quad 23 28 89 88
3 1 quad 28 25 78 89
4 1 quad 22 45 93 92
5 1 quad 45 47 96 93
.
.
.
388 1 quad 416 402 427 462
389 1 tri 441 419 464
390 1 tri 419 394 417
391 1 tri 419 417 464
392 1 tri 465 369 31
393 1 quad 466 370 369 465
394 1 tri 464 417 466
395 1 tri 417 368 370
396 1 tri 417 370 466
```

Appendix 3.3 - Methods for Calculating Yarn Intersections in the Kinematic Drape Model.

Theory

If the next yarn intersection (node) occurs on the same patch as the two nodes it is derived from, then its co-ordinates can be calculated directly from the vectors of the previous yarns attached to those nodes. If the above solution is not valid, then three simultaneous equations defining the patch surface and the possible co-ordinates of the node must be solved.

Method 1 - Vector Addition.

The simplest case occurs when the node is on the same patch as its predecessors (Figure 3.3.1). The node point $P_{m,n}$ co-ordinates can be determined from the vectors of the yarns attached to the previous two points, as shown in equation (3.3.1).

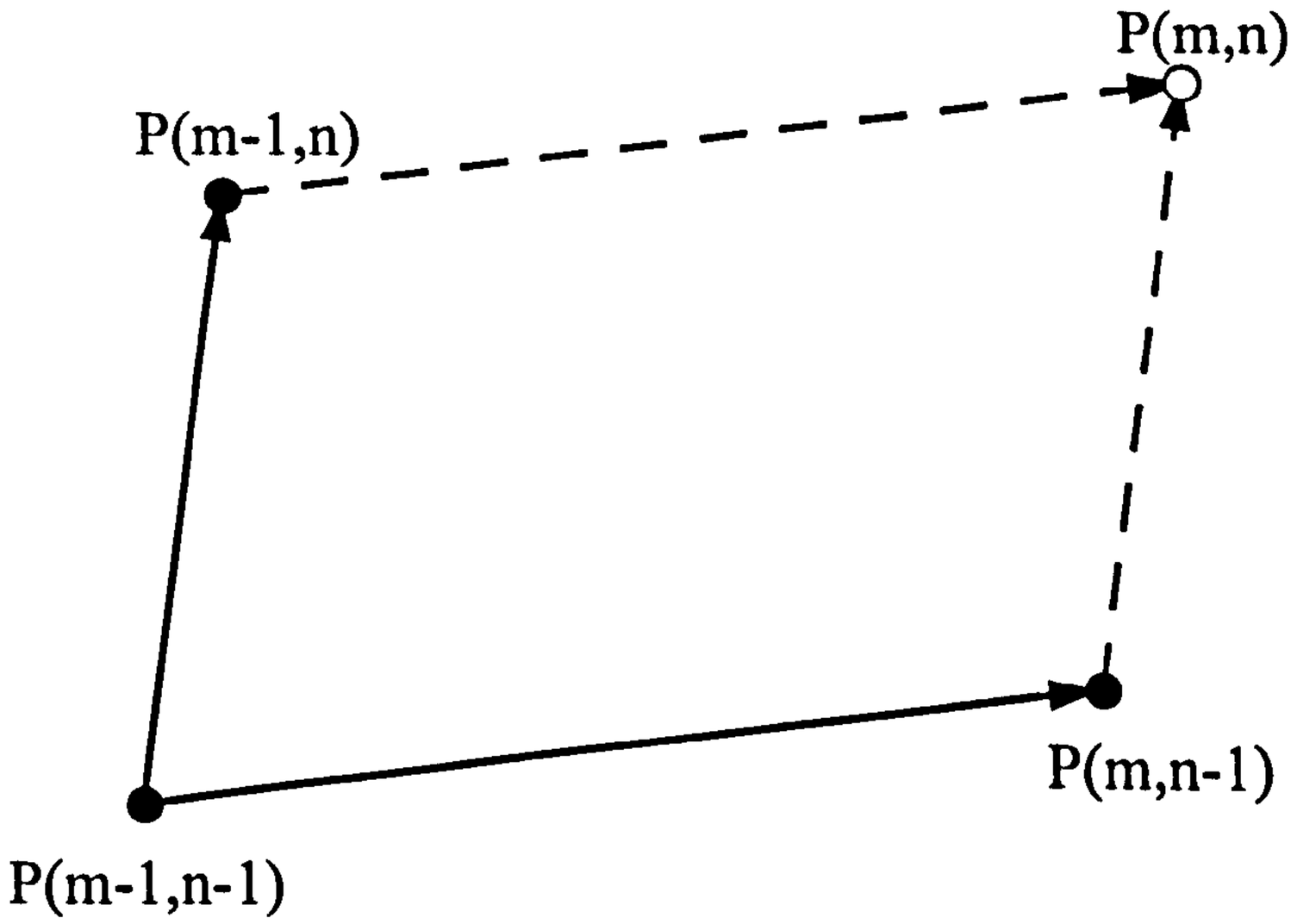

Figure 3.3.1 Calculation of point P(m,n) by vector addition

$$\overline{P_{m,n}} = \overline{P_{m-1,n}} + \left(\overline{P_{m,n-1}} - \overline{P_{m-1,n-1}} \right) \qquad (3.3.1)$$

This solution is tried first, as the majority of cases will fall into this category. To check that the solution is on the same patch as the two nodes it is derived from (and therefore that this method of solution is valid), a containment algorithm is used. This

determines if the point is on a patch by counting the number of times that a line from the point on the patch to another arbitrary point outside the patch cuts the patch boundary (Figure 3.3.2). If the boundary is cut once then the point is on the patch. An algorithm for this method is described in full by Long [26].

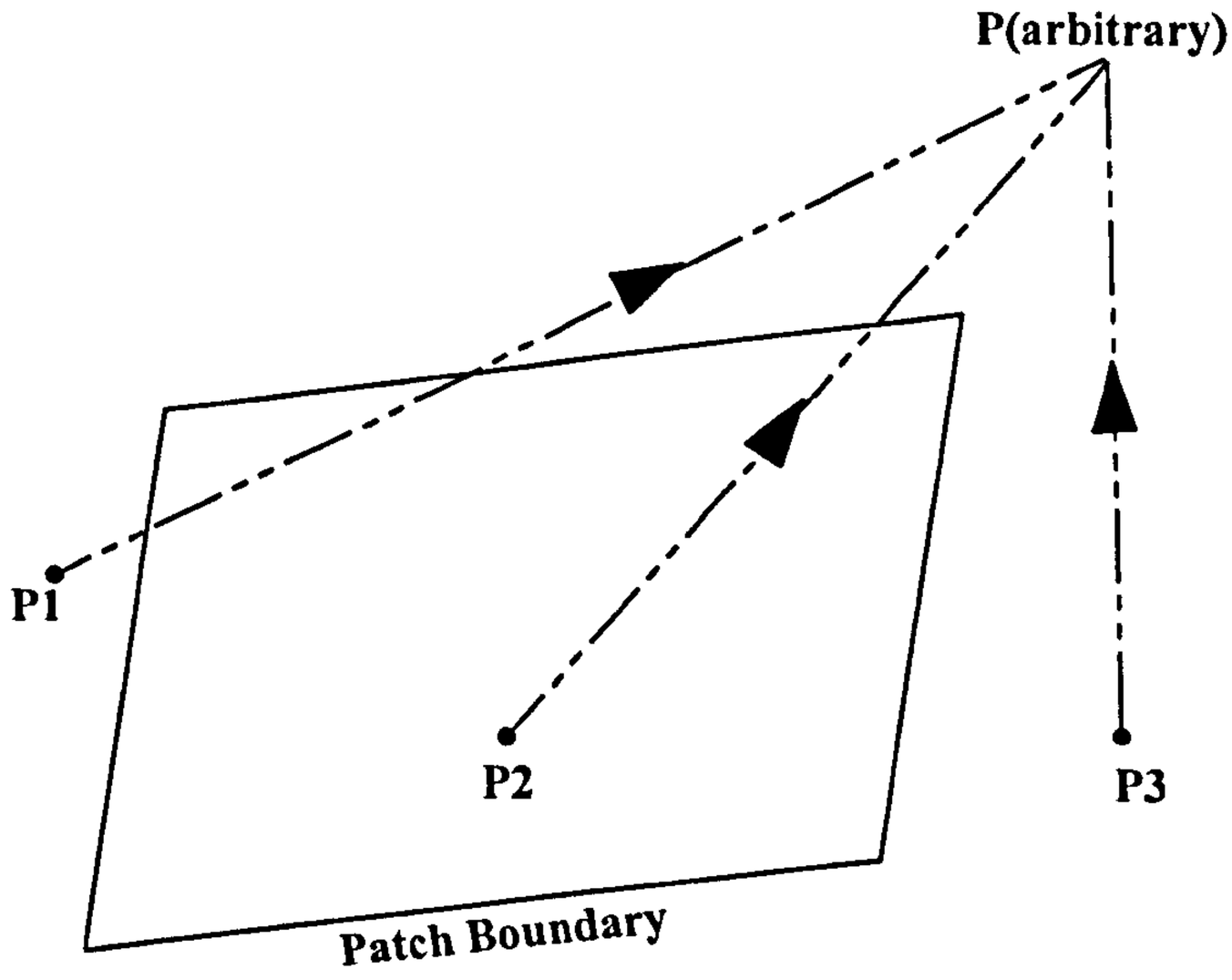

Figure 3.3.2 Method of determining if point is within a patch boundary

Method 2 - Quadratic Equations.

The co-ordinates of any point on a sphere surface can be derived using:-

$$x^2 + y^2 + z^2 = R^2 \qquad (3.3.2)$$

Since it is assumed that the yarns can rotate about their node points, a third node can be found from the intersection of the arcs of two previous nodes (Figure 2.2). This is done by finding the intersection point of two spheres centred on the previous nodes and the plane of the surface that the point lies on. The equation (3.3.2) can be therefore be expanded into 2 equations for the distance of a point on a sphere surface from its centre, with each centre being a previous node (m-1, n) and (m, n-1), giving:-

$$S_m^2 = (x_{m,n} - x_{m-1,n})^2 + (y_{m,n} - y_{m-1,n})^2 + (z_{m,n} - z_{m-1,n})^2 \qquad (3.3.3)$$

$$S_n^2 = (x_{m,n} - x_{m,n-1})^2 + (y_{m,n} - y_{m,n-1})^2 + (z_{m,n} - z_{m,n-1})^2 \qquad (3.3.4)$$

The equation of the flat plane that the node lies on is defined by:-

$$ax_{m,n} + by_{m,n} + cz_{m,n} = d \qquad (3.3.5)$$

Where the coefficients of the equation a, b and c are calculated from the vector product:-

$$\begin{bmatrix} a \\ b \\ c \end{bmatrix} = \left(\overline{P_{10}} - \overline{P_{00}} \right) x \left(\overline{P_{01}} - \overline{P_{00}} \right) \qquad (3.3.6)$$

and d is found by substituting a, b, c and the point P_{11} into equation (3.3.5).

Depending upon the projection of the plane of the patch with respect to the axes, one of the patch constants can be eliminated from the equations. For a patch that is almost perpendicular to the z-axis, constant c will have a magnitude greater than zero, and can therefore be eliminated safely. For patches than are almost perpendicular to the x, or y planes, constants a and b respectively can be eliminated. The patch in the following example is assumed to be almost perpendicular to the z axis.

By dividing equation (3.3.5) through by c, only three constants are required to describe the plane of any patch. Substituting this into equations (3.3.3) and (3.3.4) gives:-

$$x_{m,n}{}^2(1+a^2)+y_{m,n}{}^2(1+b^2)+2abx_{m,n}y_{m,n}+2x_{m,n}(az_{m-1,n}-ad-x_{m-1,n})$$
$$+2y_{m,n}(bz_{m-1,n}-bd-y_{m-1,n})=S_m{}^2+2dz_{m-1,n}-d^2-(x_{m-1,n}{}^2+y_{m-1,n}{}^2+z_{m-1,n}{}^2) \qquad (3.3.7)$$

and,

$$x_{m,n}{}^2(1+a^2)+y_{m,n}{}^2(1+b^2)+2abx_{m,n}y_{m,n}+2x_{m,n}(az_{m,n-1}-ad-x_{m,n-1})$$
$$+2y_{m,n}(bz_{m,n-1}-db-y_{m,n-1})=S_n{}^2+2dz_{m,n-1}-d^2-(x_{m,n-1}{}^2+y_{m,n-1}{}^2+z_{m,n-1}{}^2) \qquad (3.3.8)$$

Subtracting equation (3.3.7) from equation (3.3.8) gives:-

$$k_1 x_{m,n} + k_2 y_{m,n} = k_3 \qquad (3.3.9)$$

where:-

$$k_1 = 2\left[a\left(z_{m,n-1} - z_{m-1,n}\right) - x_{m,n-1} + x_{m-1,n}\right] \qquad (3.3.10)$$

$$k_2 = 2\left[b\left(z_{m,n-1} - z_{m-1,n}\right) - y_{m,n-1} + y_{m-1,n}\right] \qquad (3.3.11)$$

$$k_3 = 2d(z_{m,n-1}-z_{m-1,n})-(x_{m,n-1}{}^2+y_{m,n-1}{}^2+z_{m,n-1}{}^2)$$
$$-(x_{m-1,n}{}^2+y_{m-1,n}{}^2+z_{m-1,n}{}^2)+S_n{}^2-S_m{}^2 \qquad (3.1.12)$$

Method 2a - Simplified Quadratic Equations.

If in equation (3.3.9), k_2=0 then the equation can be simplified to:-

$$x_{m,n} = \frac{k_3}{k_1} \tag{3.3.13}$$

and if in equation (3.3.5) b=0:-

$$z_{m,n} = d - ax_{m,n} \tag{3.3.14}$$

Substituting into equation (3.3.8) gives:-

$$y_{m,n} = y_{m,n-1} \pm \sqrt{S_n^2 - (x_{m,n} - x_{m,n-1})^2 - (z_{m,n} - z_{m,n-1})^2} \tag{3.3.15}$$

But if b≠0 then a combining equations (3.3.5),(3.3.7) and (3.3.13) gives:-

$$a_2 y_{m,n}^2 + b_2 y_{m,n} + c_2 = 0 \tag{3.1.16}$$

where:-

$$a_2 = 1 + b^2 \tag{3.1.17}$$

$$b_2 = 2\left(bz_{m,n-1} + abx_{m,n} - bd - y_{m,n-1}\right) \tag{3.1.18}$$

$$c_2 = y_{m,n-1}^2 + (x_{m,n} - x_{m,n-1})^2 - S_n^2 + d^2 - 2adx_{m,n} + a^2 x_{m,n}^2 - 2dz_{m,n-1} + 2ax_{m,n} z_{m,n-1} + z_{m,n-1}^2 \tag{3.1.19}$$

The equation can then be solved by standard methods such as :-

$$q = -\frac{1}{2}\left(b + sgn(b)\sqrt{b^2 - 4ac}\right) \tag{3.1.20}$$

Where,

$$x_2 = \frac{c}{q} \tag{3.1.21}$$

and

$$x_1 = \frac{q}{a} \tag{3.1.22}$$

Method 2b - Standard Quadratic Equations.

If $k_2 \neq 0$, then combining equations (3.3.8) and (3.3.9) gives a quadratic equation that can be solved for $x_{m,n}$:-

$$a_1 x_{m,n}^2 + b_1 x_{m,n} + c_1 = 0 \qquad (3.3.23)$$

where:-

$$a_1 = 1 + a^2 + (1 + b^2)\left[\frac{k_1}{k_2}\right]^2 - 2ab\frac{k_1}{k_2} \qquad (3.3.24)$$

$$b_1 = 2\left[ab\frac{k_3}{k_2} - \frac{k_1 k_2}{k_2}(1+b^2) - \frac{k_1}{k_2}(bz_{m,n-1} - bd - y_{m,n-1}) + (az_{m,n-1} - ad - x_{m,n-1})\right] \qquad (3.3.25)$$

$$c_1 = d^2 + (x_{m,n-1}{}^2 + y_{m,n-1}{}^2 + z_{m,n-1}{}^2) - S_n{}^2 - 2dz_{m,n-1} + (1 = b^2)\left(\frac{k_3}{k_2}\right)^2$$

$$+2\frac{k_3}{k_2}(bz_{m,n-1} - bd - y_{m,n-1}) \qquad (3.3.26)$$

Once the solution for $x_{m,n}$ has been found, $y_{m,n}$ and $z_{m,n}$ can be found using equations (3.3.5) and (3.3.9).

Choosing the Correct Solution.

The solution of the simultaneous equations can give rise to the following occurrences:-

i) No Solution - the node does not lie on the plane of the currently defined patch (as defined in equation (3.3.5)). The equation of the surrounding patches must be substituted into equation (3.3.5) and the solution recalculated until the correct patch is found.

ii) One solution - node found correctly.

iii) Two solutions - choose the node that is the greatest distance from the (m-1,n-1) node. This occurs when the node is on a different patch from its 'parents'. The solution will give two nodes, one on the plane of the new patch with co-ordinates approximately equal to those of the node (m-1,n-1), and the one for the

required solution (m,n). Therefore the node furthest from the (m-1,n-1) node is the one required.

Checking if Solution is on the Patch

When the position of each new point has been determined, the algorithm must check whether the point is on the current patch. To determine this firstly a check is made on whether the point is in the same plane as the patch. If this is true then a test is made to check if the point is within the boundary of the polygon as described previously.

Appendix 3.4 - Kinematic Drape Model Algorithm

The basic kinematic drape model algorithm is as follows:-

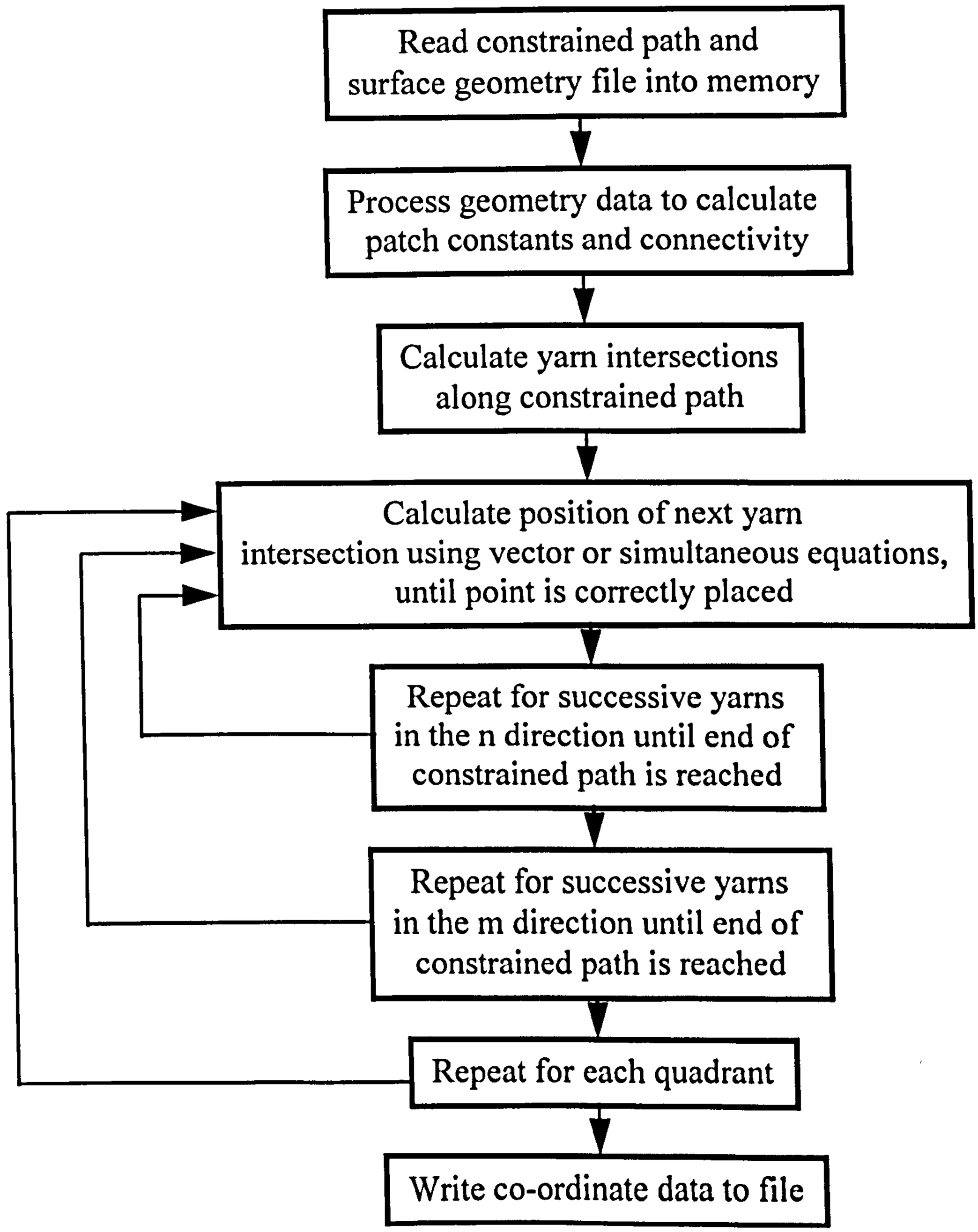

Appendix 4.1 - Calculation of Fabric Shear Resistance from Crosshead Displacement and Force

Derivation of Inter-Yarn Shear Angle

The inter-yarn shear angle (θ_s) can be calculated from the crosshead displacement (δx) using:-

$$\theta_s = 90 - \Phi_{Frame} \tag{4.1.1}$$

where the frame angle (Φ_{Frame}) is defined by:-

$$\Phi_{Frame} = 2.\cos^{-1}\left(\frac{x+\delta x}{l}\right) \tag{4.1.2}$$

and l is the length of edge between the parallelogram pivots and x is half the original distance between diagonals of the parallelogram (See Figure 4.5).

In-Plane Shear Force

The in-plane shear force (F_s) can be calculated from the crosshead force (F_{xhd}) and the frame angle (Φ_{Frame}) using:-

$$F_s = \frac{F_{xhd}}{2.\cos\left(\frac{\Phi_{Frame}}{2}\right)} \tag{4.1.3}$$

In-Plane Shear Stiffness

The in-plane shear stiffness (S) of a fabric is defined as the shear coupling per unit area per unit shear deformation [100], therefore:-

$$S = \frac{F_s.h}{h.l.\theta_s} \tag{4.1.4}$$

where h is the distance between the restrained fabric edges across the parallelogram, h.l is the surface area of the fabric being sheared, and θ_s is the shear angle in radians. The unit of shear stiffness is N/m.rad.

Appendix 4.2 - Calculation of Yarn Intersection Area and Shear Rigidity

Derivation of Yarn Intersection Area and Shear Rigidity

From measurement of several yarns using vernier calipers, it was estimated that the yarn width to height ratio (AspectRatio) was 3:1. Therefore the yarn width (W_{yarn}), thickness (t_{Yarn}), and the cross sectional area of one yarn intersection was calculated from the yarn linear density using:-

$$A_{Yarn} = \frac{m}{\rho_{Glass}} \quad (mm^2) \tag{4.2.1}$$

$$t_{Yarn} = \sqrt{\frac{A_{Yarn}}{AspectRatio}} \quad (mm) \tag{4.2.2}$$

$$W_{Yarn} = AspectRatio.t_{Yarn} \quad (mm) \tag{4.2.3}$$

$$A_{Int} = W_{Yarn}^{\ 2} \quad (mm^2) \tag{4.2.4}$$

The number of yarn intersections per square metre was calculated from the yarn spacing (L_{Yarn}) by:-

$$\text{No of Intersections} = \left(\frac{1000}{L_{Yarn}}\right)^2 \tag{4.2.5}$$

where the yarn spacing was defined by $L_{Yarn.}$ (mm). The ratio of yarn intersection area to fabric area was determined using:-

$$\text{Ratio}_{Crossover} = \frac{A_{Int}.\text{No of Intersections}}{1000000} \quad (\%) \tag{4.2.6}$$

The fabric shear rigidity was calculated from the linear portion (between θ_s = 8° and θ_s = 32° shear) of the shear force (F_θ) plot using:-

$$ShearRigidity = \frac{F_{32} - F_8}{32^o - 8^o} \quad (N/deg) \tag{4.2.7}$$

Appendix 5.1 - The CamSys ASAME Process

This appendix describes the CamSys Automated Strain Analysis and Measurement Environment (ASAME) process used in Chapters 5, 6 and 7, using a quadrant from a 19 mm high disc shaped preform as an example. Two digital images which include the desired area were captured from different angles using the equipment described in section 5.4.1 (Figure 5.1.1).

The image outside of the area of interest was selected in each image and discarded (Figure 5.1.2). Software processing of each image reduced the line thickness about the centre of the line to produce a single pixel line grid (Figure 5.1.3). This was then edited to ensure then grids were complete, replacing any line segments which were lost during image capture or subsequent processing, and removing superfluous spurs that were caused by shadows on the fabric.

A mesh was mapped onto each grid defining the points of intersection of each grid line (Figure 5.1.4 - right hand image). The two meshes were combined by the software using the two sets of co-ordinates from the grids, a user defined datum on each grid, the angle of the turntable and focal length of the camera to define a three dimensional geometry (Figure 5.1.5). The software is based on a translation of co-ordinates method, and is described in full by Vogel and Lee [80].

The surface deformation could be viewed as major and minor principal strains or strain vectors. Figure 5.1.6 shows the major principal strain distribution for a 19 mm high disc. Displaying principal strains shows the data from a metals (isotropic property) view point. To process the data into a form applicable to fabric deformation, the co-ordinates for each grid intersection were output to a text file (Figure 5.1.7). The method of post-processing the data to determine the fabric deformation in terms of slip and shear mechanisms is described in Appendix 5.2.

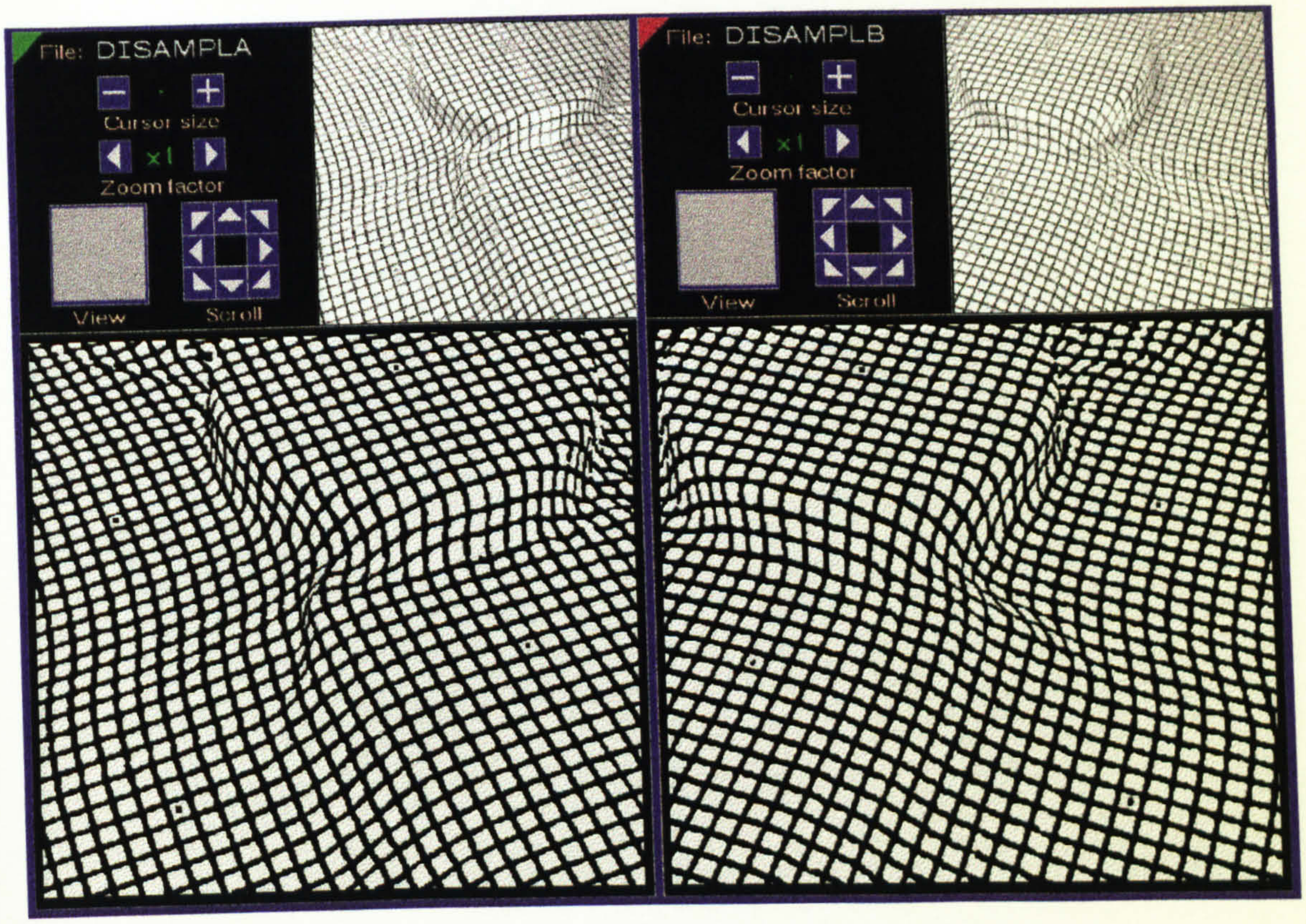

Figure 5.1.1 Raw images from ASAME equipment.

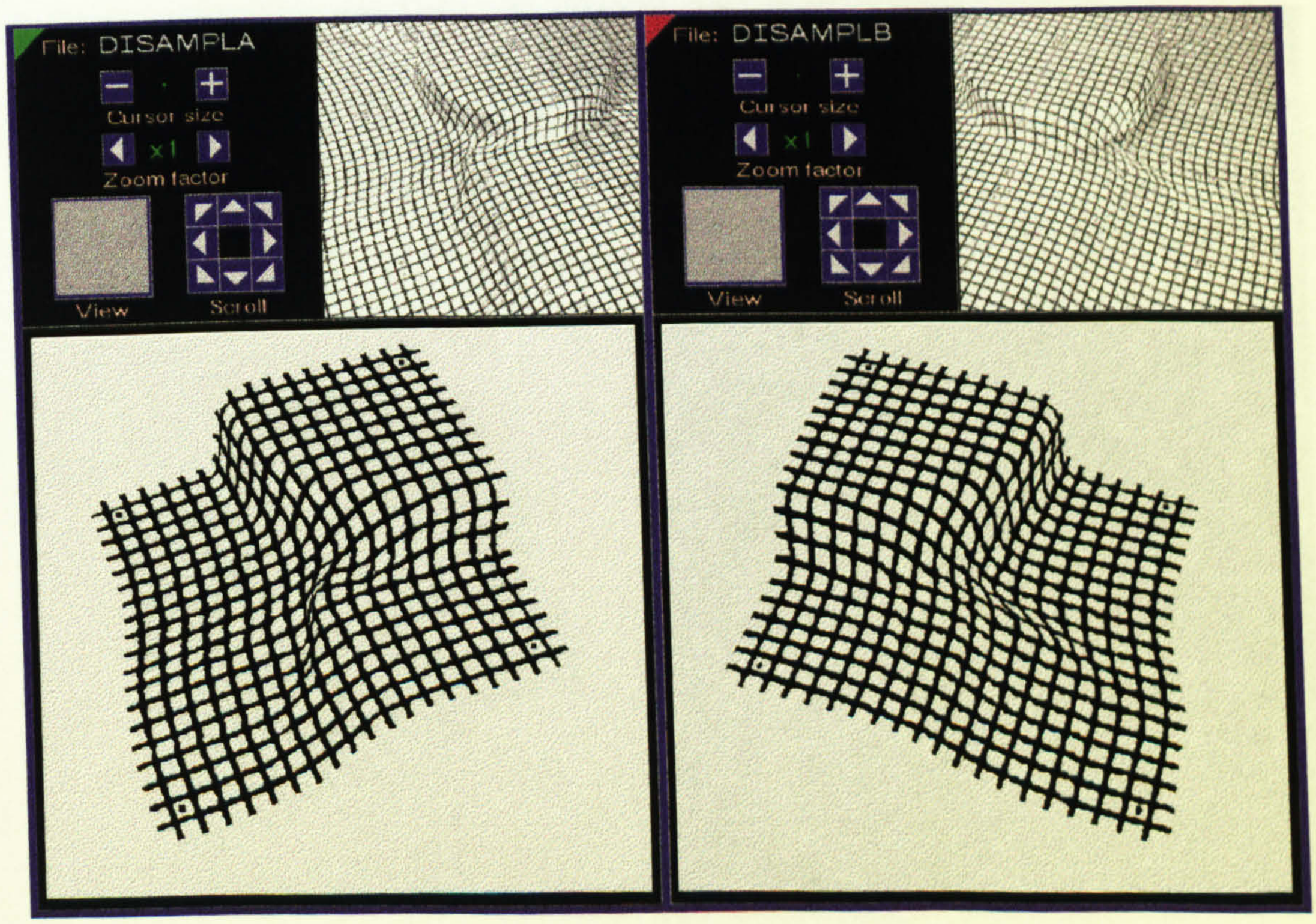

Figure 5.1.2 ASAME image processed to exclude unwanted areas.

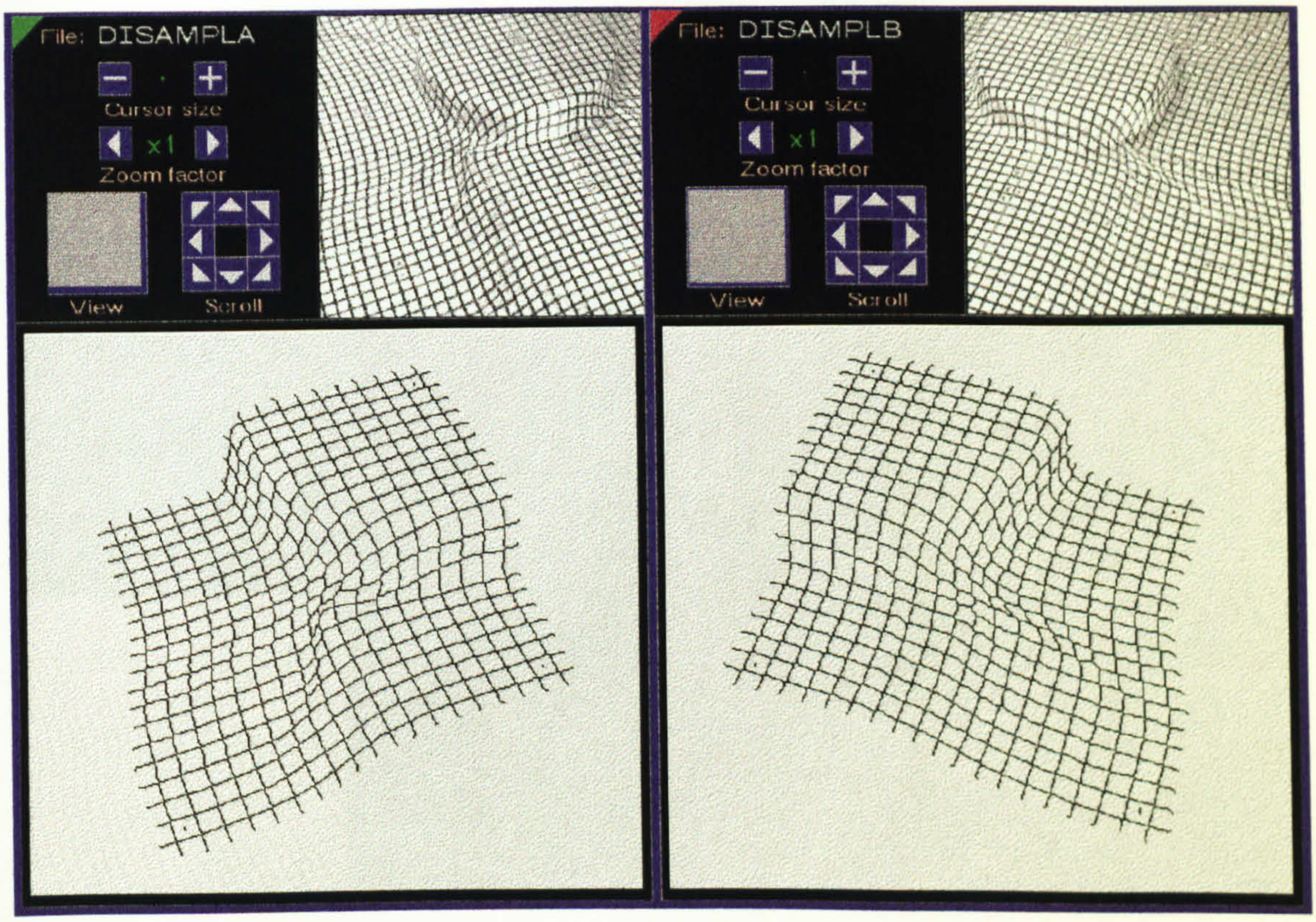

Figure 5.1.3 Images processed to produce a single pixel grid.

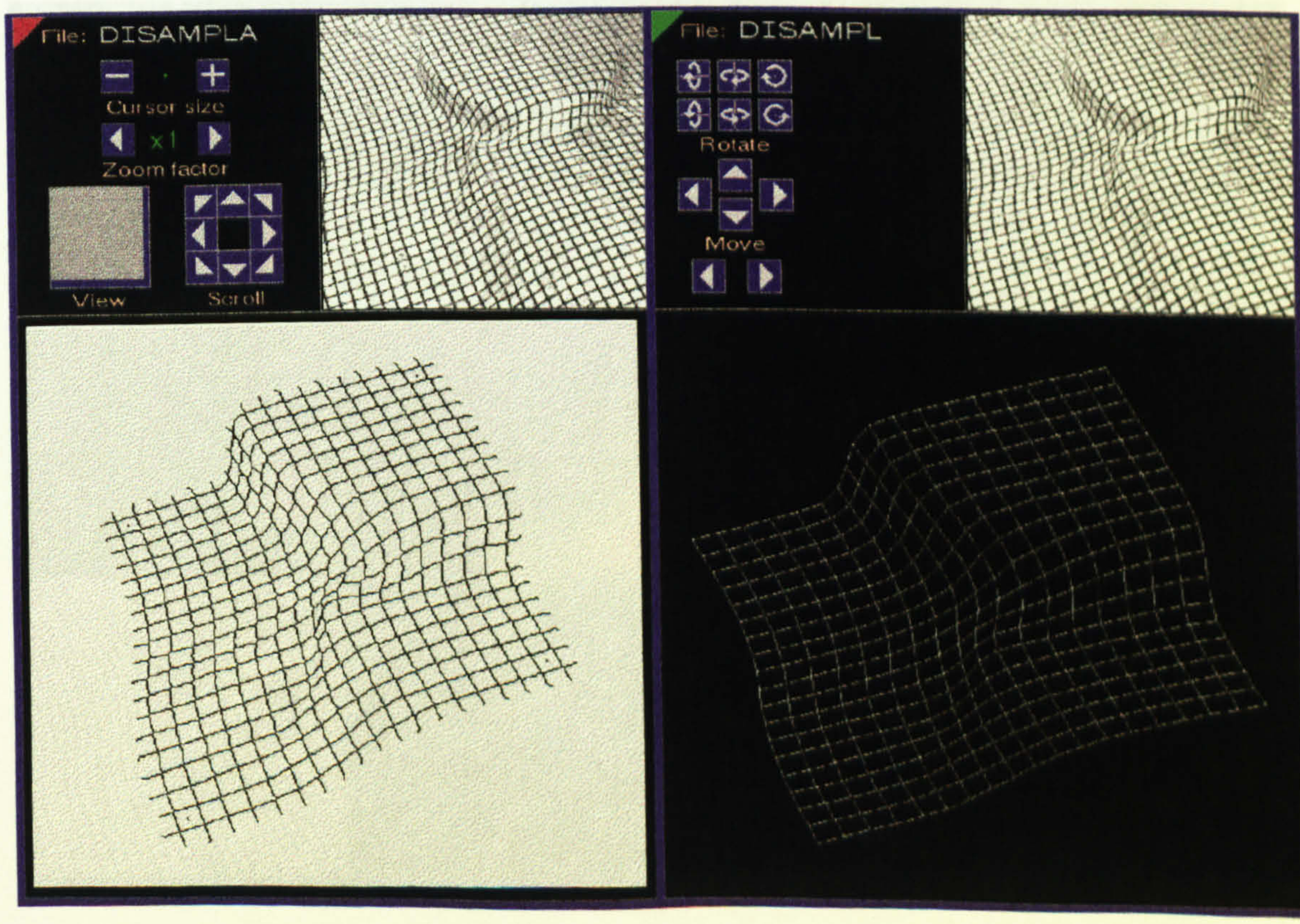

Figure 5.1.4 Thin line grid (left) and software mapped 2D grid (right).

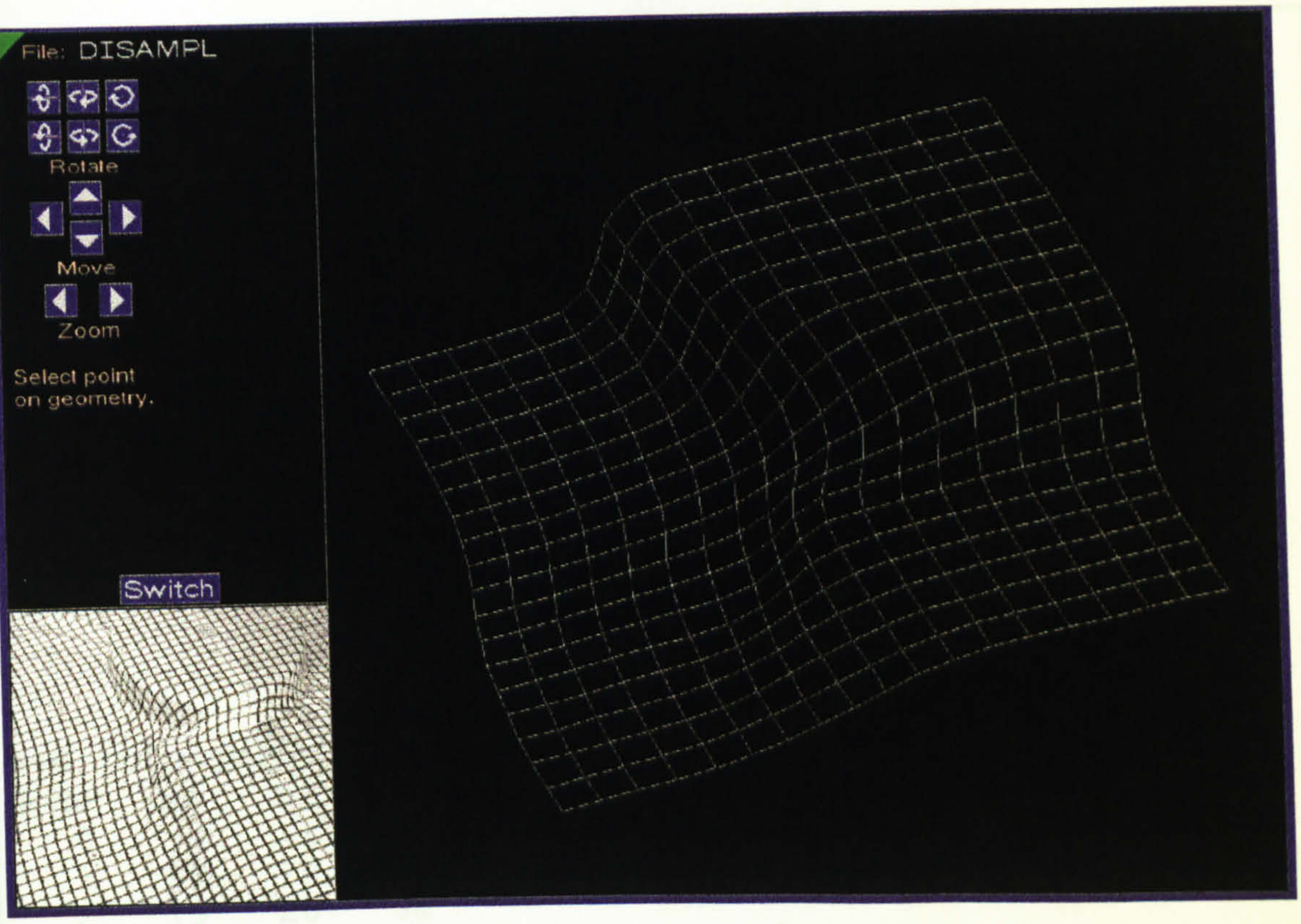

Figure 5.1.5 3D grid calculated from two 2D images.

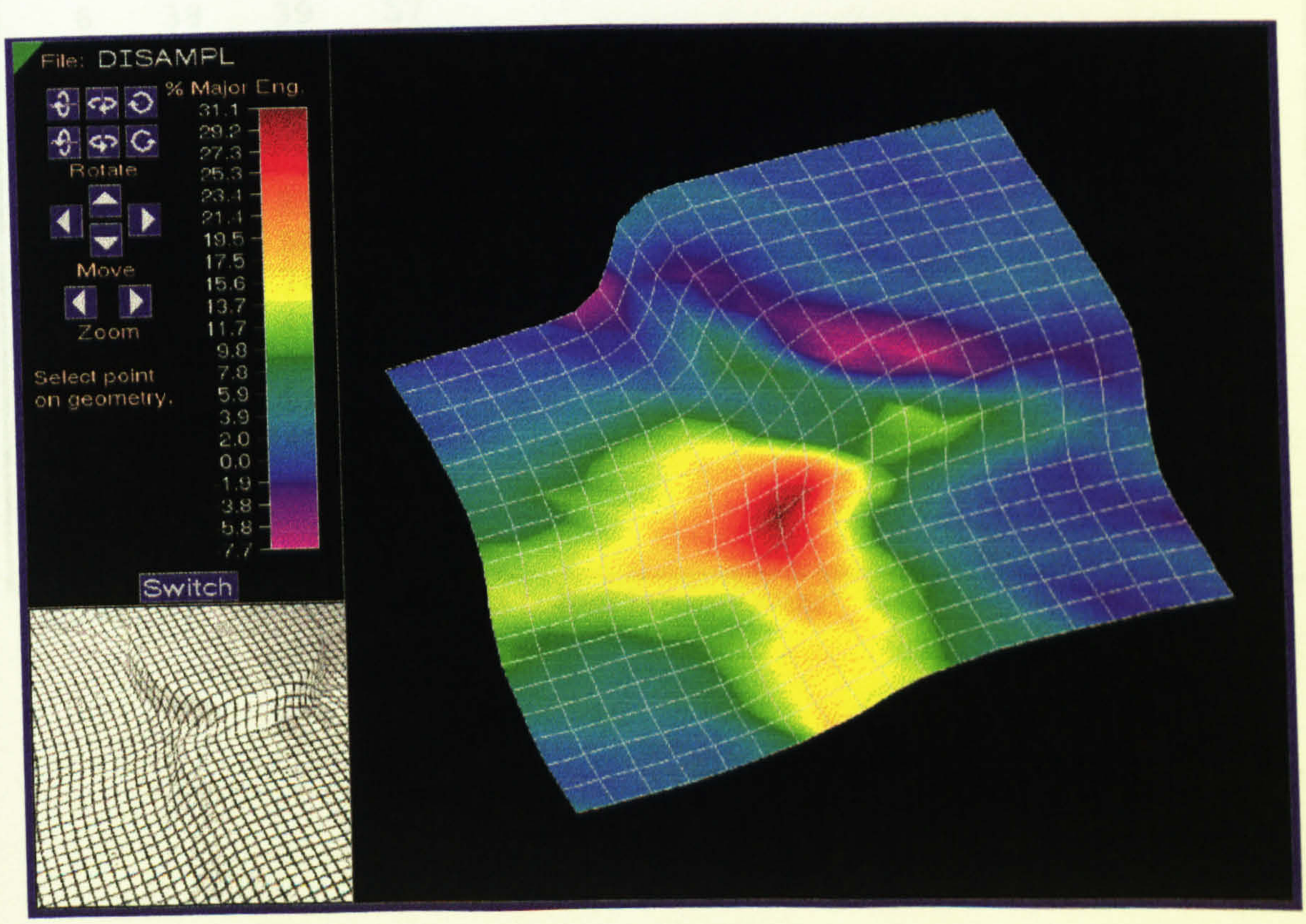

Figure 5.1.6 3D grid with major engineering strain mapped onto surface.

361 nodes (mm)

Node	X	Y	Z	Percent ENGINEERING strain Major	Minor	Dir
0	22.75	64.74	-26.30	0.86	-0.71	-0.02
1	16.73	63.22	-24.53	1.73	-1.07	-0.18
2	10.52	61.89	-22.70	1.48	-2.74	-0.61
3	4.75	60.44	-21.13	-0.30	-4.19	-1.00
4	-1.07	59.10	-19.62	0.16	-2.97	-1.07
5	-7.06	57.65	-18.04	0.31	-0.44	-1.24
6	-13.00	56.14	-16.08	0.39	-1.19	0.12
7	-19.01	54.66	-14.53	0.59	-0.92	-1.55
8	-24.85	53.11	-12.90	2.78	-4.59	1.41
9	-30.06	51.00	-11.85	2.88	-11.23	1.35
10	-33.87	46.91	-12.73	2.95	-12.92	1.18
11	-35.26	41.71	-15.30	0.07	-12.79	0.92
12	-37.06	37.02	-17.69	-6.35	-15.09	1.06

...
...
...

648 triangular elements

Node	n1	n2	n3
0	0	1	19
1	20	19	1
2	19	20	38
3	39	38	20
4	1	2	20
5	21	20	2
6	38	39	57
7	58	57	39
8	20	21	39
9	40	39	21
10	2	3	21
11	22	21	3
12	57	58	76
13	77	76	58
14	39	40	58
15	59	58	40
16	21	22	40
17	41	40	22

...
...
...

Figure 5.1.7 ASAME grid data output in text format

Appendix 5.2 - Shear and Slip Calculations

Deriving Shear and Slip from Grid Co-ordinates

The slip is defined as the change in the distance between consecutive nodes. The distance between the two nodes (D_{Actual}) is calculated from their respective co-ordinates, and compared with the original grid spacing (Figure 5.2.1) where:-

$$D_{Actual} = \sqrt{(x_1 - x_2)^2 + (y_1 - y_2)^2 + (z_1 - z_2)^2} \qquad (5.2.1)$$

$$\overline{P_{1n}} = \overline{P_{n+1}} + \left(\overline{P_{n1}} - \overline{P_{n+1}}\right) \qquad (5.2.2)$$

The inter-fibre angle is defined as the angle between two fibres (Figure 5.2.2), which is derived from the scalar product of two vectors:-

$$\cos\phi = \frac{V_1 \cdot V_2}{|V_1||V_2|} \qquad (5.2.3)$$

Giving:-

$$\cos\phi = \frac{x_1 \cdot x_2 + y_1 \cdot y_2 + z_1 \cdot z_2}{\sqrt{(x^2_1 + y^2_1 + z^2_1).(x^2_2 + y^2_2 + z^2_2)}} \qquad (5.2.4)$$

The inter-fibre shear angle is defined as the change of inter-fibre angle when compared to the undeformed fabric.

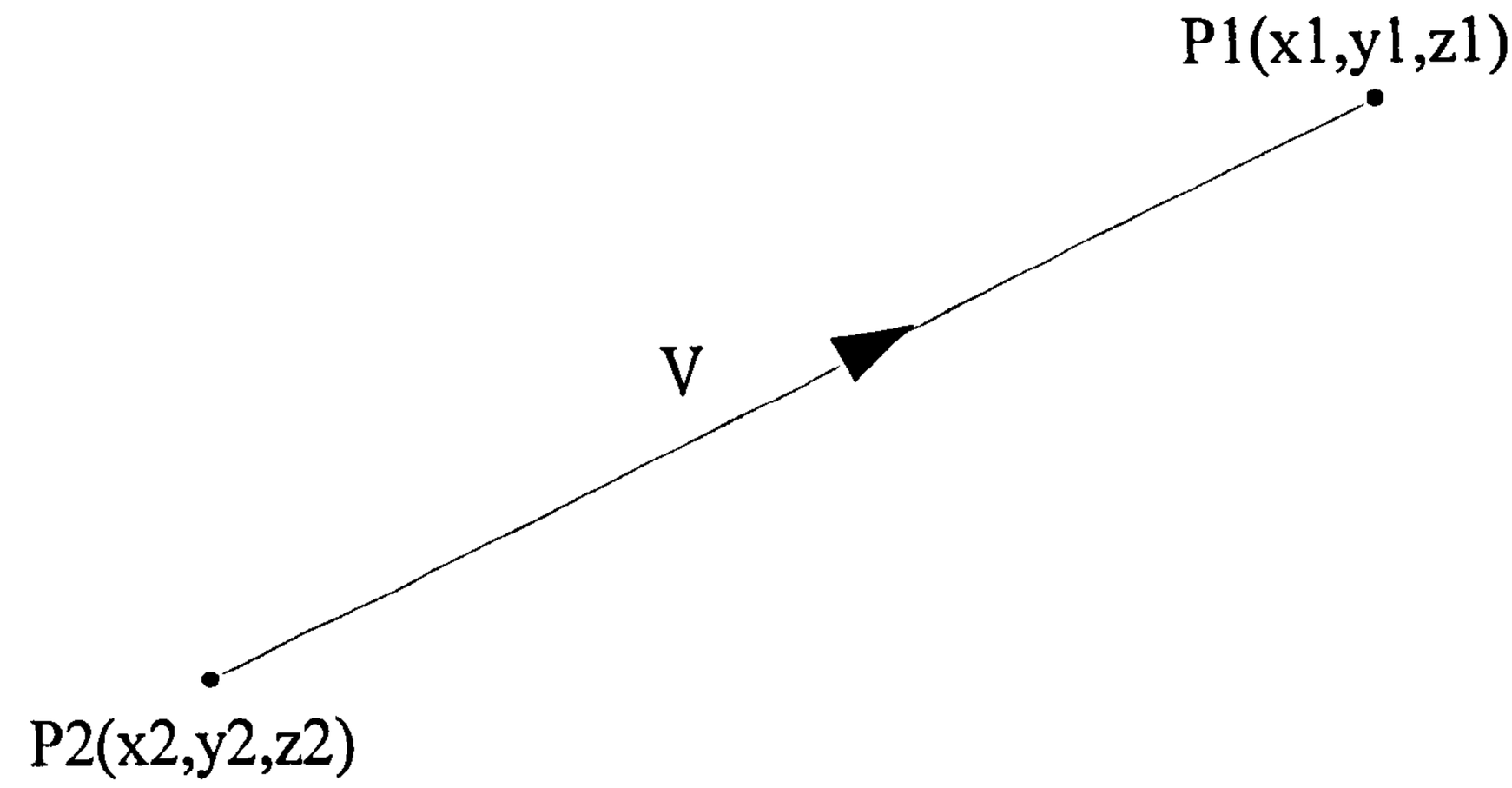

Figure 5.2.1 Calculation of distance between two points.

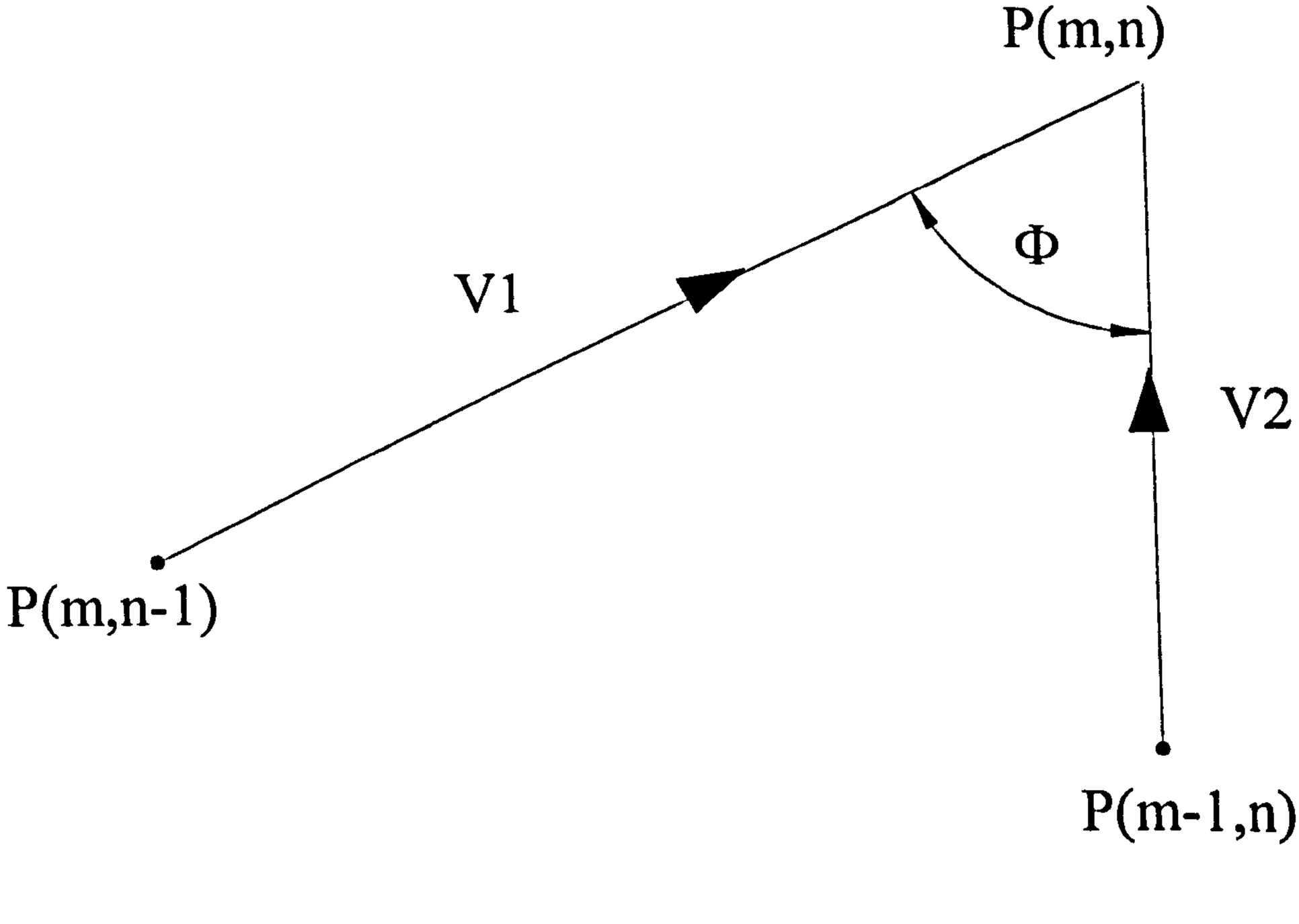

Figure 5.2.2 Calculation of included angle between two vectors.

Appendix 5.3 - Error in Slip Calculation over Curved Surfaces

The curvature of the hemispherical punch used to produce the preforms described in Chapter 6 and Chapter 7 will create errors in the slip data as described in section 5..4. The error is due to an assumption that the fibres take a straight path between grid intersection points, which does not occur on curved surfaces.

For a known hemisphere radius and grid spacing the angle between two grid intersection points from the centre (Figure 5.3.1) can be calculated:-

$$\theta = \left(\frac{L}{2.\pi.r}\right).360^{o} \qquad (5.3.1)$$

For the 50 mm radius hemisphere and 6.4 mm grid spacing used in the work reported in this thesis, $\theta = 7.33$ degrees. The direct distance (L`) between two points on a hemispherical circumference at a known angle from the centre can be found from:-

$$L` = 2.(R.\sin(\theta/2)) \qquad (5.3.2)$$

Therefore the error due to the method of calculation of slip is:-

$$Error = \frac{(L`-L)}{L} \qquad (5.3.3)$$

For the data presented in this thesis the error in the slip data due to the curvature was 0.07%, which was less than the accuracy of the ASAME process, and was therefore ignored.

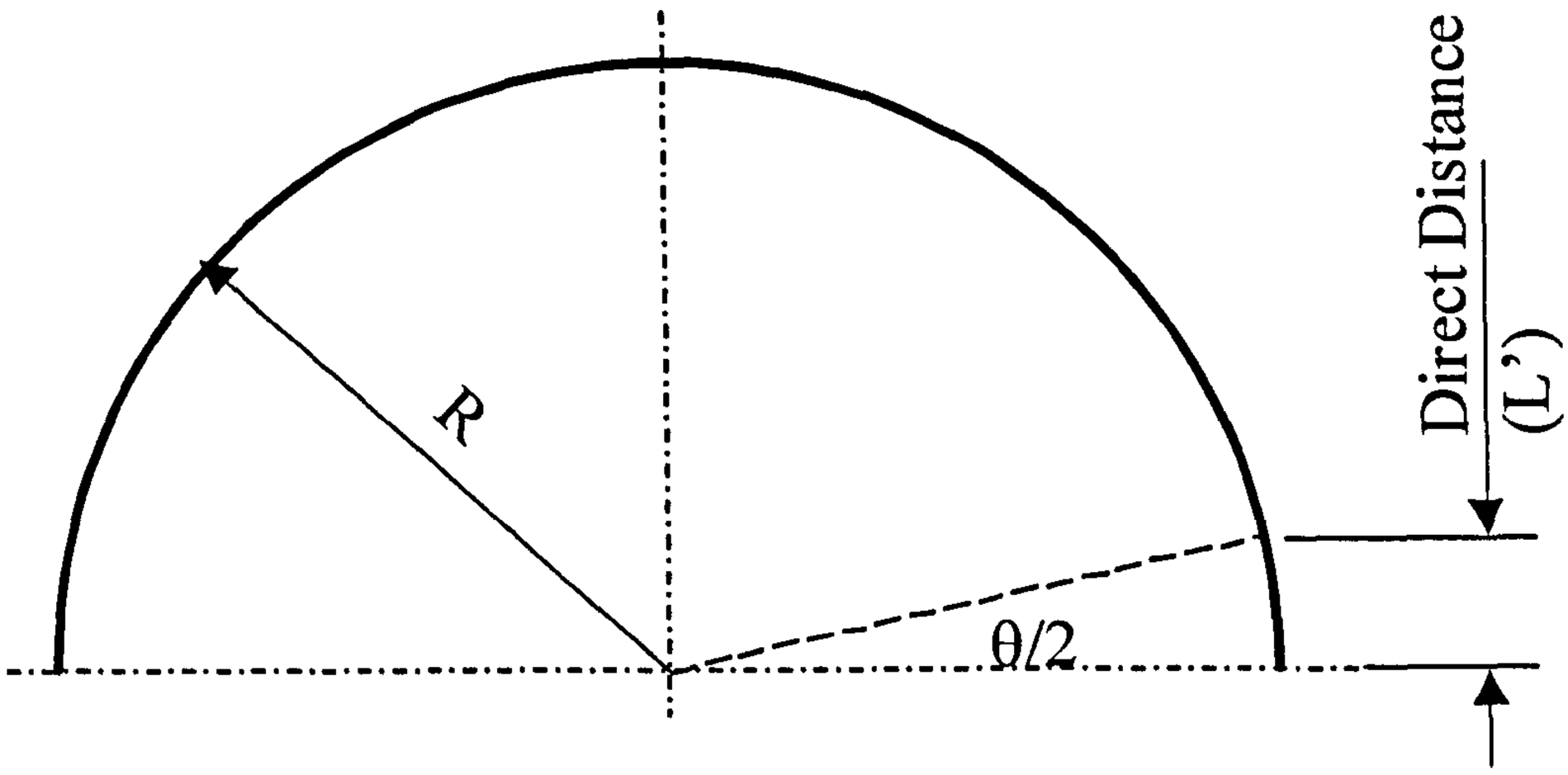

Figure 5.3.1 Diagram of variables used in the calculation of slip error over a hemispherical geometry.